

Durham E-Theses

Essays in Risk Management and Asset Pricing with High Frequency Option Panels

YANG ZHANG

How to cite:

ZHANG, YANG (2018) Essays in Risk Management and Asset Pricing with High Frequency Option Panels. Doctoral thesis, Durham University.

Use policy

The full-text may be used and/or reproduced, and given to third parties in any format or medium, without prior permission or charge, for personal research or study, educational, or not-for-profit purposes provided that:

- a full bibliographic reference is made to the original source
- a <https://etheses.durham.ac.uk/id/eprint/12601/> is made to the metadata record in Durham E-Theses
- the full-text is not changed in any way

The full-text must not be sold in any format or medium without the formal permission of the copyright holders.

Please consult the [full Durham E-Theses policy](#) for further details.

Essays in Risk Management and Asset Pricing
with High Frequency Option Panels



Yang ZHANG

Durham University Business School

Durham University

A Thesis Submitted for the Degree of

Doctor of Philosophy in Finance

2018

Essays in Risk Management and Asset Pricing with High Frequency Option Panels

Yang ZHANG

Abstract

The thesis investigates the information gains from high frequency equity option data with applications in risk management and empirical asset pricing. Chapter 1 provides the background and motivation of the thesis and outlines the key contributions. Chapter 2 describes the high frequency equity option data in detail. Chapter 3 reviews the theoretical treatments for Recovery Theorem. I derive the formulas for extracting risk neutral central moments from option prices in Chapter 4.

In Chapter 5, I specify a perturbation theory on the recovered discount factor, pricing kernel, and the physical probability density. In Chapter 6, a fast and fully-identified sequential programming algorithm is built to apply the Recovery Theorem in practice with noisy market data. I document new empirical evidence on the recovered physical probability distributions and empirical pricing kernels extracted from both index and single-name equity options. Finally, I build a left tail index from the recovered physical probability densities for the S&P 500 index options and show that the left tail index can be used as an indicator of market downside risk.

In Chapter 7, I uniquely introduce the higher dimensional option-implied average correlations and provide the procedures for estimating the higher dimensional option-implied average correlations from high frequency option data. In Chapter 8, I construct a market average correlation factor by sorting stocks according to their risk exposures to the option-implied average correlations. I find that (a) the market average correlation factor largely enhances the model-fitting of existing risk-adjusted asset pricing models. (b) the market average correlation factor yields persistent positive risk premiums in cross-sectional stock returns that cannot be explained by other existing risk factors and firm characteristic variables. Chapter 9 concludes the thesis.

Contents

Contents	1
List of Tables	6
List of Figures	7
Acronyms	17
Table of Notation	17
1 Introduction	21
1.1 Overview and Background	21
1.2 Findings and Contributions	27
1.2.1 Empirical Recovery and Risk Management	27
1.2.2 Option-implied Average Correlations and Empirical Asset Pricing	37
1.3 Structure of the Thesis	39
2 OPRA and High Frequency Option Data Panel	41
2.1 Overview	41
2.2 The OPRA Option Data System	42
2.3 The TRTH and Option Data Structure	45
2.4 The High Frequency Option Data Panel	48
2.4.1 The S&P 500 Index Constituents Sample	48
2.4.2 The Selected Sector Index Sample	49
2.4.3 Construct the Option Data Panel	50

2.5	Features of the High Frequency Option Data Panel	52
2.6	Summary and Remarks	57
3	Review of Recovery Theorem	58
3.1	Overview	58
3.2	The Ross [2015] Derivation	62
3.3	The Carr and Yu [2012] Derivation	65
3.4	The Borovička, Hansen, and Scheinkman [2016] Interpretation	68
3.5	Summary and Remarks	71
4	Extract the Risk Neutral Central Moments from Option Prices	73
4.1	Overview	73
4.2	Derive the Generic Spanning Contracts	74
4.3	Extract the Risk Neutral Central Moments from Option Prices	77
4.4	Summary and Remarks	80
5	Hansen-Scheinkman Factorisation and Ross Recovery from High Frequency Option Prices via Nonlinear Programming: The Perturbation Theory	82
5.1	Introduction	82
5.2	Eigenfunction Analysis of Risk Neutral State Price Transition Matrices	86
5.2.1	The Borovička et al. [2016] Derivation	88
5.2.2	The Ross [2015] Recovery Theorem	90
5.3	Motivating the Problem: Revisiting the Ross Recovery Calculation	92
5.3.1	Experiment One Direct Solution for \mathbf{Q}	93
5.3.2	Experiment Two Non-Negative Least Squares Solution for \mathbf{Q}	94
5.3.3	Experiment Three My Implementation for \mathbf{Q}	94
5.4	A Perturbation Theory of Recovery	96
5.4.1	Continuity of Recovered Discount Factor and Pricing Kernel	96

5.4.2	Asymptotic Properties of a Parametric Recovery Theorem	98
6	Hansen-Scheinkman Factorisation and Ross Recovery from High Frequency Option Prices via Nonlinear Programming: The Empirical Recovery	100
6.1	Empirical Recovery	100
6.1.1	Procedure Setup	102
6.1.2	Recovering the State Price Matrix Using Intraday Data	103
6.1.3	Determining the Risk Neutral State Price Transition Matrix	107
6.1.4	An Empirically Identified Recovery Theorem	115
6.1.5	Additional Issues for Numerical Implementations . . .	117
6.2	Simulation	120
6.2.1	A-priori Known Number of States	120
6.2.2	A-priori Unknown Number of States	124
6.3	Empirical Example and Application	128
6.3.1	S&P 500 Index and Apple Inc.	128
6.3.2	The Market Left Tail Index	142
6.4	Concluding Remarks	144
7	Higher Dimensional Option-implied Average Correlations: Constructing the Cross Sectional Correlation Measures	146
7.1	Introduction	146
7.2	The Higher Dimensional Average Correlations	152
7.3	Data	164
7.3.1	Daily Market Capitalisation Data for S&P 500 Index Constituents	164
7.3.2	High Frequency Option Data Panels for S&P 500 Index and its Constituents	164
7.3.3	High Frequency Option Panels for Selected Sector Index	169
7.4	Estimate the Higher Order Risk Neutral Central Moments . .	170
7.5	Estimate the Higher Dimensional Option-implied Average Correlations	177

7.5.1	Market Option-implied Average Correlations	177
7.5.2	Sectorial Option-implied Average Correlations	180
7.6	Validity of the Market Portfolio Moments Decomposition	183
7.7	Concluding Remarks	188
8	The Information Content of Higher Dimensional Option-implied Average Correlations: Measuring Diversification Risk and Cross Sectional Asset Pricing	190
8.1	Introduction	190
8.2	Data and Variables	193
8.2.1	Data	193
8.2.2	Firm-specific Control Variables	193
8.2.3	Portfolio-based Control Variables	198
8.3	Empirical Identification of the Price of Market Correlation Risk	199
8.3.1	Measure Market Diversification Risk	200
8.3.2	Construct The Market Average Correlation Factor	203
8.3.3	Market Average Correlation Factor and Expected Stock Returns	207
8.4	Robustness Check	217
8.4.1	Sub-Periods	217
8.4.2	Length of the Portfolio Formation Period	219
8.4.3	Options with Longer Time to Maturity	222
8.5	Concluding Remarks	222
9	Conclusions	225
9.1	Summary and Remarks	225
9.2	Future Work	226
10	Appendix	229
A.1	S&P 500 Index Constituents Sample List	229
A.2	Selected Sector Index Sample List	242
A.3	MATLAB Codes for Data Extraction	251
A.4	Proofs for Chapter 5	255
A.4.1	Proof for Lemma 5.1	255

A.4.2 Proofs for Unimodality of the State Price Transition Matrix	264
A.4.3 Proofs for Sub-stochasticity of the State Price Transition Matrix	269
A.4.4 Full Steps of the SQP Process on the Discount Factor Constrain	271
Bibliography	276

List of Tables

6.1	Error Bounds Analysis Tenor: 71 Days	126
6.2	Error Bounds Percentile Analysis Tenor: 71 Days	127
6.3	Sample Description	130
6.4	Option Implied Pricing Kernel for SPX and AAPL	142
7.1	Descriptive Statistics for Option Implied Correlations	179
7.2	Validity of the Market Portfolio Moments Decomposition	185
8.1	Option-implied Average Correlations and the Market Risks	201
8.2	Contemporaneous Univariate-sorted Portfolios on Option-implied Average Correlation Risk Exposure	205
8.3	Market Average Correlation Factor and Sectors Portfolio Returns	208
8.4	Fama-MacBeth Regression Analyses on Market Average Correlation Portfolio	214
8.5	Fama-MacBeth Regression Analyses for the Pre and Post OPRA Sub-Periods	218
8.6	Single-sorted Portfolios and Fama-MacBeth Regression Analyses with Different Length of Portfolio Formation Period	220
A. 1	Sample Description	229
A. 2	Sector Sample Description	242

List of Figures

1.1	Equity Option Trading Volumes in the U.S.	22
1.2	The Recovery Process	28
1.3	The Tail Truncation Problem	29
1.4	Challenges in Identifying the Transition Matrix	31
1.5	Risk Neutral Density V.S. Recovered Physical Density	34
1.6	Recovered Pricing Kernel	35
1.7	Recovered Market Left Tail Index	36
1.8	Option-implied Average Correlations	38
2.1	Option Trading Volumes on CBOE	43
2.2	Equity Option Trading Volumes in U.S.	45
2.3	High Frequency Option Data Sample	54
2.4	High Frequency Option Data Sample	55
2.5	High Frequency Option Data Sample	56
5.1	Experiments on Computing the State Transition Matrix with Ross Data	95
6.1	Extrapolating the Tail of the Option Implied Risk Neutral State Price.	118
6.2	Simulation Test of the RT Algorithm	123
6.3	Under and Over Estimation of the Number of States	125
6.4	Price Fitted for SPX on April 27, 2011	132
6.5	Price Fitted for AAPL on on April 27, 2011	133
6.6	Implied Volatility Fitted for SPX on April 27, 2011	134

6.7	Implied Volatility for AAPL on on April 27, 2011	135
6.8	Risk Neutral Density Fitted and Recovered Physical Density for SPX on April 27, 2011	137
6.9	Risk Neutral Density Fitted and Recovered Physical Density for AAPL on April 27, 2011	138
6.10	Option Implied Pricing Kernel for SPX on April 27, 2011 . . .	140
6.11	Option Implied Pricing Kernel for AAPL on April 27, 2011 . .	141
6.12	Recovered Market Left Tail Index	145
7.1	The Option-implied Average Correlation Smile Surface and Term Structure	150
7.2	Three Dimensional Decomposition	161
7.3	High Frequency Option Data Sample	167
7.4	High Frequency Option Data Sample	168
7.5	Term Structure of Estimated Risk Neutral Second Central Moments	173
7.6	Term Structure of Estimated Risk Neutral Third Central Moments	174
7.7	Term Structure of Estimated Risk Neutral Fourth Central Moments	175
7.8	Term Structure of the Option-implied Average Correlations . .	178
7.9	Option-implied Sectorial Option-implied Average Correlations: I	181
7.10	Option-implied Sectorial Option-implied Average Correlations: II	182
9.1	The Two Option-implied Risk Measures	227

Acronyms

BE book value of the equity. [194](#), [195](#)

BM book to market ratio. [194](#), [213](#)

BVPS book value of preferred stock. [195](#)

CAPM Capital Asset Pricing Model. [191](#), [207](#), [216](#), [217](#)

CBOE Chicago Board of Option Exchange. [42–45](#), [146](#), [148](#), [149](#), [151](#), [199](#),
[200](#), [202](#), [216](#), [223](#)

CKT realised co-kurtosis. [195](#), [213](#)

CLASS The capital and loss assessment under stress scenarios. [228](#)

CRRA constant relative risk aversion. [116](#), [117](#), [121](#), [124](#), [140](#), [141](#)

CRSP Centre for Research in Security Prices. [164](#), [193](#), [194](#), [198](#)

CSK realised co-skewness. [195](#), [213](#)

ETFs exchange-traded funds. [49](#), [169](#), [213](#), [223](#)

FF3 Fama-French 3-factor Model. [207](#), [216](#)

FFC4 Fama-French-Carhart 4-factor Model. [204](#), [206](#), [207](#), [212](#), [216](#)

GARCH The generalised autoregressive conditional heteroskedasticity. [228](#)

GDP Gross Domestic Product. [228](#)

- HML** book-to-market factor. [199](#), [207](#)
- HPI** House Price Index. [228](#)
- IDIO** idiosyncratic volatility. [196](#), [213](#)
- IEEE** Institute of Electrical and Electronics Engineers. [117](#), [121](#), [158](#)
- ILLIQ** illiquidity. [197](#), [213](#)
- ITCB** investment tax credit. [195](#)
- LIQ** traded liquidity factor. [199](#), [207](#), [212](#)
- MAC** market average correlation factor. [203](#), [207](#), [212](#), [213](#), [216](#), [217](#), [219](#), [222](#), [223](#)
- ME** market capitalisation. [194](#)
- MKT** market factor. [198](#), [207](#), [213](#)
- MOM** momentum. [197](#), [213](#)
- NMS** National Market System. [41](#), [44](#), [128](#)
- OCC** Option Clearing Corporation. [22](#), [44](#)
- OLS** ordinary least squares. [184](#)
- OPRA** Option Pricing Report Authority. [41](#), [44–48](#), [57](#), [85](#), [101](#), [116](#), [128](#), [130](#), [172](#), [202](#), [217](#), [219](#), [223](#)
- OTC** over the counter. [116](#), [128](#)
- PRTKRV** redemption value. [195](#)
- PSTK** par value. [195](#)
- PSTKL** liquidating value. [195](#)

- QE** Quantitative Easing. 129
- REV** reversal. 197, 213
- RKT** realised kurtosis. 196, 213
- RSK** realised skewness. 196, 213
- RT** Recovery Theorem. 23–28, 31, 32, 58–62, 83, 86, 87, 92, 97, 100, 106, 115, 116, 123, 139, 225, 228
- SEQ** book value of the shareholders' equity. 195
- SHROUT** total number of outstanding shares. 152, 194
- SIZE** the natural logarithm of market capitalisation. 194, 213
- SMB** stock size factor. 198, 199, 207
- SPDR** The Standard & Poor's Depository Receipts. 49, 169, 213
- SQP** sequential quadratic programming. 5, 102, 110, 115, 119, 271
- TRTH** Thomson Reuters Tick History. 41, 46–48, 50, 57, 164, 165
- TXDB** deferred taxes. 195
- U.S.** the United States. 22, 41, 44, 45, 57, 101, 129, 198
- UMD** momentum factor. 199, 207
- WRDS** Wharton Research Data Services. 164, 198

Declaration

I, Yang ZHANG, hereby declare that the work on which the thesis is based is my original work (except where acknowledgements indicate otherwise) and that neither the whole work nor any part of it has been, is being, or is to be submitted for another degree in this or any other university for a degree or a qualification.

Statement of Copyright

The copyright of this thesis rests with the author. No quotation from it should be published without the author's prior written consent and information derived from it should be acknowledged.

Acknowledgements

Undertaking this PhD has been a truly life-changing experience for me and it would not have been possible to do without the support and guidance that I received from many people.

Firstly, I would like to express my sincere gratitude to my primary supervisor Professor Julian Williams for all the continuous support and encouragement he gave me during the time of the PhD research and writing this thesis. The joy and enthusiasm he has for his research was contagious and motivational for me. My PhD has been an amazing experience and I thank Julian wholeheartedly for his tremendous support and guidance. I am blessed for having such a supervisor and mentor who has inspired me, gave me smiles, guided me through tough times, and always had an open ear for problems that even unrelated to research.

My deeply thanks also goes to Professor Fabio Massacci from University of Trento for his guidance and help. It has been a wonderful experience to work with him. Besides my primary supervisor, I would like to thank the rest of my supervisory team: Dr. Dennis Philip and Professor Panayiotis Andreou for their support. Many thanks also to my annual progress reviewer, Dr. Damian Damianov for his insightful comments, which intent me to widen my research from various perspectives.

Part of this thesis has been completed whilst visiting Sloan School of Management, Massachusetts Institute of Technology

and Kellogg School of Management, Northwestern University. I would like to pay special tribute to Professor Stephen Ross, who provided valuable insights on my work relating to empirical implementing on his Recovery Theorem when I visited him in MIT. He will be deeply missed. A very special gratitude goes out to Professor Viktor Todorov, Professor Torben Anderson, and Professor Ravi Jagannathan, who gave valuable comments on the thesis when I visited at Kellogg School of Management in Northwestern University.

I would like to thank my fellow colleagues, Dr. Jing Nie, Handing Sun, and Xiao Liang for the stimulating discussions, for the sleepless nights that we work together before deadlines, and for all the fun we have had in the last four years. My colleagues have played a substantial role in my academic success and the assistance they provided at critical times is greatly appreciated. My years as a doctoral student have been joyous and I attribute this to my wonderful friend, Yanjun Tan, thank you for listening, offering me advice, and supporting me through this entire process.

Last but not the least, I would like to thank my parents for supporting me throughout my PhD journey and my life in general. I always knew that you believed in me and wanted the best for me. Thank you for teaching me that my job in life was to learn, to be happy, and to know and understand myself; only then could I know and understand others.

I would like to acknowledge the financial support I received from the Economic and Social Research Science (ESRC) scholarship programme by the Northern Ireland and North East Doctoral Training Partnership (NINE DTP) in North East Doctoral Training Centre (NEDTC) under grant NO. 1447815 through my PhD research.

Dedication

*With great respect, love and appreciation,
I would like to dedicate this thesis to my loving parents,
who raised me to who I am and
encourage me to go on every adventure,
especially this one.*

Commonly Used Notation

The table below lists the general notations used throughout the thesis. A single coherent notation is used for a specific variable unless mentioned separately in the main text.

Symbol	Description
N	number of individual stocks in the market portfolio
N^*	number of independent elements in the co-moments matrices
\mathcal{N}	number of evenly spaced points in numerical integration
$S_{i,t}$	underlying stock i price at time t
$S_{m,t}$	market portfolio m price at time t
S_0	spot price
S_T	forward price
R	log return
K	option strike price
r_f	risk-free rate
T	option maturity date
τ	option time to maturity (tenor)
$C(\tau, K)$	call option price with strike K and time to maturity τ
$P(\tau, K)$	put option price with strike K and time to maturity τ
$\sigma(\tau, K)$	option-implied volatility with strike K and time to maturity τ
w	individual stock market capitalisation weights
σ_i^2	variance (second moment) for stock i
s_i^3	skewness (third moment) for stock i

Continued on next page

Continued from previous page

Symbol	Description
k_i^4	kurtosis (fourth moment) for stock i
$\sigma_{i,j}$	covariance between stocks i and j
$s_{i,j,k}$	co-skewness among stocks i , j , and k
$k_{i,j,k,l}$	co-kurtosis among stocks i , j , k , and l
$\rho_{i,j}$	quadratic correlation between stocks i and j
$\rho_{i,j,k}$	cubic correlation among stocks i , j , and k
$\rho_{i,j,k,l}$	quartic correlation among stocks i , j , k , and l
ρ_Σ	quadratic average correlation
ρ_Γ	cubic average correlation
ρ_Θ	quartic average correlation
Λ	symmetric multipliers
W	terminal wealth
δ	the discount factor
L_t	numéraire portfolio
\mathbf{w}	the individual stock market capitalisation weights vector
$\boldsymbol{\sigma}$	standard deviation (second moment root) vector
\mathbf{s}	standard skewness (third moment root) vector
\mathbf{k}	standard kurtosis (fourth moment root) vector
$\boldsymbol{\tau}$	time to maturity vector
\mathbf{K}	strike price vector
\mathbf{v}_R	right Perron vector
\mathbf{v}_L	left Perron vector
Σ	covariance matrix
Γ	co-skewness matrix
Θ	co-kurtosis matrix
\mathbf{I}	identity matrix
\mathbf{M}	M-matrix
\mathbf{S}	state price matrix with elements $s_{i,j}$
\mathbf{Q}	state price transition matrix with elements $q_{i,j}$

Continued on next page

Continued from previous page

Symbol	Description
\mathbf{P}	physical transition matrix with elements $q_{i,j}$
$\tilde{\mathbf{P}}$	the recovered physical transition matrix with martingale process
Φ	the transition kernel matrix with elements $\phi_{i,j}$
\mathbf{D}	the diagonal pricing kernel matrix with elements $d_{i,j}$
Ψ	the stochastic discount factor matrix with elements $\psi_{i,j}$
\mathbf{H}	the positive martingale process matrix with elements $h_{i,j}$
$\mathcal{N}_Q^{n,n}$	set of irreducible matrices
\mathbb{P}	physical measure operator
\mathbb{Q}	risk neutral measure operator
$+$	maximize operator
$\mathbb{E}[\cdot]$	expectation operator
\otimes	Kronecker product
\circ	Hadamard product operator
$'$	matrix transpose operator
D	Drazin inverse operator
$\#$	group inverse operator
$\text{vec}[\cdot]$	column-wise stacking vectorise operator
$\text{mat}[\cdot]$	reshape matrix operator
$\text{diag}_k[\cdot]$	k th order diagonal operator
$\text{triu}_k[\cdot]$	k th order upper triangular operator
$\text{tril}_k[\cdot]$	k th order lower triangular operator
$[\cdot]^k$	k th order power operator
$[\cdot]^{[k]}$	k th order permuted outer product operator
$U^{(k)}(\cdot)$	k th order derivative of the utility function $U(\cdot)$
$\text{CRRA}(\gamma)$	CRRA iso-elastic power utility function
$\mathcal{R}(\cdot)$	Perron root function
$\mathcal{V}(\cdot)$	Perron vector function
$\mathcal{S}(\cdot)$	simple eigenvalue function
$\mathcal{L}(\cdot)$	Lagrangian function

Continued on next page

Continued from previous page

Symbol	Description
∇	first-order derivative operator
∇^2	second-order derivative operator
∇	first-order partial derivative operator
∇^2	second-order partial derivative operator

Chapter 1

Introduction

... the plan of Thales of Miletus, which is a device for the business of getting wealth, but which, though it is attributed to him because of his wisdom, is really of universal application. Thales, so the story goes, because of his poverty was taunted with the uselessness of philosophy; but from his knowledge of astronomy he had observed while it was still winter that there was going to be a large crop of olives, so he raised a small sum of money and paid round deposits for the whole of the olive-presses in Miletus and Chios, which he hired at a low rent as nobody was running him up; and when the season arrived, there was a sudden demand for a number of presses at the same time, and by letting them out on what terms he liked he realised a large sum of money, so proving that it is easy for philosophers to be rich if they choose, but this is not what they care about.

*Aristotle, Politics 1.1259a.*¹

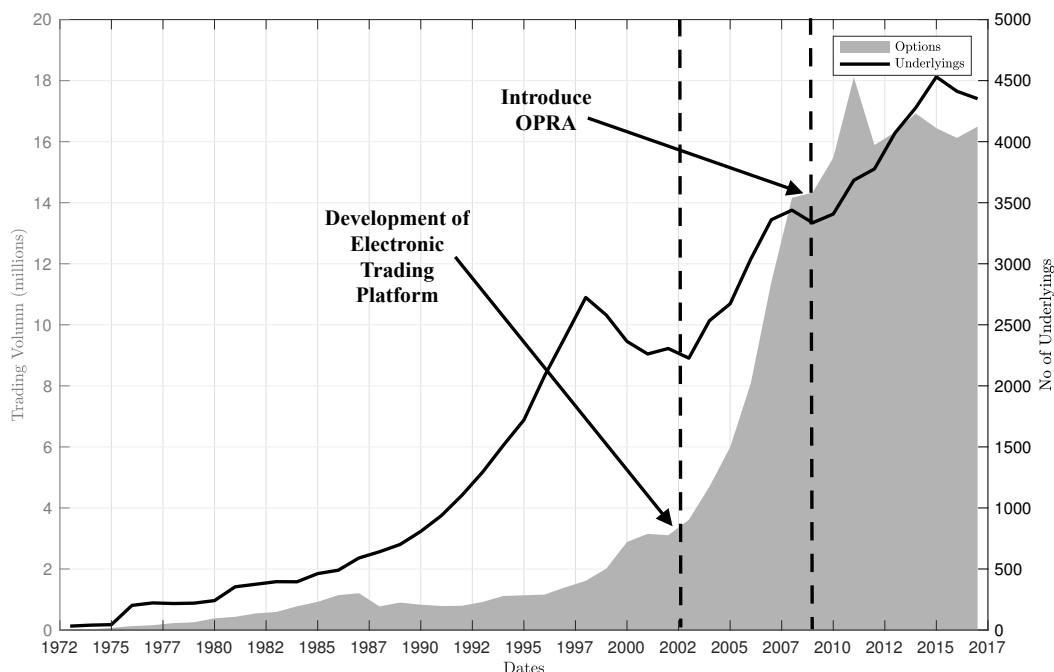
1.1 Overview and Background

Thales of Miletus has been believed as the oldest reference to derivatives as it has been recorded in the works of *Aristotle* more than 2400 years ago. It tells a story of a poor philosopher named Thales, who designed an olive-presses rent contract to answer the challenging question that “*If you are so smart, why ain’t you rich?*” The deposit gives him the right to use the olive-presses but not the obligation to use them. This could be called an option contract

¹Aristotle, *Politics* 1.1259a, from *Aristotle in 23 Volumes*, Vol. 21, translated by H. Rackham. Cambridge, MA, 1944.

on the olive-presses, which is perhaps the earliest example we can find to demonstrate the usage of derivatives.

Figure 1.1: Equity Option Trading Volumes in the U.S.



Note. Figure 1.1 reports the equity option trading volumes (in million) traded on all option exchanges in the U.S. from 1972 to 2017. The total daily trading volumes are plot by the light grey area and labeled with the left axis while the number of underlying stocks issuing options is given by the hard black line with the right axis.

With the introduction of the electronic trading platform in the mid-2000s, the trading activities and market value of derivatives have seen a surge. As Edward Swan pointed out: “*Derivatives trading is now the world’s biggest business, with an estimated daily turnover of over U.S. \$ 2.5 trillion and an annual growth rate of around 14 percent.*”² In particular, as shown in Figure 1.1, there are more than 3,500 single-name stocks issuing equity options and the daily average trading volumes for equity options in the U.S. market are more than 14 millions since 2005.³ Indeed, the increasing popularity of equity

²From Swan [2000], Building the Global Market: A 4000 Year History of Derivatives

³The trading volumes and underlying stocks data are from the Option Clearing Corporation (OCC) Daily Market Statistic: <https://www.theocc.com/webapps/historical-volume-query>.

options suggests that equity derivatives play an important role in modern financial markets.

Motivated by the growing popularity of equity options, the thesis focus on investigating the information gains from high frequency equity option panels with applications in risk management and empirical asset pricing. Specifically, I introduce two innovative risk measures extracted from option prices, mainly the left tail index and the higher dimensional option-implied average correlations. Utilising a unique high frequency option dataset, the information content of these option-implied measures are examined through a series of empirical analyses, especially with applications in risk management and empirical asset pricing.

Since the breakthrough work by [Black and Scholes \[1973\]](#) and [Merton \[1973\]](#), a vast literature has been developed in option pricing. Conventionally, options are priced under risk-neutral measures (\mathbb{Q}) while underlying equities are priced under physical measures (\mathbb{P}). A long existing cottage of literature in option pricing is to investigate the relationship between equity options and underlying equity markets. For example, the dynamics of the trading interactions between stock and option markets has been largely discussed by [Anthony \[1988\]](#), [Easley et al. \[1998\]](#), and [Liu and Pan \[2003\]](#) among others. Indeed, equity and equity-based index options provide various economic benefits to spot market, though in theory under complete market, the option market should not convey any new information and the arrival of new information should be reflected simultaneously in spot and option markets. In general, the thesis builds on various strands of existing literature in option pricing and empirical asset pricing.

The first part of the thesis builds on the newly proposed Recovery Theorem (hereafter [RT](#)), a theorem proposed by [Ross \[2015\]](#) on inferring investors' risk preference and future physical probability distributions from the observed market option prices. It is well understood that option prices are forward looking and contingent on investors' belief on future returns for the underlying equities. Traditionally, the information extracted from option prices, such as the implied volatility, is well-known as an indicator of the true spot volatility under risk-neutral measure. The innovative work by [Ross](#)

[2015] challenges the conventional wisdom by proposing the RT, stating that under mild assumptions, we can recover investors' risk preference, which is the pricing kernel and the physical probability distributions for underlying equities from the risk-neutral state price extracted from observed option prices.

The path-breaking work by Arrow [1964] and Debreu [1987] introduce the *Arrow-Debreu security*, which is a contingent claim that pays \$1 if the contingent state is true or nothing vice versa and the price of the *Arrow-Debreu security* is the so-called state price. Breeden and Litzenberger [1978] show that state price can be uniquely extracted from option prices via the risk-neutral densities, which is the second-order derivatives of the option prices with respect to the strike prices. In order to convert the risk-neutral probabilities into physical rational pricing probabilities, the *Radon-Nikodym derivative* is extensively used. Specifically, the Radon-Nikodym derivative states that the physical density is a combination of the risk-neutral density and the pricing kernel, which is formed by investors' risk preference and discounting factor.

Initially, Ross [2015] derive the RT in a discrete Markov chain framework with bounded state space. The *Perron-Frobenius theorem* is applied to recover investors' risk preferences and physical probabilities of the underlying equities' future returns. A little cottage of literature has built up on generalising the RT by loosing its initial assumptions. Carr and Yu [2012] re-derive the RT in a continuous time framework using the *Regular Sturm-Liouville theorem*. Walden [2017] looses the bound restriction and derives necessary and sufficient conditions in an unbounded diffusion framework. More discussions on the theoretical settings of the RT can be found in Dubynskiy and Goldstein [2013], Liu [2014], Park [2015], Qin and Linetsky [2016], and Qin and Linetsky [2017] among others.

A large body of literature has been developed in comparing the recovered probability densities from the RT with the historical physical probability densities. Borovička et al. [2016] point out that the recovered probability distribution from RT is misspecified, as the Perron Frobenius approach employed by Ross [2015] recovers a probability measure that reflects

long-run pricing risk. Moreover, the stochastic discount factor process assumed in [Ross \[2015\]](#) implies a unity martingale transitory component. [Ngoc-Khanh and Xia \[2014\]](#) suggests that the uniqueness of the recovered pricing kernel and the corresponding physical probability transition matrix largely depends on the dimension of the states space.

A three-step procedure is suggested by [Ross \[2015\]](#) for applying the RT in practice. The first step is to obtain the risk-neutral state price matrix from the observed option prices. The path-independent risk-neutral transition matrix is then derived from the state price matrix. Finally, the pricing kernel and the physical transition density matrix are determined by employing the *Perron-Frobenius theorem*. The approach for extracting the state price matrix from observed option prices is well-understood in the literature, which can be obtained by various parametric or non-parametric methods, see for example [Aït-Sahalia and Lo \[1998\]](#), [Andersen and Wagener \[2002\]](#), [Yatchew and Härdle \[2006\]](#), [Yuan \[2009\]](#), and [Andersen et al. \[2015\]](#).

Indeed, the most challenge step in applying the RT is to determine the risk-neutral transition density from the state price matrix. [Spears \[2013\]](#) compares nine different methods for estimating the transition density matrix under various constraints. [Audrino et al. \[2014\]](#) solve the ill-posed problem in the estimation process by applying Tikhonov regularisation, see also [Backwell \[2015\]](#). Following the example given in [Ross \[2015\]](#), several empirical studies attempt to test the reliability of the recovered results. Utilising neural networks, [Audrino et al. \[2014\]](#) demonstrate a time-series analysis of the implication of the recovered probability distribution in trading strategies with S&P 500 Index option. [Schneider and Trojani \[2018\]](#) recover the time series of conditional physical moments of market index returns from a model-free projection of the pricing kernel and find that the recovered moments predict S&P 500 returns, especially for longer horizons.

In the similar spirits of my thesis, [Jensen et al. \[2018\]](#) generalise the time-homogeneous stationary model of [Ross \[2015\]](#) and show that the recovery is feasible when the number of maturities with observable option prices is higher than the number of states of the economy. A closed-form linearised solution is provided and implemented empirically to test the predictive power of the

recovered expected return. A detailed review of the literature related to the RT and the various derivations of the RT are provided in Chapter 3.

An alternative literature strand the thesis built on is the spanning role of option contracts. In a pioneering paper, Ross [1976] first demonstrates the spanning role of derivatives such that derivatives can complete the market and improve market efficiency. Following in the spirits of Ross [1976] and Brown and Ross [1991], Bakshi and Madan [2000] and Carr and Madan [2001] explicitly examine the implications of the generic spanning contracts from two different perspectives. Specifically, Bakshi and Madan [2000] show that it is possible to analytically price options on any arbitrary transformation of underlying uncertainty using the characteristic function.

Alternatively, Carr and Madan [2001] explicitly demonstrate the decomposition of an arbitrary payoff into a portfolio of risk-free assets (bonds), risky assets (stocks), and derivatives (options written on stocks) with the optimal positions taken in each of the assets. Built on the results of Bakshi and Madan [2000] and Carr and Madan [2001], Bakshi et al. [2003a] uniquely derive the non-parametric expressions for the risk-neutral variance, skewness, and kurtosis swaps. A detailed review of the generic spanning contracts and the derivations of the risk-neutral central moments are provided in Chapter 4.

Finally, the thesis also relates to the vast literature on using pricing factors extracted from option prices in explaining cross-sectional stock returns, especially the risk-neutral moments and co-moments. Many prior studies have carefully documented empirical evidence illustrating that the market volatilities, skewness, and kurtosis extracted from the individual equity options play important role in explaining and forecasting cross-sectional stock returns, see Chang et al. [2013], Conrad et al. [2013], and Bali et al. [2015] for the most recent examples.

In addition to the risk-neutral moments, the role of option-implied correlations has also been seen as important pricing factors in explaining the cross-sectional stock returns. Correlations vary through time and a growing body of research has been motivated to investigate the role of correlations based on historical information set, see for example Von Furstenberg et al.

[1989] and Longin and Solnik [1995]. Longstaff et al. [2001] and De Jong et al. [2004] provide evidence that interest rate correlations implied by cap and swaption prices differ from realised correlations.

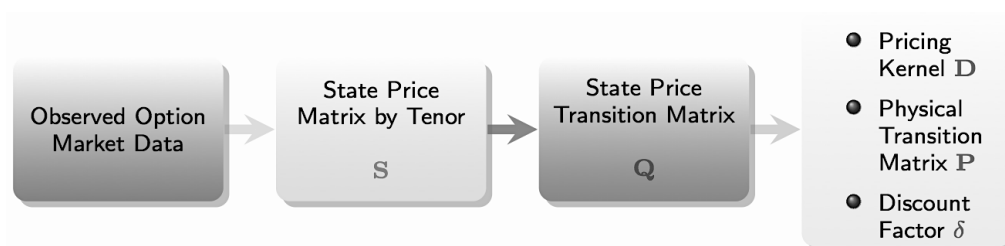
Option-implied correlations have been computed extensively in the foreign exchange markets, see for example Bodurtha and Shen [1995], Campa et al. [1998], Walter and Lopez [2000], and Mueller et al. [2016] among others. For equities, Skintzi and Refenes [2005] proposes a method to extract correlations from option prices of the individual underlying assets and the market index. Driessen et al. [2009] provide a stochastic correlation model and estimate the option-implied correlations and the correlation premium risk. Driessen et al. [2013] provided further evidence showing that the option-implied average correlations have remarkable predictive power for future stock market returns.

1.2 Findings and Contributions

1.2.1 Empirical Recovery and Risk Management

To begin with, Chapter 5 and Chapter 6 contribute to the literature on the RT by building a fully-identified non-linear algorithm for applying the RT in practice with noisy market data. The procedure for applying the RT is given in Figure 1.2, where \mathbf{S} represents the state price matrix, \mathbf{Q} is the risk-neutral state price transition matrix, δ is a scalar denoting the recovered discount factor, \mathbf{D} is a matrix with the pricing kernel sitting on the diagonal, and \mathbf{P} is the recovered physical transition matrix.

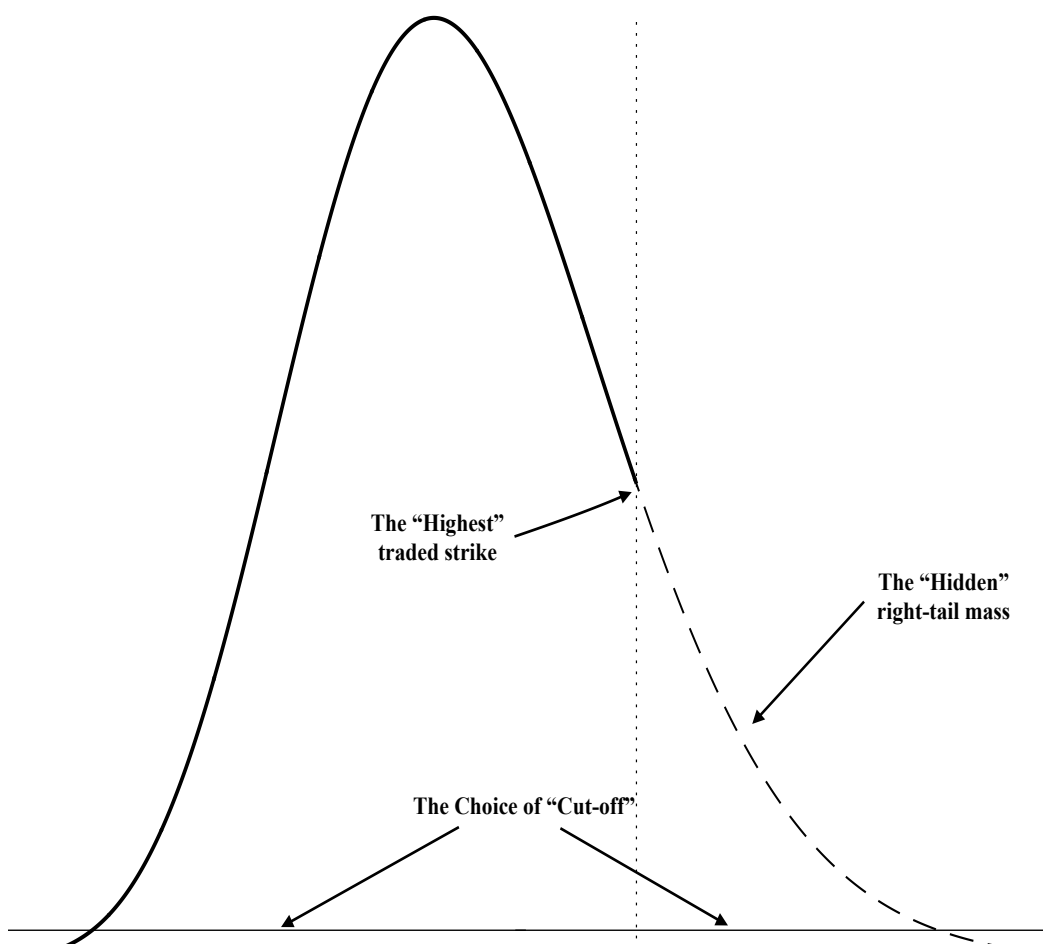
Figure 1.2: The Recovery Process



Note. Figure 1.2 gives the step-by-step procedure for applying the RT in practice. The \mathbf{S} represents the state price matrix, \mathbf{Q} is the state price transition matrix, δ is a scalar denoting the recovered discount factor, \mathbf{D} is a diagonal matrix with the pricing kernel sitting on the diagonal, and \mathbf{P} is the recovered physical transition matrix.

Theoretically, various parametric and non-parametric methods can be used to extract the state price matrix \mathbf{S} from the observed option prices. However, the noisy market data makes it difficult to recover the full distribution of the risk-neutral densities. Figure 1.3 demonstrates the (upper) tail truncation problem. Specifically, a large portion of the right-tail mass of the risk-neutral densities is hidden due to the asymmetric distribution of available strike prices for call and put options traded in the market.

Figure 1.3: The Tail Truncation Problem

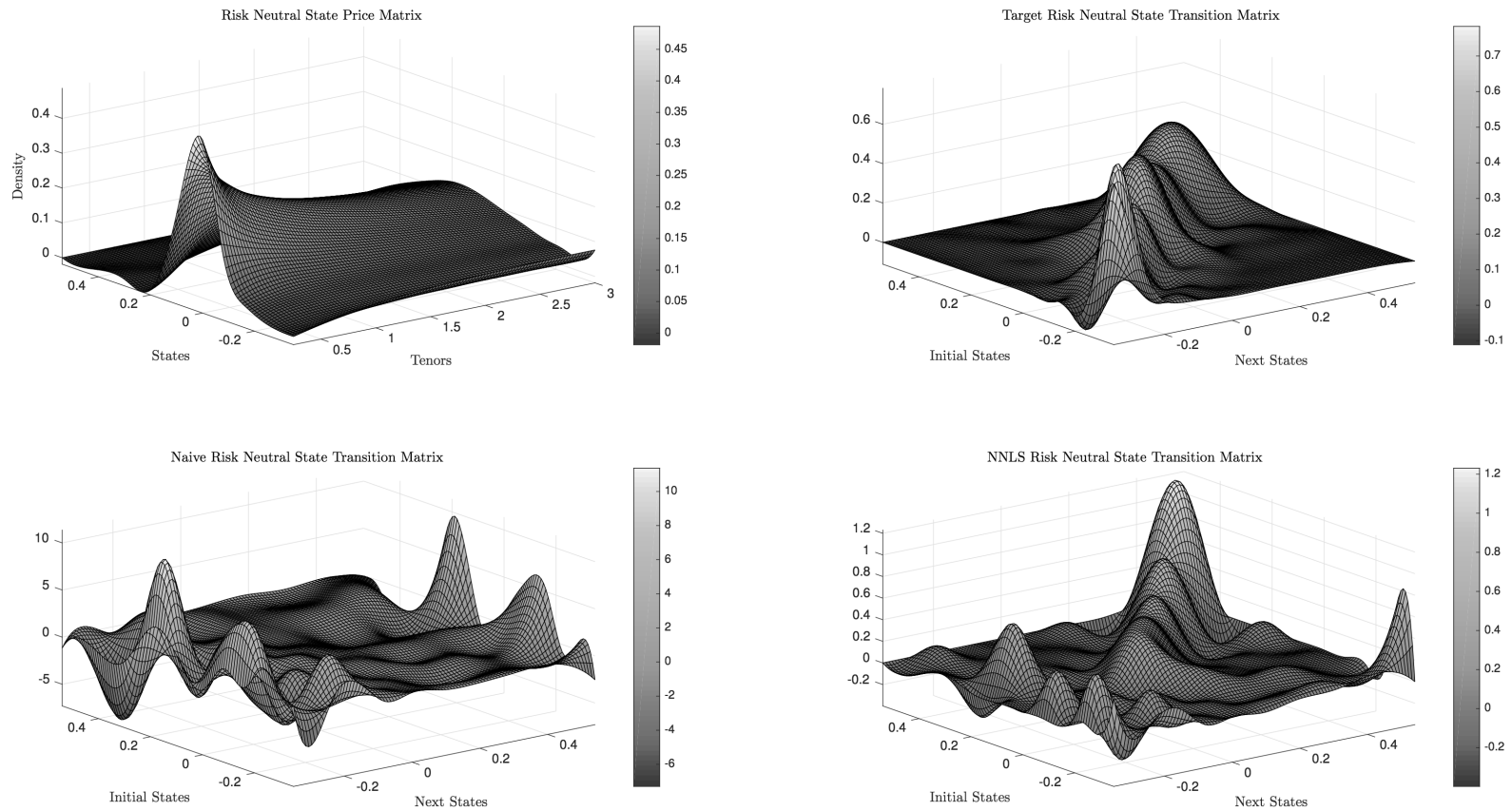


Note. Figure 1.3 demonstrates the (upper) tail truncation problem. The continuous black line represents the risk-neutral density, the vertical dotted line represents the highest traded strike price, the dash line represents the best fitting parametric curve, presumed to be a weighted mixture of up to three lognormal distributions, and the horizontal line represents the choice of cut-off level such that avoids the state price matrix numerically equal to zero.

To deal with the tail truncation issue, I employ a two-stage semi-parametric curve-fitting method to extract the full distribution of the risk-neutral densities from the noisy market data. Specifically, the market option data is smoothed by fitting the Black-Scholes implied volatility with a polynomial function over a continuous range of strike prices. I then utilise the [Breedon and Litzenberger \[1978\]](#) method to calculate the risk-neutral density curve non-parametrically. Finally, a mixture of two or three log-normals provides a fit that matches the available points in the curve and the exit trajectory of the tails from the point the coverage of the range of strikes and intraday spot prices.

The biggest challenge for applying the [RT](#) in practice is identifying the transition matrix from the state price matrix with a desired structure. In order to apply the *Perron-Frobenius theorem* to recover the discount factor and pricing kernel, the state price transition matrix needs to be unimodal with the modals sitting on the diagonal and be sub-stochastic reflecting the discounting process. As illustrated in [Figure 1.4](#), the naive un-constrained least square method yields a wild transition matrix with negative densities and a simple non-negative least square approach returns a multi-modal transition matrix violating the non-arbitrage assumption.

Figure 1.4: Challenges in Identifying the Transition Matrix



Note. Figure 1.4 illustrates the challenge in identifying the proper transition matrix from the state price matrix. The left subplot in the upper panel gives the state price matrix while the right one is the target state price transition matrix. The lower panel present two failure cases on identifying the transition matrix via un-constrained least square method (left) and non-negative least square method (right).

In Chapter 5, I uniquely derive a perturbation theory for the Perron-Frobenius eigenvalue and eigenfunction and the resulting discount factor and pricing kernel. In Chapter 6, I use this insight to develop a fast non-linear programming approach such that attained minimum formally satisfies the desired mathematical and economical constraints (e.g. the de-facto discount factor being smaller than unity and the unimodality of the transition matrix). The efficiency of the optimisation algorithm is checked through simulations with a-priori known number of states. I also examine the sensitivity of the algorithm to a-priori unknown number of states.

Besides the perturbation theory, Chapter 6 also contributes to the RT literature by providing new empirical evidence on the recovered physical densities and pricing kernels from both index options and single-name equity options. Figure 1.5 displays two examples showing the risk-neutral density versus the recovery physical density for the S&P 500 index option and options written on Apple Inc. (AAPL.O) separately. Consistent with the example in Ross [2015], the recovered physical distribution exhibits considerably thinner left tails than the nearest equivalent maturity risk-neutral distribution for both the S&P 500 index and Apple Inc.

Figure 1.6 displays the recovered pricing kernel for different number of states along with the theoretical pricing kernel with various risk aversion coefficients for the CRRA iso-elastic power utility function from the S&P 500 index options and options written on AAPL. The first obvious point to note is that for both the SPX and AAPL the shape of the kernel is (a) U-shaped (or more precisely W-shaped) and (b) asymmetric. The shape of the kernel converges as the number of states increases.

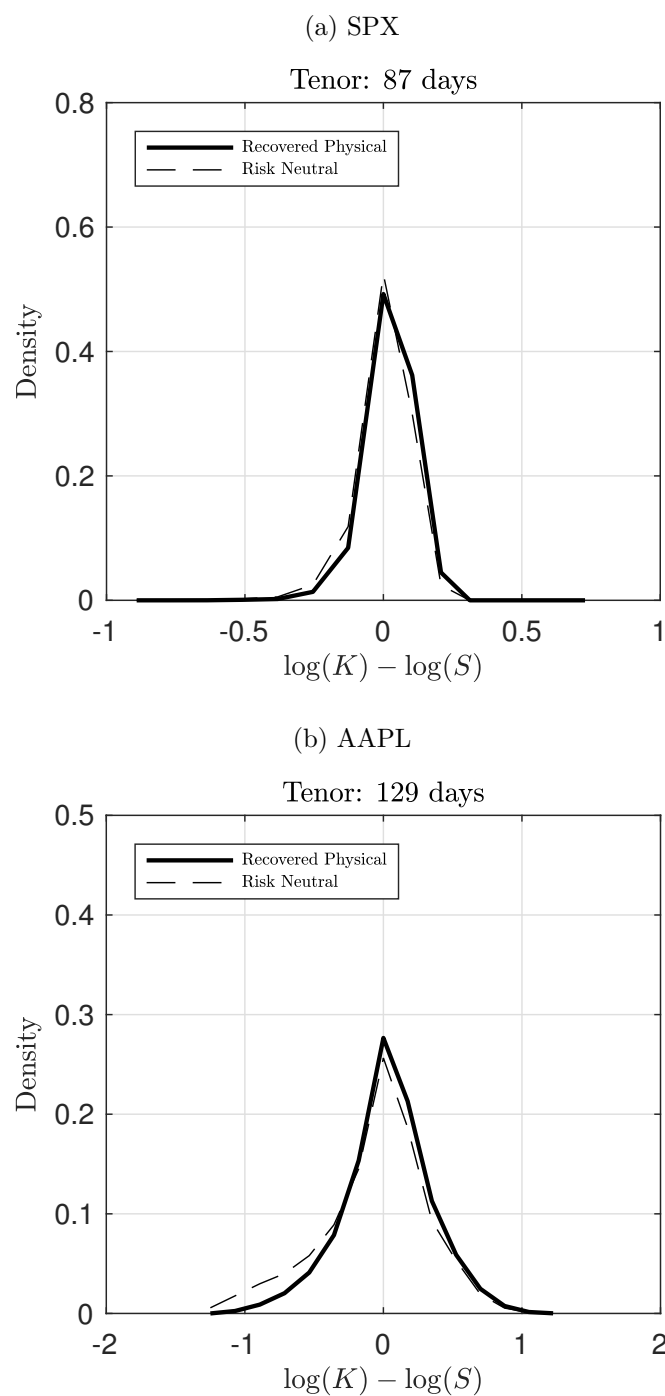
The U-shaped (or W-shaped) pricing kernels are neither inconsistent with the example in Ross [2015] nor with the theoretical pricing kernel given by the CRRA iso-elastic power utility function. Indeed, though Ross [2015] recovers a strictly decreasing pricing kernel, the U-shaped empirical pricing kernel has been widely documented as ‘pricing kernel puzzle’, see Brown and Jackwerth [2004], Hens and Reichlin [2013], and Cuesdeanu [2017] among others. In a most recent paper, Song and Xiu [2016] also find either heavily kinked or markedly U-shaped empirical pricing kernels using historical data or parallel

derivatives markets such as the VIX options.

Finally, utilising the time-series of recovered physical probability densities for options written on S&P 500 Index, I build a left tail index capturing the market downside risks. Figure 1.7 plots the left tail index from January 1, 1996 through January 31, 2015. In particular, I set the uniform state grid to be 5 states ranging from -50% to $+50\%$ (with 0% sitting in the middle) and the tenor grid to be 6 tenors ranging from 90 days to 540 days with quarterly interval. The left tail index (black hard line) is then formed by the recovered cumulative probabilities for the -50% and -25% states while the dash and dot lines are the recovered probability densities for the -50% and -25% separately. The grey areas highlight the financial crisis and economic recessions periods. It can be seen that the left tail index tracks the markets very well. The recovered probability densities provide valuable information for risk management, especially the market downside risks.

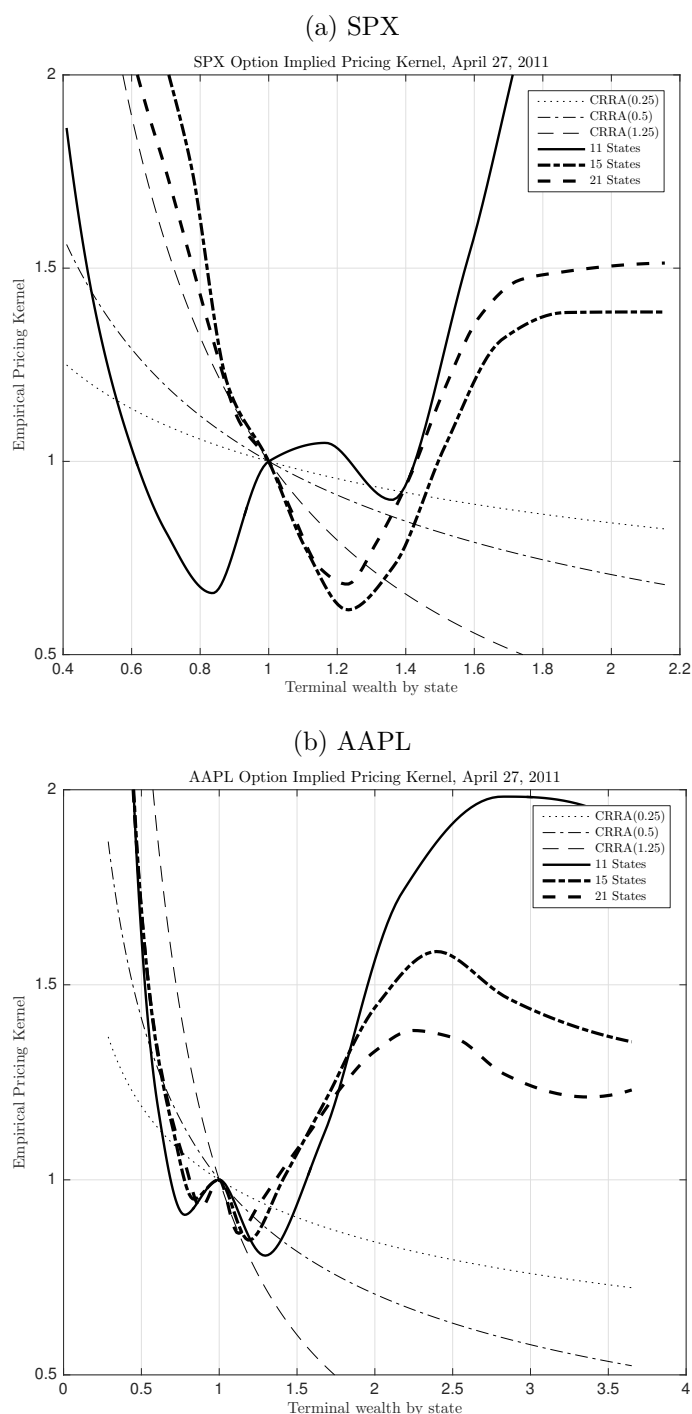
To summarise, Chapter 5 and Chapter 6 contribute to the literature on RT from three perspectives: First and foremost, I specified a perturbation theory for the discount factor and pricing kernel. A fast and fully-identified sequential quadratic programming algorithm is built to apply the RT in practice with noisy market option prices. Secondly, I provide new empirical evidence for applying the RT with single-name equity options. I find consistent evidence on the recovered probability distributions with Ross [2015]. In contrast to Ross [2015], I recover U-shaped pricing kernels, which is consistent with the ‘pricing kernel puzzle’ literature. Lastly, using the time series of the recovered probability distributions for the S&P 500 Index, I construct a left tail index, which can be used as an indicator for the long-run market downside risk.

Figure 1.5: Risk Neutral Density V.S. Recovered Physical Density



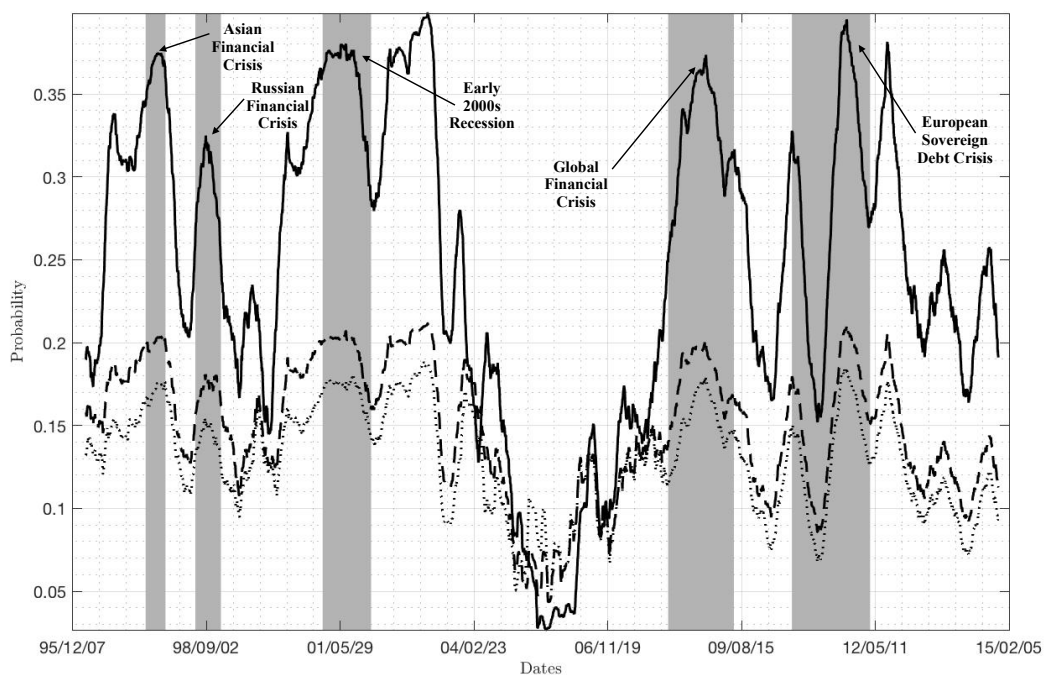
Note. Figure 1.5 plots the risk-neutral densities against the recovered physical densities using the empirical recovery algorithm given in Chapter 6. Subplot (a) is for the S&P 500 index options with 87 days to maturity while subplot (b) is for the single-name equity option written on AAPL with 129 days to maturity. In both subplots, the hard line represents the recovered physical densities while the dash line is the risk-neutral densities.

Figure 1.6: Recovered Pricing Kernel



Note. Figure 1.6 displays the recovered pricing kernel with different number of states along with the theoretical pricing kernel with various risk aversion coefficients for the CRRA iso-elastic power utility function from the S&P 500 index options and options written on AAPL stocks.

Figure 1.7: Recovered Market Left Tail Index



Note. Figure 1.7 plots the left tail index formed by the recovered physical probability distributions of S&P 500 index. The dot line represents the probability that the markets drop 50% while the dash line demonstrates the probability for market going down 25%. The hard line is the cumulative probability that the markets drop down. The grey shaded areas represent the financial crisis and economic crisis defined according to the NBER over the sample period running from January 1, 1996 through January 31, 2015.

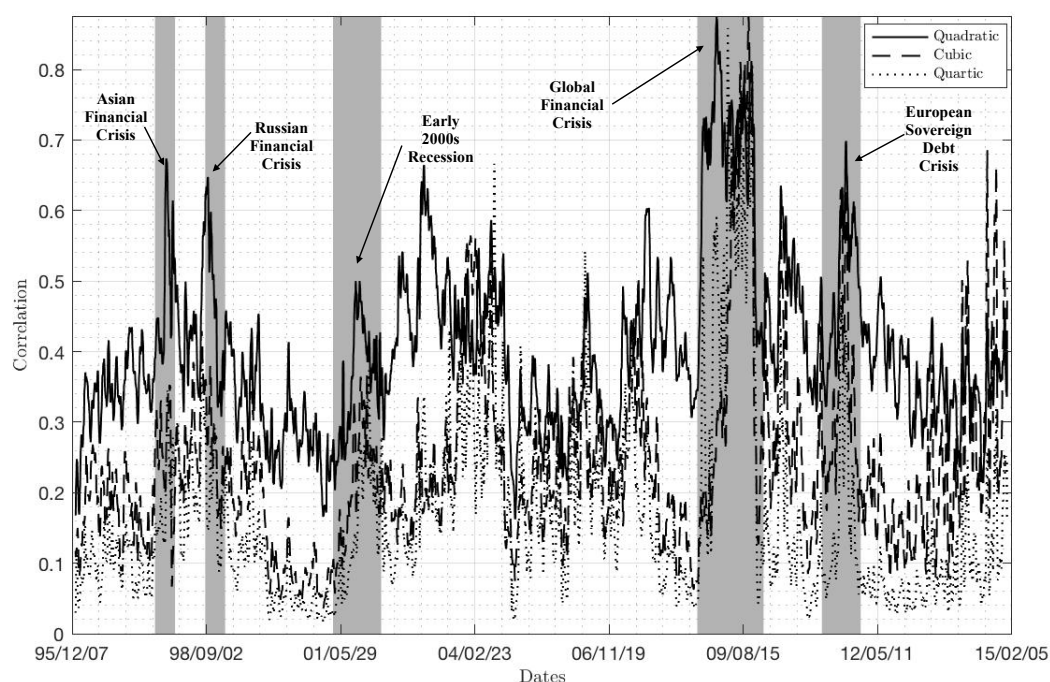
1.2.2 Option-implied Average Correlations and Empirical Asset Pricing

Motivated by the vast literature on the spanning role of derivatives, the second part of the thesis focus on investigating the information content of option-implied high moments and co-moments. Specifically, Chapter 4 contributes to the literature by uniquely deriving the explicit expressions for the risk-neutral second, third, and fourth central moments for the expected returns of underlying assets. The main contribution of the second part of the thesis sits in Chapter 7 and Chapter 8. In Chapter 7, I introduce a series of correlation analogous, namely the option-implied average quadratic, cubic, and quartic correlations, and derive the explicit formulas for extracting the higher dimensional option-implied average correlations from a high frequency option dataset.

In order to specify the calculations of the higher dimensional option-implied average correlations, I take advantage of the symmetric structure of multi-dimensional tensors, especially for the third and fourth moments. By carefully identifying the symmetric structure of the multi-dimensional tensors, I derive the explicit formulas for calculating the quadratic, cubic, and quartic option-implied average correlations in Proposition 7.1. The risk-neutral central moments for the index and all index components are estimated using the generic spanning contracts derived in Proposition 4.1. Figure 1.8 presents the one-month to maturity option-implied average correlations with the grey shaded areas representing the financial crisis and economic crisis defined according to the NBER from January 1, 1996 through January 31, 2015.

As shown in Figure 1.8, the quadratic, cubic, and quartic average correlations move closely with each other. The quadratic correlation is higher than both cubic and quartic correlations over the calm period but the higher order correlations are much higher than the quadratic correlation during the volatile periods. Together with the quadratic average correlation, the higher dimensional average correlations provide a multi-dimensional description of the correlation structure of the market portfolio, which can

Figure 1.8: Option-implied Average Correlations



Note. Figure 1.8 plots the one-month to maturity option-implied average correlations with the grey shaded areas representing the financial crisis and economic crisis defined according to the NBER over the sample period running from January 1, 1996 through January 31, 2015.

also be interpreted as a measure of the market diversification level. A higher correlation level indicates a lower diversification in the market portfolio such that individual stocks tend to move together towards the same direction, especially during the volatile periods.

In Chapter 8, I examine the role of the higher dimensional option-implied average correlations in explaining the cross-sectional stock risk premium. I employ the two-stage [Fama and MacBeth \[1973\]](#) cross-sectional regressions by regressing the excess monthly returns of S&P 500 index component stocks on the excess returns of market portfolio and the option-implied average correlations. I further consider firm characteristics and existing priced factors in the literature, such as the firm size, firm value, momentum, liquidity, idiosyncratic volatility, realised skewness, realised kurtosis, co-skewness, and co-kurtosis.

I then uniquely form a market average correlation factor as the average expected excess returns of three correlation-based portfolios. The performance of the market average correlation factor is first examined by a series of time-series regressions across 11 sector portfolios. In particular, I find the market average correlation factor largely enhances the fitting of the existing asset pricing models with higher adjusted R^2 . The relation between the risk premium of the market average correlation factor and cross section stock returns is further investigated via the [Fama and MacBeth \[1973\]](#) methodology across the whole sample. As expected, a positive significant risk premium has been detected and the significance is consistent when controlling other variables such as the firm size, firm value, momentum, liquidity, idiosyncratic volatility, realised skewness, realised kurtosis, co-skewness, and co-kurtosis.

To summarise, [Chapter 4](#), [Chapter 7](#), and [Chapter 8](#) contribute to the literature on the spanning role of derivatives in three ways: Firstly, [Proposition 4.1](#) provides explicit expressions for extracting the risk-neutral second, third, and fourth central moments from option prices. Secondly, I introduce a set of higher dimensional option-implied average correlations, namely quadratic, cubic, and quartic correlations. Lastly, the information content of the option-implied average correlations is investigated through a series of empirical analyses. I show that the correlation risk is priced in cross-sectional stock returns and form a market average correlation factor, which yields persistent positive risk premium.

1.3 Structure of the Thesis

The rest of the thesis is structured as follows. [Chapter 2](#) provides a review of the high frequency equity option dataset used through the thesis. A detailed survey of the derivations and extensions of the Recovery Theorem is given in [Chapter 3](#). In [Chapter 4](#), I first review the derivation of the generic spanning contract and then derive the formulas for extracting risk neutral central moments of expected returns from option prices. I derive a perturbation theory in [Chapter 5](#) for the recovered discount factor and

pricing kernel. Chapter 6 investigates the empirical implementations of Recovery Theorem with applications in risk management. Chapter 7 derives the estimations of the higher dimensional option-implied average correlations. Chapter 8 examines the information content of higher dimensional option-implied average correlations with applications in empirical asset pricing. Chapter 9 concludes the thesis. All chapters are self-contained and can be read independently of each other.

Chapter 2

OPRA and High Frequency Option Data Panel

2.1 Overview

The empirical analyses in this thesis are based on a high frequency equity option data panel, which sources from the Thomson Reuters Tick History (hereafter [TRTH](#)) database. In particular, I look at the *vanilla options* written on both market index and individual stocks in the United States. Specifically, we take advantage of the introduction of the Option Pricing Reporting Authority (hereafter [OPRA](#)) under the [U.S.](#) National Market System (hereafter [NMS](#)), which makes it possible to collect all of the exchange-traded equity option data from one venue rather than aggregating data from different channels. Moreover, in order to conduct the cross-sectional analyses, I uniquely construct a large scale equity option panel, including all of the S&P 500 index constituents over the sample period from January 1, 1996 through January 1, 2015.

To my knowledge, this is the most comprehensive equity option data panel within the field of this kind of research. Indeed, the data included in this thesis, whilst available publicly (for a fee) requires such high computation power to extract, I believe that this is the first usage of it outside of practitioners in high frequency option trading. Thus, I provide a

detail description of the characteristics of the high frequency equity option data panel, including the techniques used to extract and category the raw data, the various filters employed to clean the noise prices in order to construct the option data panel, and finally, I list a few data examples from the sample, showing the unique features of the high frequency option data compared to the daily data.

2.2 The OPRA Option Data System

Basket options such as the S&P 500 and the S&P 100 index options have been largely used in the studies of option pricing for many decades while single-name equity options are hardly appeared in the literature due to the limitation of the option data on individual equity option. However, with the emergence of computerised trading systems and the development of the electronic trading platform, a far more viable and liquid options trading market has been created. Both the trading volumes and number of issued underlying stocks have largely increased. In particular, options written on single-name equities have become the main players in the exchange-based option markets.

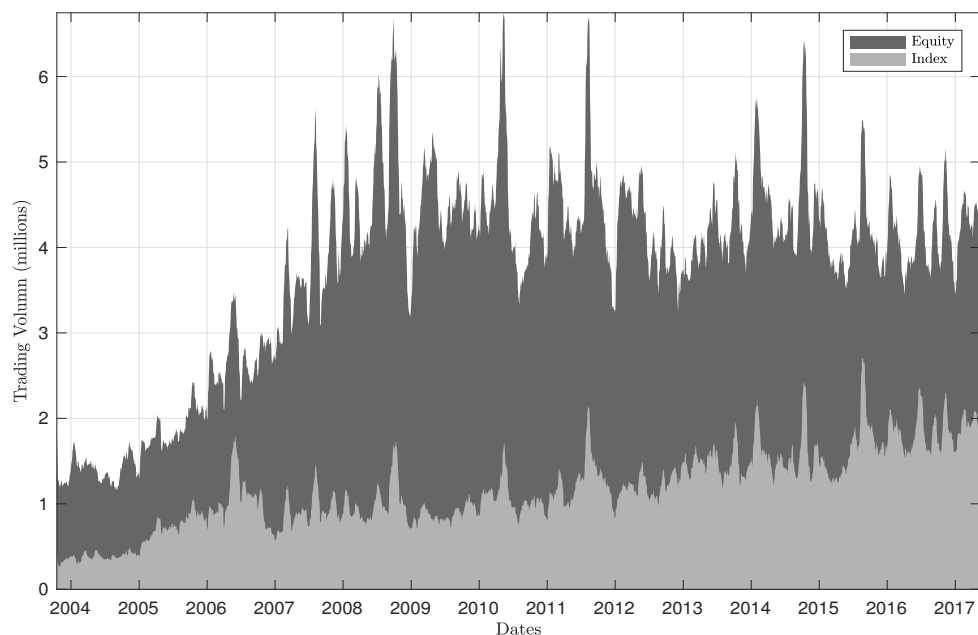
I plot the time series of trading volumes for index and single-name equity options traded on Chicago Board Options Exchange (CBOE) in Figure 2.1¹. Subplot (a) reports the daily trading volumes of index and single-name equity options on CBOE over the period October 2004 through May 2017. The trading activities of single-name equity options have increased largely since 2006 and more than half of the total trading volumes come from single-name equity options. Subplot (b) presents the daily trading volumes of single-name equity options (in million) and the number of underlying stocks issuing options on CBOE over January 1998 through May 2017. The number of underlying stocks issued equity options has climbed from less than 500 to more than 3000 over the period from 1998 to 2017.

In addition to the CBOE, a few new players have entered the

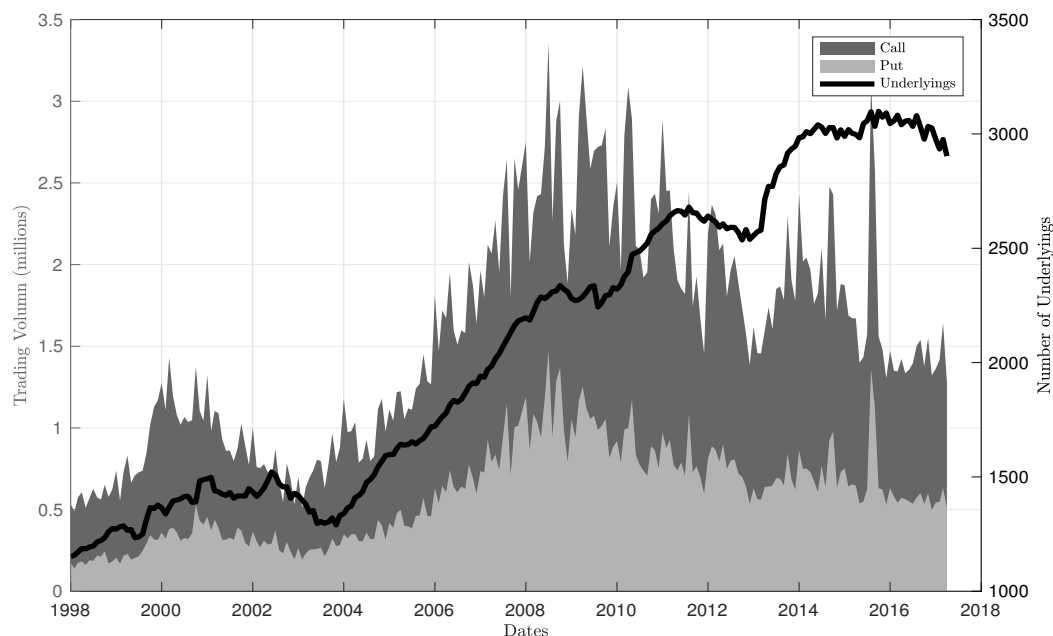
¹The trading volumes data source from the CBOE Daily Market Statistics: <http://www.cboe.com/data/current-market-statistics/cboe-daily-market-statistics>.

Figure 2.1: Option Trading Volumes on CBOE

(a) Index and Single-name Equity Option Trading Volume on CBOE



(b) Single-name Equity Option Trading Volumes on CBOE



Note. Subplot (a) reports the daily trading volumes (in million) for the index and single-name equity options traded on [CBOE](#) over the period October 2004 through May 2017. The dark grey areas stand for the daily trading volumes (in million) for single-name equity options while the light grey areas represent the daily trading volumes (in million) for index options. Subplot (b) presents the daily trading volumes of single-name equity options (in million) and the number of underlying on [CBOE](#) over January 1998 through May 2017. The dark grey and light grey areas plot the trading volume in millions of the single-name equity options marked by the left axis while the black hard line plots the number of underlying stocks issued in the option market labeled by the right axis.

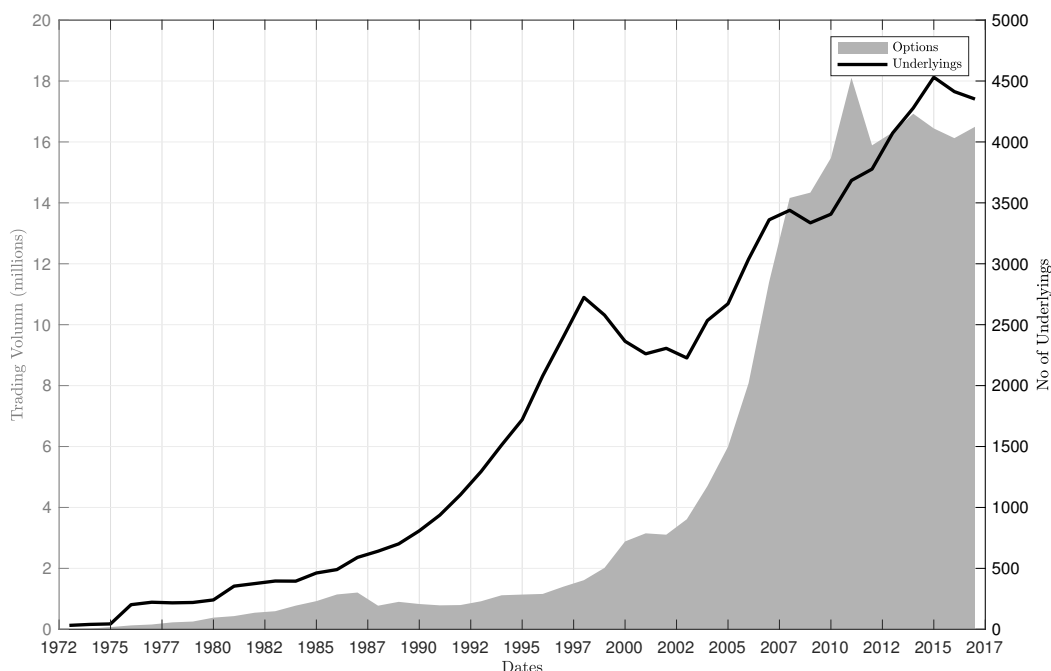
marketplace, such as the Boston Stock Exchange, International Securities Exchange, NASDAQ OMX PHLX (the former Philadelphia Stock Exchange), NASDAQ Stock Market, the NYSE Amex (the former American Stock Exchange) and NYSE Arca (the former ArcaExand). Figure 2.2 reports the total daily average trading volumes of equity options (include index and single-name equity options) traded on all of option exchanges in the U.S. since 1972.² Both the number of underlying stocks issuing equity options and the total trading volumes of equity options have soared since the early 2000s. Since 2007, more than 11 million option contracts are traded on more than 3,500 securities every day and the growth continues. Comparing Figure 2.1 and 2.2, it is easy to see that though CBOE is the largest option exchange in the U.S. it only stands for around a quarter of the U.S. equity option market.

In order to standardize the data and information system for the United States option market, the OPRA was set up in October 2009 and became effective on January 1, 2010. Under the OPRA national market system plan, the trades and quotes data of all option contracts trading on the participating exchanges is gathered and consolidated or disseminated to approved vendors. The OPRA is claimed by the compliers to be the most comprehensive exchange-based option dataset in the United States option market and more than 75% of option trading is recored with the NMS. Currently, the participating exchanges include NYSE Amex Equities (AMEX), BATS Options (BATS), Boston Stock Exchange (BSE), Chicago Board Options Exchange (CBOE), International Securities Exchange (ISE), ISE Gemini, ISE Mercury, Bats EDGX Options, Miami International Securities Exchange, NYSE Arca, Nasdaq OMX BX Options, and Philadelphia Stock Exchange (PHLX).

The introduction of the OPRA data system provides a unique venue to extract trades and quotes data for options written on single-name equities. Unlike the S&P 500 and the S&P 100 index options, which are traded on CBOE, the single-name equity options are traded on different exchanges at the

²The trading volumes data source from the OCC (Options Clearing Corporation) Daily Market Statistics: <https://www.theocc.com/webapps/historical-volume-query>.

Figure 2.2: Equity Option Trading Volumes in U.S.



Note. Figure 2.2 reports the total daily average trading volumes (in million) of equity options (include index and single-name equity options) traded on all of option exchanges in the U.S. from 1972 to 2017. The total daily average trading volumes are plot by the light grey area and labeled with the left while the number of underlying stocks issuing options is given by the hard black line with the right axis.

same time. For example, options written on Apple, Amazon, Facebook, and IBM are traded on CBOE as well as on AMEX. Without the OPRA system, trades and quotes data need to be aggregated from different exchanges while under the OPRA system all the option data are consolidated to approved vendors. Indeed, as my data sample starts from January 1, 1996, which is prior the OPRA system, I back the option data on single-name equity options by aggregating the data from all available exchanges on a weighted-average basis if needed.

2.3 The TRTH and Option Data Structure

Apart from the rich data coverage of the OPRA system, an alternative key feature of the data used in this thesis is that I uniquely construct a high

frequency option price panel, which sources from the [TRTH](#) tick-by-tick option transactions and quotations. A tick is a measure of the minimum upward or downward movement in the price of a security. A tick can also refer to the change in the price of a security from trade to trade. A tick represents the standard upon which the price of a security may fluctuate. The tick provides a specific price increment, reflected in the local currency associated with the market the security in question resides, by which the overall price of the security can change. In particular, both transactions and quotations are time-stamped to the nearest tick time and tick data are converted into one-minute series using the previous-tick method. Under the previous-tick method, the equally-spaced series of one-minute prices are generated by the observations at the end of each one-minute interval.

On the one hand, compared to the commonly used end-of-day data, the intraday dataset yields several advantages. First, I will have a range of spot prices and observations for each traded strike. Second, over a given day the range of traded strikes is likely to be more heavily populated than skimming the trades and quotes at the end of day. Third, I use the mid-price of the best bid and ask quotes and again this will likely yield a far greater variation in the quoted prices, see for example [Andersen et al. \[2003\]](#). On the other hand, the high frequency data is much noisier than the end-of-day data, such as the widely known market microstructure issue, thus a more careful cleaning procedure is essential. Specifically, I describe the high frequency data filters I applied in [Section 2.4.3](#).

The trading related data is normally stored in an irregular pattern with columns representing the day, time stamp, bid price, ask price, bid and ask volumes and some other measures of activity, such as number of traders. The remaining information for the option contracts, such as the strike price, the maturity date, the type of the contract (either a call or a put), are coded in a unique Reuters Instrument Codes (hereafter RICs). Under the [TRTH](#), the RICs are the unique identifiers to parse the contract information efficiently across different trading vendors. Indeed, the structure of the RICs varies for different trading products. The RICs for the [OPRA](#) option data has the

following structure:

$$[\text{Ticker}][\text{Month}][\text{Day}][\text{Year}][\text{Strike}].[\text{ExchangeID}]$$

such that:

- Ticker: the underlying stock ticker from the exchanges;
- Month: a letter that identifies both the expiration month and the type of the option. Specifically, for call options the expired month from January to December is labeled by the letter from 'A' to 'I' while for put options the expiration month is named with letter from 'M' to 'Y'. The [Month] also provides the decimal base for the strike prices. If [Month] is capitalized then the strike price is taken to two decimal place and if month is lower case, then the strike is taken to one decimal place;
- Day: two digits integer for the expiration day;
- Year: two digits integer for the expiration year;
- Strike: five digits adjusted by the base determined in the [Month];
- ExchangeID: a capitalized letter identify the trading exchange.

For example,

$$\text{AAPLE051709000.U}$$

represents a CALL option contract written on the underlying stock AAPL that expires on 2017-May-05 and the strike price is \$90. Finally, U represents the exchange identifier for the [OPRA](#) system.

For RICs based codes, working from right to left works best as the underlying ticker can be of variable length. Hence, for each option I parse its ticker and extract the strike price and maturity date following the rules discussed above. The Matlab codes for extracting the option data from the [TRTH](#) are available in [Appendix A.3](#).

2.4 The High Frequency Option Data Panel

The empirical analyses in this thesis are conducted based on the high frequency option panel that features by a large cross-sectional equity spot and option data over a long historical period. In this section, I present the lists of the individual companies included in the data panel and the procedure for constructing the intraday one-minute option data panel over a daily grid.

2.4.1 The S&P 500 Index Constituents Sample

Utilizing the rich option data coverage of the [OPRA](#) option system, I uniquely construct a high frequency option data panel, which includes the option prices for both the S&P 500 index and all of the index constituents over the period from January 1, 1996 through January 1, 2015. The S&P 500 index is a value-weighted index with frequency rebalancing on an as-needed basis. The list of the constituents of the S&P 500 index is obtained from the COMPUSTAT data set of Standard and Poor's. There are 973 firms in the S&P 500 index over January 1, 1996 through January 1, 2015. Unlike the actively trading for options written on the S&P 500 index, trading for some single-name equity options may be quite illiquid. In fact, as documented on the [TRTH](#), the trading for single-name equity options prior 2005 is very thin and not all of the index components equities have options traded on the exchange. Thus, I limit my attention to a subset of stocks which are known to be highly traded and liquid. I have no intention to be fully comprehensive in the sample and am inclined to drop stocks for which option trading is too thin rather than including them in the analyses.

Options on the S&P 500 index are European style and expire on the third Friday of the contract month while options on individual equities are American style and usually expire on the Saturday following the third Friday of the contract month. After excluding the index components that are either illiquid traded nor have no options written on, my sample ends up with 588 constituents. The list of the companies in the sample and the

statistics of the total number of trading days, total number of price observations, and the average number of price observations per day are reported in Table A. 1 in Appendix A.1.

2.4.2 The Selected Sector Index Sample

In addition to the high frequency option panels with S&P 500 Index and its constituent companies, I uniquely construct a sub dataset with Selected Sector Index. The Standard & Poor's Depository Receipts (SPDR) funds are a family of exchange-traded funds (ETFs) traded in the United States. The Selected Sector SPDR ETFs are the unique Exchange Traded Funds (ETFs) that divide the S&P 500 into ten index funds, namely the Energy (XLE), Materials (XLB), Industrials (XLI), Consumer Discretionary (XLY), Consumer Staples (XLP), Health Care (XLV), Financial (XLF), Information Technology (XLK), Utilities (XLU), and Real Estate (XLRE). Each Selected Sector Index is calculated using a modified 'market capitalisation' methodology, which ensures that each of the component stocks within a Selected Sector Index is represented in a proportion consistent with its percentage of the total market cap of that particular index.

Each Selected Sector SPDR is designed to, before expenses, closely track the price performance and dividend yield of a particular Select Sector Index. Each Fund's portfolio is comprised principally of shares of constituent companies included in the S&P 500. Each stock in the S&P 500 is allocated to only one Selected Sector Index. The combined companies of the ten Selected Sector Index represent all of the companies in the S&P 500. The SPDR ETFs sector index are traded as stocks and can be short-sell and optioned.³

Specifically, the options written on the Selected Sector Index are American style and usually expire on the third Friday of the contract month. The options written on the Selected Sector Index are introduced separately and the options written on specific sector index are also established at different time. In order to keep the consistent of data across all sector index, I construct

³Sources: <http://www.sectorspdr.com/sectorspdr/features/about>.

a sub dataset from my high frequency option panels consisting of nine Selected Sector Index over the sample period from November 30, 2009 to January 1, 2015.⁴ The list of the companies in each sector index and the holding and weights are reported in Table A. 2 in the Appendix A.2.

2.4.3 Construct the Option Data Panel

The spot prices for both the S&P 500 index and the index components are also obtained from the TRTH at a one-minute intraday frequency. The spot price for the S&P 500 index is backed by the E-mini S&P 500 index futures traded on Chicago Mercantile Exchange (CME). Following Bollerslev et al. [2018], I roll the future contracts in every expiration months (March, June, September, December) using the most actively traded front future contracts by counting the number of valid trades (i.e. trades with a non-zero trading volume) over a day. The proxy for the risk-free rate is collected from the exchange-traded USD deposit rate from the TRTH at a one-minute intraday basis for the sample period. I use the exchange-traded deposit rate as it gives the most comprehensive information of the up-to-date risk-free rate proxy. In the literature, the yields on the US Treasury coupon bills are generally accepted as the risk-free rate of return, which are only available on specific maturities and up to 52 weeks (1 year) time to maturity. The exchange-traded USD deposit rates are available in 19 maturities and updates hourly, ranging from the over-night instant rate up to 5-year long-term rate, which makes an ideal sample for the high frequency risk-free rates.

The high frequency option data panel is constructed by matching up the option data, spot data, and risk free rate date together with the nearest tick time stamp for each observation. I then undertake the following steps to generate the representative daily panels:

1. Following Andersen et al. [2003] and Andersen et al. [2015], I first apply the following high frequency data filters:

⁴The Real Estate Index (XLRE) began trading on Oct 8th, 2015, which is out of my sample period.

- Drop any options that do not have both a bid and an ask price or have zero bid and ask size;
 - Sort the data into buckets by time to maturity and strike price; For every time stamp and for each maturity date delete options with prices that exhibit the following:
 - Have a negative bid-ask spread;
 - Have a decreasing price with moneyness;
 - Have a price less than 90% of the intrinsic value;
2. Compute the natural logarithm of the strike to current spot price ratio (the ‘log-strike’);
 3. For a given time to maturity and strike bucket if there are both puts and calls traded then sort into pairs by nearest time stamp;
 4. For this step only, discard all un-paired options (i.e. puts without calls or vice versa), then use each paired options to compute the intraday one-minute implied dividend for the stock or index using the standard put-call parity condition. Compute the median dividend for the asset for the day;
 5. Compute the Black-Scholes implied volatility for every option applying the median dividend to every traded option. For individual stocks an American option implied volatility can also be used if the put early exercise premium is deemed to potentially be sufficiently large to bias the implied volatility calculation;
 6. For each unique time to maturity and for the put and call options collect the implied volatilities and the ‘log strikes’ into two vectors;
 7. Choose a parametric or non-parametric curve fitting model and regress the implied volatilities onto the ‘log strikes’, to compute a model of the smile surface;

8. Check that the put options have a wider range of strikes than the calls options. A second alternative is to take a weighted average of the two smiles (one for the put and one for the call);
9. Choose a regular ‘log strikes’ grid that will be consistent across all days in the sample and then apply an interpolation technique to generate a set of implied volatilities for each point on this strike grid from the irregular grid computed in the previous step;
10. Using the end-of-day spot price generate a set of strike prices from the log-strike grid and combine these with the end of day deposit or swap rate (depending on maturity) and the median implied dividend yield to generate the requisite put and call prices.

For each day this yields a correctly matched pair of matrices of put and call prices versus a regular grid of strikes. In order to generate consistent time to maturity grid (as each maturity is a fixed time stamp), a second regular time to maturity grid can be constructed and a two dimensional interpolation applied. I recommend always using linear interpolation for the time to maturity and ensure that the grid from Step 9 is sufficiently fine grained to prevent bumps that may affect the index calculation.

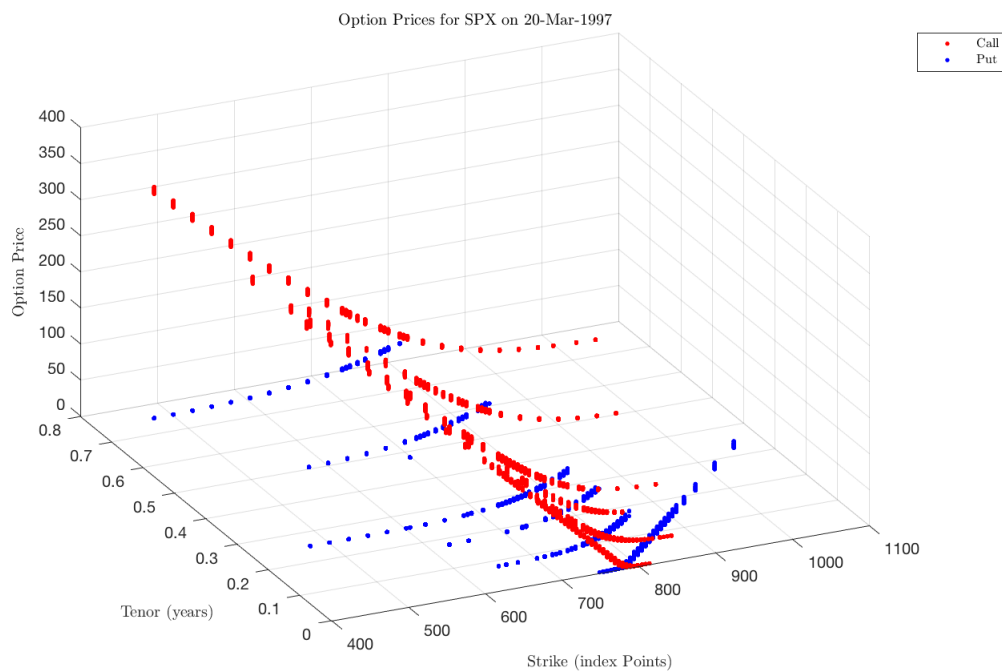
2.5 Features of the High Frequency Option Data Panel

Figures 2.3 to 2.5 provide some snapshots of my high frequency option data panel. Each of the sub plots in Figures 2.3 to 2.5 display the intraday bid-ask prices (z-axis) for option contracts traded at various strikes (x-axis) and time to maturities (y-axis) for the S&P 500 index and some selected individual companies, namely Apple Inc. (AAPL), International Business Machines Corporation (IBM), and Boeing Company (BA). The red points represents the call prices while the blue points give the put prices. The plots show that my unique high frequency option data panels provide complete

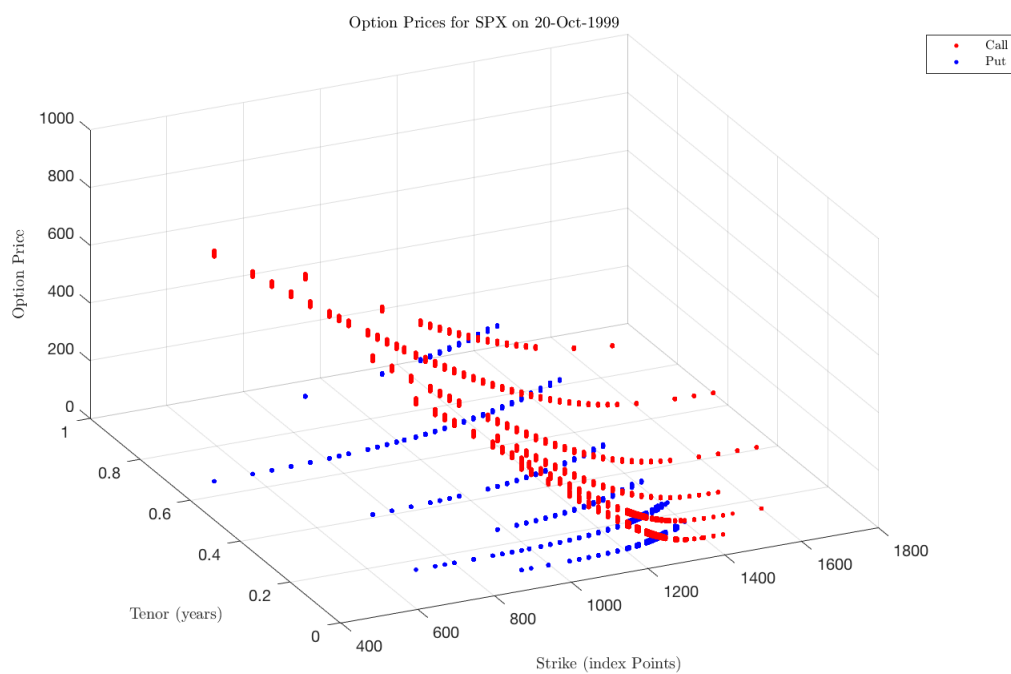
and sufficient coverage of the option prices that can be utilised to extract the various information.

It can be observed that the option trading is very thin in the early years even for the S&P 500 Index. Though the transaction activities for option written on individual equities are not as rich as those on the index, we can still observe a relative efficient coverage of price over various strikes and time to maturities that can be easily interpolated later to get the whole surface. Noted that the call and put prices are the raw market prices without applying any interpolation techniques as described in the process 8 to 11.

Figure 2.3: High Frequency Option Data Sample

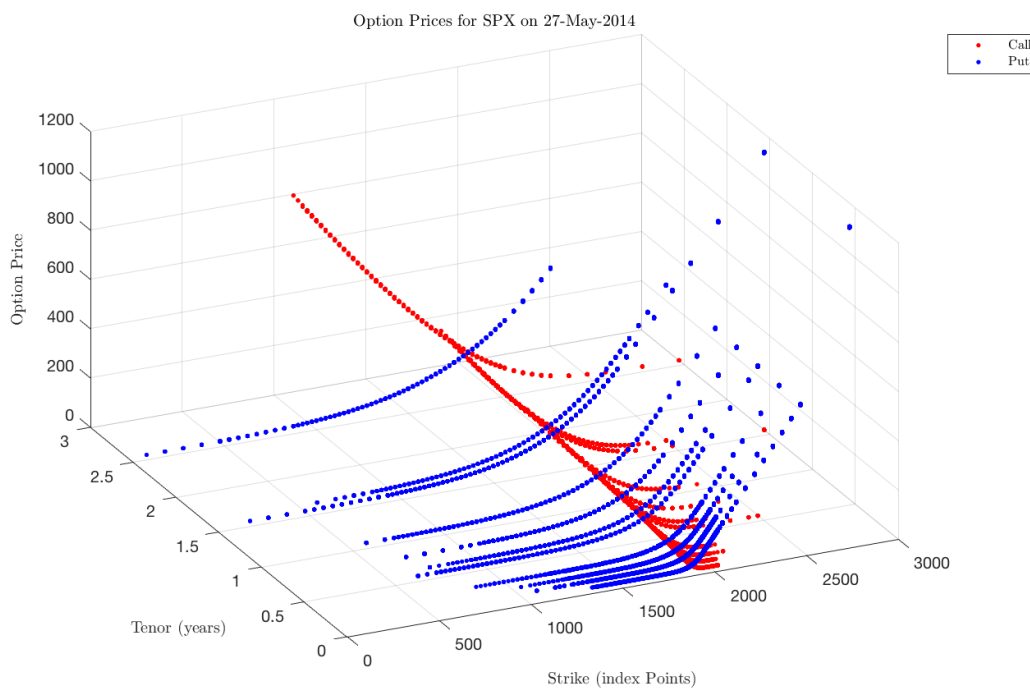


(a) SPX on 20-Mar-1997

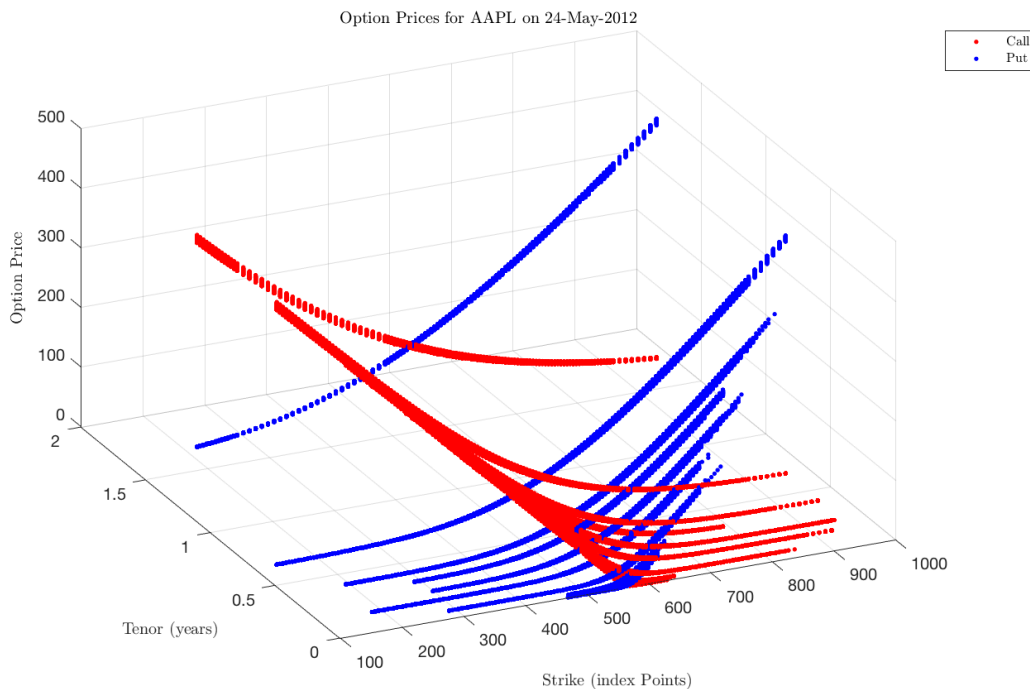


(b) SPX on 20-Oct-1999

Figure 2.4: High Frequency Option Data Sample

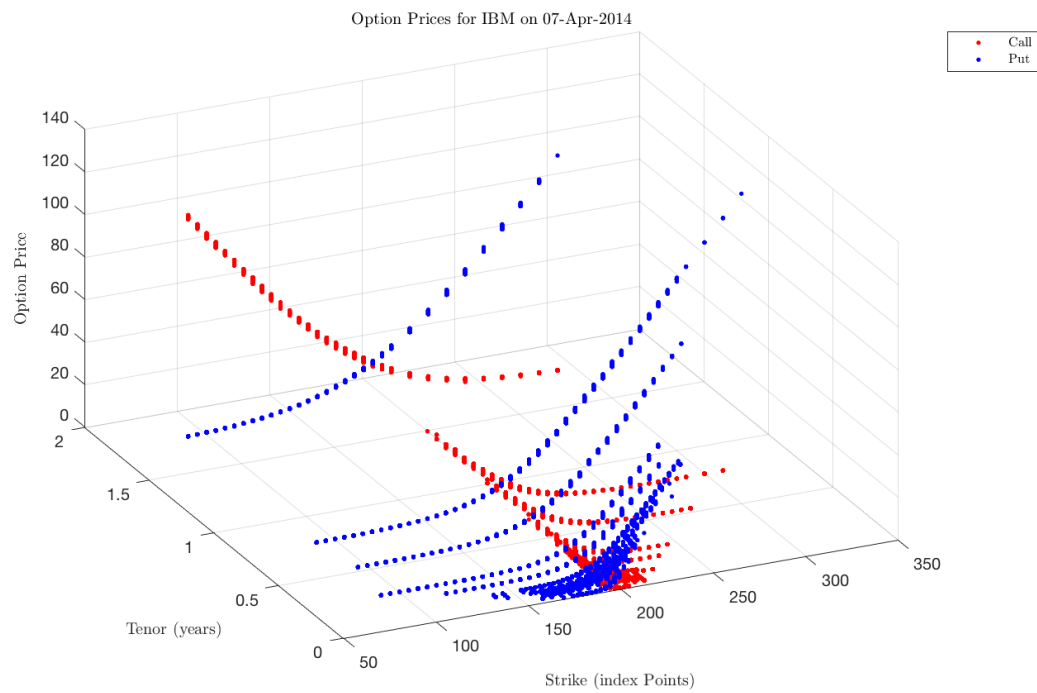


(a) SPX on 27-May-2014

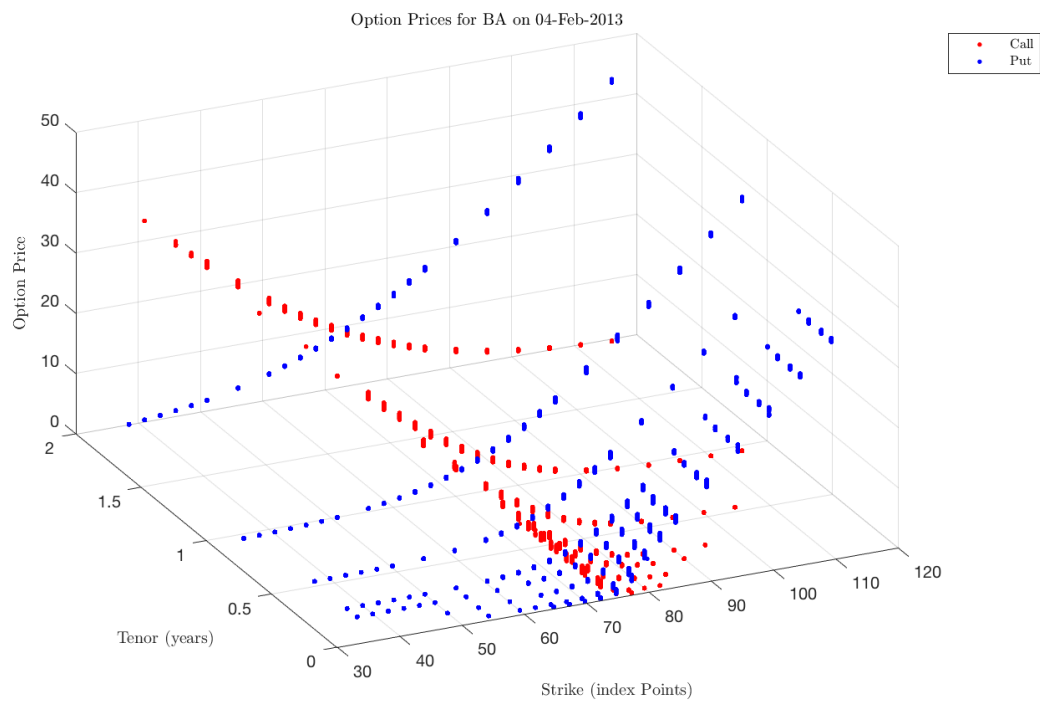


(b) AAPL on 24-May-2012

Figure 2.5: High Frequency Option Data Sample



(a) IBM on 07-Apr-2014



(b) BA on 04-Feb-2013

2.6 Summary and Remarks

The empirical analyses in this thesis are conducted based on a unique high frequency option panel, which includes the spot and option data on S&P 500 index and all of the index constituents over the sample period from January 1, 1996 through January 1, 2015. The intraday one-minute high frequency option data sources from the [TRTH](#) tick-by-tick feeds and standardized into one-minute frequency under the previous tick method. The list of the index constituents is obtained from COMPUSTAT dataset of Standard and Poor's. After applying necessary screenings, my sample ends up with 588 individual companies with options actively traded over the sample period. Another feature of my high frequency option panel is that from November 30, 2009, the [TRTH](#) option market set up the [OPRA](#) system, which records the option trading information from all of the option trading exchanges in the [U.S.](#) market. The introduction of the [OPRA](#) data system provides a unique venue to extract the option data for single-name equities options.

Chapter 3

Review of Recovery Theorem

3.1 Overview

The Recovery Theorem (hereafter [RT](#)) is about inferring market beliefs for the real-world probability distribution describing the future financial returns of the underlying asset from option price. The [RT](#) answers the question: Can we recover the physical probability density and the pricing kernel separately from the observed derivative prices. Though it is well understood that the option prices are forward looking and encode information about investors' belief of future returns of the underlings, inferring the physical probability distributions from the risk neutral densities is always questioned as options and underlying assets are priced under two different measures, namely the risk neutral measure and physical measure. The [RT](#) states that given certainty assumptions, we can go from risk neutral measure to physical measure and the derivative prices convey sufficient information on the future returns of the underlying assets as well as the time and risk preference of investors.

The path-breaking work by [Arrow \[1964\]](#) and [Debreu \[1987\]](#) introduces the *Arrow Debreu security*, which states that the asset price is a combination of investor risk aversion and probabilities used to assess risk. The Arrow-Debreu security price is so-called state price or risk-neutral density. Typically, the Arrow-Debreu security is not traded in the real-world market and hence [Breedon and Litzenberger \[1978\]](#) indicate that the risk-neutral densities can

be extracted from the observed market option prices. Various methods have been suggested to extract the risk-neutral density from the option prices, for example [Aït-Sahalia and Lo \[1998\]](#), [Yatchew and Härdle \[2006\]](#), and [Yuan \[2009\]](#) among others.

Traditionally, the information extracted from option prices, such as the implied volatility, is well-known as an indicator of the market risk level. For example, the VIX (the implied volatility of S&P 500 index options) is often referred to as the market ‘fear index’, which gauges the market’s expectation of stock market volatility over the next 30-day period. However, the information extracted from option prices turns to be silent when it comes to predict the future return of the underlying assets. The innovational work by [Ross \[2015\]](#) challenges the conventional wisdom by proposing the RT, suggesting that under mild assumptions, the pricing kernel and the real-world probability can be recovered uniquely from the observed option price.

Initially, [Ross \[2015\]](#) derive the RT in a discrete Markov chain framework with bounded state-space. The market is assumed to be complete and non-arbitrage. Two key assumptions have been imposed to derive the recovery: (a) There exists a representative agent with risk averse preference and (b) The pricing kernel is transition independent, which requires a state transition matrix that is presumed to be path independent. Armed with these assumptions, [Ross \[2015\]](#) utilizes the *Perron-Frobenius theorem* to recover the preferences of the representative agent and the real world probabilities of the underlying assets’ future returns from the observed option prices.

Several very recent papers attempt to generalize the theoretical framework of the RT by loosing its initial assumptions. [Carr and Yu \[2012\]](#) derive the unique recovery of pricing kernel and natural probability distribution in a continuous time framework with the state prices of the underlying assets following bounded stochastic process. [Carr and Yu \[2012\]](#) map the state price dynamics using the numéraire portfolio and employ the *Sturm-Liouville theorem* to determine the unique unambiguous recovery. [Walden \[2017\]](#) looses the bound restriction and derives necessary and sufficient conditions in an unbounded diffusion-type states. More discussions

on the theoretical settings of the RT can be found in [Dubynskiy and Goldstein \[2013\]](#), [Liu \[2014\]](#), [Qin and Linetsky \[2014\]](#), [Park \[2015\]](#), [Qin and Linetsky \[2016\]](#), and [Qin and Linetsky \[2017\]](#) among others.

There is no surprise that a large body of literature has developed to examine the reliability of the recovered results from both theoretical and empirical aspects. [Martin and Ross \[2013\]](#) demonstrate that the stochastic discount factor can be identified with the unconditional expected log returns on long-maturity bonds. [Borovička et al. \[2016\]](#) point out that the recovered probability distribution is misspecified, as the Perron Frobenius approach employed by [Ross \[2015\]](#) recovers a probability measure that reflects long-term pricing factor. Moreover, the stochastic discount factor process used by [Ross \[2015\]](#) implies a unity martingale transitory component. [Bakshi et al. \[2017\]](#) further test the restrictions on the recovery theorem empirically use the data on 30-year Treasury bond and options written on the 30-year Treasury bond. They show that the implicit assumption of the recovery theorem that the martingale component of the stochastic discount factor is identical to unity is rejected.

[Ngoc-Khanh and Xia \[2014\]](#) suggests that the uniqueness of the recovered pricing kernel and the corresponding physical probability transition matrix largely depends on the dimension of the states. In other words, under unique respective set of market data, the recovered beliefs, time and risk preference may be very sensitive to with the states dimensions. In a most recent study, [Jensen et al. \[2018\]](#) generalise the time-homogeneous stationary model in [Ross \[2015\]](#) and suggest that the recovery is feasible when the number of maturities with observable prices is higher than the number of states of the economy. A closed-form linearized solution has been provided and implemented empirically, testing the predictive power of the recovered expected return and other recovered statistics.

As [Ross \[2015\]](#) also provides an empirical example in the paper, there are also several empirical studies attempting to test the RT. In general, there are three steps to employ the RT. The first step is to obtain the state price matrix from the observed derivative prices, however the state price matrix is assumed to be known a-prior in Ross setting. The following step is to derive the

state price transition matrix from the state price matrix. Finally, the pricing kernel and the physical transition density matrix are determined by solving an eigenvalue and eigenvector problem employing the Perron Frobenius Theorem.

The approach of extracting the state price matrix from observed option prices is well-understood in the literature, which can be obtained by various parametric or non-parametric methods. The most challenge stage in applying the RT is to determine the transition density function from the state price matrix. [Spears \[2013\]](#) compares nine different methods for estimating the transition density matrix under various constraints and points out that the instructive method of [Ross \[2015\]](#) is inaccurate. [Audrino et al. \[2014\]](#) solve the ill-posed problem in the estimation process by applying Tikhonov method, a standard regularisation method for ill-posed problems, see also [Backwell \[2015\]](#).

The final step is simply a direct implication of the Perron Frobenius Theorem. Most of the empirical work follows [Ross \[2015\]](#), only providing a snapshot of one day date to test the RT with the market data. Within a neural network system, [Audrino et al. \[2014\]](#) demonstrate a time-series analysis of the implication of the recovered probability distribution in trading strategies with S&P 500 Index option. [Schneider and Trojani \[2018\]](#) also recover the time series of conditional physical moments of market index returns from a model-free projection of the pricing kernel and find that the recovered moments predict S&P 500 returns, especially for longer horizons. [Jensen et al. \[2018\]](#) also provide empirical evidence on testing the predictive power of the recovered expected returns and other recovered statistics.

This chapter aims to provide a theoretical review for the innovational RT. I illustrate the basic properties of the RT under two current standard treatment, first the classic derivation in discrete time by [Ross \[2015\]](#), utilizing the assumptions of a representative agents asset holdings and second, the more general framework in continuous time by [Carr and Yu \[2012\]](#), taking advantage of the results of [Long \[1990\]](#). This is then followed by a recent critical interpretation by [Borovička et al. \[2016\]](#), suggesting the recovered physical probability distributions are misspecified in the long term by a positive martingale process. I conclude this chapter with a brief

summary and remarks on the [RT](#).

3.2 The [Ross \[2015\]](#) Derivation

The objective of [RT](#) is to determine the unique real world transition probability matrix and the pricing kernel from the state price matrix separately. Given the physical transition matrix, the physical probability distribution can then be determined. The state price matrix is extracted from the observed market price of derivatives (options in most cases) written on the underlying assets. To solve for the real-world transition probability matrix, the *Perron Frobenius Theorem* is applied. [Ross \[2015\]](#) directly appeals to the standard *Arrow-Debreu* framework to map the risk neutral contingent claim and hence determine the risk neutral state transition matrix. By further imposing the representative agent assumption on the pricing kernel, [Ross \[2015\]](#) imposes enough identifying restrictions to recover the discount factor, the pricing kernel and the real world physical density matrix.

Let the evolution of the spot price of an Arrow-Debreu asset be driven by a bounded Markov chain with an $M \times N$ state price by tenor matrix \mathbf{S} with columns \mathbf{s}_n denoted by:

$$\mathbf{S} = \begin{pmatrix} s_{1,1} & s_{1,2} & \cdots & s_{1,n} \\ s_{2,1} & s_{2,2} & \cdots & s_{2,n} \\ \vdots & \vdots & \ddots & \vdots \\ s_{m,1} & s_{m,2} & \cdots & s_{m,n} \end{pmatrix} \quad (3.1)$$

where the state is indexed by M and tenor is indexed by N respectively. There is presumed to exist a state independent state price transition matrix, \mathbf{Q} , such that the state price in the next state satisfies $\mathbf{s}_{n+1} = \mathbf{Q}\mathbf{s}_n$, where \mathbf{Q}

is a $M \times M$ transition matrix such that:

$$\mathbf{Q} = \begin{pmatrix} q_{1,1} & q_{1,2} & \cdots & q_{1,m} \\ q_{2,1} & q_{2,2} & \cdots & q_{2,m} \\ \vdots & \vdots & \ddots & \vdots \\ q_{m,1} & q_{m,2} & \cdots & q_{m,m} \end{pmatrix} \quad (3.2)$$

Note, that if we know \mathbf{S} with precision then the risk neutral state price transition matrix \mathbf{Q} is uniquely determined from the given state price matrix \mathbf{S} , when $N = M + 1$. Any further columns of \mathbf{S} offer redundant information. Another point to note is that \mathbf{Q} for a positive discount rate, \mathbf{Q} is *sub-stochastic*. The relationship between \mathbf{Q} and the physical transition matrix \mathbf{P} , is the object of interest. Let

$$\mathbf{P} = \begin{pmatrix} p_{1,1} & p_{1,2} & \cdots & p_{1,m} \\ p_{2,1} & p_{2,2} & \cdots & p_{2,m} \\ \vdots & \vdots & \ddots & \vdots \\ p_{m,1} & p_{m,2} & \cdots & p_{m,m} \end{pmatrix} \quad (3.3)$$

give the physical transition probabilities. Under the non-arbitrage assumption, the risk neutral state price transition matrix $\mathbf{Q}^{\mathbb{Q}}$ and the physical transition matrix $\mathbf{P}^{\mathbb{P}}$ are related by $\phi_{ij} = q_{ij}/p_{ij}$, where ϕ_{ij} is the transition kernel.¹ The corresponding transition kernel matrix is:

$$\mathbf{\Phi} = \begin{pmatrix} \varphi_{1,1} & \varphi_{1,2} & \cdots & \varphi_{1,m} \\ \varphi_{2,1} & \varphi_{2,2} & \cdots & \varphi_{2,m} \\ \vdots & \vdots & \ddots & \vdots \\ \varphi_{m,1} & \varphi_{m,2} & \cdots & \varphi_{m,m} \end{pmatrix} \quad (3.4)$$

¹This is in fact the discrete expression of the Radon-Nikodym derivative and the existence of a positive kernel is equivalent to the non-arbitrage condition stated earlier. We drop the blackboard font superscript markers to avoid notational cluttering.

Furthermore, ϕ_{ij} is assumed to be transition independent such that

$$\phi_{ij} = \delta \frac{h(i)}{h(j)},$$

where δ and h are a positive discount factor and a positive function of the state price respectively based on a representative agent assumption. If define the diagonal matrix

$$\mathbf{D} = \begin{pmatrix} h(1) & 0 & \cdots & 0 \\ 0 & h(2) & \cdots & 0 \\ \vdots & \vdots & \ddots & \vdots \\ 0 & 0 & \cdots & h(M) \end{pmatrix}$$

the transition kernel can then be written as

$$\Phi = \delta \mathbf{D}^{-1} \mathbf{D}.$$

Simple re-arrangement yields the important result that

$$\mathbf{Q} = \mathbf{P}\Phi = \delta \mathbf{D}^{-1} \mathbf{P}\mathbf{D}. \quad (3.5)$$

Solving for the physical transition matrix:

$$\mathbf{P} = \delta^{-1} \mathbf{D}\mathbf{Q}\mathbf{D}^{-1}, \quad (3.6)$$

and hence by construction \mathbf{P} is right stochastic, as such $\mathbf{P}\mathbf{1}_{M \times 1} = \mathbf{1}_{M \times 1}$, where $\mathbf{1}_{M \times 1} = (1, 1, \dots, 1)'$. Hence,

$$\mathbf{P}\mathbf{1}_{M \times 1} = (1/\delta) \mathbf{D}\mathbf{Q}\mathbf{D}^{-1}\mathbf{1}_{M \times 1} = \mathbf{1}_{M \times 1},$$

Rearranging yields

$$\mathbf{Q}\mathbf{D}^{-1}\mathbf{1}_{M \times 1} = \delta \mathbf{D}^{-1}\mathbf{1}_{M \times 1}.$$

Set $\mathbf{v} = \mathbf{D}^{-1}\mathbf{1}_{M \times 1}$, then:

$$\mathbf{Q}\mathbf{v} = \delta \mathbf{v}. \quad (3.7)$$

Ross [2015] demonstrates that according to the *Perron-Frobenius theorem*, given an irreducible and non-negative \mathbf{Q} , δ and \mathbf{v} can be uniquely determined by the largest Perron root and the corresponding eigenvector. Thus, the discount factor δ and the pricing kernel \mathbf{D} can be uniquely recovered from the risk neutral state price transition matrix and hence the physical transition matrix \mathbf{P} .

3.3 The Carr and Yu [2012] Derivation

In contrast to the assumption on the existence of the risk-aversion representative agent, Carr and Yu [2012] generalize the RT by taking advantage of the diffusion properties of the *numéraire portfolio* introduced by Long [1990].

Consider an economy continuous at time and state space and the uncertainty is modelled by the probability space $\{\Omega, \mathcal{F}, \mathbb{P}\}$, where \mathbb{P} is the unknown physical probability measure needs to be uniquely determined and the corresponding risk neutral probability measure is denoted by \mathbb{Q} . There exist a risk-free asset such that

$$dS_t^0 = r_t S_t^0 dt,$$

with the initial condition that $S_0^0 = 1$ and stochastic growth rate r_t at time t . There also exists n risky assets, whose spot prices S_t^i are semi-martingales over a finite time interval $[0, T]$. Assume that no arbitrage opportunities exist between the risk-free asset and the n risky assets.

To map the risk neutral dynamics, Carr and Yu [2012] utilize the *numéraire portfolio*, which is a strictly positive self-financing portfolio introduced by Long [1990]. Formally, let L be the numéraire portfolio such that: $L_t = S_t^0/M_t$, where $M_t = S_t^i/L_t$ is a local martingale under \mathbb{P} measure. The dynamics of the numéraire portfolio L under \mathbb{P} measure can be derived by Itô's lemma:

$$\frac{dL_t}{L_t} = (r_t + \sigma_t^2)dt + \sigma_t dB_t^{\mathbb{P}} \quad (3.8)$$

where r_t is the stochastic interest rate. σ_t denotes the lognormal volatility of L and B is a standard Brownian motion. Long [1990] suggests that the risk-premium of the numéraire portfolio is equal to its instantaneous variance, which means if we can determine the volatility process of the numéraire portfolio then the \mathbb{P} dynamics of any contingent claim can be determined.

Let X be the solely driver of the uncertainty of the n risky assets and be a univariate time-homogeneous diffusion process such that:

$$dX_t = \beta(X_t)dt + \alpha(X_t)dW_t^{\mathbb{Q}}, \quad (3.9)$$

where $\beta(x)$ and $\alpha^2(x)$ are the known drift function and variance rate function respectively and W is a standard Brownian motion. Accordingly, the price of the risk-free asset can be written as $S_t^0 = S_0(X_t, t)$ and the stochastic interest rate as $r_t = r_t(X_t, t)$ in terms of X .

In fact, the numéraire portfolio L plays the same role as the Arrow-Debreu asset in Ross [2015]. Carr and Yu [2012] assume that the price of the numéraire portfolio L_t depends only on the current value of the driver X and both the interest rate process r_t and the volatility process σ_t are time-homogeneous, such that:

$$L_t \equiv L(X_t, t), \quad r(x, t) \equiv r(x), \quad \sigma(x, t) \equiv \sigma(x), \quad (3.10)$$

the corresponding dynamics of L under risk neutral measure \mathbb{Q} is:

$$\frac{dL_t}{L_t} = r(X_t)dt + \sigma(X_t)dW_t^{\mathbb{Q}}, \quad (3.11)$$

which suggests that L_t is a time-homogeneous process under \mathbb{Q} . Given the assumptions in Equation (3.10), the dynamics of X and L under the \mathbb{P} measure can be expressed as:

$$\begin{aligned} dX_t &= (\beta(X_t) + \sigma(X_t)\alpha(X_t))dt + \alpha(X_t)dB_t^{\mathbb{P}}, \\ \frac{dL_t}{L_t} &= (r(X_t) + \sigma^2(X_t)dt) + \sigma(X_t)dB_t^{\mathbb{P}}. \end{aligned} \quad (3.12)$$

Applying Itô's lemma to $L_t \equiv L(X_t, t)$ returns $\sigma(x) = \alpha(x)\partial/\partial x \ln L(x, t)$. Integrating over x and rearranging yields $\ln L(x, t) = \int^x \sigma(y)/\alpha(y)dy + C(t)$, where $C(t)$ is the integration constant. Define $\rho(x) = e^{\int^x \sigma(y)/\alpha(y)dy}$ and $\gamma(t) = e^{C(t)}$, then the value of the numéraire portfolio L can be expressed by two separated terms such as:

$$L(x, t) = \rho(x)\gamma(t).$$

Substituting this into the extended generator function and rearranging yields:

$$\frac{\alpha^2(x)}{2}\rho''(x) + \beta(x)\rho'(x) - r(x)\rho(x) = -\frac{\gamma'(t)}{\gamma(t)}\rho(x), \quad (3.13)$$

which is an eigenvalue and eigenfunction problem in the form stated by the *Regular Sturm-Liouville theorem*. Let $\mathcal{G}[\cdot]$ be the infinitesimal generator operator such that:

$$\mathcal{G}_x \equiv \frac{\partial}{\partial t} + \frac{\alpha^2(x)}{2} \frac{\partial^2}{\partial x^2} + \beta(x) \frac{\partial}{\partial x}.$$

The valuation function for the i risky asset solves the linear parabolic partial differential equation (PDE):

$$\mathcal{G}_x^{\mathbb{Q}}[S^i(x_t, t)] = r(x, t)S^i(x, t),$$

where the extended generator \mathcal{G}_x^E has the form

$$\mathcal{G}_x^E = \frac{\partial}{\partial t} + \frac{\alpha^2(x)}{2} \frac{\partial^2}{\partial x^2} + \beta(x) \frac{\partial}{\partial x} - r(x, t).$$

In fact, Carr and Yu [2012] show that the solutions are the first eigenvalue and corresponding eigenfunction of the system, denoted by $(\delta, \Theta(x))$. The real world transition density of the model driver X can be uniquely determined from the change of the numéraire portfolio L :

$$d\mathbb{P} = \frac{\Theta(X_T)}{\Theta(X_0)} e^{\tilde{\delta}T} e^{-\int_0^T r(X_t)dt} d\mathbb{Q}. \quad (3.14)$$

where $\tilde{\delta}$ is the discount rate.

Hence, Carr and Yu [2012] demonstrates that the real world transition density and the pricing kernel can be separately uniquely determined from the numéraire portfolio in a bounded continuous economy. The primary assumption of this version of the RT is the existence of a strictly positive numéraire portfolio as opposed to having a fully representative agents holdings.

3.4 The Borovička, Hansen, and Scheinkman [2016] Interpretation

Whilst Ross [2015] derives the RT in a finite-state Markov environment and Carr and Yu [2012] demonstrates similar separability and recoverability in a bounded continuous time setting, Borovička et al. [2016] utilizing results from Hansen and Scheinkman [2009], argue that the recovered probability density from applying the *Perron-Frobenius theory* is in fact reflecting the long-term implications for risk pricing.

Borovička et al. [2016] demonstrate that the full identification result found in Ross [2015] requires certain restrictive assumptions. Specifically, in the presence of a stochastic discount factor with a martingale component the long horizon forecasts of the density function will be miss-specified. However, both Hansen and Scheinkman [2009] Borovička et al. [2016] stress the usefulness of the eigensystem as a mechanism for refining our understanding of the price formation mechanism in financial markets.

Let $\mathbf{S} := \{s_{mn} : 1 \leq m \leq M, 1 \leq n \leq N\}$ the state price by tenor matrix, such that a column \mathbf{s}_n is the vector of risk neutral state prices for a particular tenor, with element being the risk neutral price of an asset paying a single unit in that state for that tenor only. The finite state markov chain that determines the transition from time index n to $n + 1$ is characterized by the risk neutral state price transition matrix $\mathbf{Q} := \{q_{ij} : 1 \leq i \leq M, 1 \leq j \leq M\}$, whereby $\mathbf{s}_{n+1} = \mathbf{Q}\mathbf{s}_n$. When $\mathbf{S} := \{s_{mn} : 1 \leq m \leq M, 1 \leq n \leq N\}$ is known with precision, the minimum number of tenors needed for identification of \mathbf{Q} is $N = M + 1$.

A risk free instrument pays off in every state and has current period value of $\sum_{m=1}^M s_{mn} = \exp(r_n)$, where r_n is the continuously discounted risk free return for the tenor indexed by n . When $\exp(r_{n+1}) > \exp(r_n)$ for all $n \in \{1, \dots, N\}$ the Markov process described by the risk neutral transition matrix \mathbf{Q} is sub-stochastic, hence $\lim_{\kappa \rightarrow \infty} \mathbf{Q}^\kappa = \mathbf{0}_{M \times M}$. The risk neutral measure is an artificially constructed measure that is not the observed real world or physical measure. Let $\mathbf{P} := \{p_{ij} : 1 \leq i \leq M, 1 \leq j \leq M\}$ be the physical transition matrix of the Markov chain driving observed asset prices. Setting $\delta = \exp(r)$ to be the discount factor and approximating $r_n = nr$ the standard neoclassical asset pricing framework posits the following ratio:

$$\Psi = [\psi_{ij}], \quad \text{where} \quad \psi_{ij} = \frac{q_{ij}}{p_{ij}}, \quad (3.15)$$

where $[\psi_{ij}]$ is the stochastic discount factor, as such $q_{ij} = \psi_{ij}p_{ij}$. However, from forward looking derivatives prices we only observe q_{ij} and, as such, we do not have sufficient information to fully recover ψ_{ij} and p_{ij} .

The identification challenge is simply illustrated by considering the dimensions of \mathbf{P} , \mathbf{Q} and Ψ . \mathbf{Q} has $M \times M$ entries and so does the stochastic discount factor matrix Ψ , while the physical transition matrix \mathbf{P} only have $M \times (M - 1)$ free entrances as \mathbf{P} is, by definition, right stochastic and with rows summing to unity. As such, instead of having the observed physical transition probabilities $\mathbf{P} = [p_{ij}]$, we could have an alternative such that

$$\tilde{\mathbf{P}} = [\tilde{p}_{ij}], \quad \text{such that} \quad \tilde{p}_{ij} = h_{ij}p_{ij}, \quad (3.16)$$

where h_{ij} are elements of the positive matrix $\mathbf{H} = [h_{ij}]$ such that $h_{ij} > 0$ and $\sum_{j=1}^M h_{ij}p_{ij} = 1$. As h_{ij} is obtained as a ratio of probabilities, the process H is a positive martingale under P . For each choice of the restricted matrix \mathbf{H} , the state-dependent discount factors can be formed such as $\tilde{\psi}_{ij} = \psi_{ij}/h_{ij}$, which gives the corresponding risk neutral transition probabilities such as:

$$q_{ij} = \psi_{ij}p_{ij} = \tilde{\psi}_{ij}\tilde{p}_{ij} \quad (3.17)$$

Therefore, given the flexibility in constructing the always positive martingale

process H , the physical probabilities can be recovered from the risk neutral state prices in a variety ways.

In order to recover the physical transition probabilities \mathbf{P} from the risk neutral transition probabilities \mathbf{Q} uniquely, [Borovička et al. \[2016\]](#) demonstrate that additional restrictions on the stochastic discount factor need to be imposed. Specifically, [Borovička et al. \[2016\]](#) derive the recovery under the long-term pricing restriction using Perron-Frobenius theory, which is an eigenfunction approach. Following the Perron-Frobenius theory, when all of the entries of the risk neutral transition matrix \mathbf{Q} are positive, the largest eigenvalue of \mathbf{Q} is positive and unique, which can be written as $\delta = \exp(r)$. The associated right eigenvector $\tilde{\mathbf{v}}$ also has strictly positive entries denoting the i entry of the eigenvector as \tilde{v}_i . By construction we can recover a probability matrix $\tilde{\mathbf{P}}$ with the entries such that:

$$\tilde{p}_{ij} := \delta^{-1} q_{ij} \frac{\tilde{v}_i}{\tilde{v}_j}. \quad (3.18)$$

Since $\mathbf{Q}\tilde{\mathbf{v}} = \delta\tilde{\mathbf{v}}$, thus $\sum_{j=1}^n \tilde{p}_{ij} = 1/\delta(\tilde{v}_i)^{-1} \sum_{j=1}^n q_{ij}\tilde{v}_j = 1$, hence $\tilde{\mathbf{P}}$ is a valid transition matrix. Thus the risk neutral transition probabilities can be written as

$$q_{ij} = \delta \frac{\tilde{v}_i}{\tilde{v}_j} \tilde{p}_{ij} = \tilde{\psi}_{ij} \tilde{p}_{ij} \quad (3.19)$$

Both [Ross \[2015\]](#) and [Borovička et al. \[2016\]](#) use the eigenfunction approach stated in Equation 5.5 to construct the recovered probability distribution. [Borovička et al. \[2016\]](#) show that combining Equation 5.4 together with Equation 5.5 gives the following decomposition:

$$q_{ij} = \delta \frac{\tilde{v}_i}{\tilde{v}_j} \frac{\tilde{p}_{ij}}{p_{ij}}, \quad p_{ij} = \delta \frac{\tilde{v}_i}{\tilde{v}_j} \tilde{\psi}_{ij} p_{ij} \quad (3.20)$$

hence the stochastic discount factor can be derived as

$$\tilde{\psi}_{ij} = \delta \frac{\tilde{v}_i}{\tilde{v}_j} h_{ij}, \quad \text{where} \quad h_{ij} = \frac{\tilde{p}_{ij}}{p_{ij}} \quad (3.21)$$

[Hansen and Scheinkman \[2009\]](#) show that the stochastic discount factor

derived in Equation 5.7 can be used as to study long-term valuation and h_{ij} is termed as long-term risk-neutral probability.

Borovička et al. [2016] further show that the derivation of the discount factor in Ross [2015] is a special case of their more general derivation. Ross [2015] assumes that the stochastic discount factor is state-independent and can be written as

$$\psi_{ij} = \delta \frac{\tilde{v}_i}{\tilde{v}_j} \quad (3.22)$$

and the physical transition probabilities are recovered by $\tilde{\mathbf{P}} = [\tilde{p}_{ij}]$. It is easy to see that Ross [2015]'s derivation Equation 3.22 is in fact a special case of Equation 5.7 with the condition such that:

$$\psi_{ij} = \delta \frac{\tilde{v}_i}{\tilde{v}_j} \quad \text{for some vector } \tilde{\mathbf{v}} \iff h_{ij} \equiv 1 \quad (3.23)$$

which also means the recovered physical transition probabilities are in fact $\tilde{\mathbf{P}} = \mathbf{H} \circ \mathbf{P} \equiv [h_{ij}p_{ij}]$, where \circ is the element by element product of identical dimension matrices. Hence, Ross [2015] is a special case where $h_{ij} = 1$ and hence there is no martingale component in the discount factor. In this special case $\tilde{\mathbf{P}} = \mathbf{P}$ and hence the eigenfunction recovers the physical probability. In this specific case, the risk preferences, \tilde{v}_i/\tilde{v}_j , are separate from the from the time preferences, δ , and $\tilde{v}_i/\tilde{v}_j = U'(c_i)/U'(c_{(M+1)/2})$ is the pricing kernel of the representative investor. Where $U(\cdot)$ is the at least once differentiable utility function of the representative investor and C_i is the consumable wealth in i state.

3.5 Summary and Remarks

The objective of the RT is to separately recover the discount factor, pricing kernel and the real world probabilities of the future returns of the underlying assets from the traded option prices. The original derivation by Ross [2015] depends largely on the assumption that the existence of a representative agent with risk averse preference, which restricts the empirical application of the RT to index options that can proxy for an aggregated risky asset driving the

volatility of consumption in the representative agent. However, subsequent work by Carr and Yu [2012] has illustrated the generalization of the RT to a broader domain of assets. Within a continuous time setting, the RT is derived under the less restrictive assumptions on the diffusion dynamics of a numéraire portfolio. The further interpretation of the recovered discount factor by Borovička et al. [2016] indicate that the recovered physical transition matrix depends on the presumed structure of the true Markov chain that drives the asset prices.

Ross [2015] provides an example for applying the RT in practice with a snapshot data, however, a standard algorithm for recovering is strongly called in the empirical studies. A significant gap in the contemporary RT is the absence of a fully-identified RT framework that provides both a solid theoretical interpretation of the recovered results and a practical algorithm that is easy to apply but robust to the noisy market data. Chapter 5 and Chapter 6 address these problems by firstly introducing a full perturbation theory for the RT and subsequently an efficient and robust non-linear programming algorithm to permit recovery and identify the constraints needed for full identification. In addition to the theoretical derivation, I also demonstrate detailed empirical implications of the RT algorithm from intraday option prices for both index options and single-name equity options.

Chapter 4

Extract the Risk Neutral Central Moments from Option Prices

4.1 Overview

The pioneering idea that introducing options on existing assets in an uncertain economy opens new spanning opportunities is first established by [Ross \[1976\]](#). Specifically, [Ross \[1976\]](#) shows that any complex contracts can be spanned by a portfolio of simple option contracts and without loss of efficiency, all options can be written on a single portfolio assets. In a later work, [Brown and Ross \[1991\]](#) derive the characterization of the generic spanning contracts based on a Riesz space valued Riemann-Stieltjes integral and show that the [Breedon and Litzenberger \[1978\]](#) pricing formula is a direct implication of the integral representation theorem.

Following the spirits of [Ross \[1976\]](#) and [Brown and Ross \[1991\]](#), [Bakshi and Madan \[2000\]](#) and [Carr and Madan \[2001\]](#) explicitly examine the implications of the generic spanning contracts from two different perspectives. In particular, [Bakshi and Madan \[2000\]](#) show that it is possible to analytically price options on any arbitrary transformation of underlying uncertainty using the characteristic function. Moreover, [Bakshi and Madan](#)

[2000] demonstrate the implication of the characteristic function based spanning contract valuation for pricing average-interest options, correlation options, and discretely monitored knock-out options.

Alternatively, Carr and Madan [2001] treat the valuation of the spanning contract from the perspective of portfolio management. Specifically, for the first time, Carr and Madan [2001] explicitly exhibit the decomposition of an arbitrary payoff into a portfolio of risk-free assets (bonds), risky assets (stocks), and derivatives (options written on stocks) with the optimal positions taken in each of the assets. Built on the results of Bakshi and Madan [2000] and Carr and Madan [2001], Bakshi et al. [2003a] uniquely derive the non-parametric expressions for the risk neutral variance, skewness, and kurtosis swaps by defining the volatility, cubic, and quartic contracts.

In this chapter, I first illustrate the detailed derivation of the decomposition of the generic spanning contracts based on the work by Carr and Madan [2001]. Following the spirits of Bakshi et al. [2003a], I then uniquely derive the explicit formulas for extracting the risk neutral central moments for expected returns from option prices, which are intensively used in the formation of the option-implied average correlations in the next chapter. I conclude this chapter with a brief summary and remarks on the implications of generic spanning contracts.

4.2 Derive the Generic Spanning Contracts

The derivation of the valuation of the generic spanning contracts is based on the decomposition of an arbitrary payoff into a portfolio of bonds, stock, and options as given in Carr and Madan [2001]. Let $(\Omega, \mathcal{F}, \mathcal{F}_t, \mathbb{P})$ be a filtered probability space satisfying usual conditions (e.g., Protter [2013]), where Ω is a nonempty set, $\mathcal{F}_t(t \geq 0)$ is a σ -algebra of subsets of Ω , and \mathbb{P} denotes the objective or physical probability measure. Given no-arbitrage assumption in the market, there exists an equivalent risk-neutral probability measure denoting by \mathbb{Q} . \mathbb{E} is the expectation operator and $\mathbb{E}^{\mathbb{Q}}$ is the corresponding risk neutral expectation operator.

Let S denote the price for the individual stock or the market portfolio. The uncertainty for the individual asset and hence the market portfolio is driven by the probability density, which is denoted by $p(S)$ for the physical density and $q(S)$ for the equivalent risk neutral density. The risk-neutral expectation at time t for any integrable claim payoff $L(S)$ can be expressed by:

$$\mathbb{E}_t^{\mathbb{Q}}[L(S)] = \int_0^{\infty} L(S)q(S)dS \quad (4.1)$$

where $\mathbb{E}_t^{\mathbb{Q}}$ is the risk neutral expectation operator. Thus, the prices of the European call and put options on S can be expressed as:

$$\begin{aligned} C(\tau, K) &= \int_0^{\infty} e^{-r_f\tau}(S - K)^+q(S)dS, \\ P(\tau, K) &= \int_0^{\infty} e^{-r_f\tau}(K - S)^+q(S)dS. \end{aligned} \quad (4.2)$$

where K is the strike price, r_f is the risk-free rate, and τ is the time to maturity. The maximise operator $^+$ defines the functions such that $(S - K)^+ \equiv \max(0, S - K)$ and $(K - S)^+ \equiv \max(0, K - S)$.

As shown in Carr and Madan [2001], the claim payoff $L(S)$ can be spanned by a continuum of out-of-the-money European call and put options, with optimal positioning in risk-free assets (bonds) and risky underlying assets (stocks). Specifically, for any twice-continuously differentiable claim payoff function $L(S)$ we have,

$$\begin{aligned} L(S) &= L(S_t) + (S - S_t)L'(S_t) \\ &\quad + \int_0^{S_t} L''(K)(K - S)^+dK + \int_{S_t}^{\infty} L''(K)(S - K)^+dK \end{aligned} \quad (4.3)$$

Applying the risk-neutral expectation operator on the present value of the claim payoff, $e^{-r_f\tau}L(S)$, the arbitrage-free price of the claim payoff is simply:

$$\begin{aligned} \mathbb{E}_t^{\mathbb{Q}}[e^{-r_f\tau}L(S)] &= e^{-r_f\tau}(L(S_t) - S_tL'(S_t)) + L'(S_t)S_t \\ &\quad + \int_{S_t}^{\infty} L''(K)C(\tau, K)dK + \int_0^{S_t} L''(K)P(\tau, K)dK \end{aligned} \quad (4.4)$$

which suggests that the risk-neutral expectation of the claim payoff $L(S)$ at time t can be spanned by holding $(L(S_t) - S_t L'(S_t))$ units bonds with risk-free rate r_f , $L'(S_t)$ units underlying assets at price S_t and $L''(K)$ units of calls and puts. Interestingly, the derivation of Equation 4.3 is in fact a direct consequence of the integral representation theorem. Referring to Carr and Madan [2001], we detail the derivation for Equation 4.3 in the following.

Recall $L(S)$ is an integrable function in terms of S , where $S \in [0, +\infty)$. Assume S_t is a fixed point over the domain of S , so according to the fundamental theorem of calculus the value of any unknown point over the domain of S , $L(S)$ can be expressed as $L(S_t)$ plus the difference between the two integrals from both sides of S_t , which is:

$$\begin{aligned} L(S) &= L(S_t) + 1_{S>S_t} \int_{S_t}^S L'(u) du - 1_{S<S_t} \int_S^{S_t} L'(u) du \\ &= L(S_t) + 1_{S>S_t} \int_{S_t}^S \left[L'(S_t) + \int_{S_t}^u L''(v) dv \right] du \\ &\quad - 1_{S<S_t} \int_S^{S_t} \left[L'(S_t) - \int_u^{S_t} L''(v) dv \right] du \end{aligned} \quad (4.5)$$

The Fubini's theorem results state that double integrals can be computed doing two one-variable integrals. For example, for $R \in \mathbf{R}^2 \rightarrow \mathbf{R}$, if $f(x, y)$ is continuous in $R = [a, b] \times [c, d]$, then

$$\int \int_R f(x, y) dx dy = \int_a^b \int_c^d f(x, y) dy dx = \int_c^d \int_a^b f(x, y) dx dy.$$

In our case, from Equation 4.5, $R = [S_t, S]$, if we set $[a, b] = [S_t, S]$, $[c, d] = [v, S]$, then we have:

$$\int_{S_t}^S \int_{S_t}^u L''(v) dv du = \int_{S_t}^S \int_v^S L''(v) du dv \quad (4.6)$$

Thus we have:

$$\begin{aligned}
L(S) &= L(S_t) + L'(S_t)(S - S_t) \\
&\quad + 1_{S > S_t} \int_{S_t}^S \int_v^S L''(v) du dv + 1_{S < S_t} \int_S^{S_t} \int_v^S L''(v) du dv \\
&= L(S_t) + L'(S_t)(S - S_t) \\
&\quad + 1_{S > S_t} \int_{S_t}^S L''(v)(S - v) dv + 1_{S < S_t} \int_S^{S_t} L''(v)(v - S) dv
\end{aligned} \tag{4.7}$$

Finally, expand the domain to the whole domain of the function $L(S)$, we have:

$$\begin{aligned}
L(S) &= L(S_t) + L'(S_t)(S - S_t) \\
&\quad + \int_{S_t}^{\infty} L''(v)(S - v)^+ dv + \int_0^{S_t} L''(v)(v - S)^+ dv
\end{aligned} \tag{4.8}$$

and simply replacing v with K gets Equation 4.3.

Carr and Madan [2001] demonstrate the implication of the decomposition of the payoff of the spanning contracts in portfolio allocation while Bakshi et al. [2003a] provide a non-parametric method to extract the risk neutral moments for expected returns from option prices by defining a series of expected return contracts. In the next section, I follow the spirits of Bakshi et al. [2003a] to derive the risk neutral central moments of expected returns via the spanning contracts.

4.3 Extract the Risk Neutral Central Moments from Option Prices

The moments for expected returns can be estimated using the time-series of the historical stock prices, which are known as the realised moments. A strand of literature has investigated various methods for estimating the realised moments from historical equity prices, especially using intraday high frequency data, see Andersen et al. [2001], Barndorff-Nielsen [2002],

Andersen et al. [2003], Neuberger [2012], and Buckle et al. [2014] among others.

Alternatively, we can extract the risk neutral moments for expected returns from option prices utilising the generic spanning contracts. A vast literature has documented significant evidence that the option-implied moments play important roles in explaining and forecasting cross section stock expected returns. In the following, we derive the estimations of the risk neutral central moments using the generic spanning contracts introduced in Bakshi and Madan [2000] and Carr and Madan [2001].

The beauty of the generic spanning contract is that given any twice-differentiable function $L(\cdot)$, we can replicate its risk neutral payoff by a portfolio forming by bonds, underlying stocks and the out of money call and put options written on the underlying stock. In the following proposition, we derive the estimations for the second, third, and fourth risk neutral central moments following the procedures suggested in Bakshi et al. [2003a]:

Proposition 4.1 (Risk Neutral Central Moments). Denote the central second moment (quadratic), third moment (cubic), and fourth moment (quartic) contracts for the expected returns for asset S as $L_2(S)$, $L_3(S)$, and $L_4(S)$ such that:

$$\begin{aligned} L_2(S) &:= (R_\tau - \mathbb{E}[R])^2; \\ L_3(S) &:= (R_\tau - \mathbb{E}[R])^3; \\ L_4(S) &:= (R_\tau - \mathbb{E}[R])^4. \end{aligned} \tag{4.9}$$

where $R_\tau = \ln S_T - \ln S_t$ is the τ period log-return, where $T - t = \tau$. The risk neutral second, third and fourth central moments can be extracted from

the option prices via the generic spanning contracts such that:

$$\begin{aligned}
M_2^{\mathbb{Q}}(t, K, \tau, r_f) &= \mathbb{E}_t^{\mathbb{Q}}[e^{-r_f\tau} L_2(S)] \\
&= e^{-r_f\tau} [(r_f\tau)^2 + 2r_f\tau] - 2r_f\tau \\
&\quad + \int_{S_t}^{\infty} \frac{2 \left[1 - \left(\ln \frac{K}{S_t} - r_f\tau \right) \right]}{K^2} C(\tau, K) dK \\
&\quad + \int_0^{S_t} \frac{2 \left[1 + \left(\ln \frac{S_t}{K} + r_f\tau \right) \right]}{K^2} P(\tau, K) dK
\end{aligned} \tag{4.10}$$

$$\begin{aligned}
M_3^{\mathbb{Q}}(t, K, \tau, r_f) &= \mathbb{E}_t^{\mathbb{Q}}[e^{-r_f\tau} L_3(S)] \\
&= e^{-r_f\tau} [(r_f\tau)^3 - 3(r_f\tau)^2] + 3(r_f\tau)^2 \\
&\quad + \int_{S_t}^{\infty} \frac{6 \left(\ln \frac{K}{S_t} - r_f\tau \right) - 3 \left(\ln \frac{K}{S_t} - r_f\tau \right)^2}{K^2} C(\tau, K) dK \\
&\quad - \int_0^{S_t} \frac{6 \left(\ln \frac{S_t}{K} + r_f\tau \right) + 3 \left(\ln \frac{S_t}{K} + r_f\tau \right)^2}{K^2} P(\tau, K) dK
\end{aligned} \tag{4.11}$$

$$\begin{aligned}
M_4^{\mathbb{Q}}(t, K, \tau, r_f) &= \mathbb{E}_t^{\mathbb{Q}}[e^{-r_f\tau} L_4(S)] \\
&= e^{-r_f\tau} [(r_f\tau)^4 + 4(r_f\tau)^3] - 4(r_f\tau)^3 \\
&\quad + \int_{S_t}^{\infty} \frac{12 \left(\ln \frac{K}{S_t} - r_f\tau \right)^2 - 4 \left(\ln \frac{K}{S_t} - r_f\tau \right)^3}{K^2} C(\tau, K) dK \\
&\quad + \int_0^{S_t} \frac{12 \left(\ln \frac{S_t}{K} + r_f\tau \right)^2 + 4 \left(\ln \frac{S_t}{K} + r_f\tau \right)^3}{K^2} P(\tau, K) dK
\end{aligned} \tag{4.12}$$

Proof for Proposition 4.1. The proof for Proposition 4.1 follows from the derivation of the generic spanning contract formula in Equation 4.3 and Equation 4.4. Under the risk-neutral measure, it is easy to see that $S_T = S_t e^{r_f\tau}$. Thus we have $\mathbb{E}[R] = r_f\tau$, where r_f is the risk-free rate over the period τ . The first-order derivative of the quadratic, cubic and quartic central moment contracts with respect to S evaluating at S_t can be

derived as:

$$\begin{aligned} L_2'(S_t) &= -\frac{2r_f\tau}{S_t}; \\ L_3'(S_t) &= \frac{3(r_f\tau)^2}{S_t}; \\ L_4'(S_t) &= -\frac{4(r_f\tau)^3}{S_t}. \end{aligned} \tag{4.13}$$

while the second-order derivative of the quadratic, cubic and quartic central moment contracts with respect to S evaluating and K can be derived as:

$$\begin{aligned} L_2''(K) &= \frac{2 \left[1 - \left(\ln \frac{K}{S_t} - r_f\tau \right) \right]}{K^2}; \\ L_3''(K) &= \frac{6 \left(\ln \frac{K}{S_t} - r_f\tau \right) - 3 \left(\ln \frac{K}{S_t} - r_f\tau \right)^2}{K^2}; \\ L_4''(K) &= \frac{12 \left(\ln \frac{K}{S_t} - r_f\tau \right)^2 - 4 \left(\ln \frac{K}{S_t} - r_f\tau \right)^3}{K^2}. \end{aligned} \tag{4.14}$$

Substituting Equation 4.13 and 4.14 back into the arbitrage-free price of the spanning claim payoff formula in Equation 4.5 we derive the payoff of the quadratic, cubic, and quartic contracts at time t over time to maturity τ , which are the risk neutral second, third, and fourth central moments for expected returns of asset S over the period τ , which are Equations 4.10, 4.11, and 4.12 given in Proposition 4.1. \square

4.4 Summary and Remarks

Inspired by the pioneering work of Ross [1976] and Brown and Ross [1991], Bakshi and Madan [2000] and Carr and Madan [2001] exhibit the valuation of the generic spanning contracts. In particular, the arbitrary payoff of any second-differentiable function over a period can be spanned by the payoff of risk-free bonds, underlying stocks, and the price of the out of money call and put options written on the underling assets. I illustrate the derivations of the generic spanning contract in detail referring the method proposed by

[Carr and Madan \[2001\]](#). In Proposition [4.1](#), by defining a series of central moments contracts for expected returns, I uniquely derive the formulas for extracting the risk neutral central moments for expected returns of underlying assets using the generic spanning contracts. In [Chapter 7](#) and [Chapter 8](#), utilising risk neutral central moments derived in Proposition [4.1](#), I introduce a sets of high dimensional option-implied average correlation measures and demonstrate the implication of the option-implied average correlations in cross-section asset pricing.

Chapter 5

Hansen-Scheinkman

Factorisation and Ross

Recovery from High Frequency

Option Prices via Nonlinear

Programming: The

Perturbation Theory

5.1 Introduction

Recovering the physical expected forward density function of an asset from prices observed from the asset's associated derivatives market is one of the foundational research problems in asset pricing. The contractual design of derivatives, such as options, are priced under a risk-neutral measure, often referred to as the \mathbb{Q} measure, following the fact that a fully 'delta-neutral' offsetting position can be constructed by inclusion of an appropriate derivatives position within a portfolio that contains the underlying asset. In finance, 'delta-neutral' describes a portfolio of related financial securities, in which the portfolio value remains unchanged when small changes occur in

the value of the underlying security. As such, any valuation of the derivatives position presumes a fully risk-free combination of the underlying asset and derivative is achievable. Hence, any inference on the physical (or observed) measure, usually referred to as the \mathbb{P} measure, from forward looking derivatives prices must account for the representative preferences of the market participants in the underlying asset.

Recent work by Hansen and Scheinkman [2009], Ross [2015] and Borovička et al. [2016] has established that the eigenfunction of the risk-neutral state price transition matrix has a useful economic interpretation, in respect to gaining a better understanding of the \mathbb{P} measure from derivative prices observed under the \mathbb{Q} measure. Indeed, Ross [2015] proposes a Recovery Theorem (henceforth RT) that posits that the eigenfunction of a risk-neutral state price transition matrix can be used to fully identify the discount factor, pricing kernel and physical probabilities of assets in a finite state economy.

A more general interpretation is outlined in Borovička et al. [2016], who follow up on preceding results in Hansen and Scheinkman [2009] by demonstrating that whilst the eigenfunction approach generates useful objects of interest, the recovered state price transition function may contain a martingale component that biases longer time horizon forecasts of the physical probability density function. Further work by Carr and Yu [2012] extends the exact identification case of Ross [2015] to a continuous time (with a continuum of states) setting to demonstrate that the eigenfunction approach can be utilised with individual assets as opposed to the representative consumption asset presumed in Hansen and Scheinkman [2009], Ross [2015], and Borovička et al. [2016].

The contribution of this chapter is to provide a perturbation theory for the eigenfunction analysis and embed this theory in an algorithm that can be implemented on market data. The usefulness of the perturbation theory is both in the theoretical treatment of recovery and for use in empirical applications. With it we can specify the anticipated structure (subject to theoretical predictions) on the risk-neutral state price transition matrix as a series of restrictions within a non-linear programming problem. Indeed, this

is the first implementation of such an algorithm which permits selective imposition of such constraints with a fully tractable set of derivatives on the objective and constraints. This permits specification of a recovery algorithm on very large datasets (in this case tick by tick options data).

Hence, I fully close a gap in the literature on how to implement the [Ross \[2015\]](#) and [Borovička et al. \[2016\]](#) style eigenfunction analysis on market data while systematically varying the properties of the resulting state transition matrix, discount factor and pricing kernel. Specifically, I introduce to the existing literature the use of a new type of inverse, the ‘group’ or more generally the ‘Drazin’ inverse which provides a mathematical platform to semi-parametrically identify the risk-neutral Markov transition matrix, by allowing us to present an exact perturbation theory for any type of discrete Markov chain with an irreducible state transition matrix.

In the fully identified case outlined in [Ross \[2015\]](#), a three-step framework for recovering the physical (or real world) density function is proposed. First, compute the risk-neutral state price matrix (by state by tenor) from option market prices. Second, determine the risk-neutral state price transition matrix from the Markov chain process. Finally, apply the *Perron Frobenius theorem* to recover the objects of interest. For any interpretation of the recovered state price density function, with or without the martingale component in [Borovička et al. \[2016\]](#) the empirical steps are the same, albeit with different interpretations on the recovered quantities.

My formulation allows the empirical researcher to impose this property on the recovered matrix via the imposition of linear and non-linear restrictions on the estimated risk-neutral state price transition matrix imputed from forward looking state price densities. Hence, the martingale property in the discount factor is only relevant when the specific interpretation of the recovered transition matrix is that it describes the physical evolution of assets. Under most plausible specifications for the martingale component, [Borovička et al. \[2016\]](#) demonstrate that the bias effect of the martingale component only substantiates itself at longer forecasting horizons.

My approach is to make use of the perturbation properties of the

eigensystem determined under the *Perron Frobenius theorem*. Typically eigenfunctions of square matrices do not generally have continuous real derivatives and those that do often do not have tractable analytic derivatives. However, for fields of irreducible matrices the eigenfunction of the largest eigenvalue sits in one of these cases. Indeed, not only is the first derivative continuous, the eigenfunction is in fact smooth. Indeed, by use of *Bolzano Weierstrass theorem*, I can derive two equivalent forms of the first derivative and determine explicit forms for higher derivatives using the group inverse and generate a full perturbation theory for the recovered quantities.

My final contribution is in combining this analysis with the current literature on extracting the risk-neutral density function from noisy option data. Identifying the risk-neutral density (RND) with precision, something that has eluded the literature since the original contribution of [Breeden and Litzenberger \[1978\]](#), see for example [Jackwerth and Rubinstein \[1996\]](#), [Bondarenko \[2003\]](#), and [Jackwerth \[2004\]](#) among others. [Monteiro et al. \[2008\]](#) provide a new approach to estimate the RND in the space of cubic spline functions, which ensures the positivity of the estimated RND by posing linear inequality constraints at the spline nodes and solving a convex quadratic or semidefinite programming problem within a numerical optimisation system.

My approach is the first algorithm of its type that can be both employed on intraday data and easily extrapolated to fill gaps in the coverage of tail states for certain tenors. I illustrate the significant advantage gained from having high frequency data in this setting. I illustrate my approach using intraday options data directly from the option pricing reporting authority (hereafter [OPRA](#)) feed for some sample days of S&P 500 index options and Apple Inc., a single-name American option.

I separate the theoretical work and empirical applications into two parts. In the remainder of this chapter: Section [5.2](#) presents a short review of the Recovery Theorem. I then derive a full perturbation theory of recovery in Section [5.4](#). The perturbation theory illustrates the continuity of the derivatives of the discount factor and pricing kernel. The empirical

applications are detailed in Chapter 6. Section 6.1 outlines an exact algorithm focusing on the fast non-linear programming approach in determining the risk-neutral state price matrix. A simulation analysis in Section 6.2 illustrates the consistency of my algorithm under the Ross [2015] assumptions. Section 6.3 is devoted to a completed empirical analysis of applying my approach to publicly available market data sample, namely the S&P 500 index options and the single-name equity option written on Apple Inc stock. Section 6.4 concludes the two chapters.

5.2 Eigenfunction Analysis of Risk Neutral State Price Transition Matrices

Analysis of the implications of arbitrage free pricing on the valuation of assets is arguably at the foundation of financial economics. As a standard pillar of financial economics, Arrow [1964] and Debreu [1987] introduced the concept of an Arrow-Debreu state security, one that pays a single unit of a numéraire only if a particular state occurs. The complete set of state securities may then be linearly combined and re-combined into the observed set of traded securities.

Typically, we do not observe Arrow-Debreu securities directly; however, Breeden and Litzenberger [1978] provided the insight that the second derivative of observed option prices as a function of their strikes should provide the risk-neutral valuations of the Arrow-Debreu state securities. Hansen and Scheinkman [2009] first noted that for long run asset pricing models that an eigensystem analysis of the Markov chain reveals useful quantities about the asset price process and the time and risk preferences of representative agents. The innovation of Ross [2015] is in setting out the conditions that allow full identification of the physical transition density function and hence the market expectations of the physical densities at different time horizons.

Follow up work by Carr and Yu [2012] derive the RT in a bounded continuous setting and Walden [2017] who further loosens this boundary

restriction and derives necessary and sufficient conditions for unbounded Markovian diffusion. A useful result in Carr and Yu [2012] is that the RT can be shown to work for individual assets, using the Long [1990] numéraire portfolio as a solution device.

Further loosening of the original assumptions can be found in Dubynskiy and Goldstein [2013], Liu [2014], Qin and Linetsky [2014], Schneider and Trojani [2018], Jensen et al. [2018], Bakshi et al. [2017] and Park [2015]. Utilising a spectral theory of Markovian asset pricing models, Qin and Linetsky [2016], extend the Ross [2015] RT from a discrete time, finite state irreducible Markov chains to a general continuous-time Markov process with recurrent Borel right process. Within their model setting, the uniqueness of Hansen and Scheinkman [2009] factorisation of the Markovian stochastic discount factor is proved and the long maturity asymptotic of the pricing operator is also obtained.

In a pre-cursor to my main perturbation results, Ngoc-Khanh and Xia [2014] indicates that the uniqueness and structure of the recovered kernels, discount factors and real world probabilities are sensitive to the choice of dimension of the states. I will show that the whilst the discount factor is highly sensitive this can be from two sources: inherent sensitivity to perturbation and numerical stability of the solution space.

Borovička et al. [2016] demonstrate that the full identification result found in Ross [2015] requires certain restrictive assumptions. Specifically, in the presence of a stochastic discount factor with a martingale component the long horizon forecasts of the density function will be misspecified. However, both Hansen and Scheinkman [2009] Borovička et al. [2016] stress the usefulness of the eigensystem as a mechanism for refining our understanding of the price formation mechanism in financial markets.

From an empirical perspective Audrino et al. [2014], Spears [2013], and Backwell [2015] have provided some methodological steps towards a practical implementation of the Ross [2015] three-step approach. However, in each case there are gaps, either in data coverage or in the details of the methodology. A key issue is the inherent difficulty in implementing the Breeden and Litzenberger [1978] analysis on actual market data. We address

this in two ways, first we have a two-step algorithm to smooth the traded prices (using implied volatilities as an interpolation and smoothing device) and then extrapolating the tails using mixtures of parametric distributions.

At this juncture it is useful to outline the current theoretical insights in applying eigenfunction operators to the risk-neutral state price transition matrix. To this end I adhere to the framework of [Borovička et al. \[2016\]](#) and [Ross \[2015\]](#) for which my perturbation treatment and subsequent algorithm development are most closely suited. For a more detailed discussion of various theoretical treatments of the Recovery Theorem, see Chapter 3.

5.2.1 The [Borovička et al. \[2016\]](#) Derivation

Let $\mathbf{S} := \{s_{mn} : 1 \leq m \leq M, 1 \leq n \leq N\}$ the state price by tenor matrix, such that a column \mathbf{s}_n is the vector of risk-neutral state price for a particular tenor, with element being the risk-neutral price of an asset paying a single unit in that state for that tenor only. Noted, the word ‘state’ refers to the potential outcomes of the stock price (or the market level). Through this chapter, I use ‘tenor’ to stand for the time to maturity of the option contract. The finite state Markov chain that determines the transition from time index n to $n + 1$ is characterised by the risk-neutral state price transition matrix $\mathbf{Q} := \{q_{ij} : 1 \leq i \leq M, 1 \leq j \leq M\}$, whereby $\mathbf{s}_{n+1} = \mathbf{Q}\mathbf{s}_n$. When $\mathbf{S} := \{s_{mn} : 1 \leq m \leq M, 1 \leq n \leq N\}$ is known with precision, the minimum number of tenors needed for identification of \mathbf{Q} is $N = M + 1$.

A risk free instrument pays off in every state and has current period value of $\sum_{m=1}^M s_{mn} = \exp(r_n)$, where r_n is the continuously discounted risk free return for the tenor indexed by n . When $\exp(r_{n+1}) > \exp(r_n)$ for all $n \in \{1, \dots, N\}$ the Markov process described by the risk-neutral transition matrix \mathbf{Q} is sub-stochastic, hence $\lim_{\kappa \rightarrow \infty} \mathbf{Q}^\kappa = \mathbf{0}_{M \times M}$. The risk-neutral measure is an artificially constructed measure that is not the observed real world or physical measure. Let $\mathbf{P} := \{p_{ij} : 1 \leq i \leq M, 1 \leq j \leq M\}$ be the physical transition matrix of the Markov chain driving observed asset prices. Setting $\delta = \exp(r)$ to be the discount factor and approximating $r_n = nr$ the standard

neoclassical asset pricing framework posits the following ratio:

$$\Psi = [\psi_{ij}], \quad \text{where} \quad \psi_{ij} = \frac{q_{ij}}{p_{ij}}, \quad (5.1)$$

where $[\psi_{ij}]$ is the stochastic discount factor, as such $q_{ij} = \psi_{ij}p_{ij}$. However, from forward looking derivatives prices we only observe q_{ij} and, as such, we do not have sufficient information to fully recover ψ_{ij} and p_{ij} .

The identification challenge is simply illustrated by considering the dimensions of \mathbf{P} , \mathbf{Q} and Ψ . \mathbf{Q} has $M \times M$ entries and so does the stochastic discount factor matrix Ψ , while the physical transition matrix \mathbf{P} only have $M \times (M - 1)$ free entrances as \mathbf{P} is, by definition, right stochastic and with rows summing to unity. As such, instead of having the observed physical transition probabilities $\mathbf{P} = [p_{ij}]$, we could have an alternative such that

$$\tilde{\mathbf{P}} = [\tilde{p}_{ij}], \quad \text{such that} \quad \tilde{p}_{ij} = h_{ij}p_{ij}, \quad (5.2)$$

where h_{ij} are elements of the positive matrix $\mathbf{H} = [h_{ij}]$ such that $h_{ij} > 0$ and $\sum_{j=1}^M h_{ij}p_{ij} = 1$. As h_{ij} is obtained as a ratio of probabilities, the process H is a positive martingale under P . For each choice of the restricted matrix \mathbf{H} , the state-dependent discount factors can be formed such as $\tilde{\psi}_{ij} = \psi_{ij}/h_{ij}$, which gives the corresponding risk-neutral transition probabilities such as:

$$q_{ij} = \psi_{ij}p_{ij} = \tilde{\psi}_{ij}\tilde{p}_{ij} \quad (5.3)$$

Therefore, given the flexibility in constructing the always positive martingale process H , the physical probabilities can be recovered from the risk-neutral state price in a variety ways.

In order to recovered the physical transition probabilities \mathbf{P} from the risk-neutral transition probabilities \mathbf{Q} uniquely, [Borovička et al. \[2016\]](#) demonstrate that additional restrictions on the stochastic discount factor need to be imposed. Specifically, [Borovička et al. \[2016\]](#) derive the recovery under the long-term pricing restriction using Perron-Frobenius theory, which is an eigenfunction approach. Following the Perron-Frobenius theory, when all of the entries of the risk-neutral transition matrix \mathbf{Q} are positive, the

largest eigenvalue of \mathbf{Q} is positive and unique, which can be written as $\delta = \exp(r)$. The associated right eigenvector $\tilde{\mathbf{v}}$ also has strictly positive entries denoting the i entry of the eigenvector as \tilde{v}_i . By construction we can recover a probability matrix $\tilde{\mathbf{P}}$ with the entries such that:

$$\tilde{p}_{ij} := \delta^{-1} q_{ij} \frac{\tilde{v}_i}{\tilde{v}_j}. \quad (5.4)$$

Since $\mathbf{Q}\tilde{\mathbf{v}} = \delta\tilde{\mathbf{v}}$, thus $\sum_{j=1}^n \tilde{p}_{ij} = 1/\delta(\tilde{v}_i)^{-1} \sum_{j=1}^n q_{ij}\tilde{v}_j = 1$, hence $\tilde{\mathbf{P}}$ is a valid transition matrix. Thus the risk-neutral transition probabilities can be written as

$$q_{ij} = \delta \frac{\tilde{v}_i}{\tilde{v}_j} \tilde{p}_{ij} = \tilde{\psi}_{ij} \tilde{p}_{ij} \quad (5.5)$$

Both [Ross \[2015\]](#) and [Borovička et al. \[2016\]](#) use the eigenfunction approach stated in Equation 5.5 to construct the recovered probability distribution. [Borovička et al. \[2016\]](#) show that combining Equation 5.4 together with Equation 5.5 gives the following decomposition:

$$q_{ij} = \delta \frac{\tilde{v}_i}{\tilde{v}_j} \frac{\tilde{p}_{ij}}{p_{ij}}, \quad p_{ij} = \delta \frac{\tilde{v}_i}{\tilde{v}_j} \tilde{\psi}_{ij} p_{ij} \quad (5.6)$$

Hence the stochastic discount factor can be derived as

$$\tilde{\psi}_{ij} = \delta \frac{\tilde{v}_i}{\tilde{v}_j} h_{ij}, \quad \text{where } h_{ij} = \frac{\tilde{p}_{ij}}{p_{ij}}, \quad (5.7)$$

which implies $\tilde{\mathbf{P}} = \mathbf{H} \circ \mathbf{P} \equiv [h_{ij} p_{ij}]$, where \circ is the element by element product of identical dimension matrices. [Hansen and Scheinkman \[2009\]](#) show that the stochastic discount factor derived in Equation 5.7 can be used as to study long-term valuation and h_{ij} is termed as long-term risk-neutral probability.

5.2.2 The [Ross \[2015\]](#) Recovery Theorem

If we presume that $h_{ij} = 1$ for all $i, j \in \{1, \dots, M\}$ then we obtain the full identification result of [Ross \[2015\]](#), hence $\tilde{\mathbf{P}} = \mathbf{P}$. A further benefit of this identifying assumption is that we can interpret the time and risk preferences separately, hence $\tilde{v}_i/\tilde{v}_j = U'(c_i)/U'(c_j)$, where c_i and c_j is the consumption in

state i and state j respectively of a representative agent with utility function $U(\cdot)$. It is helpful to normalise the quantity \tilde{v}_i and this normalisation is usually computed as follows. Let v_i be the i element of the eigenvector of the largest root of \mathbf{Q} then $\tilde{v}_i = v_{(M+1)/1}/v_i$. The choice of normalisation actually turns out to be important when computing the derivatives of \tilde{v}_i and we will illustrate this in the next section.

Setting $\mathbf{D} = \text{diag}[\mathbf{d}]$ where $\mathbf{d} = [d_i] = 1/v_i$, then we have an identified system such that:

$$\mathbf{P} = \delta^{-1}\mathbf{D}\mathbf{Q}\mathbf{D}^{-1}, \text{ and } \mathbf{Q} = \delta\mathbf{D}^{-1}\mathbf{P}\mathbf{D} \quad (5.8)$$

If $h_{ij} \neq 1$ for all $n \in \{1, \dots, N\}$ and does indeed describe a martingale component in the discount factor how does this instantiate itself in the misspecified calculation of \mathbf{P} ? The answer is that as time progresses the martingale component in h_{ij} results in a projected density function at the n step trending away from the expected physical density. [Borovička et al. \[2016\]](#) demonstrate that even under quite benign circumstances long horizon forecasts, without further source of information to extract the martingale component, the recovered physical density will be substantially biased as the effect of h_{ij} accumulates.

The focus of this chapter is exclusively on the perturbation theory surrounding the estimation of \mathbf{Q} and hence the derivation of $\tilde{\mathbf{P}}$ and in the following section we outline the pre-requisite perturbation theory in terms of the quantities of interest as a continuous function of \mathbf{Q} . I also outline carefully the implications of $h_{ij} = 1$ and illustrate the implied conditions (ergodicity and recurrence) needed to impose this property on the recovered $\tilde{\mathbf{P}}$ during the estimation of \mathbf{Q} from noisy market data.

5.3 Motivating the Problem: Revisiting the Ross Recovery Calculation

The most basic issue emerging in the empirical literature on the RT is how to compute the risk-neutral state price transition matrix from the imputed state price matrix derived using the Breeden and Litzenberger [1978] approach? If we look at the 11 by 12 state price matrix reported in Ross [2015], the rows each describe a state ranging from -35% to 54% returns on the index, with the middle row representing the 0% return and the columns are time to maturities from one quarter to three years (hence one more column than there are rows). The system is identified as there are eleven transitions and eleven states.

However, if we directly solve the linear algebra problem to recover the substochastic state transition matrix whereby in an unrestricted form, then we recover a physical transition matrix with negative values. So it makes sense to compute a restricted least squares on the basis that no element of the risk-neutral state transition matrix is less than zero. Repeating the solution using, for instance a Fast Non-negative Least Square (FNNLS) does yield a non-negative matrix with all elements less than unity, however the matrix is very far from row and column-wise unimodal and exhibits significant periodicity.

An instructive comparison of my approach is to compare my algorithm to the figures reported in Ross [2015], at present this is the only available comparator. The reported state transition by tenor matrix, \mathbf{S} , [Ross, 2015, Page 636] is as follows:

$$\mathbf{S} = \begin{pmatrix} 0.005 & 0.023 & 0.038 & 0.050 & 0.058 & 0.064 & 0.068 & 0.071 & 0.073 & 0.075 & 0.076 & 0.076 \\ 0.007 & 0.019 & 0.026 & 0.030 & 0.032 & 0.034 & 0.034 & 0.035 & 0.035 & 0.035 & 0.034 & 0.034 \\ 0.018 & 0.041 & 0.046 & 0.050 & 0.051 & 0.052 & 0.051 & 0.050 & 0.050 & 0.049 & 0.048 & 0.046 \\ 0.045 & 0.064 & 0.073 & 0.073 & 0.072 & 0.070 & 0.068 & 0.066 & 0.064 & 0.061 & 0.058 & 0.056 \\ 0.164 & 0.156 & 0.142 & 0.128 & 0.118 & 0.109 & 0.102 & 0.096 & 0.091 & 0.085 & 0.081 & 0.076 \\ 0.478 & 0.302 & 0.234 & 0.198 & 0.173 & 0.155 & 0.141 & 0.129 & 0.120 & 0.111 & 0.103 & 0.096 \\ 0.276 & 0.316 & 0.278 & 0.245 & 0.219 & 0.198 & 0.180 & 0.164 & 0.151 & 0.140 & 0.130 & 0.120 \\ 0.007 & 0.070 & 0.129 & 0.155 & 0.166 & 0.167 & 0.164 & 0.158 & 0.152 & 0.145 & 0.137 & 0.130 \\ 0.000 & 0.002 & 0.016 & 0.036 & 0.055 & 0.072 & 0.085 & 0.094 & 0.100 & 0.103 & 0.105 & 0.105 \\ 0.000 & 0.000 & 0.001 & 0.004 & 0.009 & 0.017 & 0.026 & 0.036 & 0.045 & 0.053 & 0.061 & 0.067 \\ 0.000 & 0.000 & 0.000 & 0.000 & 0.000 & 0.000 & 0.001 & 0.001 & 0.002 & 0.002 & 0.003 & 0.003 \end{pmatrix}$$

setting $\mathbf{s}_{i \in \{1, \dots, 12\}}$ to be a single column from \mathbf{S} . To compute the linear algebra problem I simply compute two matrices $\mathbf{S}_0 = [\mathbf{s}_1, \dots, \mathbf{s}_{11}]$ and $\mathbf{S}_1 = [\mathbf{s}_2, \dots, \mathbf{s}_{12}]$.

For the prediction states \mathbf{S}_1 , I compute $\mathbf{d} = \text{vec}[\mathbf{S}_1]$, where vec is the

column-wise stacking vec operator. Then I compute $\mathbf{C} = \text{vec}[\mathbf{S}_0 \otimes \mathbf{I}_{11}]_{i=1, \dots, 11}$.

Ross [2015] on Pages 636 and 637 suggests that the corresponding state-transition matrix is:

$$\hat{\mathbf{Q}} = \begin{pmatrix} 0.6710 & 0.2410 & 0.0530 & 0.0050 & 0.0010 & 0.0010 & 0.0010 & 0.0010 & 0.0010 & 0 & 0 \\ 0.2800 & 0.3960 & 0.2450 & 0.0540 & 0.0040 & 0 & 0 & 0 & 0 & 0 & 0 \\ 0.0490 & 0.2240 & 0.3940 & 0.2480 & 0.0560 & 0.0040 & 0 & 0 & 0 & 0 & 0 \\ 0.0060 & 0.0440 & 0.2180 & 0.3900 & 0.2500 & 0.0570 & 0.0030 & 0 & 0 & 0 & 0 \\ 0.0060 & 0.0070 & 0.0410 & 0.2110 & 0.3850 & 0.2490 & 0.0540 & 0.0020 & 0 & 0 & 0 \\ 0.0050 & 0.0070 & 0.0180 & 0.0450 & 0.1640 & 0.4780 & 0.2760 & 0.0070 & 0 & 0 & 0 \\ 0.0010 & 0.0010 & 0.0010 & 0.0040 & 0.0400 & 0.2040 & 0.3820 & 0.2510 & 0.0580 & 0.0050 & 0 \\ 0.0010 & 0.0010 & 0.0010 & 0.0020 & 0.0060 & 0.0420 & 0.2040 & 0.3730 & 0.2430 & 0.0550 & 0.0040 \\ 0.0020 & 0.0010 & 0.0010 & 0.0020 & 0.0030 & 0.0060 & 0.0410 & 0.1950 & 0.3610 & 0.2320 & 0.0570 \\ 0.0010 & 0 & 0 & 0.0010 & 0.0010 & 0.0010 & 0.0030 & 0.0350 & 0.1870 & 0.3470 & 0.3130 \\ 0 & 0 & 0 & 0 & 0 & 0 & 0 & 0 & 0.0320 & 0.1810 & 0.8750 \end{pmatrix}$$

If we compute $1/2\|\mathbf{C}\mathbf{x} - \mathbf{d}\|^2$, by setting $\mathbf{x} = \text{vec}[\hat{\mathbf{Q}}]$, then we get a sum of squared errors of 0.0487. I will now outline the difficulties in this second set of steps, starting with a direct solution using a standard unrestricted linear solver.

5.3.1 Experiment One Direct Solution for Q

Directly computing $\mathbf{Q} = \text{mat}[\mathbf{x}]$ by exact solution of $\mathbf{C}\mathbf{x} = \mathbf{d}$ recovers the following matrix:

$$\hat{\mathbf{Q}} = \begin{pmatrix} 1.2107 & -3.0672 & 1.4345 & 2.3102 & -0.2692 & 0.0798 & -0.3001 & -0.3623 & -0.0771 & 0.0551 & -2.5372 \\ 2.2855 & -0.3776 & -0.1824 & 1.5624 & 0.6314 & -0.0973 & -0.3921 & -0.8059 & -0.3600 & -0.8784 & 0.9687 \\ 4.0011 & -1.6151 & 0.4915 & 4.1111 & 0.3813 & -0.0006 & -0.7699 & -1.6137 & -0.8228 & -1.3990 & -1.0426 \\ 1.3433 & 5.0964 & -2.4741 & -1.3937 & 0.7767 & -0.1248 & 0.2284 & -0.2773 & -0.1795 & -0.9618 & 5.3256 \\ 2.6094 & 4.8992 & -2.8871 & 0.3134 & -0.2206 & 0.1627 & 0.3993 & -0.7528 & -0.4970 & -1.3014 & 5.1380 \\ -0.4332 & 2.5866 & -1.3579 & -1.5556 & 0.9438 & 0.2994 & 0.2920 & 0.2853 & 0.0711 & 0.0245 & 1.0307 \\ 1.8278 & -0.6005 & 0.4610 & 2.1488 & 0.2424 & 0.3769 & -0.0323 & -0.7056 & -0.5528 & -0.6921 & -0.8606 \\ 4.4198 & 8.7715 & -3.2561 & -0.2409 & 1.3916 & -0.2693 & -0.1274 & -1.2000 & -0.9566 & -2.7279 & 9.6482 \\ -0.2833 & -3.0165 & 0.9775 & 0.3800 & -0.0132 & -0.0052 & -0.0296 & 0.3807 & 0.8860 & 0.5299 & -3.9719 \\ -0.1691 & -5.1563 & 1.4795 & 2.0574 & -1.0753 & 0.1553 & 0.0686 & 0.1285 & 0.3430 & 1.4452 & -4.9272 \\ -1.1552 & 0.6654 & -0.2589 & -1.0936 & -0.2052 & 0.0236 & 0.2679 & 0.4899 & 0.2327 & 0.5538 & -0.6483 \end{pmatrix}$$

for which the error $1/2\|\mathbf{C}\mathbf{x} - \mathbf{d}\|^2$ is 1.0279e-31. The transition matrix recovered through the direct solution is neither a basic Markov chain transition matrix, as there are plenty of negative entrances hence it is not irreducible, nor an economic meaningful state price transition matrix, as it is obviously not unimodal.

5.3.2 Experiment Two Non-Negative Least Squares Solution for \mathbf{Q}

The recovered matrix $\hat{\mathbf{Q}}$ obviously does not conform to any of our proceeding requirements for a Markov chain transition matrix hence we can repeat this experiment, but using non-negative least squares. This yields the matrix:

$$\hat{\mathbf{Q}} = \begin{pmatrix} 0.4101 & 0 & 0.1418 & 0.2043 & 0 & 0.0184 & 0 & 0.0565 & 0.0750 & 0.1442 & 0 \\ 0.0304 & 0 & 0 & 0.0439 & 0.0344 & 0 & 0.0391 & 0.0649 & 0.0958 & 0 & 0.7539 \\ 0.0961 & 0.4417 & 0 & 0.2526 & 0.0394 & 0.0409 & 0 & 0.0102 & 0 & 0.0064 & 0 \\ 0 & 0 & 0 & 0 & 0.1275 & 0.0121 & 0.1326 & 0.1041 & 0.1220 & 0 & 0 \\ 0 & 0.3655 & 0 & 0.0952 & 0 & 0.1842 & 0.2201 & 0.0531 & 0.0318 & 0 & 0 \\ 0 & 0 & 0 & 0 & 0.1337 & 0.4524 & 0.2293 & 0.0657 & 0 & 0 & 0 \\ 0 & 0 & 0 & 0 & 0 & 0.3647 & 0.5088 & 0.1321 & 0 & 0 & 0 \\ 0 & 0 & 0.5735 & 0 & 0 & 0 & 0.2056 & 0.5593 & 0 & 0 & 0 \\ 0.0879 & 0 & 0.0456 & 0 & 0 & 0 & 0 & 0.1474 & 0.7238 & 0 & 0 \\ 0 & 0 & 0.0096 & 0 & 0 & 0 & 0 & 0 & 0.1633 & 0.8140 & 0 \\ 0 & 0 & 0 & 0 & 0 & 0 & 0 & 0 & 0 & 0.0501 & 0 \end{pmatrix}$$

which is (a) irreducible, (as every element of $\hat{\mathbf{Q}}^4$ is greater than zero) and (b) all elements are greater than zero and less than unity. However, the row and columns exhibit considerable degrees of multi-modality.

5.3.3 Experiment Three My Implementation for \mathbf{Q}

Deploying our algorithm, without the Perron root constraint (as [Ross \[2015\]](#) finds a $\delta > 1$), on the \mathbf{S} matrix reported in [Ross \[2015\]](#) I compute the following:

$$\hat{\mathbf{Q}} = \begin{pmatrix} 0.8798 & 0.1044 & 0.0047 & 0.0047 & 0.0047 & 0.0047 & 0.0037 & 0.0000 & 0.0000 & 0.0000 & 0.0000 \\ 0.3952 & 0.5531 & 0.0047 & 0.0047 & 0.0047 & 0.0047 & 0.0037 & 0 & 0.0000 & 0.0000 & 0.0000 \\ 0.2940 & 0.4401 & 0.4401 & 0.0047 & 0.0047 & 0.0047 & 0.0037 & 0 & 0.0000 & 0.0000 & 0.0000 \\ 0.1859 & 0.3050 & 0.3050 & 0.3077 & 0.0385 & 0.0385 & 0.0197 & 0 & 0.0000 & 0.0000 & 0.0000 \\ 0.0537 & 0.0842 & 0.0961 & 0.1162 & 0.2081 & 0.1898 & 0.1284 & 0.0078 & 0.0052 & 0.0036 & 0.0029 \\ 0.0252 & 0.0252 & 0.0252 & 0.0252 & 0.0252 & 0.4549 & 0.2711 & 0.0248 & 0.0248 & 0.0225 & 0.0091 \\ 0.0252 & 0.0252 & 0.0252 & 0.0252 & 0.0252 & 0.3383 & 0.5322 & 0.0425 & 0.0330 & 0.0225 & 0.0091 \\ 0.0046 & 0.0046 & 0.0046 & 0.0046 & 0.0046 & 0.0046 & 0.2538 & 0.5568 & 0.2392 & 0.0669 & 0.0091 \\ 0.0000 & 0.0000 & 0 & 0 & 0 & 0 & 0 & 0.3026 & 0.4604 & 0.1243 & 0.0093 \\ 0.0000 & 0 & 0 & 0 & 0 & 0 & 0 & 0.0409 & 0.2272 & 0.4782 & 0.0093 \\ 0 & 0 & 0 & 0 & 0 & 0 & 0 & 0 & 0 & 0.3063 & 0.5180 \end{pmatrix}$$

This yields an error of $1/2\|\mathbf{C}\mathbf{x} - \mathbf{d}\|^2 = 0.006774$, one order of magnitude lower than the error for the computed matrix in [Ross \[2015\]](#). This matrix is both column and row-wise unimodal and the corresponding δ is 1.0032 as opposed to the value of 1.018 computed in [Ross \[2015\]](#). Using intraday market data for 11 states I compute the equivalent rate to be 3.18%, which is a factor of 0.9921, much nearer to the value expected in a standard modelling framework.

Figure 5.1: Experiments on Computing the State Transition Matrix with Ross Data

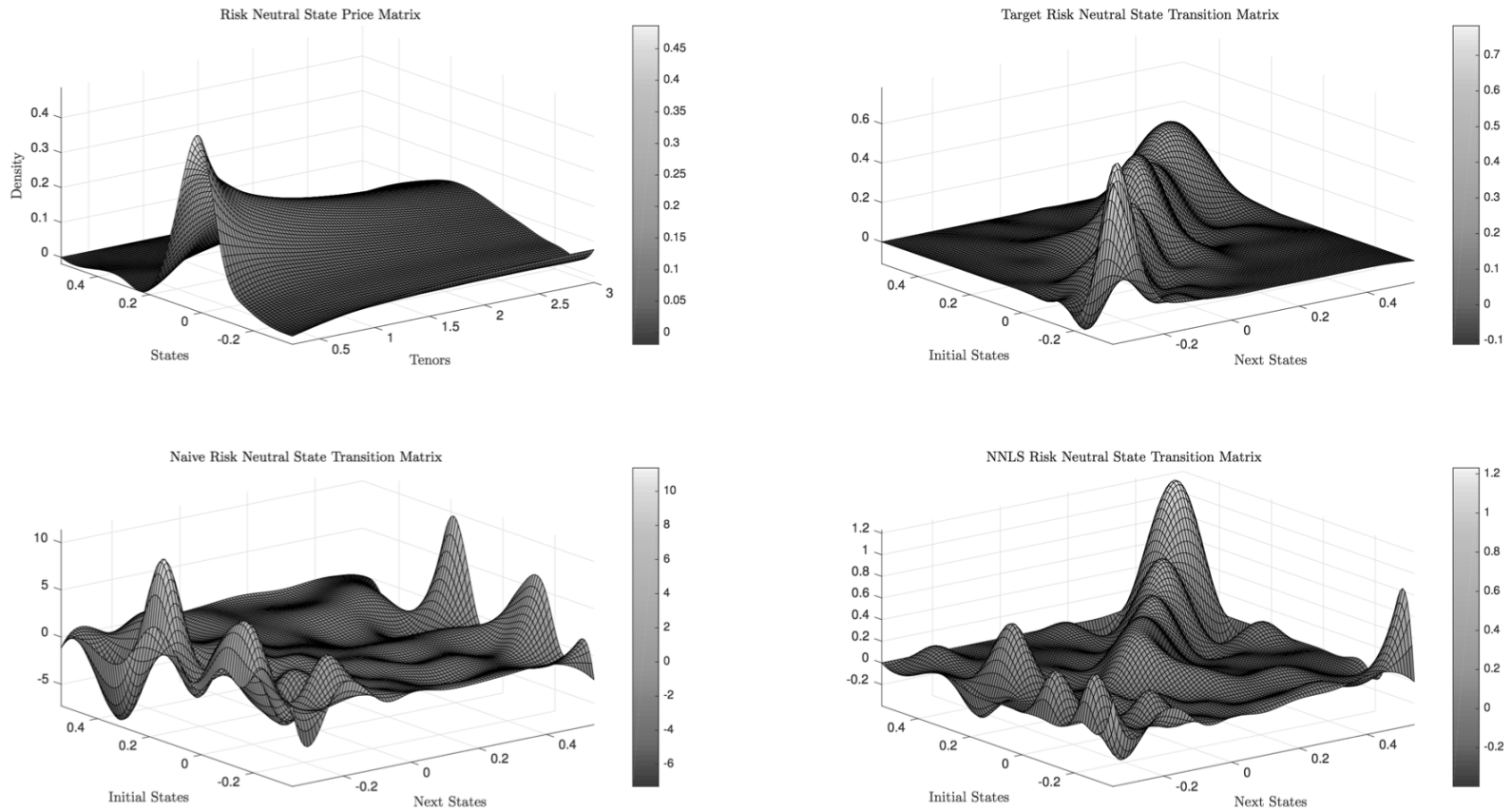


Figure 5.1 reports the experiment results all together. We can see that none of the simplest approaches yields a state price transition matrix close to one that would be considered useful for generating forward predictions. However, my final implementation does provide both a very similar matrix to that reported in Ross [2015] with a lower (by an order of magnitude) squared error in terms of the forward prediction of the state price versus those in the state price by tenor matrix.

5.4 A Perturbation Theory of Recovery

To apply the recovery theorem to empirical data, we must understand how perturbations from data affects the recovered value of interests. In particular, I can show that the discount factor and pricing kernel, as obtained from the discrete approach in Ross [2015], exhibit at least second-order continuity in the variations of the empirically recovered values of the state price matrix. This result is instrumental for proving the correctness of any empirical recovery approaches based on nonlinear programming, as it makes it possible to apply the *Karush-Kuhn-Tucker condition*.

In the next section I outline the mathematical and notational preliminaries needed for this continuity theorem by briefly recapping the results from Ross [2015] and then introduce my key theoretical result as a *Recovery Continuity Lemma*.

5.4.1 Continuity of Recovered Discount Factor and Pricing Kernel

As mentioned, to estimate the pricing kernel $\mathbf{D} = (\text{diag}[\mathbf{v}])^{-1}$ and the discount factor δ from empirical data, we must assess the robustness of such estimations to small perturbations of values of \mathbf{Q} . Hence, a desirable result is to determine the second-order continuity δ and \mathbf{v} with respect to the parameters q_{ij} .

To computing the state price transition matrix, we need to specify two operators. Let $\mathcal{N}_Q^{n,n} = \{\mathbf{Q} = (q_{ij}) | 1 > q_{ij} \geq 0\}$ be the set of irreducible matrices. Let the Perron root and Perron vector be defined by the following

two operators:

$$\mathcal{R} := \mathcal{N}_Q^{n,n} \rightarrow \mathbb{R}_+, \quad \mathcal{V} := \mathcal{N}_Q^{n,n} \rightarrow \mathbb{R}_+^n,$$

The strictly maximal eigenvalue for the non-negative and irreducible matrix \mathbf{Q} is termed the Perron root and corresponding eigenvector is referred to as the Perron vector, see Perron [1907], Frobenius [1908] and Vahrenkamp [1976] for a summary. Let the Perron root and (right) Perron vector of \mathbf{Q} be defined by the following operators:

$$\delta = \mathcal{R}(\mathbf{Q}), \quad \mathbf{v} = \mathcal{V}(\mathbf{Q}). \quad (5.9)$$

When needed, I use the subscripts R and L to denote the left and right root and vector, i.e. $\mathbf{v}_L = \mathcal{V}_L(\mathbf{Q})$ and $\mathbf{v}_R = \mathcal{V}_R(\mathbf{Q})$ are the left and right Perron eigenvectors. It should be noted that $\mathcal{V}_L(\mathbf{Q}') = \mathcal{V}_R(\mathbf{Q})$ and $\mathcal{V}_L(\mathbf{Q}) = \mathcal{V}_R(\mathbf{Q}')$. Unless explicitly specified, in the sequel by $\mathcal{V}(\mathbf{Q})$ I denote the right Perron vector.

By construction, I can derive the pricing kernel matrix $\mathbf{D} = (\text{diag}[\mathbf{v}])^{-1}$ such that:

$$\mathbf{D} = (\text{diag}[\mathbf{v}])^{-1} = (\text{diag}[\mathcal{V}_R(\mathbf{Q})])^{-1}, \quad (5.10)$$

and the physical transition matrix \mathbf{P} can then be derived according to Equation (5.8) and in my operator notation is given by:

$$\mathbf{P} = \frac{1}{\mathcal{R}(\mathbf{Q})} (\text{diag}[\mathcal{V}_R(\mathbf{Q})])^{-1} \mathbf{Q} \text{diag}[\mathcal{V}_R(\mathbf{Q})] \quad (5.11)$$

Several useful results from the linear algebra literature demonstrate that the group inverses can be used to provide a higher order perturbation theory for both the Perron root and associated eigenvector. Combining this result with the standard matrix quotient rules I can derive a full perturbation theorem for the discount factor and the pricing kernel for the RT.

Lemma 5.1. C^2 -Continuity of Recovered Discount Factor and Kernel.

Let \mathbf{I}_M be the $M \times M$ identity matrix, let \mathbf{M} be the state price transition

matrix capturing the deviations from the uniform application of the discount factor across all states, i.e. $\mathbf{M} = \delta \mathbf{I}_M - \mathbf{Q}$, and $\mathbf{M}^\#$ be the group inverse of \mathbf{M} .

1. The discount factor $\delta = \mathcal{R}(\mathbf{Q})$ is second-order continuous for variations of the elements of the state price matrix \mathbf{Q} . We have the first and second-order derivatives of the discount factor such that:

$$\begin{bmatrix} \frac{\partial \delta}{\partial q_{ij}} \end{bmatrix} = \text{vec} [(\mathbf{I}_M - \mathbf{M}\mathbf{M}^\#)'], \quad (5.12)$$

$$\begin{bmatrix} \frac{\partial^2 \delta}{\partial^2 q_{ij}} \end{bmatrix} = 2 \cdot \text{vec} [(\mathbf{M}^\#)' \circ (\mathbf{I}_M - \mathbf{M}\mathbf{M}^\#)'] \quad (5.13)$$

where \circ is the Hadamard element by element product and $\text{vec}[\cdot]$ is the stacking operator that stacks by column.

2. The recovered pricing kernel described by the M length vector \mathbf{d} is first-order continuous for variations of the elements of the state price matrix \mathbf{Q} . We have the first-order derivative of the pricing kernel such that:

$$\begin{bmatrix} \frac{\partial d_m}{\partial q_{ij}} \end{bmatrix} = \frac{\mathcal{V}(\mathbf{Q})(\tilde{\mathbf{v}}_{\tilde{c}}' \mathcal{V}_m(\mathbf{Q}) - \tilde{\mathbf{v}}_m' \mathcal{V}_{\tilde{c}}(\mathbf{Q}))}{\mathcal{V}_m^2(\mathbf{Q})} \quad (5.14)$$

where $\tilde{c} = (M + 1)/2$, $\tilde{\mathbf{v}}_m$ is the m row of the matrix formed from $\mathbf{M}^\# \partial \mathbf{Q} / \partial q_{ij}$.

For proof of Lemma 5.1, see A.4.1 and A.4.1 in Appendix A.4. \square

5.4.2 Asymptotic Properties of a Parametric Recovery Theorem

In the sequel, I utilise $\mathbf{\Delta}(\cdot)$ to represent the vector/matrix collection of first-order partial derivatives for a scalar/vector function. The Lemma 5.1 is useful to confirm the continuity of the derivatives rather than to provides actual analytical solutions due to the inherent computational difficulty in computing group inverses. Indeed, in numerical calculations when the first-order derivative of the social discount factor is needed (such as our own

algorithm), Equation (10.1) is far from satisfactory. It is numerically more convenient to use a linear algebra result due to Vahrenkamp [1976] to capture the first derivative of the Perron Root as the outer product of the associated left and right Perron eigenvectors \mathbf{v}_L and \mathbf{v}_R .

$$\begin{bmatrix} \frac{\partial \delta}{\partial q_{ij}} \end{bmatrix} = \text{vec} [\mathbf{v}_L \mathbf{v}'_R] \quad (5.15)$$

It is also possible to use the continuity Lemma to investigate by numerical simulations how different assumptions and probability distributions of the actual state price matrix might impact the recovered social discount factor and the pricing kernel. See for example Borovička et al. [2016] for a discussion of the stochastic nature of the state price matrix.

Example 5.1 (Asymptotic Properties of a Parametric Recovery Theorem). *Suppose the state price matrix $\mathbf{Q} = \mathcal{P}(\boldsymbol{\vartheta})$ is determined by a function such that:*

$$\sqrt{\mathcal{T}}(\tilde{\boldsymbol{\vartheta}} - \bar{\boldsymbol{\vartheta}}) \xrightarrow{d} \mathcal{N}(\mathbf{0}_{\mathfrak{N}}, \Gamma)$$

where $\sqrt{\mathcal{T}}$ is a problem specific attribute, such as a sample characteristic and Γ is an $\mathfrak{N} \times \mathfrak{N}$ positive definite matrix. The vectors $\tilde{\boldsymbol{\vartheta}}$ and $\bar{\boldsymbol{\vartheta}}$ are a realization and the true parameter vector respectively.

Replacing $\mathbf{M}^\# \partial \mathbf{Q} / \partial q_{ij}$ with $\mathbf{M}^\# \partial \mathcal{P}(\boldsymbol{\vartheta}) / \partial \vartheta_\nu$, the asymptotic distribution of the discount factor and pricing kernel can be computed via the Delta method. Setting, $\boldsymbol{\Delta}(\delta) = [\partial \delta / \partial \vartheta_\nu]$ and $\boldsymbol{\Delta}(\mathbf{d}) = [\partial d_m / \partial \vartheta_\nu]$ to be the $\mathfrak{N} \times 1$ vector of derivatives for the discount factor and the $\mathfrak{N} \times M$ matrix of derivatives for the pricing kernel. Hence the asymptotic distributions of the discount factor and pricing kernel maybe given by:

$$\sqrt{\mathcal{T}}(\tilde{\delta} - \bar{\delta}) \xrightarrow{d} \mathcal{N}(0, \boldsymbol{\Delta}(\delta)' \Gamma \boldsymbol{\Delta}(\delta)) \quad (5.16)$$

$$\sqrt{\mathcal{T}}(\tilde{\mathbf{d}} - \bar{\mathbf{d}}) \xrightarrow{d} \mathcal{N}(\mathbf{0}_M, \boldsymbol{\Delta}(\mathbf{d})' \Gamma \boldsymbol{\Delta}(\mathbf{d})). \quad (5.17)$$

I take advantage of this convergence identity in Section 6.2 to conduct a simulation on the consistency of our algorithm under relatively benign identification conditions.

Chapter 6

Hansen-Scheinkman Factorisation and Ross Recovery from High Frequency Option Prices via Nonlinear Programming: The Empirical Recovery

6.1 Empirical Recovery

From the previous chapter we can see that there are three discrete steps to implementing the [RT](#): Step 1 is extracting the state price from observed option price to form the state price matrix \mathbf{S} ; Step 2 is determining the risk-neutral state price transition matrix \mathbf{Q} from \mathbf{S} ; Step 3 is applying the *Perron-Frobenius theorem* to recover the discount factor δ , the pricing kernel \mathbf{D} and the physical transition matrix \mathbf{P} .

Step 1 is the well established problem of estimating the risk-neutral density function extracted from option prices. Step 3 is the application of the *Perron-Frobenius theorem*. Step 2 is the most challenging part, in particular when

the requirements of the Step 2 and Step 3 rely on Step 1 identifying the risk-neutral density with precision, something that has eluded the literature since the original contribution of [Breedon and Litzenberger \[1978\]](#). My approach to integrating Steps 2 and 3 is to presume that Step 1 yields a state price by tenor matrix that is estimated with noise and gaps and therefore Step 2 must be adjusted from straightforward algebra to be robust.

To deal with option prices with gaps, I utilise intraday data to provide a wider coverage of prices and then use the Black-Scholes implied volatility as a device that allows us to determine a continuous polynomial functional form for the implied volatility surface and yield a curve that I can evaluate over arbitrary points to yield the risk-neutral density. Unlike [Ross \[2015\]](#), I impose the risk-free discount rate on the state price, by normalisation of the fitted density and discounting by the current prevailing deposit rate for the particular tenor in question. It should be emphasised that I use the Black-Scholes implied volatility as a normalised price and that our approach is not tied to the assumptions of the Black-Scholes model.

A major issue with any empirical analysis is that real market data, even at the high frequency level, has lots of gaps and it is noisy. The [OPRA](#) data tapes from the [U.S.](#) national market service, are quoted by specific maturity date and strike prices and are rarely in a neatly comparable grid. Directly using the market prices to recover the density function results in a tight balancing exercise: too smooth fitting and the major features of the distribution are lost, too coarse and the calculation of the second-order derivative is ill-defined. Most importantly, is the issue of truncation. Without some functional form to delineate the tail structure near date, tenors will often have major gaps and these will need to be filled in some form to allow us to estimate the state price transition matrix.

Given that the computation of the tails of the risk-neutral density are approximations, relying on the sum of the states is often inaccurate. Indeed [Ross \[2015\]](#) notes that the recovered “risk-free” rates are somewhat away from quoted deposit and swap rates. This issue is discussed at length in [Breedon and Litzenberger \[1978\]](#), [Ait-Sahalia and Lo \[1998\]](#) and [Figlewski \[2008\]](#). The general approach is to normalise the state price to the risk-neutral density and

then discount with the quoted rates and I follow this strategy. My approach is intrinsically linked to the yield curve as I use the implied volatility as a device to smooth the call price as a function of strike and tenor.

Step 2, estimation of the risk-neutral state price transition matrix, is the least comprehensively discussed problem. Several preceding applications have outlined procedures and these have included artificial neural networks, [Audrino et al. \[2014\]](#) and least squares [Ngoc-Khanh and Xia \[2014\]](#). In this section, I use a constrained non-linear least square optimisation algorithm based on the sequential quadratic programming (SQP), where I can formally prove that the resulting minimum form satisfies the desired mathematical and economics constraints (e.g. having a discount factor lower than unity).

I have also tried a number of other strategies for recovering the state price matrix. These include the parametric method of [Song and Xiu \[2016\]](#) amongst others. The major issue is that the approaches are designed to accurately recover the risk-neutral density function over the precise range of strikes for an individual tenor. My approach works also even if the range of traded strikes is unavailable for certain tenors, as found on empirical data.

6.1.1 Procedure Setup

Consider a discrete-time economy with finite state space. The current time is denoted by t and T is the maturity dates of the given option contracts, where $\tau = T - t$ is time to maturity. \mathbf{T} is the vector of available time to maturity (tenors). For any given day, let K be the available strike prices of the options traded during the day and S be the spot prices. I construct the state variables using the log-returns such that $R = \log(K/S)$ and let \mathbf{R} be the vector of available states. $\tilde{\mathbf{S}}$ is the state price matrix estimated by the observed option prices with errors while the true empirical state price matrix is $\bar{\mathbf{S}}$.

6.1.2 Recovering the State Price Matrix Using Intraday Data

In order to determine the state price transition matrix, the state price matrix needs to be built on a uniformly specified states and tensors grid. However, the market data is not always uniformly specified. To tackle this issue, I first build the market realised state price matrix on a grid with states and tensors indexed by the market data. Then, I interpolate the market realised state price matrix on a uniform grid, which is bounded by the minimum and maximum of the market realised grid and equally spaced.

Let $\mathcal{S}_{I \times J}$ be the collection of state price functions $\mathcal{P}_j(\log(K/S))$, where $j \in 1, \dots, J$ is the index of the observed tensors. The collection of functions $\mathcal{P}_j(\log(K/S))$ are parametric approximations of the numerical evaluations of the [Breedon and Litzenberger \[1978\]](#) formulation extracted from market data. My objective is to estimate the $M \times N$ state price matrix denoted $\tilde{\mathbf{S}} = \{\tilde{s}_{mn} : 1 \leq m \leq M, 1 \leq n \leq N\}$ from $\mathcal{S}_{I \times J}$ by interpolation.

I employ a modification of the non-parametric approach of [Ait-Sahalia and Lo \[1998\]](#) and [Figlewski \[2008\]](#) to determine $\mathcal{P}_j(\log(K/S))$. For a given observed tenor τ_j let the collection of call and put prices traded over a day for a given tenor be denoted by $\mathcal{C}_j = \{\mathcal{C}_a(K_i, S_t, \tau_j)\}$ and $\mathcal{P}_j = \{\mathcal{P}_b(K_i, S_t, \tau_j)\}$, where $\{1 \leq a \leq \tilde{A}_j\}$ and $\{1 \leq b \leq \tilde{B}_j\}$ are the index of observed prices per tenor over a day and $\{1 \leq t \leq \tilde{T}\}$ is the index of intraday observations of the spot price.

Let r_j be a deposit rate with maturity close to τ_j quote. My first operation is to recover the implied continuous dividend ς_t for a given pair of put and call options traded at time t , denoted by the tuple $\{\mathcal{C}_a(K_i, S_t, \tau_j), \mathcal{P}_b(K_i, S_t, \tau_j)|t\}$.¹ Once I have the implied continuous dividend I can then compute the Black-Scholes implied volatility for the put and call options $\tilde{\sigma}_a|[K_i/S_t]_a$ and $\tilde{\sigma}_b|[K_i/S_t]_b$. Following convention I utilise the put implied

¹The implied dividend is derived from the put-call parity:

$$\varsigma(K_i, \tau_j) = -\frac{1}{\tau_j} \log \left(\frac{\mathcal{C}_a(K_i, S_t, \tau_j) - \mathcal{P}_b(K_i, S_t, \tau_j) + K_i e^{-r_j \tau_j}}{S_0} \right).$$

volatilities to construct the smoother call prices rather than the calls themselves, see Figlewski [2008] for commentary. I solve numerically for the Black-Scholes implied volatility using a bisection approach in the standard manner from the standard formulation

$$\mathcal{C}_a(K_i, S_t, \tau_j) = S_t e^{-\varsigma\tau} \mathbf{N}(d_1) - K e^{-r\tau} \mathbf{N}(d_2), \quad (6.1)$$

$$\mathcal{P}_b(K_i, S_t, \tau_j) = -S_t e^{-\varsigma\tau} \mathbf{N}(-d_1) + K e^{-r\tau} \mathbf{N}(-d_2), \quad (6.2)$$

where

$$d_1 = \frac{\log S_t/K + (r - \varsigma + \frac{1}{2}\sigma)\tau}{\sigma\sqrt{\tau}}, \quad \text{and} \quad d_2 = d_1 - \sigma\sqrt{\tau}.$$

For each tenor, indexed by j , I have a matched data set of implied volatilities, intraday spot prices and a cross section of strikes $\{\tilde{\sigma}_b, [K_i/S_t]_b\}_j$. Several choices are now available at this juncture, for instance the non-parametric method of Ait-Sahalia and Lo [1998] is very popular. However, for the purpose of building the set of functions in \mathcal{S} I choose to follow in the spirit of Figlewski [2008] and proceed in two steps. First I smooth the implied volatilities by fitting a polynomial function to the implied volatilities over the range $\{\min[\log(K_i/S_t)], \max[\log(K_i/S_t)]\}_j$, I then fit a weighted mixture of log-normals to the smoothed state price imputed from over the range $\{\min[\log(K_i/S_t)], \max[\log(K_i/S_t)]\}_j$.

This procedure is implemented as follows, first I estimate a V -order polynomial for each tenor:

$$\left\{ \tilde{\sigma}_b = \sum_{v=0}^V \beta_v R_b^v + \xi_b, \quad R_b = [\log(K_i/S_t)]_b, \quad \xi_b \sim \mathcal{N}(0, \zeta^2) \right\}_j.$$

I construct a grid with regular intervals $R_g : 1 \leq g \leq G$ over the range $\{\min[\log(K_i/S_t)], \max[\log(K_i/S_t)]\}_j$ of arbitrary precision, in this case I choose G to be five thousand points. Using the estimated polynomial coefficients $\hat{\beta}$ I construct a smooth curve $\tilde{\sigma}_g = \sum_{v=0}^V \hat{\beta}_v R_g^v$.

Setting S_0 to be the median spot price from S_t for the day and ς_0 to be the median continuous implied dividend I build a new range of strikes $K_g = S_0 \exp(R_g)$. Hence I can build a new range of smooth call prices using

the Black-Scholes implied volatility as a fitting device; whereby $\{C_g = \bar{\mathfrak{C}}(\tilde{\sigma}_g, S_0, K_g, r_j, \varsigma_0, \tau_j)\}_j$. I can then apply the [Breedon and Litzenberger \[1978\]](#) result to the smoothed call prices to create the following coordinate system

$$\{R_g, \hat{\mathcal{P}}_j(R_g)\} := \left\{ \log(K_g/S_0), \frac{C_{g-1} + C_{g+1} - 2C_g}{\left[\frac{1}{2}(K_{g-1} - K_{g+1})\right]^2} \right\}_j. \quad (6.3)$$

If each tenor had a regular number of strikes then we could have interpolated out the desired states, in terms of continuous return from the median spot prices S_0 , and moved on to recovering the estimated state price transition matrix $\tilde{\mathbf{Q}}$. Unfortunately, in most cases we need a parametric functional form to generate both the tails and a regular set of states.

A two-stage approach works well in this scenario. Polynomials provide a fast fit over the data range from $\min[\log(K_i/S_t)]$ to $\max[\log(K_i/S_t)]_j$ and provides the overall shape and the trajectory of the tails. However, polynomials are unreliable for extrapolating tails themselves and a parametric representation of the distribution is required. Fitting an integrated form of the mixture distribution directly to the call prices is: (a) slow and (b) highly unreliable in terms of generating a reasonable results. Hence the polynomial approach provides an effective device for computing the central mass of the RND and the parametric distribution is useful for fitting the tails. It is also useful to be able to use the put prices via the implied volatility device as these tend to have a wider range of available strikes from market data, particularly for low strikes.

[Figlewski \[2008\]](#) recommends using a generalised extreme value (GEV) distribution to model the tails and a normal distribution to model the central mass for end of day data. However, empirical testing on intraday data from my sample indicates that a mixture of two or three log-normals provides a fit that matches the available points in the curve and the exit trajectory of the tails from the point the coverage of the range of strikes and intraday spot prices stops far better than the GEV–normal combination.

Let the mixture probability density function be given by:

$$\mathcal{F}(z|\theta) = \sum_{v=1}^V \omega_v \mathcal{F}_v(z|\theta_v), \quad \forall z \in \mathbb{R}, \quad (6.4)$$

where $\mathcal{F}_v(z|\theta_v)$ is the v indexed probability density function with parameter vector θ_v and weighting ω_v and the global parameter vector is $\theta = (\omega_1, \theta'_1, \dots, \omega_V, \theta'_V)'$. The parameter vector θ is estimated via:

$$\left\{ \hat{\theta} \triangleq \arg \min_{\theta} \frac{1}{2} \|\hat{\mathcal{P}}_j(R_g) - \mathcal{F}(K_g|\theta)\|^2 \right\}_j, \quad (6.5)$$

where $\|\cdot\|^2$ is the square of the p-2 norm of a vector (hence the sum of squares), as such, this is a second stage non-linear least squares fitting problem.

Hence, I have a two-step parametric representation of the state price function which is collected up by $\mathcal{S}_{I \times J} = \{\mathcal{P}_j(R) := \{\mathcal{F}(S \exp(R)|\hat{\theta})\}_j\}$. To recover the actual state price state price from the state price function, I first specify the grid of returns corresponding to each state $\mathbf{R}_M = \{R_m : \min R_i \leq R_i \leq \max R_i, 1 \leq m \leq I, R_{(M+1)/2} = 0\}$. I then evaluate $\{\psi_{ij} = \mathcal{P}_j(R_i)\}_j$. The estimated state price for each state is then simply computed from:

$$\hat{s}_{mj} = \frac{\psi_{ij}}{\sum_{i=1}^I \psi_{ij}} e^{-r_j \tau_j}, \quad m \in \{1, \dots, M\}, j \in \{1, \dots, \tilde{J}\}. \quad (6.6)$$

Unfortunately, we have still not quite computed $\tilde{\mathbf{S}} = [\tilde{s}_{mn}]$ as the number of observed tenors \tilde{J} is commonly insufficient or too irregular for the purposes of the RT. We now need to apply one last two dimensional linear interpolation to move from $j \in \{1, \dots, \tilde{J}\}$ observed tenors to $n \in \{1, \dots, N\}$ interpolated tenors.

Let $\tau_{j=A} \leq \tau_n \leq \tau_{j=B}$ with tuples $(\tau_{j=A}, \hat{s}_{mj=A}), (\tau_{j=B}, \hat{s}_{mj=B})$, then the

mn element of the the estimated state price matrix is:

$$\tilde{s}_{mn}^* = \hat{s}_{mj=A} + \frac{\hat{s}_{mj=B} - \hat{s}_{mj=A}}{\tau_{j=B} - \tau_{j=A}}(\tau_n - \tau_{j=A}), \quad (6.7)$$

$$\tilde{s}_{mn} = \frac{\tilde{s}_{mn}^*}{\sum_{i=1}^I \tilde{s}_{mn}^*} e^{-r_n \tau_n}, \quad m \in \{1, \dots, \tilde{M}\}, n \in \{1, \dots, N\}, \quad (6.8)$$

and as such, we finally have $\tilde{\mathbf{S}} = [\tilde{s}_{mn}]$. The second normalisation corrects any distortions to $\tilde{\mathbf{S}} = [\tilde{s}_{mn}]$ caused by the linear interpolation to the uniform grid of tenors indexed by $n \in \{1, \dots, N\}$.

6.1.3 Determining the Risk Neutral State Price Transition Matrix

To ensure clarity within the following discussion I specify a series of naming conventions for a discrete time Markov chain I follow [Norris \[1998\]](#) for my definitions. Let $\mathbb{Q}[A]$ be the probability of an event A and \mathcal{M} be a Markov chain, with countable state space $x \in \mathcal{X}$. Let X_0, X_1, \dots be a sequence of random variables and let $\mathcal{H}_{t-1} \cap_{h=0}^{t-1} \{X_s = x_s\}$ be the history of events satisfying $\mathbb{Q}[\mathcal{H}_{t-1} \cap \{X_s = x_s\}]$ hence for a pair of states $x_a \in \mathcal{X}$ and $x_b \in \mathcal{X}$, then

$$\mathbb{Q}[X_{t+1} = x_b | \mathcal{H}_{t-1} \cap \{X_t = x_a\}] = \mathbb{Q}[X_{t+1} = x_b | X_t = x_a] = q(x_a, x_b),$$

which I denote by short hand as q_{ab} . The matrix of transitions between all states in $x_i \in \mathcal{X}$, is denoted by a bold latin letter, for instance \mathbf{Q} . For the $\kappa \in \mathbb{N}^+$ forward step, the κ transition matrix is denoted $\mathbf{Q}_\kappa \equiv [q_{ab,\kappa}] = \mathbf{Q}^\kappa$.

A Irreducible – a state b is accessible from any other state a after a finite number of κ steps, hence the probability of transitioning from a to b at the κ step, denoted $q_{ab,\kappa} > 0$, for an integer step $\kappa > 0$. Hence a state transition matrix \mathbf{Q} is irreducible if for a finite $\kappa \in \mathbb{N}^+$, $q_{ab,\kappa} > 0, \forall x_a, x_b \in \mathcal{X}$. That is the matrix \mathbf{Q} describes a strongly connected graph.

B *A-periodic* – Let $\mathcal{T}[x_a] \triangleq \{t \geq 1 : q_{aa,t} > 0\}$ be the set of times when it is possible for the chain to return to a starting position x_a , the period of \mathcal{M} is defined as the greatest common divisor (gcd) of $\mathcal{T}[x_a]$. If \mathcal{M} is an irreducible Markov chain then $\text{gcd } \mathcal{T}[x_a] = \text{gcd } \mathcal{T}[x_b]$, $\forall \{x_a, x_b \in \mathcal{X}\}$. If $\text{gcd } \mathcal{T}[x] = 1$, $\forall \{x \in \mathcal{X}\}$ then \mathcal{M} is termed a-periodic.

C *Ergodic* – For an irreducible Markov chain \mathcal{M} , let $\mathbb{Q}\{\lim_{t \rightarrow \infty} t^{-1} \sum_{h=0}^{t-1} \mathbf{1}_{X_a=x} = \pi[x]\} = 1$, the quantity $\pi[x]$ is the proportion of time that \mathcal{M} spends in state $x \in \mathcal{X}$. If \mathcal{M} has a unique invariant measure $\pi[x]$, then \mathcal{M} is an ergodic Markov chain.

D *Mixing* – Suppose that \mathcal{M} is an irreducible and aperiodic Markov chain, let $\tilde{\sigma}$ be a limiting distribution.

$$\max_{\{x, x_a\} \in \mathcal{X}} 1/2 \sum_{x \in \mathcal{X}} |q_{xx_a,t} - \tilde{\sigma}| \leq \Psi \psi^t,$$

where $\Psi > 0$ and $\psi \in (0, 1)$ are constants. For a given pair of constants Ψ^* and ψ^* the corresponding time t^* is termed the ‘mixing’ time and the Markov chain \mathcal{M} is termed a ‘mixing’ Markov chain.

E *Unimodality* – For a Markov chain \mathcal{M} , strong diagonal dominance is where $q_{aa} > q_{ab}$, $\forall x_a \neq x_b \in \mathcal{X}$. Strict diagonal unimodality imposes that for an arbitrary ordering of states $x_1 < x_2 \dots, x_M$ the following conditions for a collection of ordered states $\{x_a, x_b, x_c\} \in \mathcal{X}$ and hence $\{a, b, c\} \in \{1, \dots, M\}$:

$$q_{ab} \begin{cases} > q_{ac}, & \text{if } b > a \ \& \ c > b \\ < q_{ac}, & \text{if } b < a \ \& \ c < b \end{cases}, \quad \text{and} \quad q_{ab} \begin{cases} > q_{cb}, & \text{if } b > a \ \& \ c > a \\ < q_{cb}, & \text{if } b < a \ \& \ c < a \end{cases}$$

F *Sub-stochastic* a Markov chain \mathcal{M} is sub-stochastic if for the transition matrix \mathbf{Q} , every element of the vector $[a_m] := \mathbf{a} = \mathbf{Q}\mathbf{1}_{M \times 1}$, is in the range $0 < a_m < 1, \forall m \in \{1, \dots, M\}$.

With the current set-up in mind, we can specify the Markov chain that connects the actual vector of states $\bar{\mathbf{s}}_{n+1}$ to the preceding state $\bar{\mathbf{s}}_i$, via the true

state transition time-homogenous matrix $\mathbf{Q} \in \mathcal{N}^{n,n}$, such that

$$\bar{\mathbf{s}}_{n+1} = \bar{\mathbf{Q}}\bar{\mathbf{s}}_n, \quad \forall i \in \{1, \dots, M\}, \quad (6.9)$$

We do not observe the true state price matrix $\bar{\mathbf{S}}$, but the noisy approximation $\tilde{\mathbf{S}}$ from the preceding step. Hence, directly solving for $\bar{\mathbf{P}}$ from $\bar{\mathbf{S}}$ is infeasible as I illustrated in Section 5.3. In fact, we could solve for $\tilde{\mathbf{Q}}$ from $\tilde{\mathbf{S}}$ within a constrained optimisation programming process. Through necessity, we need to find a minimum distance between $\sum_i \|\tilde{\mathbf{s}}_{n+1} - \tilde{\mathbf{Q}}\tilde{\mathbf{s}}_n\|^2$ subject to the constraints that ensure that $\tilde{\mathbf{Q}}$ describes a Markov chain with the desired properties.

Essential Constraints on $\tilde{\mathbf{Q}}$

Constraints E.1 to E.3 ensure that $\tilde{\mathbf{Q}}$ describes a Markov process:

E.1 $\tilde{\mathbf{Q}}$ is irreducible.

E.2 $\tilde{\mathbf{Q}}$ is sub-stochastic. The progression of the sum of the risk-neutral state price describes the equivalent discount on a risk free asset, $\sum_m \tilde{\mathbf{Q}}\mathbf{s}_n = \exp(-r_{n+1}\tau_{n+1}) \equiv \sum_m \mathbf{s}_{n+1}$.

E.3 The elements of $\tilde{\mathbf{Q}}$, q_{ij} are in the domain, $0 \leq q_{ij} < 1$.

Economically Meaningful Constraints on $\tilde{\mathbf{Q}}$

The following constraints are desirable in terms of the subsequent implications for asset pricing:

D.4 $\tilde{\mathbf{Q}}$ is unimodal, about the diagonal.

D.5 The largest eigenvalue of $\tilde{\mathbf{Q}}$ with a non-negative eigenvector is less than unity.

D.6 The Markov chain described by $\tilde{\mathbf{Q}}$ is aperiodic (redundant if E.2 is imposed).

Constraints E.2, E.3 and D.4 can be imposed as linear constraints, whilst E.1, D.5 and D.6 result in a non-linear constraint for determining $\tilde{\mathbf{Q}}$.

Let \mathbf{S}_1 and \mathbf{S}_0 be the subsets of the $M \times N$ state price matrix \mathbf{S} respectively, such that:

$$\mathbf{S}_1 = [\mathbf{s}_2, \dots, \mathbf{s}_N]; \quad \mathbf{S}_0 = [\mathbf{s}_1, \dots, \mathbf{s}_{N-1}].$$

The basic case is when $N = M + 1$, thus both \mathbf{S}_1 and \mathbf{S}_0 are in size $M \times M$. I now specify the vector $\mathbf{s}_0 = \text{vec}[\mathbf{S}_0]$ and $\mathbf{s}_1 = \text{vec}[\mathbf{S}_1]$. Let $\mathbf{G} = [\mathbf{s}'_n \otimes \mathbf{I}_M]_{n=1, \dots, N-1}$ be the $M^2 \times M^2$ matrix of lagged states, where \mathbf{I} is a matrix with unity on the diagonals. Setting $\mathbf{x} = \text{vec}[\mathbf{Q}]$, the vectorised optimisation is now of the following form:²

SQP Identification of the State Price Transition Matrix

$$\hat{\mathbf{Q}} = \text{mat}[\hat{\mathbf{x}}], \quad \hat{\mathbf{x}} = \arg \min_{\mathbf{x}} \frac{1}{2} \|\mathbf{G}\mathbf{x} - \mathbf{s}_0\|^2,$$

$$\text{s.t.} \begin{cases} \mathbf{A}\mathbf{x} \leq \mathbf{0}_{2M(M-1) \times 1} & \text{D.4} \\ \mathbf{B}\mathbf{x} = \mathbf{b}_{M \times 1} & \text{E.2} \\ \mathbf{0}_{M \times 1} \leq \mathbf{x} \leq \mathbf{e}_M & \text{E.3} \\ \mathcal{R}(\text{mat}(\mathbf{x})) - 1 \leq 0 & \text{D.5} \\ \mathcal{Q}(\text{mat}[\mathbf{x}]) < 0 & \text{E.1} \end{cases} \quad (6.10)$$

The matrix \mathbf{A} is of dimension $2M(M - 1) \times M^2$ and imposes the row and column-wise unimodality constraint on $\text{mat}[\mathbf{x}]$ and hence $\hat{\mathbf{Q}}$. $\mathbf{e}_{(M+1)/2}$ represents a null vector except for element $(M + 1)/2$ which is one. The matrix \mathbf{B} is of dimension $M \times M^2$ and imposes the summation constraint that $\sum_m \mathbf{s}_{n+1} = \sum_m \hat{\mathbf{Q}}\mathbf{s}_n$. The non-linear constraint $\mathcal{R}(\text{mat}(\mathbf{x})) - 1 \leq 0$ imposes (a) the existence of the Perron root of $\text{mat}(\mathbf{x})$ and (b) that the root is less than unity, hence is a valid discount factor. Finally, $\mathcal{Q}(\text{mat}[\mathbf{x}]) < 0$ imposes the irreducibility condition. I will approach the constraints in order of complexity.

²Following the convention in non-linear programming, see [Fletcher \[1971\]](#), I set out the optimisation in the following order, linear inequality constraints, linear equality constraints, variable domains and non-linear inequality constraints.

Imposing Unimodality – D.4, Linear Inequality Constraint

The precise form of \mathbf{A} depends on the stacking operation of $\text{vec}[\cdot]$. Following the convention in econometrics, I assume that the $\text{vec}[\cdot]$ operator stacks by column. The matrix \mathbf{A} is constructed in two parts \mathbf{A}_r and \mathbf{A}_c for the rows and column unimodality restrictions respectively. Set $\mathbf{A}_{ru} = \text{trimr}_M[\mathbf{I}_M + \text{diag}_1[-\mathbf{e}_{M-1}]]$, where $\text{diag}_w[\cdot]$ is the operator that transforms a vector into a matrix with the elements of the vector placed on the w upper diagonal and $\text{trimr}_W[\cdot]$ trims the row or collection of rows W from a matrix or a vector. Hence \mathbf{A}_{ru} is of the following form:

$$\mathbf{A}_{ru} = \begin{pmatrix} 1 & -1 & 0 & \cdots & 0 & 0 \\ 0 & 1 & -1 & \cdots & 0 & 0 \\ \vdots & \vdots & \vdots & \ddots & \vdots & \vdots \\ 0 & 0 & 0 & \cdots & 1 & -1 \end{pmatrix}. \quad (6.11)$$

The matrix \mathbf{A}_r is constructed by placing combinations of \mathbf{A}_{ru} and \mathbf{A}_{rl} on the block diagonal. Let $\mathbf{A}_{rm} = [\text{trimr}_{m,\dots,M-1}[\mathbf{A}_{ru}]', \text{trimr}_{1,\dots,m-1}[-\mathbf{A}_{ru}]']'$, then \mathbf{A}_r is:

$$\mathbf{A}_r = \begin{pmatrix} \mathbf{A}_{r1} & \mathbf{0} & \cdots & \mathbf{0} \\ \mathbf{0} & \mathbf{A}_{r1} & \cdots & \mathbf{0} \\ \vdots & \vdots & \ddots & \vdots \\ \mathbf{0} & \mathbf{0} & \cdots & \mathbf{A}_{rM} \end{pmatrix}. \quad (6.12)$$

The column-wise unimodality constraint is similar, albeit the restrictions are now in front to back blocks. Set $\mathbf{A}_{cu} = \text{trimr}_M[\mathbf{I}_M \otimes \mathbf{e}_{c,m} + \text{diag}_m[\mathbf{e}_{M-1}] \otimes -\mathbf{e}_{c,m}]$, where $\mathbf{e}_{c,m}$ is an $M - 1$ null vector with the m element set to unity. Similarly to the row-wise restriction the I set $\mathbf{A}_{cm} = [\text{trimr}_{m,\dots,M-1}[\mathbf{A}_{cu}]', \text{trimr}_{1,\dots,m-1}[-\mathbf{A}_{cu}]']'$. The blocks are then stacked one on top of the other as follows:

$$\mathbf{A}_c = \begin{pmatrix} \mathbf{A}_{c1} \\ \mathbf{A}_{c2} \\ \vdots \\ \mathbf{A}_{cM} \end{pmatrix}. \quad (6.13)$$

The matrix \mathbf{A} is then formed via vertical concatenation of the two matrices \mathbf{A}_r and \mathbf{A}_c hence $\mathbf{A} = [\mathbf{A}'_r, \mathbf{A}'_c]'$. This leads us to my first proposition.

Proposition 6.1 (Unimodality of the State Transition Matrix). *An optimisation $\min_{\mathbf{x}} \frac{1}{2} \|\mathbf{G}\mathbf{x} - \mathbf{s}_0\|_2$ that attains a minima with vector $\hat{\mathbf{x}}$ and satisfies the constraint $\mathbf{A}\mathbf{x} \leq \mathbf{0}_{2M(M-1)}$ results in an estimated state transition matrix $\hat{\mathbf{Q}} = \text{mat}[\hat{\mathbf{x}}]$ that is row and column-wise unimodal.*

For proof for Proposition 6.1 see A.4.2 in Appendix A.4. \square

Preserving the Risk Free Discount Path – E.2, Linear Equality Constraint

Constraint E.2 preserves the term structure of the risk free rates that yield the cost of an asset that pays off in all states. As noted, the risk-neutral state price transition matrix $\hat{\mathbf{Q}}$ needs to preserve the term structure of the risk-free rate and hence the sub-stochastic Markov chain is described by a state price matrix $\hat{\mathbf{S}}$ with columns whose sum determines the discount factors from the yield curve. Hence, for a sum over the j rows for a column \mathbf{s}_n , is denote $\sum_j \mathbf{s}_n$:

$$\sum_j \hat{\mathbf{Q}} \tilde{\mathbf{s}}_n = e^{-R_{i+1}\tau_{i+1}} = \sum_j \tilde{\mathbf{s}}_{n+1}, \forall i \in \{1, \dots, M\}.$$

One can also at the $i = 0$ constraint, whereby $\mathbf{s}_0 = \mathbf{e}$, where \mathbf{e} is a null vector except for the middle element (the current state) which is equal to unity. In practice, this does not matter unless (a) the yield curve is initially very steep and (b) the number of states is such that from time τ_0 to τ_1 is long enough that the yield is sufficiently different from τ_1 to τ_2 to generate a substantial error.

Let \mathbf{B} be a matrix and \mathbf{b} be a target vector such that the equality constraint $\mathbf{B}\mathbf{x} = \mathbf{b}$. The column sum of the forward shift matrix \mathbf{S}_1 maybe expressed by $\mathbf{b} = \mathbf{1}'\mathbf{S}_1$, where $\mathbf{1}$ is a unit column vector of length M . The matrix summation for the columns within the vector $\mathbf{x} = \text{vec}[\mathbf{Q}]$ is given by:

$$\mathbf{B} = [\mathbf{1}' \otimes \mathbf{s}'_n]_{n \in \{1, \dots, M\}}.$$

Hence, a sufficient condition for the constraint $\sum_j \hat{\mathbf{P}} \tilde{\mathbf{s}}_n = \sum_j \tilde{\mathbf{s}}_{n+1}$, $\forall i \in \{1, \dots, M\}$ to hold is if $\mathbf{B}\mathbf{x} = \mathbf{b}$. The proof is trivial and can be shown by the fact that for a given column n in \mathbf{S}_1 , the corresponding $1 \times M^2$ row vector in \mathbf{B} given by $\mathbf{1}' \otimes \mathbf{s}'_n$, when matrix multiplied by the $M^2 \times 1$ column vector \mathbf{x} is the equivalent to the double sum $\sum_i \sum_j \hat{q}_{ij} s_{m=i,n}$, where \hat{q}_{ij} is the ij element of $\hat{\mathbf{Q}}$. This leads to my second proposition³.

Proposition 6.2 (Sub-stochasticity of the State Price Transition Matrix). *An optimisation $\min_{\mathbf{x}} \frac{1}{2} \|\mathbf{G}\mathbf{x} - \mathbf{s}_0\|_2$ that attains a minima with vector $\hat{\mathbf{x}}$ and satisfies the constraint $\mathbf{B}\mathbf{x} = \mathbf{b}$ results in an estimated state transition matrix $\hat{\mathbf{Q}} = \text{mat}[\hat{\mathbf{x}}]$ that is sub-stochastic.*

For proof for Proposition 6.1 see A.4.3 in Appendix A.4. □

Irreducibility – E.1, Nonlinear Inequality Constraint

If the initial construction of $\tilde{\mathbf{S}}$ does not have any rows such that the elements of $\mathbf{1}_{N \times 1} \tilde{\mathbf{S}}'$ are numerically indistinguishable from zero then we empirically found the resulting estimated $\hat{\mathbf{Q}}$ to be usually irreducible. However, it is not guaranteed and it is important to check this property, especially if the subsequent constraint on the Perron root is not imposed.

The traditional approach for irreducibility is to test the strong connectedness of the graph whose adjacency matrix is constructed by replacing every element greater than 0 in \mathbf{Q} with 1. The elements $q_{ij,\kappa}$ of the κ -power of the matrix \mathbf{Q}^κ corresponds to the connectedness of the two elements after κ steps. Hence, if we can find some $\kappa < \infty$, such that $q_{ij,\kappa} > 0$, $\forall i, j \in \{1, \dots, M\}$ then \mathbf{Q} would be irreducible.

By itself this condition is only sufficient and not necessary. The square matrix $\begin{pmatrix} 0 & 1 \\ 1 & 0 \end{pmatrix}$ is the simplest counterexample of an irreducible matrix in which for any power κ there are always some elements that are zero. To achieve a necessary and sufficient condition one would need to test whether

³It is important to note that the ordering of the Kronecker product, in many econometric applications the matrices are Hermitian, hence vectorised sums are often, although not always, symmetrical.

$(\mathbf{Q} + \mathbf{I}_M)^k$ was larger than zero. However, Proposition 6.1 guarantees that the matrix is unimodal and therefore the elements of the diagonal are always non zero. Hence, when replacing every element greater than 0 with 1, the matrix \mathbf{Q} and the matrix $\mathbf{Q} + \mathbf{I}_M$ would generate exactly the same adjacency matrix.

From graph theory we know that the longest path for M states is long at most M steps and then we can set out a non-linear constraint as follows:

$$\mathcal{Q}(\text{mat}[\mathbf{x}]) = -\text{vec}[\mathbf{Q}^M] < \mathbf{0}_{M^2 \times 1}, \quad \mathbf{Q} = \text{mat}[\mathbf{x}], \quad (6.14)$$

with the following first-order derivative:

$$\frac{\partial \mathcal{Q}(\text{mat}[\mathbf{x}])}{\partial \mathbf{x}'} = \frac{d(\mathbf{Q}^{M-1}\mathbf{Q})}{d\mathbf{Q}} \equiv (\mathbf{Q}' \otimes \mathbf{I}_M) \frac{d\mathbf{Q}^{M-1}}{d\mathbf{Q}} \equiv \sum_{j=1}^M (\mathbf{Q}')^{M-j} \otimes \mathbf{Q}^{j-1}, \quad (6.15)$$

which is an $M^2 \times M^2$ matrix of gradients.

Proposition 6.3 (Irreducibility of the State Transition Matrix). *An optimisation $\min_{\mathbf{x}} \frac{1}{2} \|\mathbf{G}\mathbf{x} - \mathbf{s}_0\|_2$ that attains a minima with vector $\hat{\mathbf{x}}$ and satisfies the constraint $\mathcal{Q}(\text{mat}[\mathbf{x}]) = \text{vec}[\mathbf{Q}^M] > \mathbf{0}_{M^2 \times 1}$ is a necessary and sufficient condition for the unimodal state transition matrix \mathbf{Q} to be irreducible.*

The proof for Proposition 6.3 follows from the preceding text. □

In practice, this number of non-linear constraints and derivatives is very high and significantly slows down the algorithm. What I found to be practically more effective is to run the algorithm without this constraint and simply compute the M -th power of the estimated matrix and test whether $\hat{q}_{ij,M} > 0, \forall i, j \in \{1, \dots, M\}$. If the test succeeds, then by Proposition 6.3 the estimated matrix $\hat{\mathbf{Q}}$ is irreducible. In the rare cases when the test failed, then one can re-run the algorithm by adding the irreducibility constraint.

The Existence and Domain of the Perron Root – D.5, Nonlinear Inequality Constraint

The [RT](#) relies on the Perron root of the risk-neutral state price transition matrix \mathbf{Q} being a discount factor that ensures $\mathbf{P}\mathbf{1} = \mathbf{1}$. As we do not directly observe \mathbf{Q} , but its estimated analogue $\hat{\mathbf{Q}}$, we can utilise resulting Perron root in the optimisation to assist in identification of the physical real world state transition matrix \mathbf{P} . The obvious constraint is on existence: the Perron root is real and positive. We can go further and impose δ to be less than unity as would be economically meaningful such that:

$$\delta = \mathcal{R}(\text{mat}(\mathbf{x})) \leq 1, \quad \mathbf{Q} = \text{mat}[\mathbf{x}], \quad (6.16)$$

For this constraint to hold, we need an algorithm to compute both the actual root and the first and the second-order derivatives of $\mathcal{R}(\text{mat}(\mathbf{x}))$ as functions of \mathbf{x} . The key intuition behind my successful approach is to decouple the actual computation of the Perron's root from the computation of a closed form of its first-order and second-order derivatives.

For the latter two, the correctness of the [SQP](#) algorithm requires their existence and the continuity Lemma 5.1 does precisely that: Equation 5.12 and Equation 5.13 guarantees respectively that for $\mathbf{x} = [\vec{\mathbf{Q}}]$ the first-order derivative $\partial\mathcal{R}(\text{mat}(\mathbf{x}))/\partial x$ and the second-order derivative $\partial^2\mathcal{R}(\text{mat}(\mathbf{x}))/\partial x^2$ exist and are continuous. Hence the satisfaction of the Karush-Kuhn-Tucker condition for the [SQP](#) minimisation problem guarantees that the minimum $\hat{\mathbf{Q}}$ also has a discount factor $\hat{\delta} \leq 1$. I provide the full steps of the of the [SQP](#) process in the optimisation system with the constraint on the discount factor D.5 in [A.4.4](#) in Appendix [A.4](#).

6.1.4 An Empirically Identified Recovery Theorem

Given the perturbation theory stated in Lemma 5.1 and the propositions derived from the [SQP](#) process for determining the state price transition matrix, I can finally obtained a *Realised Recovery Theorem* that is uniquely identified, i.e. that the identification of the state transition matrix can be

solved in closed-form and the derived discount factor, pricing kernel and physical transition matrix satisfy both the constraints embedded in the Markov process of the underlying assets and the constraints that maintain the economically meaningful results of the Recovery Theorem.

The result below combines Ross' Theorem 1 with the continuity Lemma 5.1 and Proposition 6.1 through Proposition 6.3.

Theorem 6.1 (An Empirical Recovery). *The discount factor δ , pricing kernel \mathbf{D} and the physical state transition matrix \mathbf{P} of the asset prices can be uniquely identified from the state price by tenor matrix \mathbf{S} through the risk-neutral state transition matrix \mathbf{Q} obtained by the minimisation of the optimisation constraints in (6.10) that attains a minima which, by construction, is row-wise and column-wise unimodal; sub-stochastic; irreducible; with a discount factor that is less than unity and a decreasing pricing kernel.*

Proof follows sequentially from the original RT and the proof of our perturbation theorem and the steps are detailed in proceeding sections. \square

In Ross [2015], a worked example of applying the RT using a snapshot of one day data is outlined. In this case the RT is estimated on an over the counter (hereafter OTC) dataset that has a full set of strikes for coverage and a very regular quarterly term structure. OTC data of this type is typical in FX options and some bond options. One interesting point is that whilst the pricing kernel recovered from the OTC follows a CRRA kernel very precisely, the discount factor is greater than unity, by a quite considerable amount. For the same day, I use OPRA data and the constraint above to yield a closer fit to the state price by tenor matrix, with a kernel that is less than unity. For this I end up with a pricing kernel that is more-or-less 'U-shaped', see the following sections for an extensive exploration.

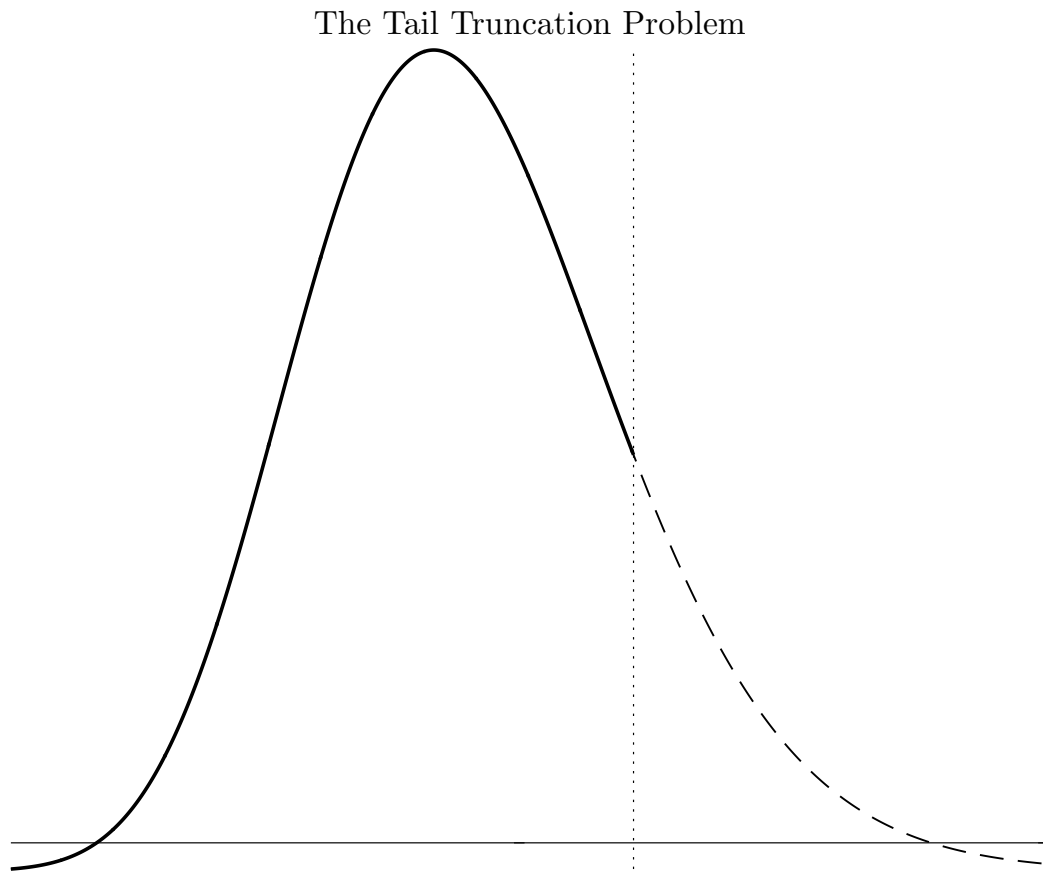
Various alternative approaches to recovering the pricing kernel, for instance by non-parametric regression on the cross section of asset prices or by use of both spot and option markets commonly yield a 'U-shaped' kernel, a classic recent example is from Song and Xiu [2016], which has a full parametric specification for the density function. Hence, whilst I have a potential restriction from the main perturbation theorem for the pricing

kernel (either parametrically or non-parametrically) I do not impose a [CRRA](#) (decreasing parabolic) shape to it.

6.1.5 Additional Issues for Numerical Implementations

There are a number of issues that stems from the numerical implementation. At first, the constraints on a-periodicity are useful when setting arbitrary ranges for the states. The primary motivation stems from the issue of tail truncation at longer maturities, leading to state price matrices $\tilde{\mathbf{S}}$ which are overly sparse. Numerical issues can occur when numerous points at the tail effectively generate rows in $\tilde{\mathbf{S}}$ that ‘close’ to zero. By ‘close’ I generally refer to the minimum absolute differences in [IEEE](#) defined double precision arithmetic between two numbers before they are considered identical at that precision. On a 64bit computer this is around $2.2204e-16$.

Figure 6.1: Extrapolating the Tail of the Option Implied Risk Neutral State Price.



Notes: This plot presents a summary of the (upper) tail truncation problem. The continuous black line represents the risk-neutral density, computed using the [Breedon and Litzenberger \[1978\]](#) approach, of a long tenor option (presumed to have widest range of strikes). The vertical dotted line represents the highest traded strike. The dotted line represents the best fitting parametric curve, presumed to be a weighted mixture of up to three lognormal distributions. The exit trajectory of the risk-neutral prices at the exit point represents the best guess for the direction and mass of the tail. From the point of view of the Recovery Theorem it is critical to a) identify a numerical cut-off point where the tail is not numerically equal to zero, resulting in a row of the state price matrix $\tilde{\mathbf{S}}$ numerically equal to zero. The horizontal line represents the choice of cut-off, I choose this to be the square root of the smallest difference that distinguishes two floating point numbers, as this permits most forms of mathematical operation to be performed without return a zero.

Figure 6.1 outlines the problem of tail truncation at longer tenors. Here, the distribution is truncated prior to approaching the right tail, with this also being the highest available strike. Hence, the terminal state that will be

defined by the vertical dotted line, will still have substantial probability mass to the right. Thus, the choice of range of states matters. Choosing upper bounds where the dotted curve is below the lower horizontal line (presumed to be an appropriately sized small number, for instance the square root of the smallest double precision number, to allow for cross products in the subsequent matrix operations).

Another issue that is hampered by numerical considerations is the direct construction of the Hessian for the SQP. The exact SQP algorithm that solves the non-linear programming problem outlined in (6.10) requires that both the first and second-order derivatives be continuous and that the objective function is convex. The first requirement is obvious from the choice of objective function and follows from the standard linear algebra arguments. I have carefully identified the derivatives of the constraint and the pricing kernel. As such I have a functional form for the second-order derivatives of the Perron Root and hence once could, in theory directly compute the Lagrangian of the optimisation problem and solve directly using Newton's method. However, the exact form of the second-order derivative can only be computed using the group inverse, as in Equation (10.13).

Numerical testing of the stability of several group inverse algorithms suggests that as the number of states increases the level of error in the resulting group inverse can rise substantially (after 20-30 states basically being pure noise). In contrast, the first-order derivative of the Perron-Root evaluated from the cross product of the left and right Perron vector, denoted $\mathbf{v}_L \mathbf{v}'_R$, is numerically more robust to an increasingly large number of states. Hence, I suggest using finite differencing to numerically approximate the second-order derivative of the Perron root. For small numbers of states the speed difference between implementation of the group inverse versus numerical approximation via finite differencing (as long as the gradients are specified) is negligible. With the functional forms of the gradients, numerical methods such as the Broyden Fletcher Goldfarb Shanno algorithm are very quick even for large numbers of states and the fact that the first derivatives are already identified results in a very fast solver.

6.2 Simulation

To test the internal consistency of my algorithm I generate simulated option data and then fit our algorithm to a repeated trails of randomly perturbed data. My baseline simulation presumes that $h_{ij} = 1$ and hence there is no martingale component to the stochastic discount factor. I first presume that the correct number of states is known a-priori, hence the simulation conditions are assumed to be correctly specified. I then provide a sensitivity analysis of my algorithm when the number of states is unknown a-priori.

6.2.1 A-priori Known Number of States

In this part, I presume that the correct number of states is known a-priori, hence the simulation conditions are assumed to be correctly specified. I start with a physical probability transition matrix \mathbf{P} with 13 states. To generate the matrix I apply the following procedure to generate a physical probability matrix with approximately exponential decay:

1. Start with an identity matrix $\mathring{\mathbf{P}}_0 = \mathbf{I}_{13}$.
2. For each successive diagonal $k \in \{1, \dots, 12\}$ such that $\mathring{\mathbf{P}}_k + \text{diag}_{\kappa}[\exp(-b\kappa\mathbf{1}_{13-\kappa}) + a] + \text{diag}_{-\kappa}[\exp(-b\kappa\mathbf{1}_{13-\kappa}) + a]$, where $\mathbf{1}_{\kappa}$ is a unit vector of length κ .
3. I then set: $\bar{\mathbf{P}}_0 = \mathring{\mathbf{P}}_0$, and $\bar{\mathbf{P}}_{r1} = [\hat{\mathbf{p}}'_{rj1}]_1$ and $\bar{\mathbf{P}}_{c1} = [\hat{\mathbf{p}}_{ci1}]_1$ are the j row and i column respectively.
4. I then normalise the rows and columns $[\hat{\mathbf{p}}'_{rj1}]_1$ and $[\hat{\mathbf{p}}_{ci1}]_1$ and compute sequentially $\hat{\mathbf{p}}'_{rj2} = \hat{\mathbf{p}}'_{rj1}(\hat{\mathbf{p}}'_{rj1}\mathbf{1})^{-1}$ and $\hat{\mathbf{p}}_{cj2} = \hat{\mathbf{p}}_{cj1}(\hat{\mathbf{p}}'_{cj1}\mathbf{1})^{-1}$.
5. I then repeatedly compute (3) until $1 - \hat{\mathbf{p}}'_{rj\kappa}(\hat{\mathbf{p}}'_{rj\kappa}\mathbf{1})^{-1} = 0$ and $1 - \hat{\mathbf{p}}'_{cj\kappa}(\hat{\mathbf{p}}'_{cj\kappa}\mathbf{1})^{-1} \leq \epsilon$, where ϵ is the smallest floating point integer.

The above algorithm converges to an approximate doubly stochastic matrix in less than 50 to 100 iterations depending on the parameters a and b . For our purposes I set both to unity.

I then specify a vector of 13 states with returns $R_i = \log(S_T/S_t)$ ranging from $-1/2$ to $1/2$. I set $\bar{\mathbf{D}} = \text{diag}[\bar{\mathbf{d}}]$, with elements $\bar{\mathbf{d}} = [\bar{d}_i]$. Given an iso-elastic utility function with $c(t) = 1$ and $c_i(T) = \exp(R_i)$ for state i , with constant relative risk aversion coefficient $\gamma = 1.25$, hence if $u(c) = (c^{1-\gamma} - 1)/(1 - \gamma)$ for $\gamma \neq 1$ and $u(c) = \log(c)$ for $\gamma = 1$, then the kernel simplifies to $d_i = \exp(-\gamma R_i)$, I denote the constant relative risk aversion (CRRA) kernel to be $\text{CRRA}(\gamma) = (U'(c(T)))/(U'(c(t)))$. Setting $\bar{\delta} = 0.994$, I generate $\bar{\mathbf{Q}}$ by $\bar{\mathbf{Q}} = \bar{\delta}\bar{\mathbf{D}}^{-1}\bar{\mathbf{P}}\bar{\mathbf{D}}$ and hence the simulated state price matrix by tenor $\bar{\mathbf{S}}$ according to:

$$\bar{s}_{n+1} = \bar{\mathbf{Q}}\bar{s}_n.$$

To generate the option prices, I interpolate a series of strikes $\bar{K}_m = \exp(R_m)$ and risk-neutral state price $\bar{\mathbf{S}}_m$ from the 13 states using a cubic spline. I set $m \in \{1, \dots, 1001\}$ then numerically evaluate the double surface integral using trapezoidal integration, where $\mathcal{G}(K)$ is $-K$ hence:

$$\bar{C}(K) = \oint_{\mathcal{G}(K_m)} \oint_{\mathcal{G}(K_m)} \bar{s}_m d\bar{K}_m d\bar{K}_m, \quad (6.17)$$

which is the direct inverse of the [Breedon and Litzenberger \[1978\]](#) procedure. The computed normalised call prices are hence computed directly from the simulated state price.⁴ I then draw the following call prices for the simulation:

$$C_\beta(K) = \bar{C}(K)e^{\xi_\beta}, \quad \xi_\beta \sim \mathcal{N}(0, \hat{\sigma}^2), \quad (6.18)$$

for $\beta \in \{1, \dots, 499\}$ and compute estimates of $\hat{\mathbf{Q}}_\beta$ and subsequently $\hat{\mathbf{P}}_\beta$, $\hat{\mathbf{D}}_\beta$ and $\hat{\delta}_\beta$ using our algorithm. For speed I bypass the implied volatility fitting step (I have one observation of $\bar{C}(K_m)$ per \bar{K}_m) and fit the log-

⁴To draw the distinction that I am cumulatively integrating from ‘right to left’, as opposed to standard convention of a line integral from left to right. The correct notation is to denote the double integral as a surface integral over the function $\mathcal{G}(K) = -K$ reversing the real line, to denote the direction from the lower bound (upper limit on K). In general the ‘lower limit’ should be when $K_m = \infty$, but in practice I follow the same truncation rule I use to extrapolate the upper tails, by truncation for tail probabilities at or below the [IEEE](#) lowest available floating point number different from zero. In practical terms this is a double cumulative trapezoidal integration with the strike price, call price pairs ‘flipped’ left to right.

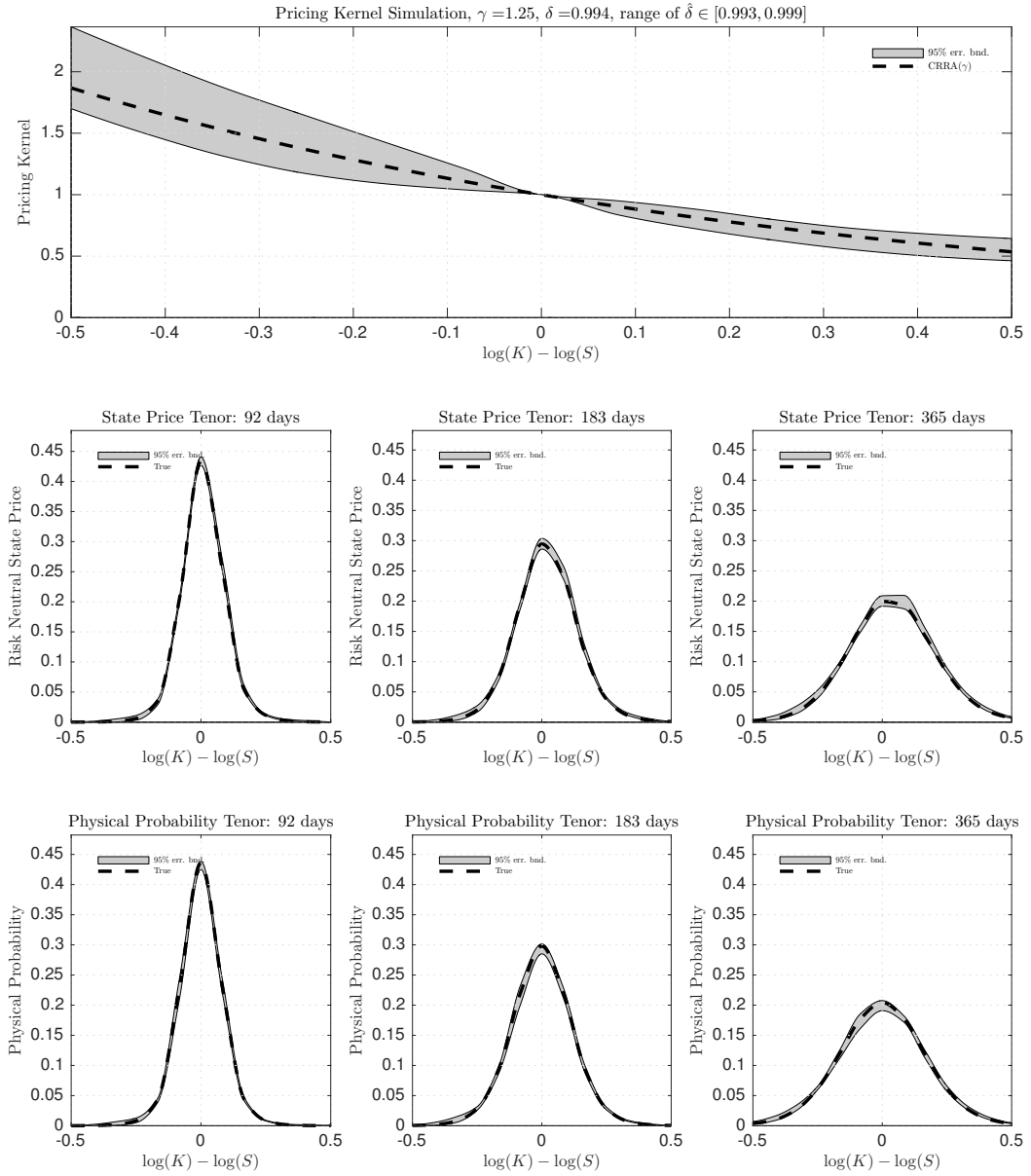
normal mixture directly to the call prices, to compute the risk-neutral density, which is $\partial^2 \hat{C}_\beta(\bar{K}_m)/\partial \bar{K}_m^2$. I set the simulation to that $\sigma = 1/10$, which is approximately the error I find in the subsequent fitting of the curves to real data after the implied volatility step.

Recall, that in my algorithm for actual market data, I compute the implied volatility and fit a polynomial curve to the implied volatility surface, I then compute smooth option prices from the volatilities that lie on this curve and then impose the log-normal mixture. The intermediate step using the implied volatilities is useful when fitting the curve against multiple options by strike. I approximate an instructive value of σ by comparing the standard deviation of the fitted options from the implied volatility step versus the corresponding market quotes. Furthermore, I presume in the simulation to have a complete range of strike prices for each tenor, a feature absent from actual data, hence the simulation serves to illustrate the consistency of the algorithm as opposed to the impact of potential mis-specification in the real-world implementation, I leave this for future work.

Figure 6.2 provides a summary of the simulation results. The grey area in each of the plots presents the 95% error bound from sorting the draws for $\text{diag}[\hat{\mathbf{d}}_\beta]$ and for a selection of columns from the risk-neutral state price by tenor matrix and corresponding physical price by tenor matrix computed from $\hat{\mathbf{Q}}_\beta$ and $\hat{\mathbf{P}}_\beta$ respectively. The dotted line reports the generating kernel and density functions.

It is striking to notice that the error bounds for the probability matrices by tenor is markedly less than the kernel, whilst the degree of accuracy in recovering $\bar{\delta}$ is very high. Proportionally the Perron root is far more tightly identified than the correct Perron vector for a given level of noise. As to be expected the level of accuracy drops with increasing tenor.

Figure 6.2: Simulation Test of the RT Algorithm



Notes. Fig.6.2 compares the risk-neutral density with the recovered physical density (lower six sub-figures) and plots the the option implied pricing kernel generated by our RT algorithm for a simulated kernel and options prices. The simulation is set up with a CRRA($\gamma = 1.25$) kernel, a unimodal physical transition matrix \mathbf{P} , which is right stochastic and a true discount factor of $\delta = 0.994$. I generate a 13 state, risk-neutral state price by tenor matrix \mathbf{S} . I interpolate this matrix over a range of $\log(K/S)$ from $-1/2$ to $+1/2$, with 14 quarterly tenors. I use a multiplicative variance such that $\mathbb{E}[\log(\hat{C}) - \log(C)] = \sigma \approx 10\%$, which corresponds to the observed variation we find in our empirical example versus the call options. I then draw 499 replications and recover the kernel $\text{diag}[\hat{\mathbf{d}}]$, discount factor $\hat{\delta}$ and physical probabilities by tenor matrix with columns $[\hat{\mathbf{Q}}^i \mathbf{e}_{(n+1)/2}]$ where \mathbf{e}_κ is a null vector except for element κ which is set to be unity. The grey area represents the 95% error bound from the simulation.

6.2.2 A-priori Unknown Number of States

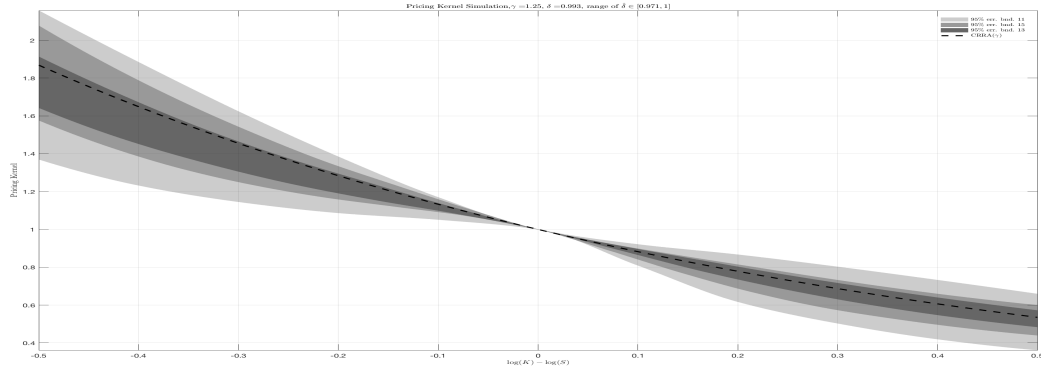
The simulation illustrated above is under the assumption that the number of states is known a-priori; that is, we recover the physical densities with the number of states implied by the state price and this is known with certainty. However, in reality, the number of states is not known a-priori and we simply observe a span of options prices measured at arbitrary intervals (fixed by the strikes available in the market).

I now examine the sensitivity of my algorithm to the under or over specification of the number of states. I assume the true number of states that generate the state price by tenor matrix is 13 and we run the recovery theorem algorithm with 9, 11, 15, and 17 states separately. I then compare the 95% error bounds of each of the recovered discount factor, pricing kernel, risk-neutral densities, and the recovered physical densities with those of the exact identified number of states case.

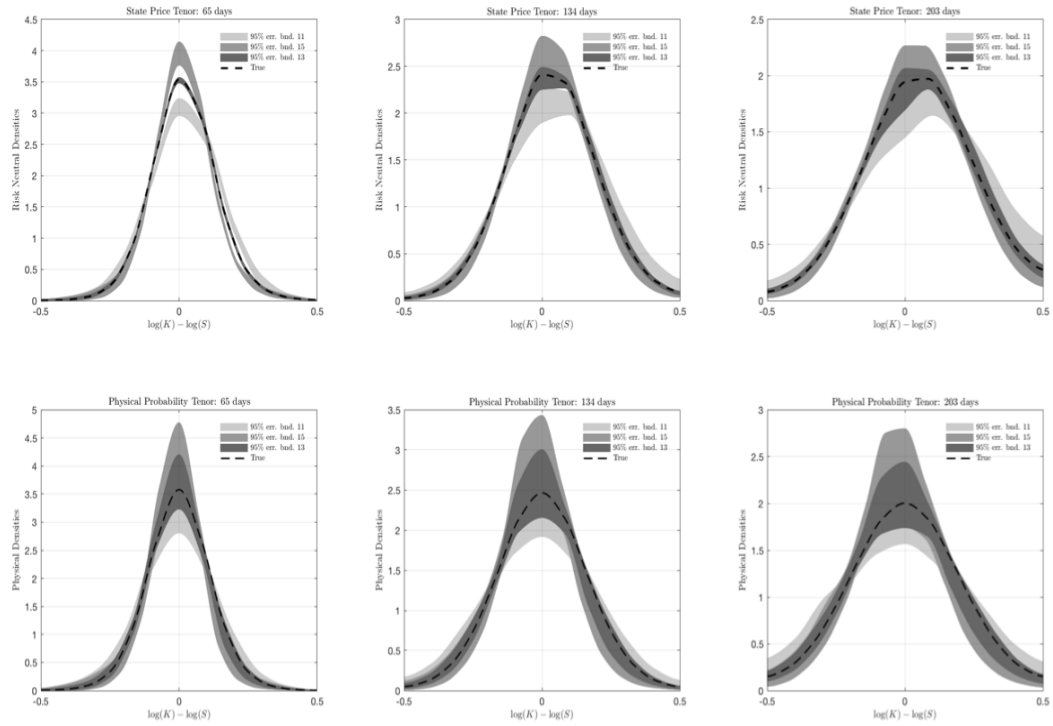
Figure 6.3 compares the recovered results between under and over specification of number of states. The upper panel plots the 95% error bounds for the recovered pricing kernel with 11, 13, and 15 states against the theoretical pricing kernel with a CRRA coefficient $\gamma = 1.25$. The error bound for 11 states is much wider than that of 15 states and the exact identified 13 states. Moreover, the deviation between the pricing kernel error bounds of the over and under identified cases and those of the exact identified case are bigger for the negative states while for the positive states, the differences are vanishing. The asymmetric pattern of the deviation for the pricing kernel is consistent with the risk aversion assumption for the investors' utility functions. The middle and bottom panels in Figure 6.3 reports the error bounds of the risk-neutral and recovered physical densities with three tenors from the simulation with 11, 13, and 15 states respectively.

Unlike the pricing kernel, the sensitivity of the error bounds of the risk-neutral densities and the recovered physical densities with under and over identified number of states is striking. In specific, under-identifying the number of states will lead to under-estimation of the densities in the peak but over-estimation of the densities at the tails while over specification yields the

Figure 6.3: Under and Over Estimation of the Number of States



(a) The Pricing Kernel



(b) The Risk-neutral and Physical Densities

Notes. Fig.6.3 reports the simulation results for under or over specification of the number of states. The upper panel compares the error bounds of the recovered discount factor and pricing kernel with different number of states against the true theoretical discount factor (0.993) and pricing kernel with CRRA($\gamma = 1.25$) respectively. The exact specification of number of states is set to be 13 states and two separate simulation with option prices generating with 11 states and 13 states are then computed. The 6 plots in the lower panel report the error bounds of the risk-neutral densities and the recovered physical densities with different tenors for under and over specification of the number of states respectively. The black dash line represents the true value and the the grey area represents the 95% error bound from the simulation.

Table 6.1: Error Bounds Analysis Tenor: 71 Days

Table 6.1 reports the error bounds analysis for under and over specification of number of states for the tenor with 71 days. Following the simulation, we set the true discount factor be 0.993 and the theoretical pricing kernel is generated with the CRRA risk aversion coefficient $\gamma = 1.25$. The exact number of states is assumed to be 13 and we generate the mis-specified simulations from number of states ranging from 9 to 17. The first panel of the table reports the range of the recovered discount factors and the size of the error bounds for the recovered pricing kernel, the risk-neutral densities and the recovered physical densities based on a 95% error bound simulation with 499 replications. The size of the error for each case is calculated by the difference between the area below the upper bound and the lower bound and the areas are calculated using trapezoidal integration. The lower panel presents the relative error for each number of states with respect to the error size of the exact specification case, which is 13 states in the middle.

Size of Error Bounds					
States	$\hat{\delta}_L$	$\hat{\delta}_U$	Pricing Kernel	Risk Neutral Den.	Physical Den.
9	0.957	0.976	1.103	0.209	0.297
11	0.981	0.995	0.901	0.148	0.249
13	0.985	0.999	0.748	0.065	0.268
15	0.989	1.000	0.815	0.149	0.380
17	0.990	1.000	0.894	0.236	0.425
Relative Error					
States	$\hat{\delta}_L$	$\hat{\delta}_U$	Pricing Kernel	Risk Neutral Den.	Physical Den.
9	0.972	0.977	1.474	3.214	1.105
11	0.996	0.996	1.204	2.277	0.926
13	1.000	1.000	1.000	1.000	1.000
15	1.004	1.001	1.089	2.286	1.414
17	1.005	1.000	1.195	3.623	1.583

opposite. It is interesting to notice that for the 71 days tenor, the error bounds of the risk-neutral densities for the three number of states only partially overlap at the tails but deviate a lot in the middle of the distribution, which indicates the level of sensitivity of the risk-neutral densities to the under or over specification of states number.

Table 6.1 and 6.2 report a more comprehensive comparison of the error bounds generating by simulations with different states number ranging from 9 states to 17 states for 71 days tenor. The upper panel in Table 6.1 lists the size of the error bounds while the lower panel reports the relative error of the error bounds for 9, 11, 15, and 17 states with respect to those for 13 states. Consistent with the patterns in Figure 6.3, the error bounds for the recovered discount factor, the pricing kernel, and the densities are increasing with under or over identified number of states compared to the exact specification number of states. The error bounds for the recovered physical densities are wider as

Table 6.2: Error Bounds Percentile Analysis Tenor: 71 Days

Table 6.2 reports the error bounds percentile analysis for under and over specification of number of states for the tenor with 71 days. Following the simulation, we set the true discount factor be 0.993 and the theoretical pricing kernel is generated with the CRRA risk aversion coefficient $\gamma = 1.25$. The exact number of states is assumed to be 13 and we generate the mis-identified simulations from number of states ranging from 9 to 17. The three panels reports the relative error of the 0.25%, 25%, 50%, 75%, and 97.5% points of the absolute distance between the upper and lower error bounds and the true values with respect to that of exact identified number of states for pricing kernel, risk-neutral densities, and recovered physical densities respectively. The 0.25% and 97.5% relative error describe the sensitivity of mis-specification of the number of states on the left and right tails of the distribution while the 50% ones summarise the error sensitivity for the peak of the distribution.

Pricing Kernel					
States	0.25%	25.00%	50.00%	75.00%	97.50%
9	2.538	1.384	1.089	0.840	0.727
11	1.767	1.067	1.208	0.962	0.936
13	1.000	1.000	1.000	1.000	1.000
15	1.160	1.071	0.484	1.015	1.003
17	1.429	1.202	0.548	0.983	1.081
Risk Neutral Density					
States	0.25%	25.00%	50.00%	75.00%	97.50%
9	1.168	3.914	13.087	7.647	1.459
11	1.926	2.198	9.319	6.464	1.939
13	1.000	1.000	1.000	1.000	1.000
15	1.967	2.748	8.838	3.567	2.195
17	2.511	3.220	18.615	5.196	4.557
Recovered Physical Density					
States	0.25%	25.00%	50.00%	75.00%	97.50%
9	1.073	2.222	1.597	2.024	2.059
11	1.537	1.559	0.796	1.369	1.927
13	1.000	1.000	1.000	1.000	1.000
15	1.682	1.510	1.309	1.166	2.172
17	3.018	1.845	2.028	1.305	4.590

both the error in the estimation of the risk-neutral densities and the pricing kernel have featured in the recovered physical densities.

In order to examine the patterns of the error bounds in further detail, I report the percentile analysis for the error bounds of pricing kernel, risk-neutral densities, and the recovered physical densities for the same tenor in Table 6.2. In specific, we calculate the relative error of each error bounds of the mis-identified case on 0.25%, 25 %, 50%, 75%, and 97.5% percentiles with respect to those of the exact-identified one. The recovered pricing kernel shows more sensitivities before the 50% percentile points across all cases and the differences tend to decrease for the positive states.

For the risk-neutral densities, the errors peak in the middle of the

distribution at the 50% percentile points and the right tails show more sensitivities across all cases compared to the left tails, which suggests that the mis-specification of number of states affects the probabilities for positive states more than that for negative states. As the recovered physical densities are a mixture of the risk-neutral densities and the pricing kernel, the difference between the deviations of the tails are not as significant as those of the middle points.

6.3 Empirical Example and Application

In this section, I first provide an example for applying the Empirical Recovery in practice with both market index and single-name stocks, mainly the S&P 500 Index and Apple Inc. I then demonstrate the empirical application of the recovered physical probability distribution by building a market left tail index from the options written on S&P 500 Index.

6.3.1 S&P 500 Index and Apple Inc.

To demonstrate my approach I utilise publicly available market price data, this is in contrast to [Ross \[2015\]](#) who has access to a proprietary [OTC](#) data source. My option data is from the [OPRA](#) feed and catalogued by Thomson Reuters and SIRCA. [OPRA](#) claims that 75% of option trading is recorded within this National Market reporting system.⁵ Both transactions and quotations are time-stamped to the nearest tick time and tick data are converted into one-minute series using the previous-tick method.⁶ Compared to the commonly used end-of-day data, the intraday dataset yields several advantages. First, I will have a range of spot prices and observations for each traded strike. Second, over a given day the range of traded strikes is likely to

⁵The SEC put forward the [NMS](#) in November 2009 and set up the [OPRA](#). Under the National Market System plan, the trades and quotes data of all option contracts trading on the participating exchanges are gathered and consolidated or disseminated to approved vendors. The [OPRA](#) is claimed by the compilers to be the most comprehensive exchange-based option dataset in the United States option market.

⁶Under the previous-tick method, the equally-spaced series of one-minute prices are generated by the observations at the end of each one-minute interval.

be more heavily populated than skimming the trades and quotes at the end of day. Third, I use the mid-price of the best bid and ask quotes and again this will likely yield a far greater variation in the quoted prices.

I collect one-minute intraday quotations information related to options on S&P 500 index (SPX) and Apple Inc. (NASDAQ: AAPL.O) respectively. For the risk free rate I utilise minute updated time matched intraday quotes for U.S. deposit rates for maturities up to three years. The yield curves are time matched to each quoted option in the dataset. I then match the minute put and call option datasets together by quote-time, strike and maturity date.

The following filters are applied on the raw data. Firstly, drop the observations with zero bids price or zero asks price. Then, I also exclude the observations with zero number of bids or zero number of asks and zero trading volumes. At last, I calculate the intrinsic value for each option and kick out the observations that violate the non-arbitrage condition. For each observation over a day, the spot price and risk free rate is matched by time stamp. The spot price for SPX is back by the intraday changes of the S&P 500 index level and that for AAPL is matched by the intraday one-minute quotations of AAPL.O.

For each matched put and call quote I generate a time matched implied dividend yield and then recover the implied volatility for both put and call options from their respective prices. For the SPX options the dividend yield is very stable at a little over 2.20% and this value is used in that case that either a put or a call is absent. I note that the AAPL.O options are of the American type and I have experimented with deducting the put early exercise premium to recover the equivalent European price, however, the results indicate that the value of this premium is very small. I obviously recommend that further applications to single-name American options check the early exercise premium as this may not be uniform across all stocks⁷.

For application I choose April 27, 2011, the same day utilised in Ross [2015]’s empirical examples. I also test the algorithm on three unique dates that correspond with the United States Quantitative Easing (hereafter QE)

⁷See for example Dupont [2001] for a detailed discussion on the effects of early exercise premium on extracting risk-neutral probability distributions from American option prices.

Table 6.3: Sample Description

Assume there are m observed time points during a day. S_0 is the median spot price during the day, computing by $S_0 = \text{median}(S_m)$. K is the available strike prices extract directly from the cleaned option price panel. τ stands for the time to maturity in days, which is $\tau = T - t$. R is the log-return calculated on an intraday frequency, such that $R_m = \log(K_m/S_m)$ for the m point during a day.

Sample	SPX				AAPL			
	20100331	20110427	20110630	20141029	20100331	20110427	20110630	20141029
Calls								
S_0	1171.67	1348.88	1318.95	1981.56	235.69	349.76	335.22	107.01
No. of Obs	91,799	73,629	16,928	104,462	26,817	67,337	63,967	54,280
No. of K	87	84	72	112	55	79	74	98
Min. K	400	550	800	1075	15	100	100	43
Max. K	1425	1700	1800	2525	350	540	490	130
No. of τ	13	10	10	11	6	8	9	12
Min. τ	17	24	16	24	17	2	1	9
Max. τ	997	969	905	779	661	633	569	814
Min. R	-108%	-90%	-50%	-61%	-276%	-126%	-121%	-92%
Max. R	20%	23%	31%	25%	40%	44%	39%	20%
Puts								
No. of Obs	85,424	69,491	14,403	126,256	17,018	49,629	51,751	56,913
No. of K	95	89	82	129	25	58	54	63
Min. K	500	550	800	1075	155	215	215	88
Max. K	1700	1800	2000	2600	350	540	520	155
No. of τ	14	10	10	11	6	8	9	12
Min. τ	1	24	16	24	17	2	1	9
Max. τ	997	969	905	779	661	633	569	814
Min. R	-85%	-90%	-50%	-61%	-42%	-49%	-45%	-20%
Max. R	38%	29%	42%	28%	40%	44%	45%	38%

timelines, which are March 31, 2010 (QE1 Ends), June 30, 2011 (QE2 Ends), and October 29, 2014 (QE3 Ends).

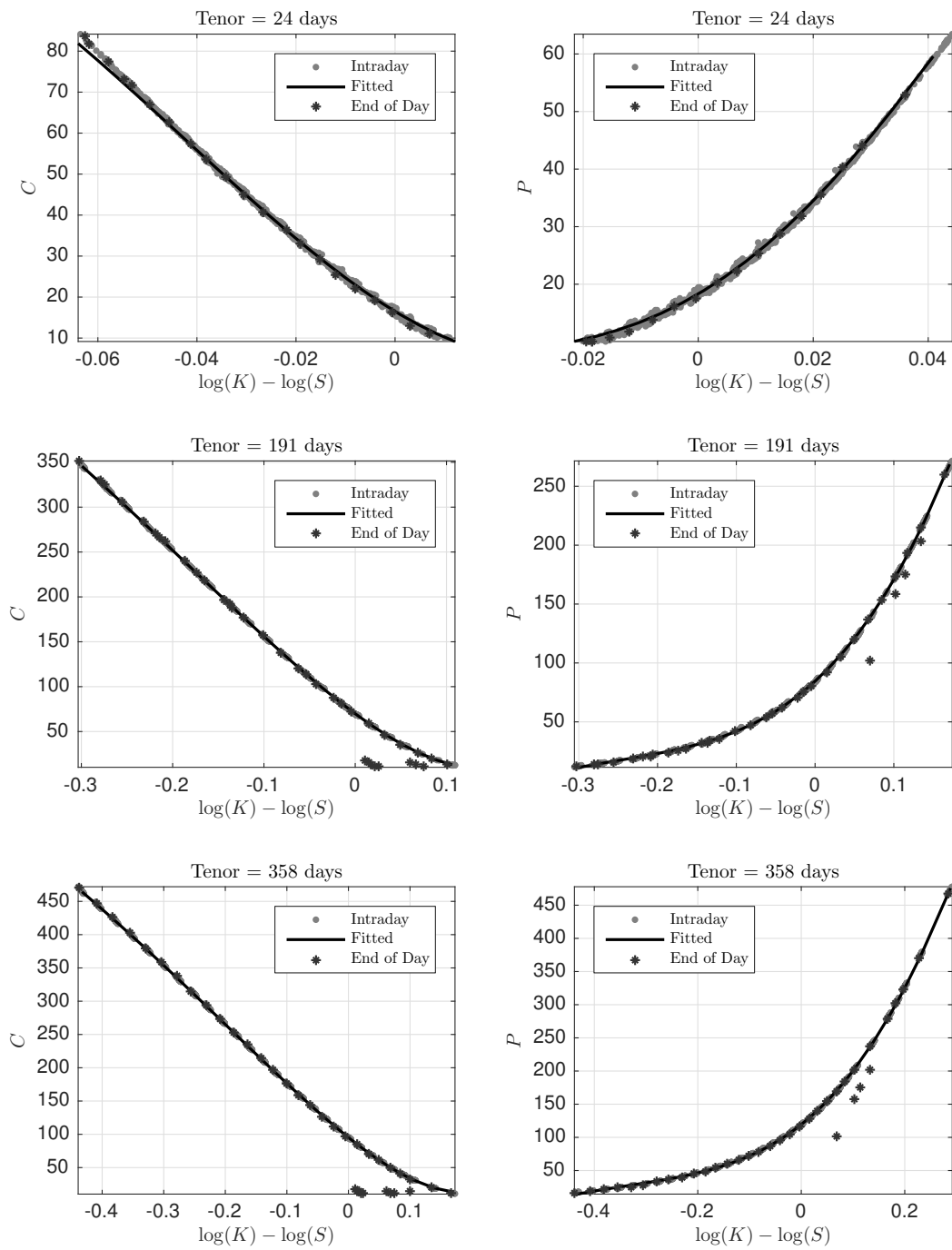
Table 6.3 reports the number of observations, the available strikes range, and the available maturities range for the samples. At a glance, we have a fine grid of both SPX and AAPL across the sample dates. For example, for SPX on April 27, 2011 we have up to 89 different available strikes ranging from 550 to 1800, with a corresponding states from -90% to 29%. In terms of the tenors, we have at least 10 tenors ranging from 24 days to 969 days (2.65 years)⁸.

I employ the algorithm on each of the eight samples. For brevity I only present a full set of steps for SPX and AAPL on April 27, 2011. I then report the recovered kernel and discount factor for the remaining days. Figures 6.4

⁸Ross [2015] reports results with tenors up to 3 years, as that dataset included some Long Term Equity Anticipation Products (LEAPs), which have a longer maturities than most commonly traded options. In general the OPRA dataset runs to around 2.5 years.

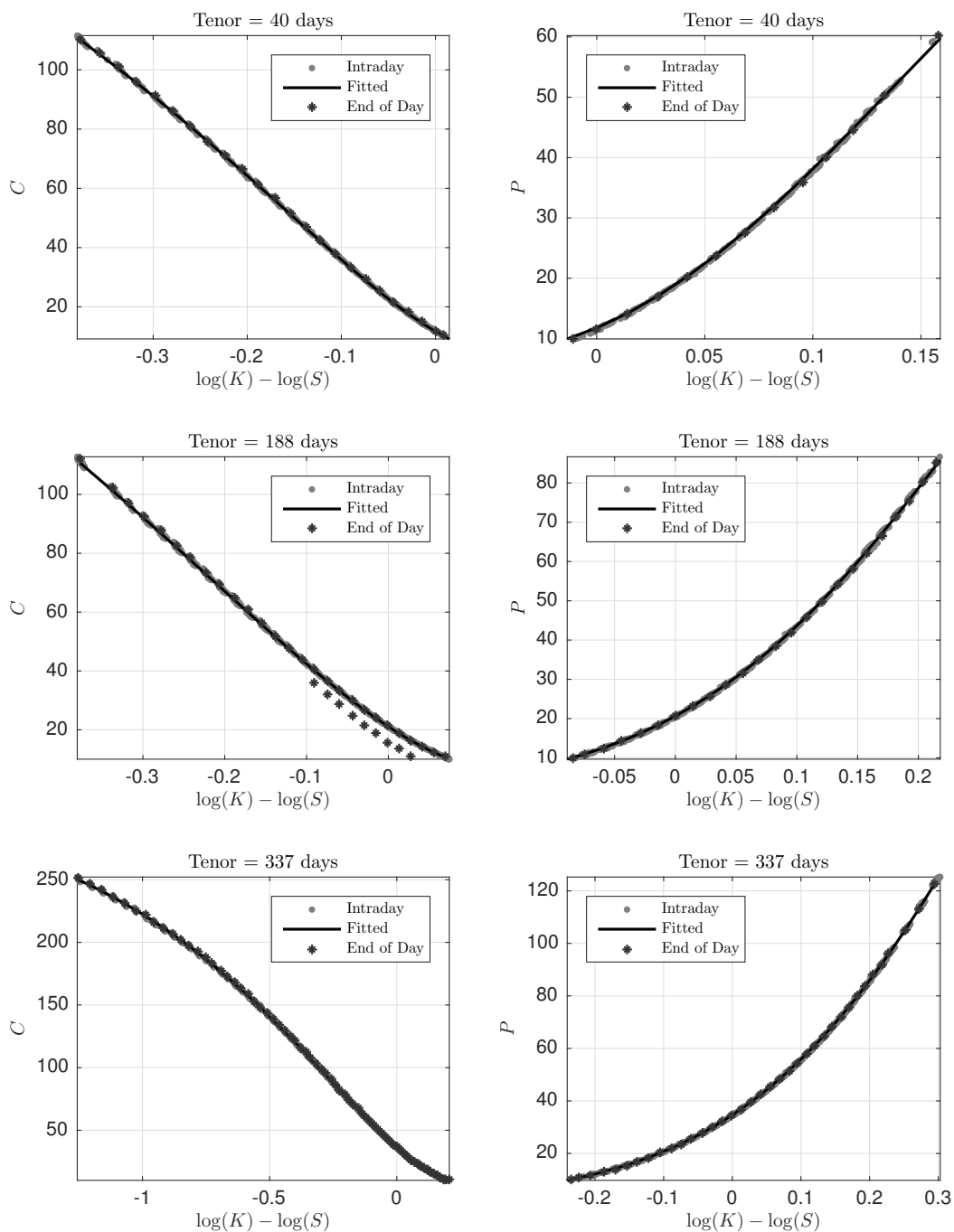
and 6.5 plot the option prices determined from the smoothed polynomial fit (alongside the traded prices) for SPX and AAPL respectively. Figures 6.6 and 6.7 present the Black-Scholes implied volatility with its fitted polynomial for the SPX and AAPL individually. I also include the end-of-day transaction data on the plots. The advantage of the intraday data is apparent in the fitting of the polynomial curve to distribution of implied volatilities traded throughout the day. The polynomial function of the implied volatility data yields exceptionally closely fitting put and call prices over the range of log moneyness $\log(K/S)$. Following convention, I use the put volatility curve to generate the call prices used in the subsequent analysis.

Figure 6.4: Price Fitted for SPX on April 27, 2011



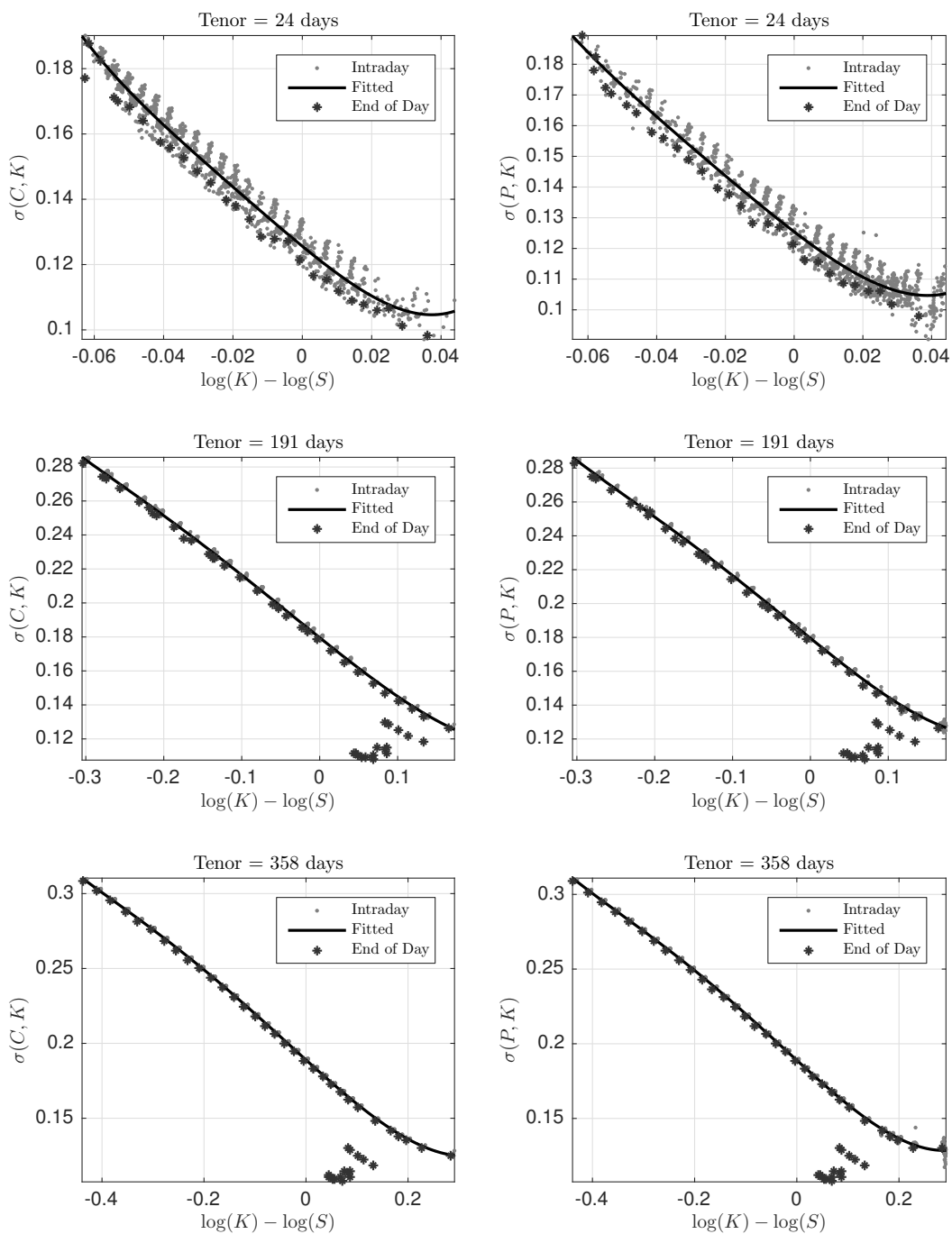
Notes. The left panel gives the Black-Scholes prices fitted for calls (C) while the right one is for puts (P) with a 4th order polynomial function for short, medium and long maturity options. The dark grey ‘.’ draws the one-minute intraday market data, the black ‘*’ is the end-of-day data and the hard line plots the polynomial fitted function.

Figure 6.5: Price Fitted for AAPL on on April 27, 2011



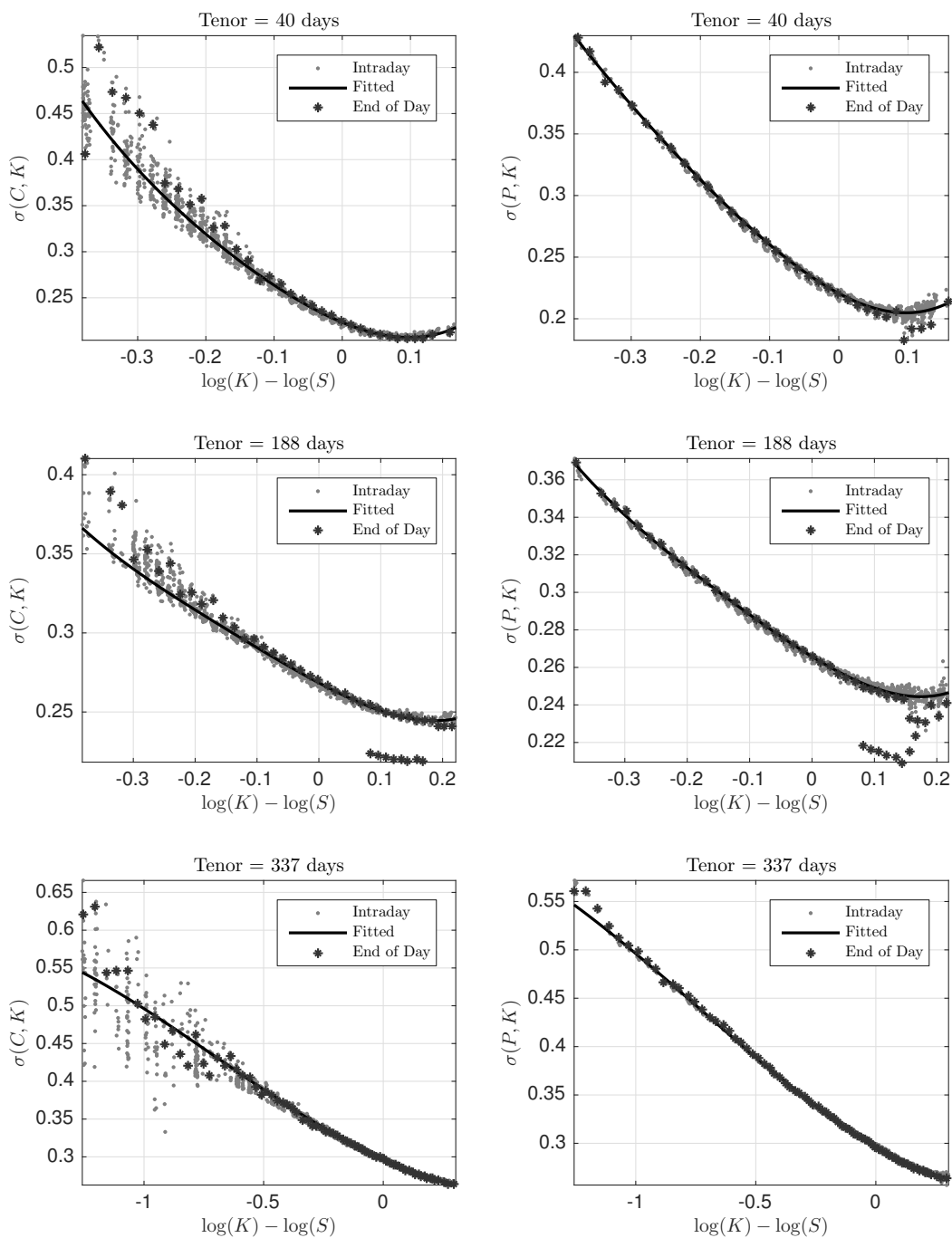
Notes. The left panel gives the Black-Scholes prices fitted for calls (C) while the right one is for puts (P) with a 4th order polynomial function for short, medium and long maturity options. The dark grey ‘.’ draws the one-minute intraday market data, the black ‘*’ is the end-of-day data and the hard line plots the polynomial fitted function.

Figure 6.6: Implied Volatility Fitted for SPX on April 27, 2011



Notes. The left panel gives the Black-Scholes implied volatility fitted from call prices ($\sigma(C, K)$) while the right one is from put prices ($\sigma(P, K)$) with a 4th order polynomial function for short, medium and long maturity options. The dark grey ‘.’ draws the one-minute intraday market data, the black ‘*’ points the end-of-day data and the hard line plots the polynomial fitted function.

Figure 6.7: Implied Volatility for AAPL on April 27, 2011



Notes. The left panel gives the Black-Scholes implied volatility fitted from call prices ($\sigma(C, K)$) while the right one is from put prices ($\sigma(P, K)$) with a 4th order polynomial function for short, medium and long maturity options. The dark grey ‘.’ draws the one-minute intraday market data, the black ‘*’ points the end-of-day data and the hard line plots the polynomial fitted function.

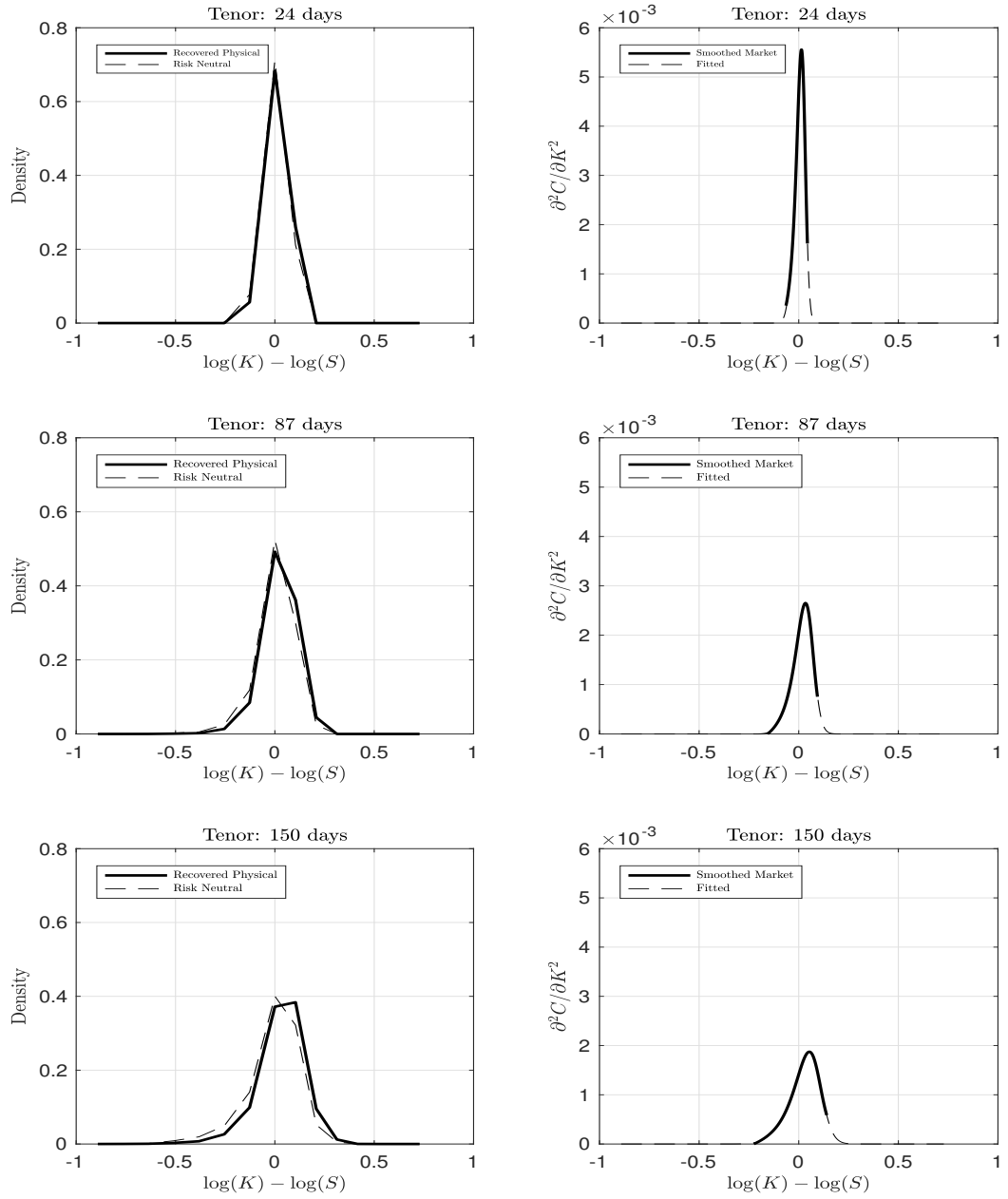
The right panels in Figures 6.8 and 6.9 plot the fitting of the risk-neutral density functions from the analysis for SPX and AAPL separately. It is worth noting that the extra information provided by the intraday data does yield a risk-neutral distribution that is exceptionally close to log-normal for each tenor (this does not mean that the driving process exhibits time-inhomogeneous volatility, simply that the individual tenor is close to log-normal). Notice, in Figure 6.9 the bottom right plot, that the shape of the 337 day risk-neutral density is quite distinct from the typical shape of a single log-normal distribution. This provides a good example of the benefit to having multiple weighted log normal distributions to capture the somewhat irregular shape indicated by the call prices derived from the polynomial fit using the put implied volatilities.

At this point I can execute the algorithm for imputing the risk-neutral state price transition matrix. It is worth commenting on the choices the econometrician has at this juncture, the most basic being the number of states. I provide full functional forms for derivatives for the objective function (simple least squares) and the constraints in addition to a scaleable matrix functional form for the Hessian of the Lagrangian hence the optimisation is (a) computed on functions that are at least continuous to order \mathcal{C}^2 and should attain the optimal matrix very quickly despite a potentially large number of variables that maybe required for the estimation.

However, this does not mean that the number of states can be set to any arbitrarily high number as the finer grid will only sit over the same information set, this is particular true for the number of tenors. Empirical observation suggests that once the number of states exceeds three times the number of observed tenors changing the choice of interpolation methodology to construct the uniform state price by tenor grid begins to have a significant impact on the recovered physical density function, size of the discount factor and shape of the pricing kernel.

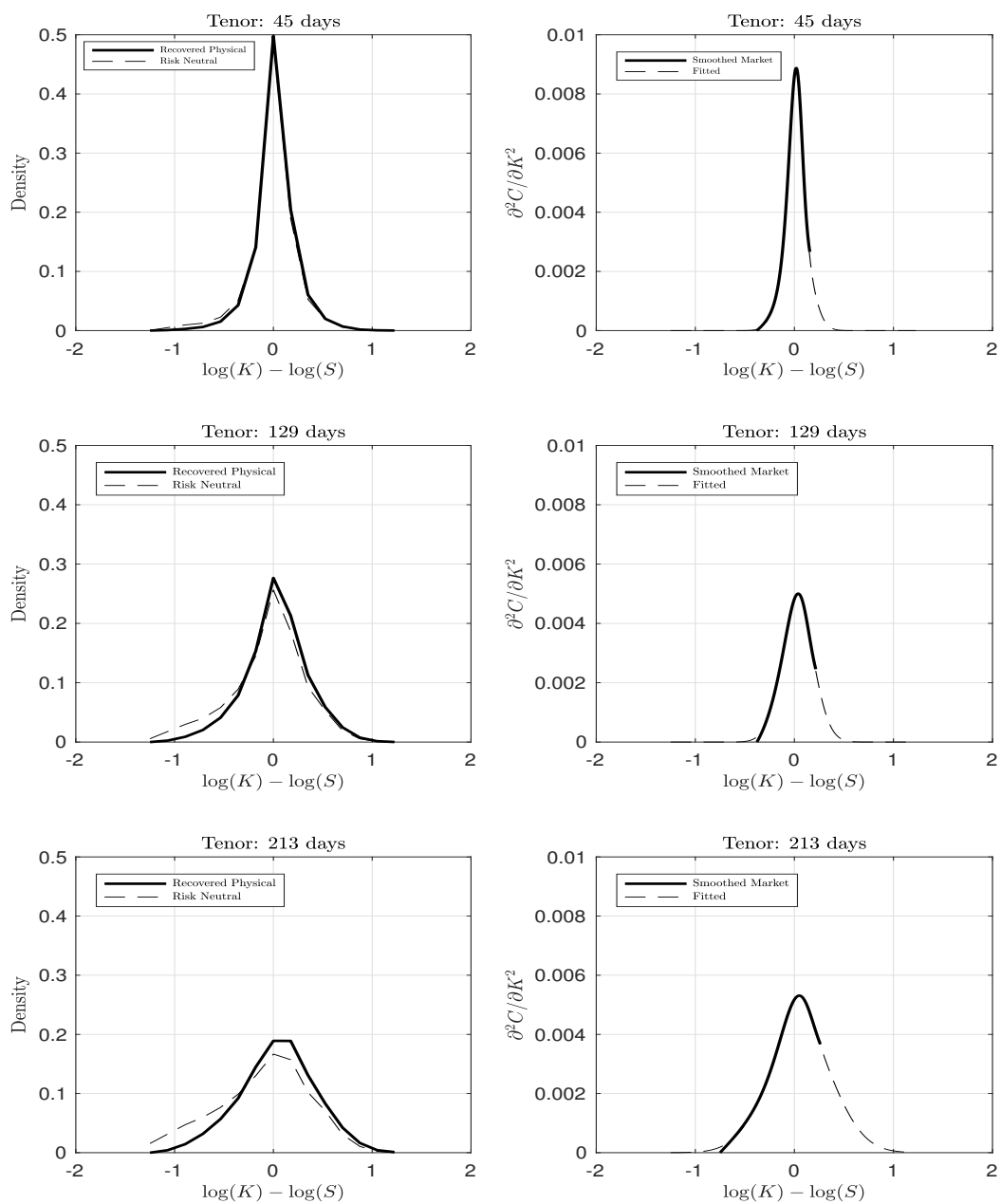
The left panels in Figure 6.8 and 6.9 illustrates the recovered physical distribution compared to the nearest actual tenor risk-neutral distribution (dashed lines). We can see that for short maturities, as expected, the recovered physical distribution exhibits considerably fatter tails than the

Figure 6.8: Risk Neutral Density Fitted and Recovered Physical Density for SPX on April 27, 2011



Notes. The right panel plots the state price densities against the parametric mixture lognormal fitted density function. The state price density is calculated by Equation 6.3. The mixture lognormal fitted density is fitted with Equation 6.4. The left panel compares the risk-neutral density with the recovered physical density. Note, the scales on the left sides plots are in the form of recovered density functions, hence, the integral over the range $\pm\infty$ under the curve, with respect to the horizontal scale is unity. In contrast the right column is in the form of recovered state price, hence their sum will be $\exp(-r_i\tau_i)$, where r_i is the nearest quoted deposit rate for that maturity.

Figure 6.9: Risk Neutral Density Fitted and Recovered Physical Density for AAPL on April 27, 2011



Notes. The right panel plots the state price densities against the parametric mixture lognormal fitted density function. The state price density is calculated by Equation 6.3. The mixture lognormal fitted density is fitted with Equation 6.4. The left panel compares the risk-neutral density with the recovered physical density. Note, the scales on the left sides plots are in the form of recovered density functions, hence, the integral over the range $\pm\infty$ under the curve, with respect to the horizontal scale is unity. In contrast the right column is in the form of recovered state price, hence their sum will be $\exp(-r_i\tau_i)$, where r_i is the nearest quoted deposit rate for that maturity.

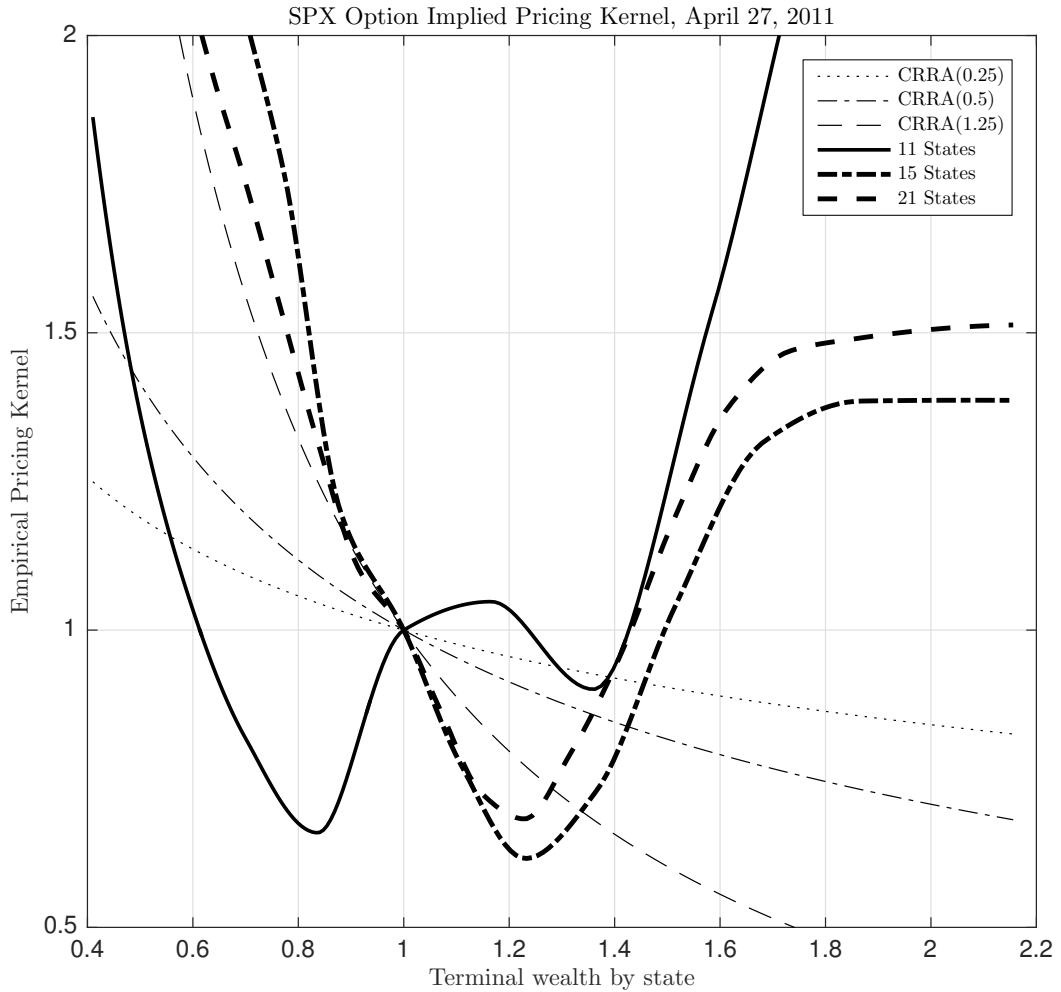
nearest equivalent maturity risk-neutral distribution. For AAPL the recovered physical distribution more-or-less converges on the risk-neutral distribution for longer maturities. However, for the SPX the tails are consistently wider out to 150 days.

Figures 6.10 and 6.11 present the estimated kernels for different choices in the number of states for the SPX and AAPL respectively. The first obvious point to note is that for both the SPX and AAPL the shape of the kernel is (a) U-shaped and (b) somewhat asymmetric. For comparison purposes I plot the pricing Kernels derived from a constant relative risk aversion, $\text{CRRA}(\gamma)$, iso-elastic power utility function with relative risk aversion parameter γ set to $\{0.25, 0.5, 1.25\}$ to provide an illustration of the range. Notice that for both the SPX and AAPL on this particular day (and I find consistent evidence across the days tested) that the shape of the kernel converges as the number of states increases. I use 11 states as a baseline to be consistent with the evaluation of Ross [2015]; however, I find that whilst the first six states yield effectively the same range of values (more-or-less tracking the $\text{CRRA}(0.25)$ curve), there is a slight hump. In contrast, Ross [2015] recovers a strictly decreasing kernel.

Indeed, as we shift to higher numbers of states, which is possible under my algorithm, the shape of the kernel matches the shape found in several previous papers, see for instance Song and Xiu [2016] for a good example, where the kernel is recovered by combining realized volatility of spot data with options prices on volatility indices. Further evidence on the U-shape of the kernel (and hence the ‘pricing kernel puzzle’) is documented in Brown and Jackwerth [2004], Hens and Reichlin [2013], and Cuesdeanu [2017] amongst others. It is useful to note that the shape of the kernel and the discount rate does not change at the number of states rises. This appears to be the case for both the SPX and AAPL for my case study days.

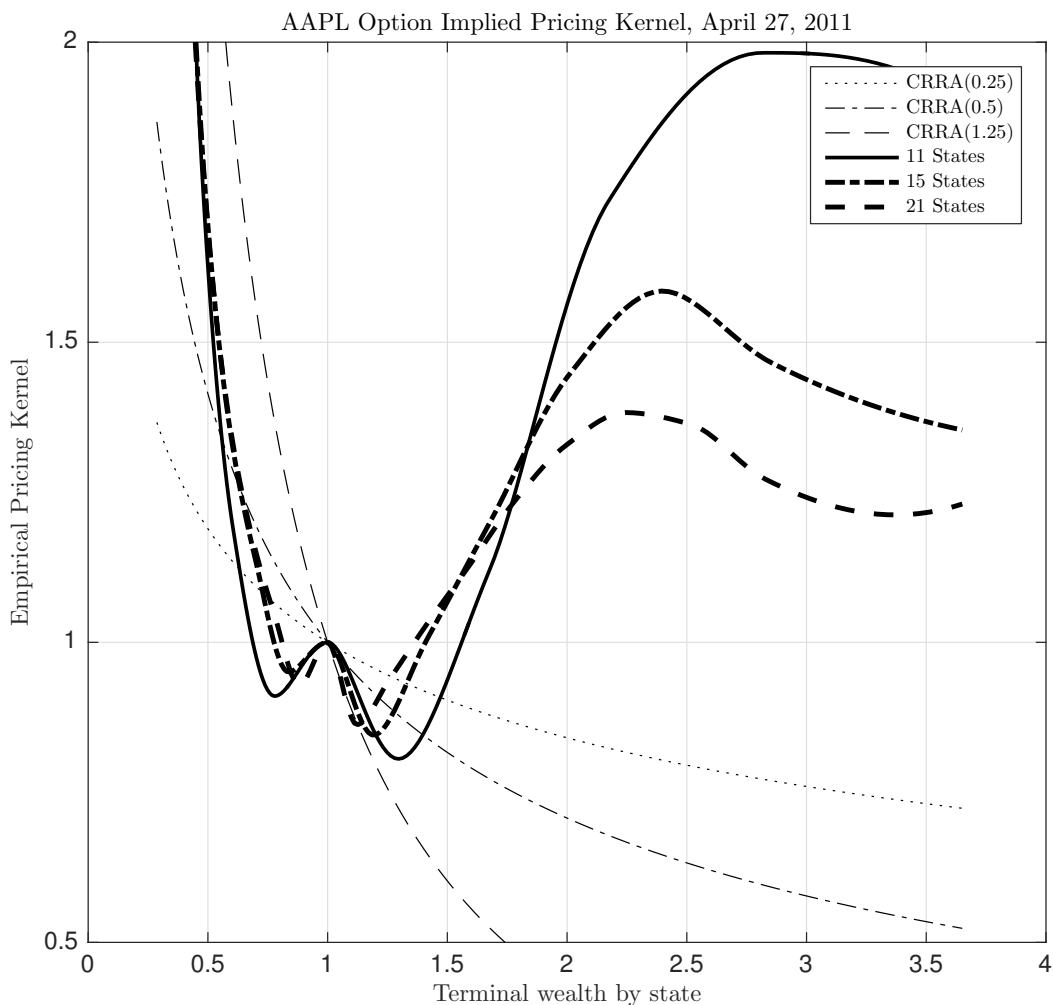
Table 6.4 summarise the option implied pricing kernel and the annualised discount factor for all of the eight samples in the case study. Noted with the RT, we could separate the discount factor and the pricing kernel. The discount factor represents time preference while the recovered pricing kernel describes the risk-aversion preference. The positive annualised discount factor

Figure 6.10: Option Implied Pricing Kernel for SPX on April 27, 2011



Notes. The plot compares our option-implied pricing kernel \mathbf{D} with the empirical constant relative risk aversion (CRRA) pricing kernel. The option-implied kernel across different states is given by Equation (5.9) and normalised by the states with 0% change. The utility function of CRRA investors is presumed to be an isoelastic power utility function of the form $u(c) = (c^{1-\gamma} - 1)/(1 - \gamma)$ for $\gamma \neq 1$ and $\log(c)$ for $\gamma = 1$. The kernel is defined by $\text{CRRA}(\gamma) = (U'(c(T)))/(U'(c(t)))$. Setting $c(t) = 1$ to be one present period dollar and $c(T) = K/S$ to be the terminal payoff per dollar (time T wealth) of a single dollar at time T for given state determined by K . Hence, defining $R = \log(K/S)$ the Kernel is $\text{CRRA}(\gamma) = \exp(-\gamma R)$. For visualisation and comparison purposes the intermediate points for the 11 and 15 state kernels has been interpolated using a piece-wise cubic spline to the 21 state frequency.

Figure 6.11: Option Implied Pricing Kernel for AAPL on April 27, 2011



Notes. The plot compares our option-implied pricing kernel \mathbf{D} with the empirical constant relative risk aversion (CRRA) pricing kernel. The option-implied kernel across different states is given by Equation (5.9) and normalised by the states with 0% change. The utility function of CRRA investors is presumed to be an isoelastic power utility function of the form $u(c) = (c^{1-\gamma} - 1)/(1 - \gamma)$ for $\gamma \neq 1$ and $\log(c)$ for $\gamma = 1$. The kernel is defined by $\text{CRRA}(\gamma) = (U'(c(T)))/(U'(c(t)))$. Setting $c(t) = 1$ to be one present period dollar and $c(T) = K/S$ to be the terminal payoff per dollar (time T wealth) of a single dollar at time T for given state determined by K . Hence, defining $R = \log(K/S)$ the Kernel is $\text{CRRA}(\gamma) = \exp(-\gamma R)$. For visualisation and comparison purposes the intermediate points for the 11 and 15 state kernels has been interpolated using a piece-wise cubic spline to the 21 state frequency.

indicates a δ that is less than unity, which is consistent with the non-arbitrage conditions. In the snapshot exercise of [Ross \[2015\]](#), a 1.018 δ is recovered, which gives an equivalent annualised rate to be -1.74%.

Table 6.4: Option Implied Pricing Kernel for SPX and AAPL

The option-implied pricing kernels reported are calculated on a uniformed 11-states space with $\mathbf{R} = \{-0.5 \leq R_m \leq 0.5\}$. The r is the percentage annualized discount factor that given by $r = -\log(\delta)/\Delta\tau$, where δ is the Perron root of the transition matrix \mathbf{Q} as given by Equation (6.9) and $\Delta\tau$ is the uniformed time-space between two states. The option-implied pricing kernel is calculated according to Equation (5.9) and normalised by the states with 0% changes.

	$r\%$	-50%	-40%	-30%	-20%	-10%	0%	10%	20%	30%	40%	50%
SPX												
20100331	0.43	1.29	1.16	1.09	1.03	1.00	1.00	0.90	0.91	0.99	1.07	1.20
20110427	3.18	1.55	1.37	1.27	1.20	1.12	1.00	0.84	0.75	0.87	1.20	1.70
20110630	0.94	5.13	4.19	3.06	2.12	1.33	1.00	0.74	0.49	0.49	0.66	0.93
20141029	28.23	6.76	5.20	3.70	2.58	1.58	1.00	0.84	0.80	1.19	2.29	4.64
AAPL												
20100331	0.88	1.15	1.04	0.98	0.97	0.98	1.00	1.03	1.03	1.02	1.03	1.10
20110427	0.07	1.24	1.11	1.04	1.02	1.01	1.00	0.99	0.97	0.95	0.94	0.97
20110630	1.20	1.32	1.15	1.06	1.03	1.02	1.00	0.97	0.96	0.93	0.92	0.96
20141029	7.55	1.42	1.18	1.06	1.01	0.99	1.00	1.00	1.07	1.14	1.27	1.52

6.3.2 The Market Left Tail Index

In this section, I demonstrate one of the empirical application of the recovered ‘physical’ probability densities in terms of risk management. Specifically, I illustrate the fact that the risk neutral densities, form a lower bound on the likelihood of a left tail outcome and we can compute a range of probabilities from the risk neutral to the recovery theorem physical probabilities and illustrates the robustness of the technique to misspecification in the [Borovička et al. \[2016\]](#) sense.

Figure 6.8 and 6.9 illustrate a common finding that the risk neutral density for a given time step n , denoted by the vector $\mathbf{q}_n = \exp(r_n)\hat{\mathbf{Q}}^n\mathbf{e}_{(M+1)/1}$ has larger tail probabilities than the physical density $\mathbf{p}_n = \hat{\mathbf{P}}^n\mathbf{e}_{(M+1)/1}$. This assumes that the martingale component \mathbf{H} is unity for elements $h_{ij}, \forall i, j \in$

$\{1, \dots, m\}$. Without detailed knowledge of the martingale measure on the stochastic component of the discount factor it is a matter of faith in the assumption that $\hat{\mathbf{P}}^n \mathbf{e}_{(M+1)/1}$ is the true probability mass function. However, from Theorem 5.1 and from our simulation evidence we can be very confident that \mathbf{q}_n is a noisy, but unbiased, estimate the risk neutral measure, even if $h_{ij} \neq 1, \forall i, j \in \{1, \dots, m\}$, as the option market already filters this problem for a give time step (indeed, this is the heart of the recovery debate).

It is also reasonable to presume, as Hansen and Scheinkman [2009] and Borovička et al. [2016] that given the most plausible set of representative preferences the stochastic trend in the martingale component, if it exists, will exhibit a positive drift, hence decreasing the downside component of the tail.⁹

We can therefore make the following conjecture: let $\tilde{\mathbf{r}} = [R_i], \forall i, j \in \{1, \dots, m\}$ be the column vector of returns associated with the i state, hence $\tilde{\mathbf{r}}' \mathbf{P}^n \mathbf{e}_{(M+1)/1} = r_n^{\mathbb{P}}$ and $\tilde{\mathbf{r}}' \exp(r_n) \mathbf{Q}^n \mathbf{e}_{(M+1)/1} = r_n^{\mathbb{Q}} = r_n$ are the physical and risk neutral expected returns. If we presume when $\mathbf{P} = \mathbf{H} \circ \tilde{\mathbf{P}}$ that $r_n^{\mathbb{P}} > r_n^{\mathbb{Q}}$ then a series of simple observations on lower bounds can be inferred. First, let $\mathbf{q}_{n,\ell} = \sum_{i=1}^{\mathbf{t}_\ell} \mathbf{q}_{n,i}$ and $\mathbf{p}_{n,\ell} = \sum_{i=1}^{\mathbf{t}_\ell} \mathbf{p}_{n,i}$ be the risk neutral and physical cumulative probabilities from the left (downside) tail, for a given downside return \underline{r} .

By inspection we can see that if the pricing kernel is the result of a concave (risk averse) utility function the left tail risk neutral probabilities $\mathbf{q}_{n,\ell} = \sum_{i=1}^{\mathbf{t}_\ell} \mathbf{q}_{n,i}$, for \mathbf{t}_ℓ that describes the tail of the density function, $R_i \leq \underline{r}$ that is given a \mathbf{t}_ℓ , such that probability masses from \mathbf{t}_ℓ to \mathbf{t}_ℓ describe a ‘point probability’ defined by $q_{n,0}$ and $p_{n,0}$, the tail probabilities will be ordered such that $\mathbf{q}_{n,\ell} > \mathbf{p}_{n,\ell}$, that is an outcome with return lower than R_ℓ in period n the physical tail probability will be strongly bounded by the risk neutral tail probability, even if we cannot define the physical probability as the martingale component is stochastically trended.

This is a very useful result as one of the major uses of this type of analysis is to provide downside risk measures over a variety of forward time horizons, potentially beyond those available from the option market. Figure 6.12 plots

⁹Indeed, this is the main example given in the quantitative illustrations in Section 5 of Borovička et al. [2016].

the left tail index formed by the recovered physical probability distributions of S&P 500 index from January 1, 1996 through January 31, 2015. In particular, I set the uniform state grid to be 5 states ranging from -50% to $+50\%$ (with 0% sitting in the middle) and the tenor grid to be 6 tenors ranging from 90 days to 540 days with quarterly interval. The left tail index (black hard line) is then formed by the recovered cumulative probabilities for the -50% and -25% states while the dash and dot lines are the recovered probabilities for the -50% and -25% separately.

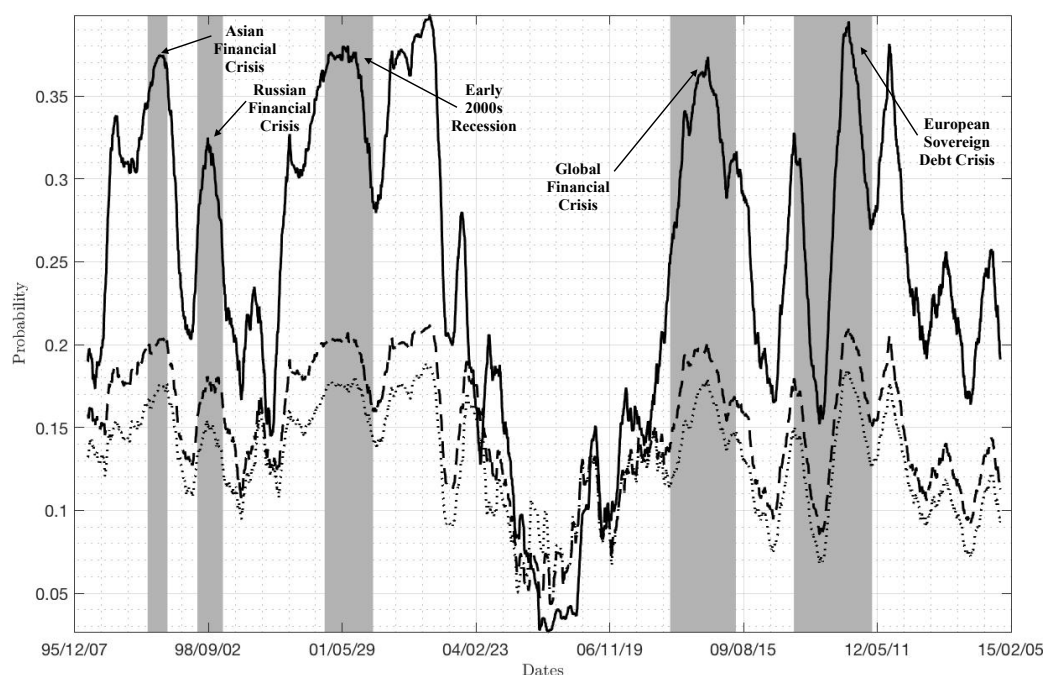
The grey areas highlight the financial crisis and economic recessions periods. It can be seen that the left tail index tracks the market volatiles very well. Thus, the recovered probability densities provide valuable information for risk management, especially the market downside risks and the left tail index can be seen as an ‘physical fear index’ alongside the ‘fear index’, VIX, which is a widely used market volatility gauge under risk-neutral measure.

6.4 Concluding Remarks

Eigenfunction operations on the risk-neutral state price transition matrices have proven a useful tool for the better understanding of asset price dynamics and aggregate behaviour of agents within asset markets. I have specified a perturbation theory for the discount factor pricing kernel and physical probabilities. Using this result I have carefully constructed a sequential quadratic programming algorithm with appropriate restrictions that allows full identification of the discount factor, pricing kernel and physical density function from the sub-stochastic risk-neutral state price transition matrix.

Using the continuous derivatives our estimation procedure is very fast as I have determined all of the mathematical preliminaries needed converge to a unique solution. In addition to the contribution to the recovery theorem directly this is the first paper to utilise intra-day data to estimate the risk-neutral density function and demonstrate the advantages of the extra available information relative to end-of-day approaches. Through simulation I demonstrate that my procedure is consistent in recovering the correct shape of the representative agents pricing kernel and discount rate alongside the

Figure 6.12: Recovered Market Left Tail Index



Note. Figure 6.12 plots the left tail index formed by the recovered physical probability distributions of S&P 500 index. The dot line represents the probability that the markets drop 50% while the dash line demonstrates the probability for market going down 25%. The hard line is the cumulative probability that the markets drop down. The grey shaded areas represent the financial crisis and economic crisis as defined according to the NBER over the sample period running from January 1, 1996 through January 31, 2015.

primary objective the recovered physical probabilities.

I outline the procedure on actual intraday data for the S&P 500 index over a series of days and by appealing to the results in Carr and Yu [2012] fit the model to Apple Inc. for the equivalent days. I find supporting evidence to the multitude of studies that use historical data or parallel derivatives markets such as VIX options, see for example Song and Xiu [2016], to compute the physical density function that the pricing kernel is in fact either heavily kinked or indeed markedly U-shaped. Finally, I provide a brief example for the application of the recovered 'physical' probability densities in risk management. A market left tail index is built using the recovered 'physical' probability densities for S&P 500 Index.

Chapter 7

Higher Dimensional Option-implied Average Correlations: Constructing the Cross Sectional Correlation Measures

7.1 Introduction

This chapter proposes a set of new pricing factors extracted from high frequency options panels that capture quadratic and higher order moments and co-moments. The Chicago Board Options Exchange ([CBOE](#)) currently provides an average implied correlation index computed using the Black-Scholes implied volatility straddle for individual constituents versus index options. However, there is mixed evidence on the usefulness of this index as a time series factor in a standard asset pricing framework.

My results show several key points, first that higher order average co-dependency does not have a unit correlation across measures. Secondly, the degree of decay in the value of the factor decreases inline with the degree expected from a simple representative agent model where current period

consumption is traded off against future consumption with non-zero higher odd moments and potentially excess kurtosis and diversification is costly. It should be emphasised that empirically comparing the advantage of the newly constructed option-implied average correlations over the ones from the existing studies is out of the scope of this thesis and left for future works.

Traditionally, options prices have been used to measure derivative market traders aggregate opinion on forward variation. Many prior studies have carefully documented empirical evidence illustrating that the higher moments extracted from the individual equity options play important role in explaining and forecasting cross-sectional stock returns, see [Chang et al. \[2013\]](#), [Conrad et al. \[2013\]](#), and [Bali et al. \[2015\]](#) for the most recent examples. In addition to the risk-neutral moments and co-moments, [Skintzi and Refenes \[2005\]](#) proposes a method to extract the option-implied correlations from the option prices of the individual stocks and the market index. [Driessen et al. \[2009\]](#) provide a stochastic correlation model to estimate the price of the correlation risk premium. The following work by [Krishnan et al. \[2009\]](#) and [Driessen et al. \[2013\]](#) document significant evidence that the option-implied average correlations have remarkable explanatory power for the variance premium.

Built on the previous studies of the option-implied moments and co-moments, the main focus of this chapter is to construct the cross-sectional correlation measures utilising high frequency option data panels. Specifically, I uniquely introduce a series of analogous correlation measures, namely the average cubic and quartic correlations, which are estimated based on the third and fourth central moments. Together with the conventional quadratic average correlation, the higher dimensional average correlations provide a multi-dimensional description of the correlation structure of the market portfolio, which can also be interpreted as a measure of the market diversification level.

My work contributes to various strands of literature in correlation structure and option-implied average correlations. Evidence from portfolio management and asset allocation has shown that correlation actually varies through time and a growing body of research has been motivated to investigate the role of correlations based on a historical information set, see for example

Von Furstenberg et al. [1989] and Longin and Solnik [1995]. Longstaff et al. [2001] and De Jong et al. [2004] provide evidence that interest rate correlations implied by cap and swaption prices differ from realised correlations.

Option-implied correlations have been computed extensively in the FX market, using currency triangles to back out the implied correlation function from the implied volatility surface. Bodurtha and Shen [1995], Campa et al. [1998], and Walter and Lopez [2000], and Mueller et al. [2016] among others have documented that these correlation surfaces do have some power in forecasting the discount on spot exchange rates. For equities, Skintzi and Refenes [2005] proposes an approach to extract correlations from option prices of the individual underlying assets and the market index. Driessen et al. [2009] provide a stochastic correlation model and intensively estimate the option-implied correlation and the correlation premium risk using data for S&P 100 index option and the components equity options.

Using a cross-sectional approach, Krishnan et al. [2009] and Driessen et al. [2013] provided evidence that the option-implied average correlation is a risk factor in market volatility and the option-implied correlations have remarkable predictive power for future stock market returns. Zhou [2013] examines the information contents of the CBOE S&P 500 Implied Correlation Index (ICJ) and concludes that the the current information set of ICJ changes can be used for predicting return of the S&P 500 Index in seven to ten months.

The CBOE option-implied average correlation index is calculated from the option-implied volatility of the index and the individual component options, which measures the market's systematic risk at the second moment. To compute this index, CBOE creates a tracking basket of the 50 largest components versus the options traded on the index and re-normalises the tracking index presuming that the 50 largest firms contain the majority of the weighted information on the implied volatility of the S&P 500. The individual and index volatilities are computed using the at-the-money straddle, which is the average of the implied volatility of the option with the nearest strike to the equivalent maturity future.

However, there are well understood limitations to the Back-Scholes models, the most particular being that the geometric Brownian motion (GBM) driving

the stochastic process has a time homogenous volatility parameter. Setting σ_i , $i \in \{1, \dots, N + 1\}$ to be the Black-Scholes implied volatilities for the individual components and the index, where we presume that the $N + 1$ asset is the index and the $i = 0$ is a pure discount bond. Average implied correlations are computed by the ratio of the implied integrated index variance minus the capitalisation weighted sum of constituent variances divided by the sum of the weighted cross products (excluding the diagonal products), which is denoted by

$$\bar{\rho} = \frac{(\sigma_{N+1} - \sum_{i=1}^N w_i^2 \sigma_i^2)}{(2 \sum_{i=1}^N \sum_{j=i+1}^N w_i w_j \sigma_i \sigma_j)}, \quad (7.1)$$

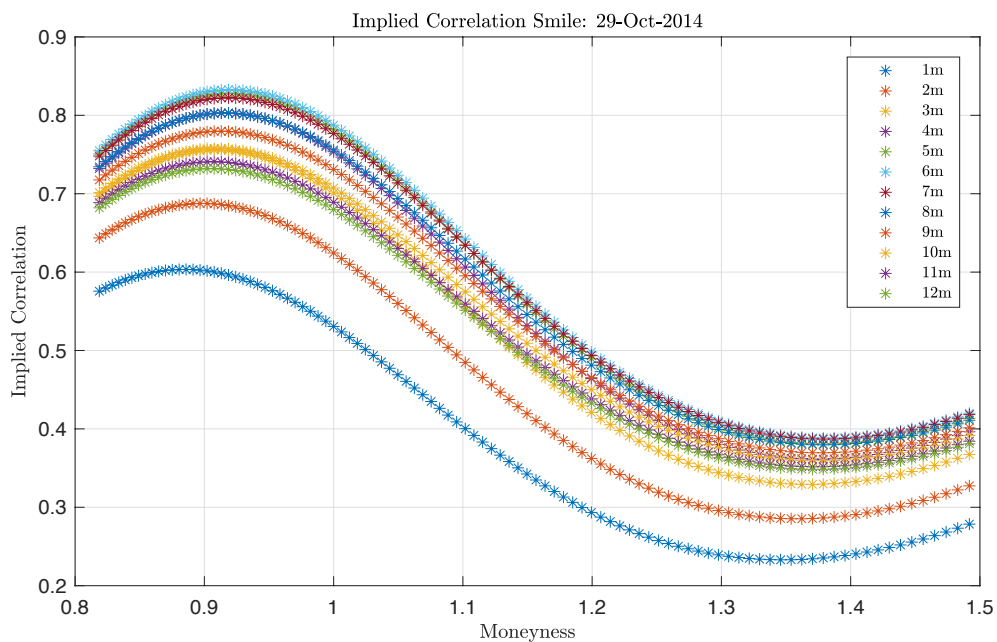
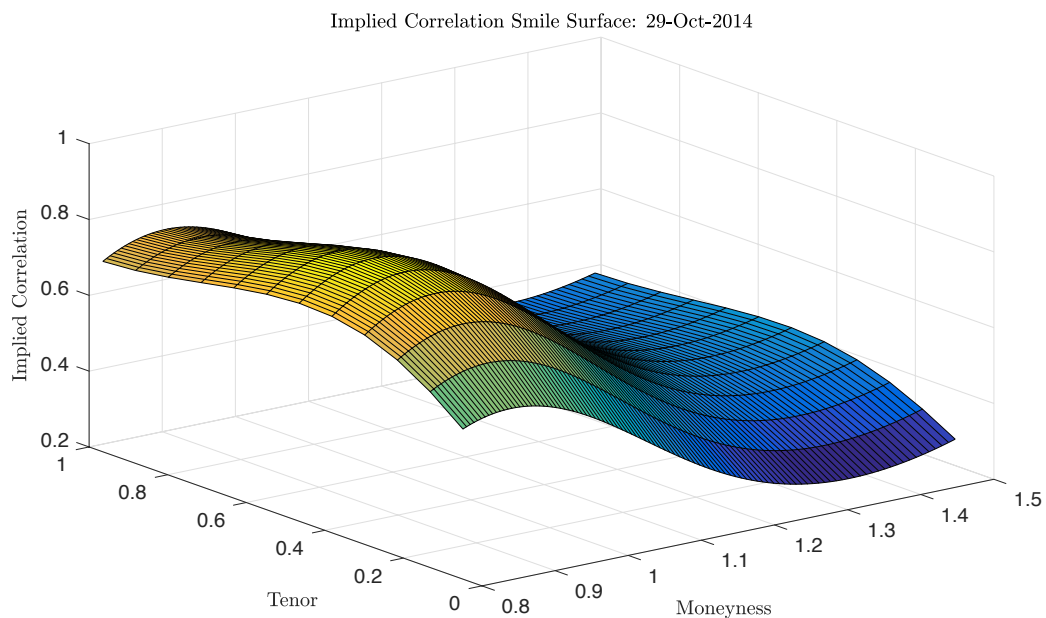
where w_i represents the holding weights for the individual stock in the index and normally is calculated based on the market capitalisation of each company in practice.

There are some issues with the [CBOE](#) approach. For example, In [Figure 7.1](#) I recompute the implied correlation for the S&P 500 for a single day on October 29, 2014 over a range of moneyness, K/S , where K is the strike price and S is the current spot price and over time to maturities from one month to twelve months. To do this I compute the implied volatility for every option traded for the S&P 500 index and all of its constituents. For each set of options I compute the average of the put and call implied volatilities and then estimate the following third order polynomial regression

$$\begin{aligned} \sigma_{i,j} = & \beta_1 + \beta_2 T_{i,j} + \beta_3 T_{i,j}^2 + \beta_4 T_{i,j}^3 + \beta_4 \log \left(\frac{K_{i,j}}{S_{i,j}} \right) \\ & + \beta_5 \log \left(\frac{K_{i,j}}{S_{i,j}} \right)^2 + \beta_6 \log \left(\frac{K_{i,j}}{S_{i,j}} \right)^3 + \epsilon_{i,j}, \end{aligned} \quad (7.2)$$

where $j \in \{1, \dots, J\}$ is the list of all options traded and $T_{i,j}$ is the time to maturity. I then create a fixed grid over T and $\log(K/S)$ and compute the implied correlations using the [CBOE](#) method and plot the implied correlations.

Figure 7.1: The Option-implied Average Correlation Smile Surface and Term Structure



Note. Figure 7.1 displays the option-implied average correlation smile surface (upper panel) and the term structure of the option-implied average correlation smiles calculated based on the Black-Scholes implied volatilities of the index and individual equity options on October 29, 2014.

Figure 7.1 clearly shows that there is a great deal of variation in the implied correlation over the range of strikes, with low values of K/S having a very high correlation. Not only does the value of the implied correlation vary across moneyness and time to maturities, but we can also see that tracking any given point on the correlation surface can have very different correlation dynamics. Hence deciding on which correlation to use is a very tricky decision, if one is sticking to a Black-Scholes type framework.

In contrast to the CBOE approach, I extract the risk-neutral moments from the option prices utilising the model-free spanning contracts proposed by Bakshi and Madan [2000] and Carr and Madan [2001], which suggests that the risk-neutral moments of assets expected returns can be spanned by the integration of a series of out-of-the-money call and put option prices. For the focus of this chapter, I derive the exact formulas for the second, third, and fourth risk-neutral central moments of assets expected returns in Chapter 4.

Motivated by the evidence that the higher order moments and co-moments are significant risk factors in cross-sectional stock returns (see for example Driessen et al. [2009], Driessen et al. [2013], and Conrad et al. [2013] among others), I extend the quadratic option-implied average correlation into higher dimensional correlations estimating from the risk-neutral higher moments and co-moments. Similar to the quadratic option-implied average correlation, the cubic and quartic correlations provide measures of the market diversification from higher dimensions.

Specifically, the cubic average correlation provides the average triple-wise correlations among the individual assets while the quartic average correlation measures the average of the quadruple-wise correlations of the portfolio. I use the options written on the S&P 500 index as the proxy for the market portfolio and the options written on all of the index components to extract the risk neutral central moments and estimate the quadratic, cubic, and quartic option-implied average correlations.

The remainder of the chapter is organised as follows: Section 7.2 details the theoretical derivations of the higher dimensional average correlations. Section 7.3 briefly describes the high frequency option data used to construct the higher dimensional option-implied average correlations. Section 7.4 illustrates

the empirical procedures for estimating the risk-neutral higher order central moments from option prices. Section 7.5 constructs the market and sectorial higher dimensional option-implied average correlation indices utilising the theoretical results in Section 7.2. The validity of the market portfolio moments decomposition is investigated in Section 7.6. Section 7.7 concludes this chapter.

7.2 The Higher Dimensional Average Correlations

In this section, I derive the analogous higher dimensional average correlations from the third and fourth central moments and co-moments of assets' returns, namely the cubic and quartic average correlations. The derivations of the higher dimensional average correlations borrow the symmetric multidimensional tensor algebra, which largely reduces the computation for the higher order co-moments arrays.

Consider a market with N continuously traded assets, indexing by $i = 1, 2, \dots, n$. The price of the i th asset at time t is denoted by $S_{i,t}$, where $t = 1, 2, \dots, T$. There exists an aggregated market index, which is a value-weighted portfolio and each of the N component individual assets contribute to the index level weighted by its market capitalisation. At a given time t , the weights of asset i in the market portfolio is defined by:

$$w_{i,t} = \frac{S_{i,t} \times \text{SHROUT}_{i,t}}{\sum_{i=1}^N S_{i,t} \times \text{SHROUT}_{i,t}}, \quad 1 \leq i \leq N \quad (7.3)$$

where $\text{SHROUT}_{i,t}$ represents the total number of outstanding shares for asset i at time t . The market index is not traded and the level of the market index is updated continuously corresponding to the price changes of the N component assets. The level of the market index at time t is denoted by $S_{m,t}$, where $t = 1, 2, \dots, T$.

Let $R_{i,t}$ and $R_{m,t}$ be the log-return for asset i and the market portfolio m

at time t such that:

$$R_t = \ln S_{t+1} - \ln S_t. \quad (7.4)$$

We can express the second, third and fourth central moments of the expected returns for asset i at time t by:

$$\begin{aligned} \sigma_{i,t}^2 &= \mathbb{E}[(R_{i,t} - \mathbb{E}[R_{i,t}])^2], \\ s_{i,t}^3 &= \mathbb{E}[(R_{i,t} - \mathbb{E}[R_{i,t}])^3], \\ k_{i,t}^4 &= \mathbb{E}[(R_{i,t} - \mathbb{E}[R_{i,t}])^4]. \end{aligned} \quad (7.5)$$

Accordingly, the *un-normalised* second, third, and fourth co-moments can be given by:

$$\begin{aligned} \sigma_{i,j} &= \mathbb{E}[(R_{i,t} - \mathbb{E}[R_{i,t}]) (R_{j,t} - \mathbb{E}[R_{j,t}])], \\ s_{i,j,k} &= \mathbb{E}[(R_{i,t} - \mathbb{E}[R_{i,t}]) (R_{j,t} - \mathbb{E}[R_{j,t}]) (R_{k,t} - \mathbb{E}[R_{k,t}])], \\ k_{i,j,k,l} &= \mathbb{E}[(R_{i,t} - \mathbb{E}[R_{i,t}]) (R_{j,t} - \mathbb{E}[R_{j,t}]) (R_{k,t} - \mathbb{E}[R_{k,t}]) (R_{l,t} - \mathbb{E}[R_{l,t}])]. \end{aligned} \quad (7.6)$$

where $\sigma_{i,j}$ is the well-known covariance between assets i and j . Analogously, $s_{i,j,k}$ represents the co-skewness among assets i , j , and k , and $k_{i,j,k,l}$ is the co-kurtosis among assets i , j , k , and l .

Recall that the market index S_m is a value-weighted portfolio of all individual assets. Let \mathbf{w}_t be the $(N \times 1)$ weight vector for the N assets such that $\mathbf{w}_t := \{w_{i,t}, 1 \leq i \leq N\}$, where $w_{i,t}$ as defined in Equation 7.3. Denote the covariance matrix by $\mathbf{\Sigma}$, the co-skewness array by $\mathbf{\Gamma}$, and the co-kurtosis array by $\mathbf{\Theta}$. Thus, the second, third, and fourth central moments of the expected return of the market portfolio at time t can be expressed by:

$$\begin{aligned} \sigma_{m,t}^2 &= \mathbb{E} [(R_{m,t} - \mathbb{E}[R_{m,t}])^2] = \mathbf{w}_t' \mathbf{\Sigma}_t \mathbf{w}_t, \\ s_{m,t}^3 &= \mathbb{E} [(R_{m,t} - \mathbb{E}[R_{m,t}])^3] = \mathbf{w}_t' \mathbf{\Gamma}_t (\mathbf{w}_t \otimes \mathbf{w}_t), \\ k_{m,t}^4 &= \mathbb{E} [(R_{m,t} - \mathbb{E}[R_{m,t}])^4] = \mathbf{w}_t' \mathbf{\Theta}_t (\mathbf{w}_t \otimes \mathbf{w}_t \otimes \mathbf{w}_t). \end{aligned} \quad (7.7)$$

where \otimes is the Kronecker product operator ¹ and $'$ is the matrix transpose operator.

The second order co-moment array Σ , i.e. the covariance matrix, is very popular and widely used in asset pricing and portfolio management. But the higher order co-moments arrays Γ and Θ are less well-understood given the complicated multidimensional structures. In particular, when it comes to portfolio with a large number of assets, the estimations of the elements of the co-moments arrays become extremely complicated.²

Instead of estimating the co-moments array directly, I derive a sets of average correlations that measure the total diversification of the portfolio from different dimensions. In the following, I first introduce a series of correlation analogues. Recall that the standard correlation coefficient between asset i and j is defined as:

$$\rho_{i,j} = \frac{\sigma_{i,j}}{\sigma_i \sigma_j}, \quad (7.8)$$

where $\sigma_{i,j}$ is the covariance between asset i and j , and σ_i and σ_j are the standard deviations for asset i and asset j , which is calculated as the square root of σ_i^2 and σ_j^2 respectively. Similarly, following [Buckle et al. \[2014\]](#), I formally define the higher dimensional correlation analogues as the following:

Definition 7.1 (Higher Dimensional Correlation). Let s_i and k_i be the cubic and quartic root of the third and fourth central moments for the expected returns of asset i such that $s_i = \sqrt[3]{s_i^3}$ and $k_i = \sqrt[4]{k_i^4}$. Further assume that the third central moments are well-defined and non-zero. The cubic correlation

¹Let \mathbf{A} be an $(n \times p)$ matrix and \mathbf{B} be an $(m \times q)$ matrix, then the Kronecker product of \mathbf{A} and \mathbf{B} yields an $(mn \times pq)$ matrix such that:

$$\mathbf{A} \otimes \mathbf{B} = \begin{pmatrix} a_{1,1}\mathbf{B} & a_{1,2}\mathbf{B} & \cdots & a_{1,n}\mathbf{B} \\ a_{2,1}\mathbf{B} & a_{2,2}\mathbf{B} & \cdots & a_{2,n}\mathbf{B} \\ \vdots & \vdots & \ddots & \vdots \\ a_{m,1}\mathbf{B} & a_{m,2}\mathbf{B} & \cdots & a_{m,n}\mathbf{B} \end{pmatrix}.$$

²There is a strand of literature in portfolio management investigating various methods to simplify the estimation of higher dimensional co-moment arrays, see for example [Martellini and Ziemann \[2010\]](#), [Ghalanos et al. \[2015\]](#), and [Boudt et al. \[2015\]](#) among others.

$\rho_{i,j,k}$ and quartic correlation $\rho_{i,j,k,l}$ among assets i, j, k , and l are defined by:

$$\rho_{i,j,k} = \frac{s_{i,j,k}}{s_i s_j s_k}, \quad \rho_{i,j,k,l} = \frac{k_{i,j,k,l}}{k_i k_j k_k k_l}, \quad (7.9)$$

where $s_{i,j,k}$ and $k_{i,j,k,l}$ are the third and fourth central co-moments among assets i, j, k, l as given in Equation 7.6

Recall that the second-order covariance matrix and the quadratic correlation matrix are symmetric about the diagonal. By construction, the cubic and quartic correlations can also be expressed by symmetric multidimensional arrays with ones sitting on the super diagonals. I further define the average correlations as the arithmetic mean of the off-diagonal correlations such that:

Definition 7.2 (Higher Dimensional Average Correlations). Let ρ_Σ , ρ_Γ and ρ_Θ be the average quadratic, cubic, and quartic correlations for the off-diagonals of the correlation arrays respectively such that:

$$\begin{aligned} \rho_\Sigma &= \frac{1}{N^2 - N} \sum_{i=1}^{N^2-N} \rho_{i,j}, \quad i \neq j, \\ \rho_\Gamma &= \frac{1}{N^3 - N} \sum_{i=1}^{N^3-N} \rho_{i,j,k}, \quad i \neq j \neq k, \\ \rho_\Theta &= \frac{1}{N^4 - N} \sum_{i=1}^{N^4-N} \rho_{i,j,k,l}, \quad i \neq j \neq k \neq l. \end{aligned} \quad (7.10)$$

where N is the number of assets in the portfolio.

The definition for the higher dimensional average correlations is very straightforward. For a k th order correlation array with N assets, there are N (super) diagonal elements and $N^k - N$ off-diagonal elements. The average higher dimensional correlations are given by arithmetic mean of the off-diagonal elements in the higher dimensional correlation arrays.

With the average higher dimensional correlations, the co-moments arrays of the portfolio expected returns can be further decomposed by the (super) diagonal in the following Lemma:

Lemma 7.1 (Diagonal Decomposition of Co-moment Arrays). Let \mathbf{x} be a $N \times 1$ vector with entries x_i , where $1 \leq i \leq N$. Denote \mathbf{x}^k as the r th power of the vector \mathbf{x} and $\mathbf{x}^{[k]}$ as the vector permuted outer product of the vector \mathbf{x} with itself. For a given portfolio with N assets, the covariance matrix Σ , third and fourth co-moments arrays Γ and Θ can be decomposed by its (super) diagonal with the off-diagonal average quadratic correlation ρ_Σ , cubic correlation ρ_Γ and quartic correlation ρ_Θ such that:

$$\begin{aligned}\Sigma &= \text{diag}_2[\boldsymbol{\sigma}^2] + \rho_\Sigma \text{triu}_2[\boldsymbol{\sigma}^{[2]}] + \rho_\Sigma \text{tril}_2[\boldsymbol{\sigma}^{[2]}] \\ \Gamma &= \text{diag}_3[\mathbf{s}^3] + \rho_\Gamma \text{triu}_3[\mathbf{s}^{[3]}] + \rho_\Gamma \text{tril}_3[\mathbf{s}^{[3]}] \\ \Theta &= \text{diag}_4[\mathbf{k}^4] + \rho_\Theta \text{triu}_4[\mathbf{k}^{[4]}] + \rho_\Theta \text{tril}_4[\mathbf{k}^{[4]}].\end{aligned}\quad (7.11)$$

where $\boldsymbol{\sigma}$, \mathbf{s} , and \mathbf{k} are the $(N \times 1)$ root moments vectors for the N assets such that

$$\begin{aligned}\boldsymbol{\sigma} &:= \left\{ \sigma_i = \sqrt{\sigma_i^2}, 1 \leq i \leq N \right\}, \\ \mathbf{s} &:= \left\{ s_i = \sqrt[3]{s_i^3}, 1 \leq i \leq N \right\}, \\ \mathbf{k} &:= \left\{ k_i = \sqrt[4]{k_i^4}, 1 \leq i \leq N \right\}.\end{aligned}\quad (7.12)$$

and $\text{diag}_k[\cdot]$, $\text{triu}_k[\cdot]$, and $\text{tril}_k[\cdot]$ are the diagonal, upper, and lower triangular operators.

Proof for Lemma 7.1. Before proceeding the proof of the decomposition of higher dimensional co-moment arrays, I first declare some useful operators. Let \mathbf{x} be a $N \times 1$ vector with entries x_i , where $1 \leq i \leq N$. Denote \mathbf{x}^k as the r th power of the vector \mathbf{x} and $\mathbf{x}^{[k]}$ as the vector permuted outer product of the vector \mathbf{x} with itself. Thus, for $k = 2, 3, 4$ we have:

$$\begin{aligned}\mathbf{x}^2 &:= \{x_i = x_i^2, 1 \leq i \leq N\}, & \mathbf{x}^{[2]} &= \mathbf{x}\mathbf{x}'; \\ \mathbf{x}^3 &:= \{x_i = x_i^3, 1 \leq i \leq N\}, & \mathbf{x}^{[3]} &= \mathbf{x}'(\mathbf{x} \otimes \mathbf{x}); \\ \mathbf{x}^4 &:= \{x_i = x_i^4, 1 \leq i \leq N\}, & \mathbf{x}^{[4]} &= \mathbf{x}'(\mathbf{x} \otimes \mathbf{x} \otimes \mathbf{x}).\end{aligned}\quad (7.13)$$

Let \mathbf{x}^k be the r th power of the vector \mathbf{x} , then $\text{diag}_k[\mathbf{x}^k]$ is the k dimensional diagonal operator that turns the $N \times 1$ vector \mathbf{x} into a k dimensional array that with the elements of the vector on the (super) diagonal and all other elements being zeros. For example, for $k = 2$, $\text{diag}_2[\mathbf{x}^k]$ results a two dimensional $N \times N$ array such that:

$$\text{diag}_2[\mathbf{x}^2] = \begin{pmatrix} x_1^2 & 0 & \cdots & 0 \\ 0 & x_2^2 & \cdots & 0 \\ \vdots & \vdots & \ddots & \vdots \\ 0 & 0 & \cdots & x_N^2 \end{pmatrix}.$$

For $k = 3$, $\text{diag}_3[\mathbf{x}^3]$ gives a three dimensional $N \times N \times N$ array with x_i^3 sitting on the super-diagonal and all the other elements being zeros.

Let $\mathbf{x}^{[k]}$ be the vector permuted outer product of the vector \mathbf{x} with itself. $\text{triu}_k[\mathbf{x}^{[k]}]$ is the upper triangular operator that returns the upper triangular part of the r dimensional array $\mathbf{x}^{[k]}$. Similarly, $\text{tril}_k[\mathbf{x}^{[k]}]$ is the lower triangular operator that returns the lower triangular part of the r dimensional array $\mathbf{x}^{[k]}$. For example, for $k = 2$, $\text{triu}_2[\mathbf{xx}']$ and $\text{tril}_2[\mathbf{xx}']$ return the following 2 dimensional $N \times N$ upper triangular and lower triangular arrays such that:

$$\text{triu}_2[\mathbf{xx}'] = \begin{pmatrix} 0 & x_1x_2 & \cdots & x_1x_N \\ 0 & 0 & \cdots & x_2x_N \\ \vdots & \vdots & \ddots & \vdots \\ 0 & 0 & \cdots & 0 \end{pmatrix}; \quad \text{tril}_2[\mathbf{xx}'] = \begin{pmatrix} 0 & 0 & \cdots & 0 \\ x_2x_1 & 0 & \cdots & 0 \\ \vdots & \vdots & \ddots & \vdots \\ x_Nx_1 & x_Nx_2 & \cdots & 0 \end{pmatrix}.$$

The proof for Lemma 7.1 then follows from the preceding text by combining the definitions of the higher dimensional average correlations, diagonal operator and the upper and lower triangular operators. \square

Substituting the decomposition results in Lemma 7.1 back into the expressions of the central moments for the portfolio in Equation 7.7, we have:

$$\begin{aligned} \sigma_m^2 &= \mathbf{w}' \text{diag}_2[\boldsymbol{\sigma}^2] \mathbf{w} + \rho_\Sigma \mathbf{w}' (\text{triu}_2[\boldsymbol{\sigma}^{[2]}] + \text{tril}_2[\boldsymbol{\sigma}^{[2]}]) \mathbf{w}, \\ s_m^3 &= \mathbf{w}' \text{diag}_3[\mathbf{s}^3] (\mathbf{w} \otimes \mathbf{w}) + \rho_\Gamma \mathbf{w}' (\text{triu}_3[\mathbf{s}^{[3]}] + \text{tril}_3[\mathbf{s}^{[3]}]) (\mathbf{w} \otimes \mathbf{w}), \\ k_m^4 &= \mathbf{w}' \text{diag}_4[\mathbf{k}^4] (\mathbf{w} \otimes \mathbf{w} \otimes \mathbf{w}) + \rho_\Theta \mathbf{w}' (\text{triu}_4[\mathbf{k}^{[4]}] + \text{tril}_4[\mathbf{k}^{[4]}]) (\mathbf{w} \otimes \mathbf{w} \otimes \mathbf{w}). \end{aligned} \quad (7.14)$$

The estimation is quite straightforward for the second central moment as the covariance array is simply a two dimensional $N \times N$ matrix while dealing with high moments can easily become algebraically cumbersome or even intractable. However, we can simplify the estimations by identifying the symmetric structure of the co-moments array.

For any n -dimensional random vector, its co-moments can be seen as multi-dimensional tensors. Specifically, the covariance array Σ is a two-way tensor with dimension $N \times N$, the co-skewness array Γ is a three-way tensor with dimension $N \times N \times N$, and the co-kurtosis array Θ is a four-way tensor with dimension $N \times N \times N \times N$. Given the super symmetric structure of the multidimensional tensors, the derivation of the higher dimensional average correlations becomes available.

In general, for N assets, the number of independent elements N^* in the covariance, third and fourth co-moments tensors can be expressed by:

$$N^* = \begin{cases} \frac{N(N+1)}{2}, & \text{out of } N^2 \text{ in } \Sigma; \\ \frac{N(N+1)(N+2)}{6}, & \text{out of } N^3 \text{ in } \Gamma; \\ \frac{N(N+1)(N+2)(N+3)}{24}, & \text{out of } N^4 \text{ in } \Theta. \end{cases} \quad (7.15)$$

Consider for $N = 500$, there are $500^4 = 62,500,000,000$ elements in the four-dimensional co-kurtosis matrix, but only $(500 \times (500 + 1) \times (500 + 2) \times (500 + 3))/24 = 2,635,531,375$ elements are unique and need to be computed, which is only around 4% of 500^4 and is computable using [IEEE](#) (Institute of Electrical and Electronics Engineers) double precision convention.

According to Equation 7.14, in order to estimate the average correlations ρ_Σ , ρ_Γ , and ρ_Θ we need to calculate the diagonal co-moment array, the upper triangular co-moment array and the lower triangular co-moment array for each moments. Noted, the average correlations ρ_Σ , ρ_Γ , and ρ_Θ are scalars and we don't need to investigate the structural arrays but the sum of the off-diagonal elements of the co-moment arrays. As I have shown in the earlier example, the off-diagonal elements in the co-moment tensors include many duplicated entries. In fact, the sum of the off-diagonals can be calculated as the product of a symmetric multiplier and the sum of the unique elements.

Taking advantage of the symmetric structure of the multidimensional co-moments tensors, I derive the formulas for estimating the average higher dimensional correlations in the following proposition:

Proposition 7.1 (Estimations for Higher Dimensional Correlations). Given the central moments for the market portfolio, σ_m^2 , s_m^3 , and k_m^4 and the holding weights for each components, w_i , and the standard root moments for the assets in the portfolio, σ_i , s_i , and k_i , the average quadratic correlation ρ_Σ , cubic correlation ρ_Γ , and quartic correlation ρ_Θ can be estimated by:

$$\begin{aligned}
\rho_\Sigma &= \frac{\sigma_m^2 - \sum_{i=1}^N w_i^2 \sigma_i^2}{\Lambda_{i,j} \sum_{i=1}^N \sum_{j>i}^N w_i w_j \sigma_i \sigma_j} \\
\rho_\Gamma &= \frac{s_m^3 - \sum_{i=1}^N w_i^3 s_i^3}{\Lambda_{i,j,k} \sum_{i=1}^N \sum_{j>i}^N w_i w_j w_k s_i s_j s_k} \\
\rho_\Theta &= \frac{k_m^4 - \sum_{i=1}^N w_i^4 k_i^4}{\Lambda_{i,j,k,l} \sum_{i=1}^N \sum_{j=i}^N \sum_{k=j}^N \sum_{l>i}^N w_i w_j w_k w_l k_i k_j k_k k_l}.
\end{aligned} \tag{7.16}$$

where $\Lambda_{i,j}$, $\Lambda_{i,j,k}$, and $\Lambda_{i,j,k,l}$ are the symmetric multipliers such that:

$$\begin{aligned}
\Lambda_{i,j} &= 2; \\
\Lambda_{i,j,k} &= \begin{cases} 6, i \neq j \neq k, \\ 3, \text{any two of } i, j, k \text{ are duplicated.} \end{cases} \\
\Lambda_{i,j,k,l} &= \begin{cases} 24, i \neq j \neq k \neq l, \\ 12, \text{one pair of } i, j, k, l \text{ are duplicated,} \\ 6, \text{two pairs of } i, j, k, l \text{ are duplicated,} \\ 4, \text{any three of } i, j, k, l \text{ are duplicated.} \end{cases}
\end{aligned} \tag{7.17}$$

Proof for Proposition 7.1. I have demonstrated the (super) diagonal decomposition of the co-moment arrays in Lemma 7.1, which yields the

following summation expression of the market portfolio moments:

$$\begin{aligned}
\sigma_m^2 &= \sum_{i=1}^N w_i^2 \sigma_i^2 + \rho_\Sigma \sum_{i=1}^N \sum_{j=1}^N w_i w_j \sigma_i \sigma_j, \\
s_m^3 &= \sum_{i=1}^N w_i^3 s_i^3 + \rho_\Gamma \sum_{i=1}^N \sum_{j=1}^N \sum_{k=1}^N w_i w_j w_k s_i s_j s_k, \\
k_m^4 &= \sum_{i=1}^N w_i^4 k_i^4 + \rho_\Theta \sum_{i=1}^N \sum_{j=1}^N \sum_{k=1}^N \sum_{l=1}^N w_i w_j w_k w_l k_i k_j k_k k_l.
\end{aligned} \tag{7.18}$$

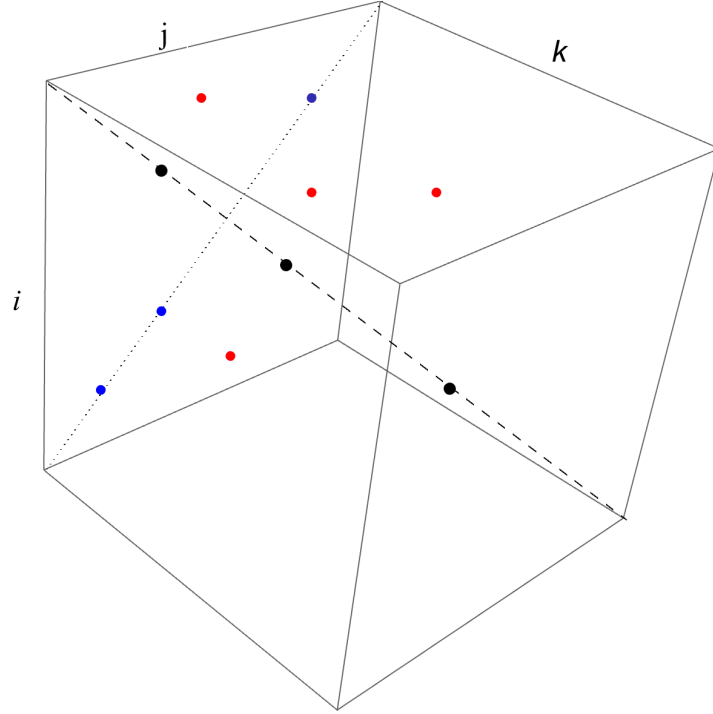
In order to estimate the sum of the off-diagonal elements in the co-moments arrays, we take advantage of the symmetric structure of the higher dimensional tensors to simplify the calculate by deriving the symmetric multiplier, Λ , for each of the co-moments tensors.

The case for the $N \times N$ two-way covariance tensor is very straightforward. When $i \neq j$, the off-diagonal elements are symmetric about the diagonal, i.e. $\sigma_i \sigma_j = \sigma_j \sigma_i$. Thus the symmetric multiplier is simply:

$$\Lambda_{i,j} = 2, \text{ All elements are unique: } i \neq j. \tag{7.19}$$

The cases for the three-way cubic correlation tensor and four-way quartic correlation tensor are more complicated. The three-way cubic correlation tensor can be seen as a cube, see Figure 7.2.

Figure 7.2: Three Dimensional Decomposition



The elements in the three-way cubic correlation tensor can be classified into three groups:

1. Group 1: When all of the three elements are duplicated, i.e. $i = j = k$, the co-moment elements lie on the super diagonal of the cube with unity cubic correlation, which are the black points on the dashed line.
2. Group 2: When only two of the elements are duplicated, i.e. either $i = j$ or $i = k$ or $j = k$, the co-moment elements lie on the planes, which are the blue points on the dot line.
3. Group 3: when all of the three elements are unique, i.e. $i \neq j \neq k$, the co-moment elements are in the three-dimensional space, which are the red interior points.

For the off-diagonal elements (the points on the plane and interior points), we can get the symmetric multiplier $\Lambda_{i,j,k}$ by the number of different

combinations by applying the binomial theory:

$$\Lambda_{i,j,k} = \begin{cases} 3! = 6, & \text{all elements are unique;} \\ 3!/2! = 3, & \text{any two of the elements are duplicated.} \end{cases} \quad (7.20)$$

Similarly, for the four-way quartic correlation tensor, we have the symmetric multiplier $\Lambda_{i,j,k,l}$ such that:

$$\Lambda_{i,j,k,l} = \begin{cases} 4! = 24, & \text{all elements are unique;} \\ 4!/2! = 12, & \text{one of the elements are duplicated;} \\ 4!/2!/2! = 6, & \text{two of the elements are duplicated;} \\ 4!/3! = 4, & \text{three of the elements are duplicated.} \end{cases} \quad (7.21)$$

Thus, the central moments of the market portfolio in Equation 7.18 can be re-written as:

$$\begin{aligned} \sigma_m^2 &= \sum_{i=1}^N w_i^2 \sigma_i^2 + \rho_\Sigma \Lambda_{i,j} \sum_{i=1}^N \sum_{j>i}^N w_{i,t} w_j \sigma_i \sigma_j, \\ s_m^3 &= \sum_{i=1}^N w_i^3 s_i^3 + \rho_\Gamma \Lambda_{i,j,k} \sum_{i=1}^N \sum_{j=i}^N \sum_{k>i}^N w_i w_j w_k s_i s_j s_k, \\ k_m^4 &= \sum_{i=1}^N w_i^4 k_i^4 + \rho_\Theta \Lambda_{i,j,k,l} \sum_{i=1}^N \sum_{j=i}^N \sum_{k=j}^N \sum_{l>i}^N w_i w_j w_k w_l k_i k_j k_k k_l. \end{aligned} \quad (7.22)$$

where $\Lambda_{i,j}$, $\Lambda_{i,j,k}$, and $\Lambda_{i,j,k,l}$ are the symmetric factors as given in Equation 7.19, 7.20 and 7.21. Reorganise and solve for ρ_Σ , ρ_Γ , and ρ_Θ we get the formulas in Equation 7.16. \square

Noted the average quadratic, cubic, and quartic correlations we derived in Proposition 7.1 are a weighted average of all pair-wise, triple-wise, and quadruple-wise correlations of the constituents of the market portfolio, which gives average measures of the degree of diversification in the market portfolio. Formally, we can derive the upper and lower bounds for the cubic-correlation and quartic-correlation from the following Corollary:

Corollary 7.1 (A Measure for Degree of Diversification). Let the pairs $\{\sigma_{m,min}^2, \sigma_{m,max}^2\}$, $\{s_{m,min}^3, s_{m,max}^3\}$, and $\{k_{m,min}^4, k_{m,max}^4\}$ be the upper and lower bound of the second, third, and fourth central moments of the market portfolio m , then the average correlations we derived in Proposition 7.1 can be interpreted as a measure for degree of diversification of the market portfolio m , which quantifies the difference between the minimum and maximum values of the portfolio moments, such that:

$$\begin{aligned}\rho_{\Sigma} &= \frac{\sigma_m^2 - \sigma_{m,min}^2}{\sigma_{m,max}^2 - \sigma_{m,min}^2} \\ \rho_{\Gamma} &= \frac{s_m^3 - s_{m,min}^3}{s_{m,max}^3 - s_{m,min}^3} \\ \rho_{\Theta} &= \frac{k_m^4 - k_{m,min}^4}{k_{m,max}^4 - k_{m,min}^4}.\end{aligned}\tag{7.23}$$

Proof for Corollary 7.1. The minimum aggregate moments for the portfolio with N assets are achieved when the assets in the portfolio are fully diversified, i.e. $\rho = 0$. Similarly, we obtain the maximum aggregate moment for the portfolio in the case that there is no diversification, i.e. $\rho = 1$. Substituting $\rho = 0$ and $\rho = 1$ into the expressions for the portfolio moments in Equation 7.16 we can obtain the lower bounds of the central moments of the market portfolio such that:

$$\begin{aligned}\sigma_{m,min}^2 &= \sum_{i=1}^N w_i^2 \sigma_i^2, \\ s_{m,min}^3 &= \sum_{i=1}^N w_i^3 s_i^3, \\ k_{m,min}^4 &= \sum_{i=1}^N w_i^4 k_i^4.\end{aligned}\tag{7.24}$$

and the upper bounds of the central moments of the market portfolio such

that:

$$\begin{aligned}
\sigma_{m,max}^2 &= \sum_{i=1}^N w_i^2 \sigma_i^2 + \Lambda_{i,j} \sum_{i=1}^N \sum_{j>i}^N w_i w_j \sigma_i; \\
s_{m,max}^3 &= \sum_{i=1}^N w_i^3 s_i^3 + \Lambda_{i,j,k} \sum_{i=1}^N \sum_{j=i}^N \sum_{k>i}^N w_i w_j w_k s_i s_j s_k; \\
k_{m,max}^4 &= \sum_{i=1}^N w_i^4 k_i^4 + \Lambda_{i,j,k,l} \sum_{i=1}^N \sum_{j=i}^N \sum_{k=j}^N \sum_{l>i}^N w_i w_j w_k w_l k_i k_j k_k k_l.
\end{aligned} \tag{7.25}$$

where $\Lambda_{i,j}$, $\Lambda_{i,j,k}$, and $\Lambda_{i,j,k,l}$ are the symmetric multipliers as given in Equation 7.17 in Proposition 7.1. The proof of the expressions in Equation 7.23 then follows. \square

7.3 Data

7.3.1 Daily Market Capitalisation Data for S&P 500 Index Constituents

The list of S&P 500 Index constituents from January 1, 1996 to January 1, 2015 is from Compustat and the daily price and number of share outstanding for each stocks are obtained from the Centre for Research in Security Prices (CRSP) archived by the Wharton Research Data Services (WRDS).

7.3.2 High Frequency Option Data Panels for S&P 500 Index and its Constituents

The option data of the S&P 500 index option and the individual equity options on all of the S&P 500 constituents are obtained from the TRTH through January 1, 1996 to January 1, 2015. Unlike the actively trading for options written on the S&P 500 index, trading for some single-name equity options may be quite illiquid. In fact, as documented on the TRTH, the trading for single-name equity options prior 2005 is very thin and not all of the index components equities have options traded on the exchange. Thus, I limit the

attention to a subset of stocks which are known to be highly traded and liquid. I have no intention to be fully comprehensive in my sample and are inclined to drop stocks for which option trading is too thin rather than including them in the analyses. After excluding the index components that are either illiquid traded nor have no options written on, the sample ends up with 588 constituents.³

Options on the S&P 500 index are European style and expire on the third Friday of the contract month while options on individual equities are American style and usually expire on the Saturday following the third Friday of the contract month. For both the S&P 500 index option and each single-name equity options, we extract the intraday one-minute quotes data for all available strike prices and maturities. For each company, I then screen the option price data according to the conventional criteria (a) drop the observations with missing quotes, or zero bids; (b) drop the observations with zero trading volume or zero quotes size; (c) drop the observation with option prices that violate the put-call parity and arbitrage restrictions.

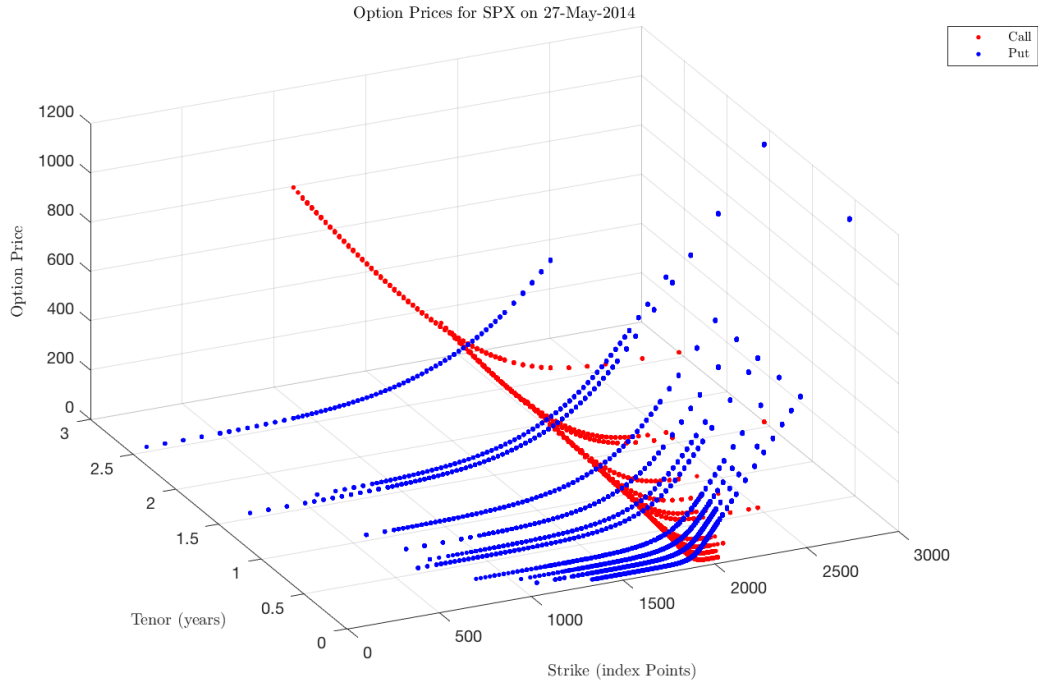
The spot prices for both the S&P 500 index and the index components are also obtained from the [TRTH](#) at a one-minute intraday frequency. The spot price for the S&P 500 index is backed by the S&P 500 index futures. The proxy for the risk-free rate is collected from the exchange-traded USD deposit rate from the [TRTH](#) at a one-minute intraday basis for the sample period. Finally, the high frequency option data panel is constructed by matching the option data, spot data, and risk-free rate data together with the nearest tick time stamp for each observation.

Figure [7.4](#) provides a snapshot of the high frequency option data panels.

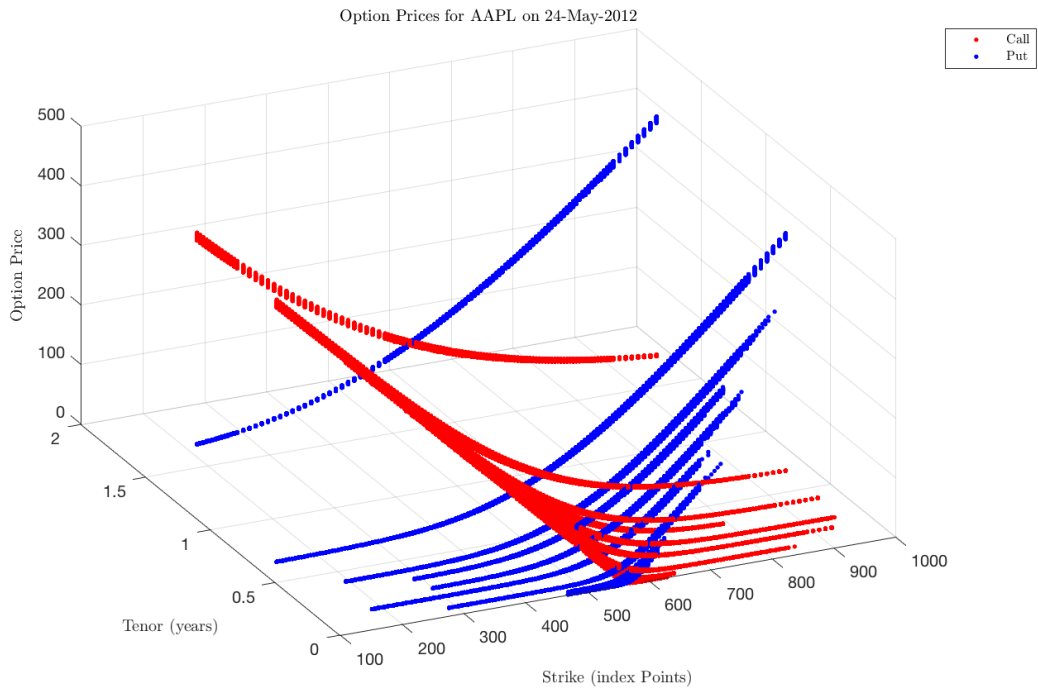
³Since 30th November, 2009, the option data on TRTH is based on the Option Price Reporting Authority national market system. OPRA was set up in 2009 and became effective on January 1, 2010. Under the OPRA National Market System plan, the trades and quotes data of all option contracts trading on the participating exchanges is gathered and consolidated or disseminated to approved vendors. The current participant exchanges include NYSE Amex Equities (AMEX), BATS Options (BATS), Boston Stock Exchange (BSE), Chicago Board Options Exchange (CBOE), International Securities Exchange (ISE), NYSE Arca, and Philadelphia Stock Exchange (PHLX). In order to keep the consistent in the data coverage, trading data before the OPRA effective dates are collected by aggregating the data from all of the participating exchanges on a weighted-average basis if needed.

Each of the sub plots in Figure 7.4 displays the intraday bid-ask prices (z-axis) for option contracts traded at various strikes (x-axis) and time to maturities (y-axis) for the S&P 500 index and some selected individual companies, namely Apple (AAPL), International Business Machines Corporation (IBM), and Boeing Company (BA). The red points represents the call prices while the blue points stand for the put prices. The plots show that the unique high frequency option data panels provide complete and sufficient coverage of the option prices that can be utilised to extract the various information.

Figure 7.3: High Frequency Option Data Sample

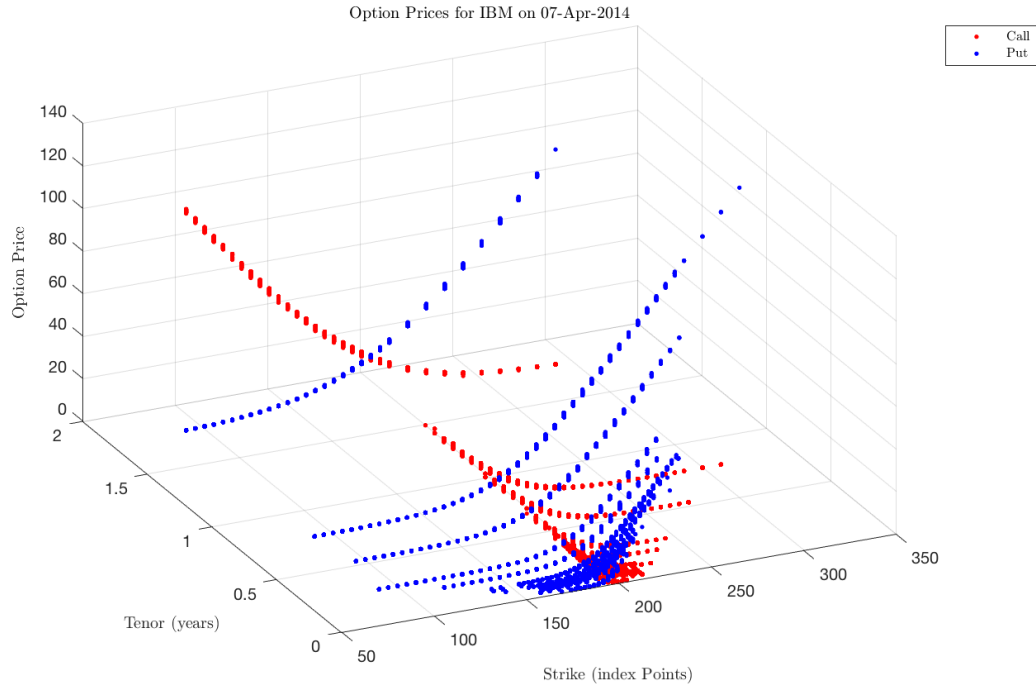


(a) SPX on 27-May-2014

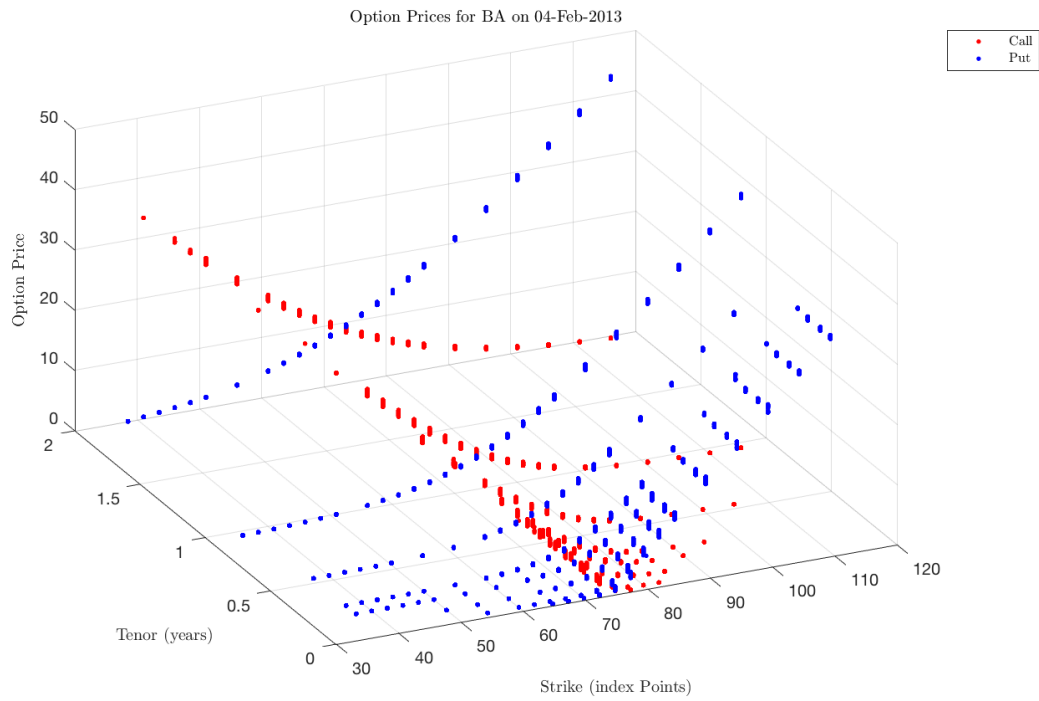


(b) AAPL on 24-May-2012

Figure 7.4: High Frequency Option Data Sample



(a) IBM on 07-Apr-2014



(b) BA on 04-Feb-2013

7.3.3 High Frequency Option Panels for Selected Sector Index

In addition to the high frequency option panels with S&P 500 Index and its constituent companies, I construct a sub dataset with Selected Sector Index. The Standard & Poor's Depository Receipts (SPDR) funds are a family of exchange-traded funds (ETFs) traded in the United States that divide the S&P 500 into ten index funds, namely the Energy (XLE), Materials (XLB), Industrials (XLI), Consumer Discretionary (XLY), Consumer Staples (XLP), Health Care (XLV), Financial (XLF), Information Technology (XLK), Utilities (XLU), and Real Estate (XLRE).

Each Selected Sector Index is calculated using a modified 'market capitalisation' methodology, which ensures that each of the component stocks within a Selected Sector Index is represented in a proportion consistent with its percentage of the total market capitalisation of that particular index. Each Selected Sector SPDR is designed to closely track the price performance and dividend yield of a particular Selected Sector Index. Each portfolio is comprised principally of shares of constituent companies included in the S&P 500. In particular, each stock in the S&P 500 is allocated to only one Selected Sector Index. The combined companies of the ten Selected Sector Index represent all of the companies in the S&P 500 Index.⁴

The SPDR ETFs sector index are traded as stocks and can be short sold and optioned. Specifically, the options written on the Selected Sector Index are American style and usually expire on the third Friday of the contract month. As the Selected Sector Index are introduced separately and the options written on specific sector index are also established at different time. In order to keep the consistent of data across all sector index, I construct a sub dataset consisting of nine Selected Sector Index over the sample period from November 30, 2009 to January 1, 2015.⁵

⁴Sources: <http://www.sectorspdr.com/sectorspdr/features/about>.

⁵I exclude the Real Estate Index (XLRE), which began trading on Oct 8th, 2015 as it is out of the range of my sample period.

7.4 Estimate the Higher Order Risk Neutral Central Moments

In this section I detail the estimation procedures for the risk-neutral high order central moments as derived in Chapter 4. In particular, I address the key issues arising in estimating the risk-neutral moments from market option prices using the non-parametric spanning contracts method. Finally, I provide summary statistics and term-structure plots of the risk-neutral high order central moments for S&P 500 Index and the single-name equity options.

The risk-neutral high order central moments of S&P 500 index and individual stocks are estimated according to Equations 4.10, 4.11, and 4.12 proposed in Proposition 4.1 in Chapter 4. The estimation procedures are as follows. For a given day t , let S_t be the spot price. Let $\boldsymbol{\tau} = \{\tau_j, j = 1, \dots, J\}$ be the vector of the available time to maturities (tenors), where $\tau = T - t$ and T is the maturity date. For a given tenor, the option prices are sorted by the available strikes such that $K_i \in \{K_{\min}, K_{\max}\}$, where K_{\min} and K_{\max} are the minimum and maximum strikes of the traded option contracts over a given day.

A few technical issues raise in estimating the integrals in Equations 4.10, 4.11, and 4.12. First is the truncation problem as we need both out-of-the-money call and put option prices over a continuous list of strike prices from 0 to infinity, while we only have limited numbers of strike prices from the options traded in the market. Thus, the integral domain will be truncated by the minimum and maximum strikes available in the market, $\{K_{\min}, K_{\max}\}$.

Another issue is the discontinuity of the strike prices. The option prices are quoted at a specific strike price pattern thus we do not have a continuous series of strike prices. For example, for the options written on S&P 500 Index traded in CBOE, the strike prices are set with a \$5 interval. To tackle this issue, I first calculate the Black-Scholes implied volatility for each observations and fit the implied volatilities with a fourth-order polynomial.⁶ I then convert

⁶The single-name equity options are American style, thus the prices are embedded with early-exercise premium. I only use the out-of-the-money options to estimate of the risk-neutral central moments defined in Equation 4.10, 4.11, and 4.12, so the early-exercise premiums

the fitted implied volatilities back to call and put prices over the fitted equal-spaced strike prices grid, which I denote by $\hat{C}(\tau_j, \hat{K}_i)$ and $\hat{P}(\tau_j, \hat{K}_i)$. It should be emphasised that I use the Black-Scholes implied volatility as a normalised price and that our approach is not tied to the assumptions of the Black-Scholes model. Finally, I estimate the integrals using trapezoidal numerical integration such that:

$$\begin{aligned} \hat{M}_2^{\mathbb{Q}}(t, \tau_j) &= e^{-r_{f,j}\tau_j} [(r_{f,j}\tau_j)^2 + 2r_{f,j}\tau_j] - 2r_{f,j}\tau_j \\ &+ \frac{K_{\max} - S_t}{2\mathcal{N}} \sum_{i=1}^{\mathcal{N}} [\mathcal{C}_2(\tau_j, \hat{K}_i) + \mathcal{C}_2(\tau_j, \hat{K}_{i+1})] \\ &+ \frac{S_t - K_{\min}}{2\mathcal{N}} \sum_{i=1}^{\mathcal{N}} [\mathcal{P}_2(\tau_j, \hat{K}_i) + \mathcal{P}_2(\tau_j, \hat{K}_{i+1})]; \end{aligned} \quad (7.26)$$

$$\begin{aligned} \hat{M}_3^{\mathbb{Q}}(t, \tau_j) &= e^{-r_{f,j}\tau_j} [(r_{f,j}\tau_j)^3 - 3(r_{f,j}\tau_j)^2] + 3(r_{f,j}\tau_j)^2 \\ &+ \frac{K_{\max} - S_t}{2\mathcal{N}} \sum_{i=1}^{\mathcal{N}} [\mathcal{C}_3(\tau_j, \hat{K}_i) + \mathcal{C}_3(\tau_j, \hat{K}_{i+1})] \\ &+ \frac{S_t - K_{\min}}{2\mathcal{N}} \sum_{i=1}^{\mathcal{N}} [\mathcal{P}_3(\tau_j, \hat{K}_i) + \mathcal{P}_3(\tau_j, \hat{K}_{i+1})]; \end{aligned} \quad (7.27)$$

$$\begin{aligned} \hat{M}_4^{\mathbb{Q}}(t, \tau_j) &= e^{-r_{f,j}\tau_j} [(r_{f,j}\tau_j)^4 + 4(r_{f,j}\tau_j)^3] - 4(r_{f,j}\tau_j)^3 \\ &+ \frac{K_{\max} - S_t}{2\mathcal{N}} \sum_{i=1}^{\mathcal{N}} [\mathcal{C}_4(\tau_j, \hat{K}_i) + \mathcal{C}_4(\tau_j, \hat{K}_{i+1})] \\ &+ \frac{S_t - K_{\min}}{2\mathcal{N}} \sum_{i=1}^{\mathcal{N}} [\mathcal{P}_4(\tau_j, \hat{K}_i) + \mathcal{P}_4(\tau_j, \hat{K}_{i+1})]. \end{aligned} \quad (7.28)$$

are negligible.

such that

$$\mathcal{C}_2(\tau_j, \hat{K}_i) = \frac{2 \left[1 - \left(\ln \frac{\hat{K}_i}{S_t} - r_{f,j} \tau_j \right) \right]}{\hat{K}_i^2} \hat{C}(\tau_j, \hat{K}_i), \quad (7.29)$$

$$\mathcal{P}_2(\tau_j, \hat{K}_i) = \frac{2 \left[1 + \left(\ln \frac{\hat{K}_i}{S_t} + r_{f,j} \tau_j \right) \right]}{\hat{K}_i^2} \hat{P}(\tau_j, \hat{K}_i);$$

$$\mathcal{C}_3(\tau_j, \hat{K}_i) = \frac{6 \left(\ln \frac{\hat{K}_i}{S_t} - r_{f,j} \tau_j \right) - 3 \left(\ln \frac{\hat{K}_i}{S_t} - r_{f,j} \tau_j \right)^2}{\hat{K}_i^2} \hat{C}(\tau_j, \hat{K}_i), \quad (7.30)$$

$$\mathcal{P}_3(\tau_j, \hat{K}_i) = \frac{6 \left(\ln \frac{S_t}{\hat{K}_i} + r_{f,j} \tau_j \right) + 3 \left(\ln \frac{S_t}{\hat{K}_i} + r_{f,j} \tau_j \right)^2}{\hat{K}_i^2} \hat{P}(\tau_j, \hat{K}_i);$$

$$\mathcal{C}_4(\tau_j, \hat{K}_i) = \frac{12 \left(\ln \frac{\hat{K}_i}{S_t} - r_{f,j} \tau_j \right)^2 - 4 \left(\ln \frac{\hat{K}_i}{S_t} - r_{f,j} \tau_j \right)^3}{\hat{K}_i^2} \hat{C}(\tau_j, \hat{K}_i), \quad (7.31)$$

$$\mathcal{P}_4(\tau_j, \hat{K}_i) = \frac{12 \left(\ln \frac{S_t}{\hat{K}_i} + r_{f,j} \tau_j \right)^2 + 4 \left(\ln \frac{S_t}{\hat{K}_i} + r_{f,j} \tau_j \right)^3}{\hat{K}_i^2} \hat{P}(\tau_j, \hat{K}_i).$$

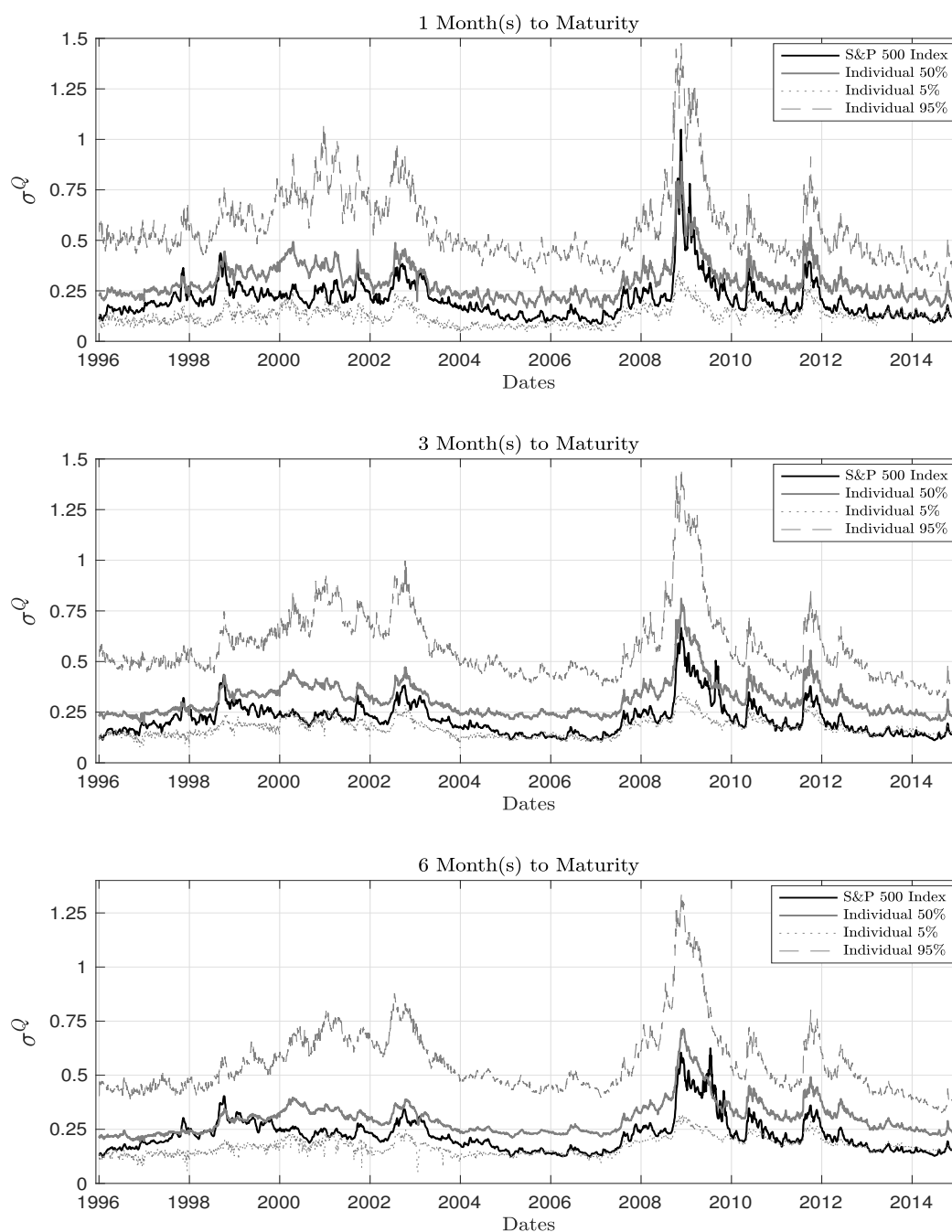
where \mathcal{N} is the number of evenly spaced points, in our case I set it to be 201 and $r_{f,j}$ is the corresponding risk free rate for the j th tenor.

Finally, I perform a linear interpolation across the tenor vector $\boldsymbol{\tau}$ on each day to get a standard tenor grid. On each day, for the index and individual equity options, I use the intraday option price panel to obtain the daily estimations. Noted that with the [OPRA](#) data from November 2009, I calculate the risk-neutral central moments for the index options with tenors from 30 days up to 2 years and up to 1.5 years for the single-name equity options. However, before the [OPRA](#) (from 1 January 1996 to 30 November 2009), due to the data limit, I calculate the risk-neutral central moments with tenors from 30 days up to 6 months for both the index option and the single-name equity options. In order to maintain the consistency of time series, I report the estimated results for the following tenors: 1 month, 3 months, and 6 months from January 1, 1996 to January 1, 2015.⁷

Figure [7.5](#), [7.6](#), and [7.7](#) plots the tenor adjusted time series of the

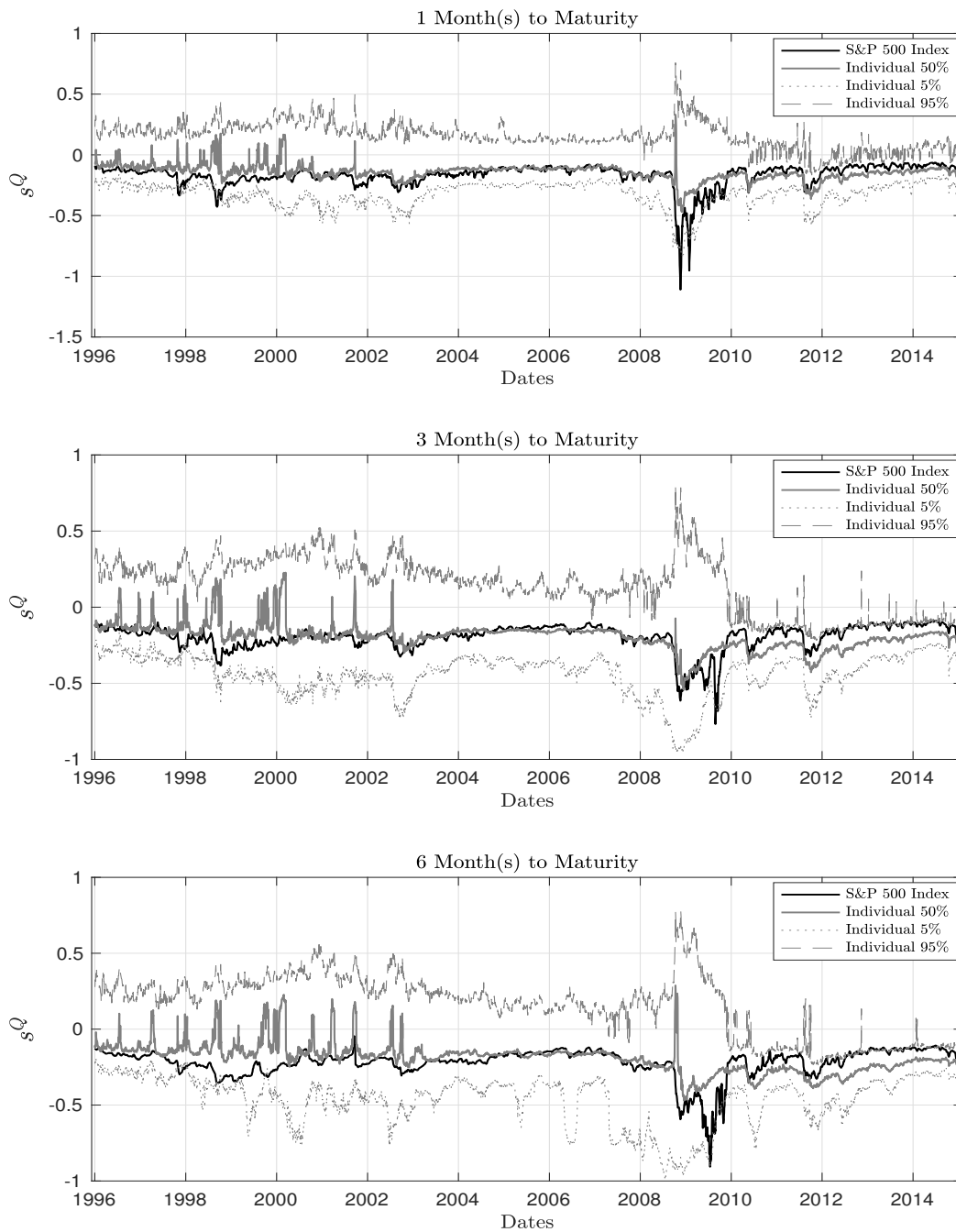
⁷The results for the other tenors for a different sample period are available on request.

Figure 7.5: Term Structure of Estimated Risk Neutral Second Central Moments



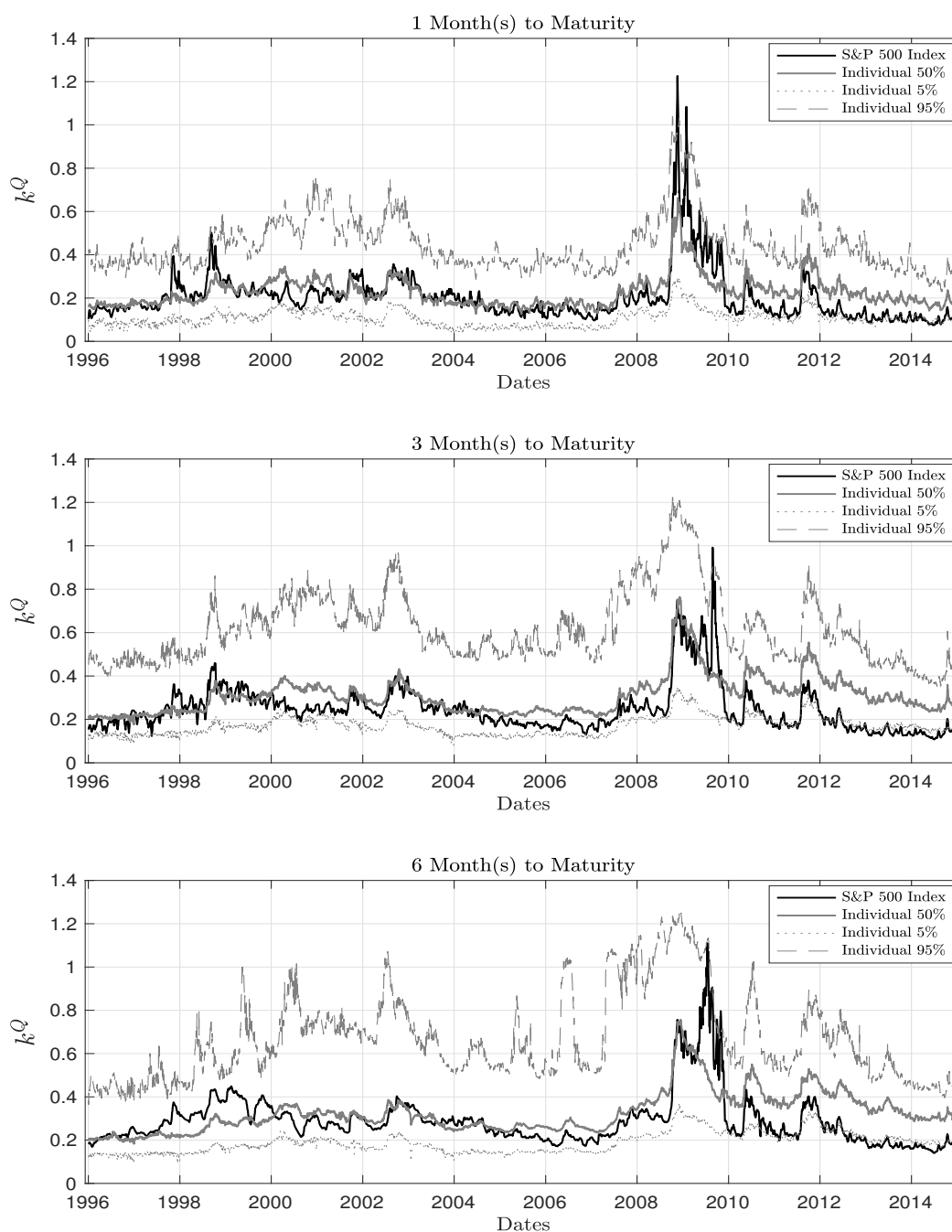
Note. Figure 7.5 plots the time series of the quadratic root of the estimated risk-neutral second central moments adjusted by the tenor, such that $\sigma^Q = \hat{M}_2^{1/2}/\tau_j$ for the S&P 500 index option and the single-name equity options over three different time to maturities, namely, 1 month, 3 months, and 6 months. The black hard line is the estimated risk-neutral second central moments for the S&P 500 index and the grey hard line and the dash lines are the median, 5% percentile, and 95% percentile of the estimated risk-neutral second central moments for the single-name equity options respectively.

Figure 7.6: Term Structure of Estimated Risk Neutral Third Central Moments



Note. Figure 7.6 plots the time series of the cubic root of the estimated third risk-neutral central moments adjusted by the tenor such that $s^Q = \hat{M}_3^{1/3} / \tau_j$ for the S&P 500 index option and the single-name equity options over three different time to maturities, namely, 1 month, 3 months, and 6 months. The black hard line is the estimated risk-neutral third central moments for the S&P 500 index and the grey hard line and the dash lines are the median, 5% percentile, and 95% percentile of the estimated risk-neutral third central moments for the single-name equity options respectively.

Figure 7.7: Term Structure of Estimated Risk Neutral Fourth Central Moments



Note. Figure 7.7 plots the time series of the quadratic root of the estimated risk-neutral fourth central moments adjusted by the tenor such that $k^Q = \hat{M}_4^{1/4}/\tau_j$ for the S&P 500 index option and the single-name equity options over three different time to maturity, namely, 1 month, 3 months, and 6 months. The black hard line is the estimated risk-neutral fourth central moments for the S&P 500 index and the grey hard line and the dash lines are the median, 5% percentile, and 95% percentile of the estimated risk-neutral fourth central moments for the single-name equity options respectively.

quadratic, cubic, and quartic root of the estimated risk-neutral central moments for the S&P 500 index option and the single-name equity options with 1 month, 3 months, and 6 months to maturity, over January 1, 1996 to January 1, 2015. For the 588 individual equities, I form three percentile portfolios, mainly the 5%, 50% (median), and the 95% percentile, which are represented by the dot, hard, and dash grey lines while the black hard line stands for the S&P 500 index option.

There are clear patterns in the time series of these moments over the sample period across different time to maturities. The 5% and 95% percentile moments of the single-name equity options act as the upper and lower bounds for the index moments. Across different time to maturities, the median second moments of the single-name equity options are always higher than the ones of the index option, especially during the crisis period, for example, the 1998 Asian Financial Crisis, the 2000 Internet Bubble, and the most recent 2009 Global Financial Crisis.

The behaviours of the third moments between the index and individual equity options are a bit different, for example, such that the third moment for the index is always negative but that for the individual equity options some time is slightly positive. Specifically, the 95% percentile of the individual equity option third moment is positive. This pattern is consistent with the evidence documented by [Bakshi and Kapadia \[2003\]](#) and [Bakshi et al. \[2003b\]](#) that some individual options are positive skewed while the index option is negative skewed. Interestingly, the upper bounds of the third moments of the single-name equity options are largely positive skewed during the crisis period while that of the lower bounds and the median are negative skewed, which is consistent with the index options. Unlike the second moments, the fourth moment of the index and the median fourth moments of the individual equity options tend to move closely with each other during the quiet period and the index fourth moments are more peaky during the crisis period.

7.5 Estimate the Higher Dimensional Option-implied Average Correlations

7.5.1 Market Option-implied Average Correlations

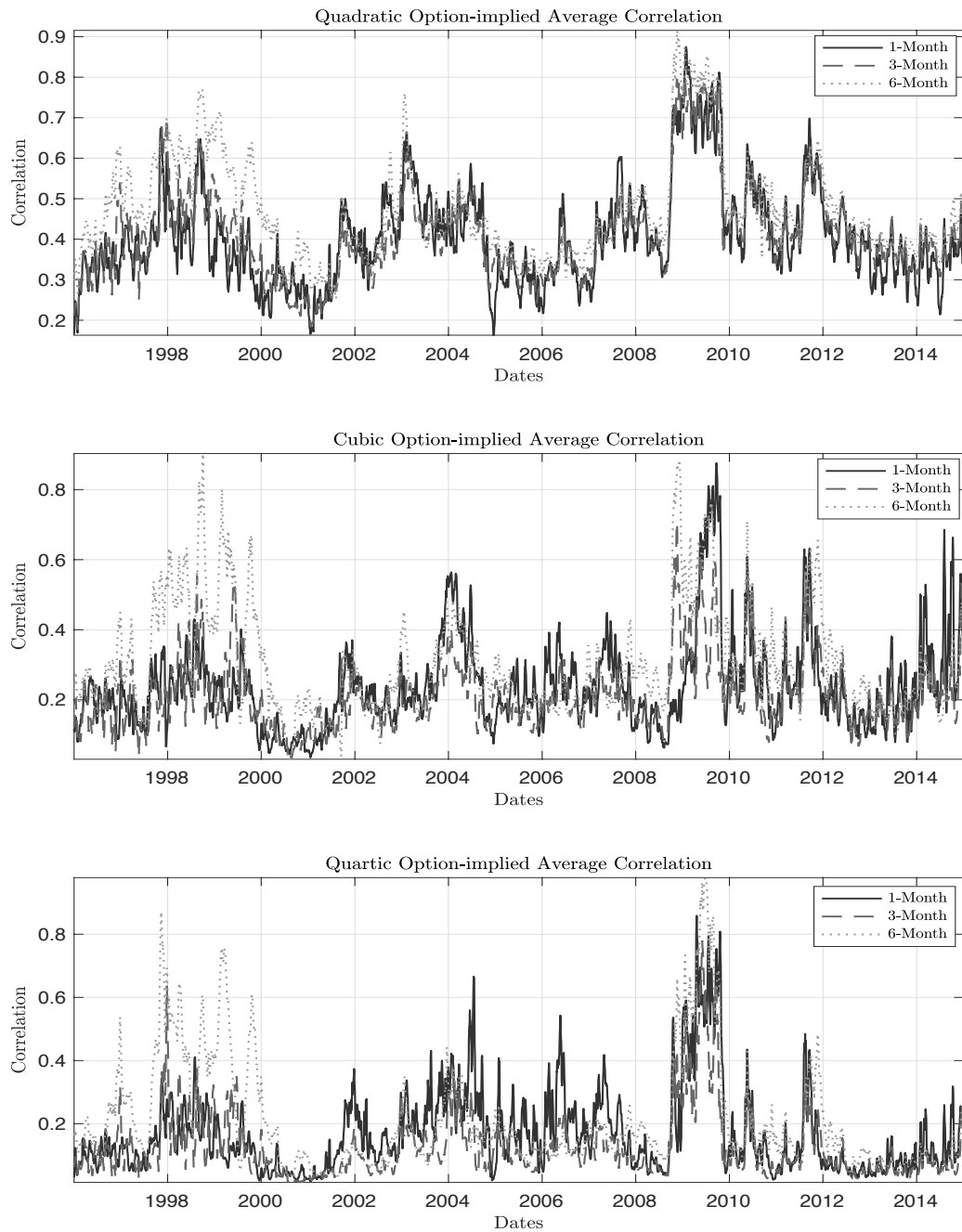
Let the estimated risk-neutral central moments at a given day t for τ_j time to maturity for the S&P 500 index and the i th single-name equity option are denoted by the triples $\{\hat{M}_2^{\mathbb{Q}}(m, t, \tau_j), \hat{M}_3^{\mathbb{Q}}(m, t, \tau_j), \hat{M}_4^{\mathbb{Q}}(m, t, \tau_j)\}$ and $\{\hat{M}_2^{\mathbb{Q}}(i, t, \tau_j), \hat{M}_3^{\mathbb{Q}}(i, t, \tau_j), \hat{M}_4^{\mathbb{Q}}(i, t, \tau_j)\}$.

The corresponding estimated quadratic, cubic, and quartic roots of the central moments are $\{\hat{\sigma}_{m,t,\tau_j}^{\mathbb{Q}}, \hat{s}_{m,t,\tau_j}^{\mathbb{Q}}, \hat{k}_{m,t,\tau_j}^{\mathbb{Q}}\}$ and $\{\hat{\sigma}_{i,t,\tau_j}^{\mathbb{Q}}, \hat{s}_{i,t,\tau_j}^{\mathbb{Q}}, \hat{k}_{i,t,\tau_j}^{\mathbb{Q}}\}$. Then according to Equation 7.16, at a given day t , I calculate the option-implied average higher dimensional correlations over τ_j time to maturity by:

$$\begin{aligned}
\hat{\rho}_{\Sigma,t,\tau_j}^{\mathbb{Q}} &= \frac{\hat{M}_2^{\mathbb{Q}}(m, t, \tau_j) - \sum_{i=1}^N w_{i,t}^2 \hat{M}_2^{\mathbb{Q}}(i, t, \tau_j)}{\Lambda_{i,j} \sum_{i=1}^N \sum_{j>i}^N w_{i,t} w_{j,t} \hat{\sigma}_{i,t,\tau_j}^{\mathbb{Q}} \hat{\sigma}_{j,t,\tau_j}^{\mathbb{Q}}} \\
\hat{\rho}_{\Gamma,t,\tau_j}^{\mathbb{Q}} &= \frac{\hat{M}_3^{\mathbb{Q}}(m, t, \tau_j) - \sum_{i=1}^N w_{i,t}^3 \hat{M}_3^{\mathbb{Q}}(i, t, \tau_j)}{\Lambda_{i,j,k} \sum_{i=1}^N \sum_{j>i}^N w_{i,t} w_{j,t} w_{k,t} \hat{s}_{i,t,\tau_j}^{\mathbb{Q}} \hat{s}_{j,t,\tau_j}^{\mathbb{Q}} \hat{s}_{k,t,\tau_j}^{\mathbb{Q}}} \\
\hat{\rho}_{\Theta,t,\tau_j}^{\mathbb{Q}} &= \frac{\hat{M}_4^{\mathbb{Q}}(m, t, \tau_j) - \sum_{i=1}^N w_{i,t}^4 \hat{M}_4^{\mathbb{Q}}(i, t, \tau_j)}{\Lambda_{i,j,k,l} \sum_{i=1}^N \sum_{j=i}^N \sum_{k=j}^N \sum_{l>i}^N w_{i,t} w_{j,t} w_{k,t} w_{l,t} \hat{k}_{i,t,\tau_j}^{\mathbb{Q}} \hat{k}_{j,t,\tau_j}^{\mathbb{Q}} \hat{k}_{k,t,\tau_j}^{\mathbb{Q}} \hat{k}_{l,t,\tau_j}^{\mathbb{Q}}}.
\end{aligned} \tag{7.32}$$

where $w_{i,t}$ is the market capitalisation for company i at day t and $\Lambda_{i,j}$, $\Lambda_{i,j,k}$, and $\Lambda_{i,j,k,l}$ are the symmetric multipliers as given in Equation 7.17 in Proposition 7.1.

Figure 7.8: Term Structure of the Option-implied Average Correlations



Note. Figure 7.8 plots the time series of the quadratic, cubic, and quartic option-implied average correlations estimated based on the risk-neutral central moments of the S&P 500 index and the single-name equity options as defined in Equation 7.32 from January 1, 1996 to January 1, 2015 over 1 month, 3 months, and 6 months to maturity, respectively. In each of the sub-plots, the black hard line represents the 1-Month to maturity, the dark grey dash line is the 3-Month to maturity, while the light grey dot line is for 6-Month to maturity.

Table 7.1: Descriptive Statistics for Option Implied Correlations

Table 7.1 reports the descriptive statistics for the estimated option-implied average correlations estimated from the S&P 500 index option and its component single-name equity options with 1 month, 3 months, and 6 months to maturity for the sample period from January 1, 1996 to January 1, 2015, namely the average quadratic option-implied correlations $\{\hat{\rho}_{\Sigma,1}^Q, \hat{\rho}_{\Sigma,3}^Q, \hat{\rho}_{\Sigma,6}^Q\}$, the average cubic option-implied correlations $\{\hat{\rho}_{\Gamma,1}^Q, \hat{\rho}_{\Gamma,3}^Q, \hat{\rho}_{\Gamma,6}^Q\}$, and the average quartic option-implied correlations $\{\hat{\rho}_{\Theta,1}^Q, \hat{\rho}_{\Theta,3}^Q, \hat{\rho}_{\Theta,6}^Q\}$. The lower panel of the table gives the correlation matrix between each of the average option-implied correlations.

	$\hat{\rho}_{\Sigma,1}^Q$	$\hat{\rho}_{\Sigma,3}^Q$	$\hat{\rho}_{\Sigma,6}^Q$	$\hat{\rho}_{\Gamma,1}^Q$	$\hat{\rho}_{\Gamma,3}^Q$	$\hat{\rho}_{\Gamma,6}^Q$	$\hat{\rho}_{\Theta,1}^Q$	$\hat{\rho}_{\Theta,3}^Q$	$\hat{\rho}_{\Theta,6}^Q$
Mean	0.406	0.412	0.469	0.239	0.213	0.303	0.167	0.125	0.210
Median	0.384	0.398	0.441	0.212	0.193	0.256	0.123	0.092	0.146
Max.	0.906	0.897	0.954	0.923	0.790	0.989	0.925	0.842	0.992
Min.	0.098	0.012	0.093	0.033	0.000	0.012	0.014	0.006	0.007
SD	0.126	0.116	0.127	0.138	0.107	0.158	0.143	0.110	0.180
Skewness	1.011	1.061	1.110	1.649	1.454	1.251	1.875	2.528	1.890
Kurtosis	4.136	4.548	4.081	6.615	6.005	4.360	7.011	11.496	6.438
$\hat{\rho}_{\Sigma,1}^Q$	1.000								
$\hat{\rho}_{\Sigma,3}^Q$	0.869	1.000							
$\hat{\rho}_{\Sigma,6}^Q$	0.757	0.870	1.000						
$\hat{\rho}_{\Gamma,1}^Q$	0.580	0.545	0.413	1.000					
$\hat{\rho}_{\Gamma,3}^Q$	0.597	0.737	0.611	0.605	1.000				
$\hat{\rho}_{\Gamma,6}^Q$	0.603	0.733	0.843	0.445	0.681	1.000			
$\hat{\rho}_{\Theta,1}^Q$	0.689	0.609	0.498	0.754	0.547	0.444	1.000		
$\hat{\rho}_{\Theta,3}^Q$	0.618	0.787	0.679	0.550	0.772	0.639	0.669	1.000	
$\hat{\rho}_{\Theta,6}^Q$	0.574	0.720	0.841	0.443	0.552	0.859	0.533	0.748	1.000

Table 7.1 reports the descriptive statistics and the correlation matrix for the estimated risk-neutral central moments time series. Figure 7.8 reports the time series of the higher dimensional option-implied average correlations estimated are based on the risk-neutral central moments of the S&P 500 index and the single-name equity options as defined in Equation 7.32 from January 1, 1996 to January 1, 2015 for 1 month, 3 months, and 6 months to maturities respectively. It can be observed that the three option-implied average correlations follow a similar trend over time. In particular, the cubic and quartic correlations move together through the time but deviate a bit from the quadratic correlations.

Across all three tenors, the feature that the cubic and quartic average implied correlations are more sensitive to the market crash is captured by

the spike clusters during the 1998 Asian Financial Crisis and the 2008-2009 Global Financial Crisis. For the 1 month and 3 months to maturity average correlation indexes, the quadratic correlations are generally larger than the cubic and quartic correlations, while the cubic and quartic correlations outperform the quadratic correlations occasionally during the extremely volatile period in the 6 months to maturity case.

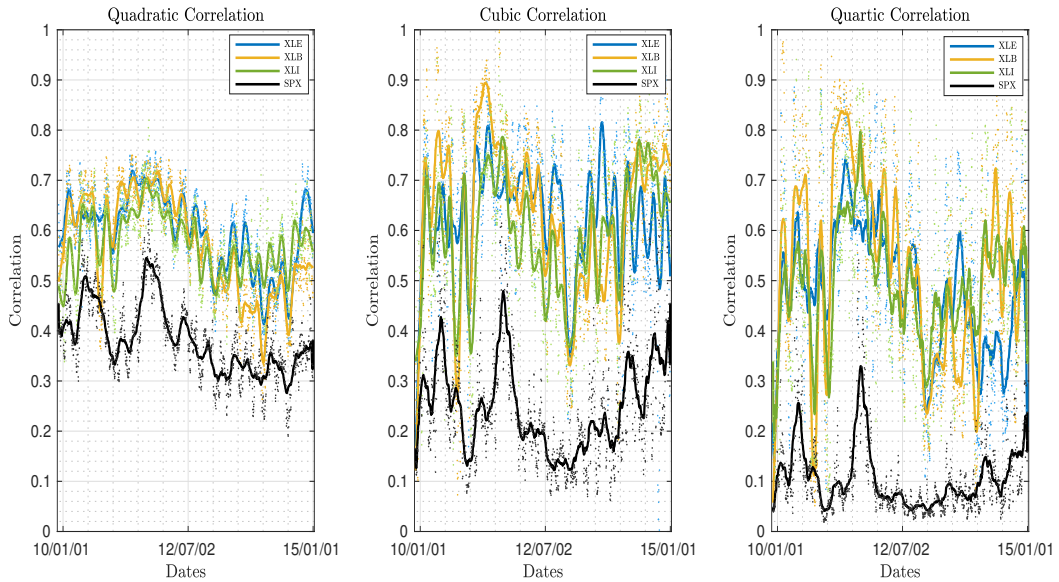
7.5.2 Sectorial Option-implied Average Correlations

Replacing the risk-neutral central moments for the S&P 500 index with the SPDR EFTs Selected Sector Index and the corresponding constituent components with the specific sector index components, I can also estimate the sectorial option-implied average correlations by Equation 7.32. Due to the limited data coverage of the SPDR EFTs Selected Sector Index options, the time series for the sectorial option-implied average correlations are only available over the post-OPRA period.

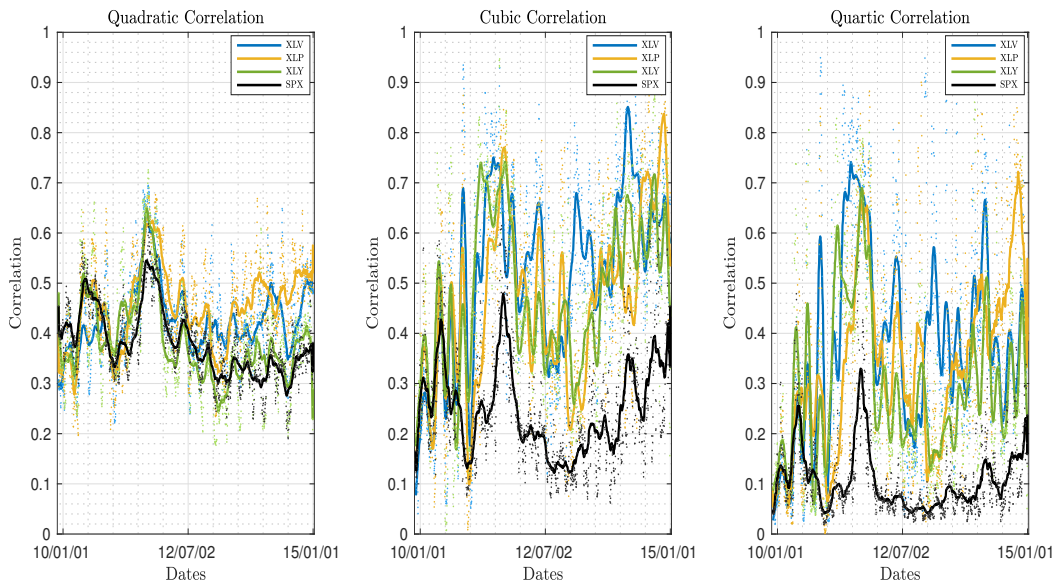
Figure 7.9 and 7.10 plot the time series of the quadratic, cubic, and quartic option-implied average correlations estimated for the SPRD EFTs Select Sector Index from November 30, 2009 to January 1, 2015 with one-month to maturity. I further group the sectors into four groups. Specifically, I put the Industrial (XLI), Material (XLB), and Energy (XLE) sectors as the industrial-related group while the Health Care (XLV), Consumer Discretionary (XLY), Consumer Staples (XLP) sectors as the consumer-related group. The Financial (XLF) and Information Technology (XLK) sectors are treated separately.

Figure 7.9: Option-implied Sectorial Option-implied Average Correlations: I

(a) Industrial (XLI) & Material (XLB) & Energy (XLE)

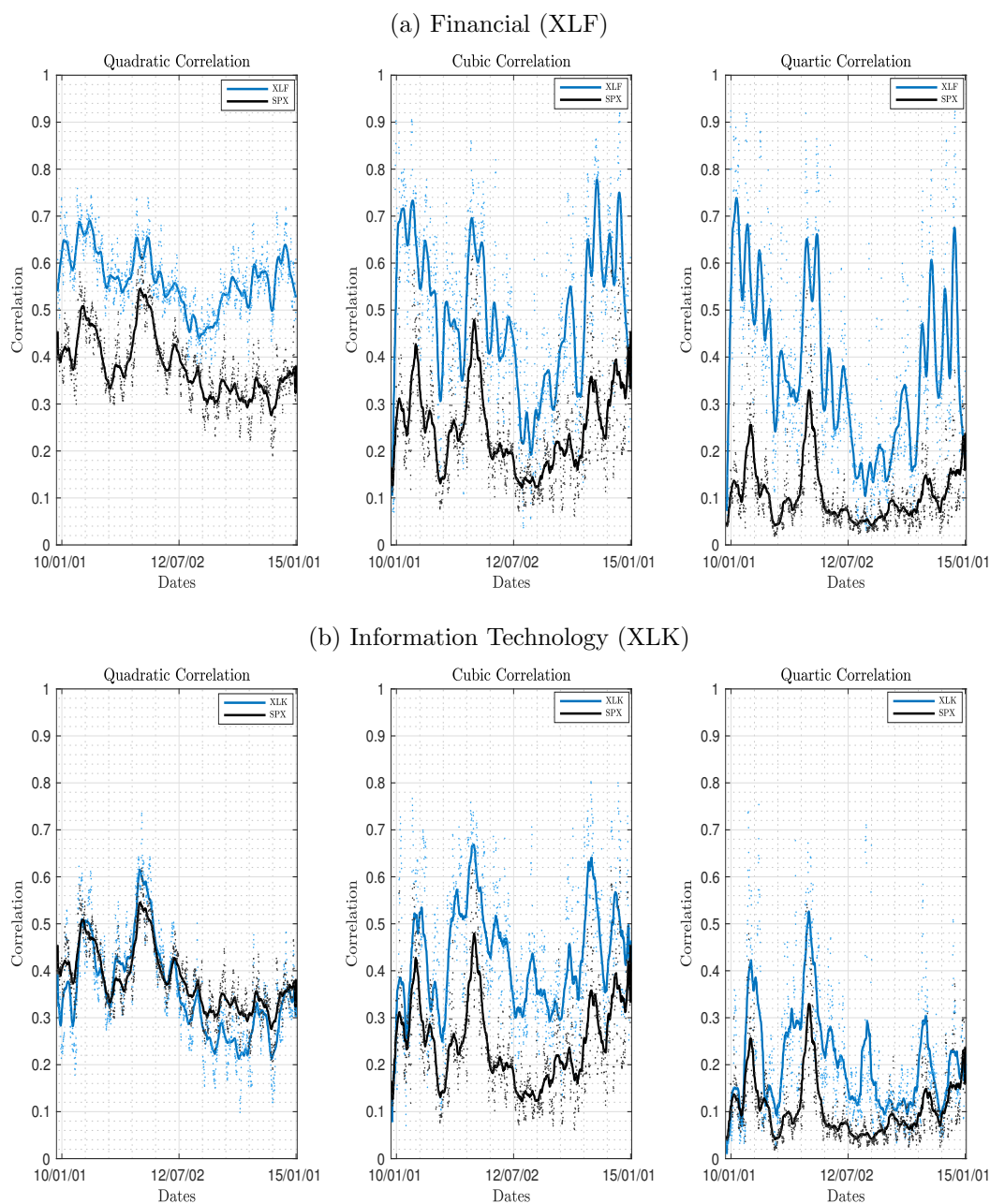


(b) Consumer Staples (XLP) & Consumer Discretionary (XLY) & Health Care (XLV)



Note. Figure 7.9 plots the time series of the sectorial higher dimensional option-implied average correlations from November 30, 2009 to January 1, 2015 over 1 month to maturity. I group the sectors into two groups. Industrial (XLI), Material (XLB), and Energy (XLE) are the industrial-related sector group and Consumer Staples (XLP), Consumer Discretionary (XLY), and Health Care (XLV) are the consumer-related sector group. In each of the sub-plots, the dots in the background plot the raw data while the corresponding lines demonstrate the smoothed results over a 30-day moving-average window. The black line represents the market-wide average correlations calculated from options written on S&P 500 index and its components while the colour lines are the sectorial correlations.

Figure 7.10: Option-implied Sectorial Option-implied Average Correlations:
II



Note. Figure 7.10 plots the time series of the higher dimensional option-implied average correlations for the Financial (XLF) and Information Technology (XLK) sectors from November 30, 2009 to January 1, 2015 over 1 month to maturity, respectively. In each of the sub-plots, the dots in the background plot the raw data while the corresponding lines demonstrate the smoothed results over a 30-day moving-average window. The black line represents the market-wide average correlations calculated from options written on S&P 500 index and its components.

In each of the subplots, the dots at the background give the raw data while the lines at the front are the smoothed series based on a 30-day moving average window. For each group, I also plot the market-wide option-implied average correlations calculated from the S&P 500 index and constituent components. In general, the sectorial option-implied average correlations are higher than the market-wide option-implied average correlations. Across the nine industrial sectors, Financial (XLF), Energy (XLE), Materials (XLB), and Industrials (XLI) sectors show consistent higher average correlation, while Health Care (XLV), Consumer Discretionary (XLY), Consumer Staples (XLP), and Information Technology (XLK) report lower average correlations, especially the quadratic option-implied average correlations for the Information Technology sector. Comparing the quadratic, cubic, and quartic option-implied average correlations, the deviation between the sectorial correlations and the market-wide correlations are increasing as moving from second moment to fourth moments, which suggests the level of diversification in the market-wide portfolio higher on high order moments than the second moments.

7.6 Validity of the Market Portfolio Moments Decomposition

Following [Pollet and Wilson \[2010\]](#), I investigate the validity of the decomposition of the moments of the market portfolio. According to Corollary [7.1](#), the option-implied average correlation provides a measure of the degree of the diversification of the risky assets in the market, we can further approximate the market portfolio's moments via the average moments and average correlations such that:

$$\sigma_m^2 \approx \rho_\Sigma \times \bar{\sigma}_N^2, \quad s_m^3 \approx \rho_\Gamma \times \bar{s}_N^3, \quad k_m^4 \approx \rho_\Theta \times \bar{k}_N^4. \quad (7.33)$$

where $\bar{\sigma}_N^2$, \bar{s}_N^3 , and \bar{k}_N^4 are the value-weighted average second moments, third moments, and fourth moments of the N risky assets in the market such that:

$$\bar{\sigma}_N^2 = \sum_i^N w_i \sigma_i^2, \quad \bar{s}_N^3 = \sum_i^N w_i s_i^3, \quad \bar{k}_N^4 = \sum_i^N w_i k_i^4. \quad (7.34)$$

Table 7.2 reports the ordinary least squares (OLS) regressions of the estimated risk-neutral moments of the S&P 500 index options over different time to maturities on various combinations of the sample estimates of average risk-neutral moments and option-implied average correlations from the single-name equity options written on the index constituents over the same time to maturities for the whole sample time period, from January 1, 1996 through January 1, 2015. The dependent variables are the risk-neutral moments estimated from the S&P 500 index options for 1 month, 3 months, and 6 months to maturity.

The independent variables are the value-weighted average risk-neutral moments, $\{\bar{\sigma}_N^2, \bar{s}_N^3, \bar{k}_N^4\}$, the option-implied average correlations, $\{\bar{\rho}_\Sigma, \bar{\rho}_\Gamma, \bar{\rho}_\Theta\}$, and the product of the average risk-neutral moments and the average correlations, $\{\bar{\sigma}_N^2 \times \bar{\rho}_\Sigma, \bar{s}_N^3 \times \bar{\rho}_\Gamma, \bar{k}_N^4 \times \bar{\rho}_\Theta\}$.

Four regressions are estimated with these independent and dependent variables respectively. Regression (1) and (2) regress the value-weighted average risk-neutral moments and the option-implied average correlations on the market risk-neutral moments separately. Regression (3) regresses the product of the average moments and the average correlations on the index moments while regression (4) tests the validity of a linear combination of the average moments and average correlations to explain the portfolio moments.

All of the independent variables are significant in explaining the market index moments variation across different time to maturities. As expected, across different moments, the product of the value-weighted average moments and the average correlations feature the best explanatory variable for the variation of the market index moments with 90.7%, 72.9%, and 72.8% R^2 individually for the 1 month to maturity experiments. The value-weighted average second moments only explain 76.2% of the variation in the index

Table 7.2: Validity of the Market Portfolio Moments Decomposition

Table 7.2 reports the regression results for the validity of the decomposition of the market portfolio risk neutral moments as described by Equation 7.33. The market portfolio is approximated by the S&P 500 index and the individual assets in the market are proxied by the constituents of the S&P 500 index. Panel A, B, and C displays the estimated coefficients, the root mean squared error (RMSE), and the adjusted R^2 for the decomposition regressions of the risk neutral moments across 1 month, 3 months, and 6 months to maturities, respectively. For the regressions in each panel, the dependent variable is the daily risk neutral moments estimated from the S&P 500 index options and the independent variables are the value-weighted average risk neutral moments estimated from the options written on the individual constituents, the option-implied average correlations, the product of the value-weighted average risk neutral moments and the option-implied average correlations. The sample is from January 1, 1996 to January 1, 2015 and consisted of 4751 daily observations. The absolute value of the t-statistics is in brackets underneath, with *** indicates the significance at 1% level, ** at 5%, and * at 10%. < 0.01% indicates the value is less than 0.01%.

	1 Month to Maturity			
	(1)	(2)	(3)	(4)
Constant	-0.003*** (32.155)	-0.007*** (24.925)	-0.001*** (17.203)	-0.008*** (46.448)
$\bar{\sigma}_N^2$	0.859*** (96.511)			0.756*** (87.728)
$\bar{\rho}_\Sigma$		0.028*** (42.918)		0.014*** (32.926)
$\bar{\sigma}_N^2 \times \bar{\rho}_\Sigma$			1.410*** (140.743)	
RMSE	0.004	0.006	0.003	0.003
Adjusted R^2	76.2%	37.9%	90.7%	72.5%
Constant	0.001*** (10.281)	-0.001*** (3.723)	< 0.01%*** (2.548)	0.002*** (9.506)
\bar{s}_N^3	2.689*** (38.668)			2.707*** (38.939)
$\bar{\rho}_\Gamma$		-0.002*** (2.072)		-0.003*** (4.532)
$\bar{s}_N^3 \times \bar{\rho}_\Gamma$			1.490*** (26.542)	
RMSE	0.004	0.007	0.003	0.005
Adjusted R^2	63.9%	23.9%	72.9%	64.3%
Constant	-0.002*** (10.196)	< 0.01% (1.503)	< 0.01% (1.397)	-0.003*** (10.549)
\bar{k}_N^4	3.053*** (35.768)			3.008*** (35.091)
$\bar{\rho}_\Theta$		0.010*** (7.734)		0.006*** (4.664)
$\bar{k}_N^4 \times \bar{\rho}_\Theta$			1.361*** (26.418)	
RMSE	0.004	0.008	0.003	0.004
Adjusted R^2	61.2%	21.2%	72.8%	61.6%

Table 7.2: Continued

	3 Months to Maturity			
	(1)	(2)	(3)	(4)
Constant	-0.003*** (20.459)	-0.017*** (35.627)	0.002*** (23.058)	-0.018*** (85.064)
$\bar{\sigma}_N^2$	0.591*** (122.801)			0.482*** (140.735)
$\bar{\rho}_\Sigma$		0.074*** (65.199)		0.044*** (79.978)
$\bar{\sigma}_N^2 \times \bar{\rho}_\Sigma$			0.915*** (198.379)	
RMSE	0.006	0.009	0.004	0.004
Adjusted R^2	76.1%	47.2%	92.8%	89.8%
Constant	< 0.01%*** (2.583)	0.006*** (18.978)	-0.001*** (6.579)	0.006*** (22.187)
\bar{s}_N^3	0.568*** (35.934)			0.434*** (27.486)
$\bar{\rho}_\Gamma$		-0.043*** (34.051)		-0.032*** (25.207)
$\bar{s}_N^3 \times \bar{\rho}_\Gamma$			1.438*** (44.105)	
RMSE	0.004	0.007	0.003	0.005
Adjusted R^2	61.4%	29.6%	79.1%	60.7%
Constant	-0.001*** (3.624)	-0.005*** (11.643)	< 0.01% (1.276)	-0.007*** (16.508)
\bar{k}_N^4	0.359*** (23.631)			0.272*** (18.071)
$\bar{\rho}_\Theta$		0.064*** (26.646)		0.052*** (21.714)
$\bar{k}_N^4 \times \bar{\rho}_\Theta$			1.434*** (32.849)	
RMSE	0.004	0.006	0.003	0.004
Adjusted R^2	60.5%	33.0%	78.5%	68.6%

Table 7.2: Continued

	6 Months to Maturity			
	(1)	(2)	(3)	(4)
Constant	-0.005*** (11.178)	-0.044*** (49.119)	0.005*** (20.058)	-0.043*** (73.624)
$\bar{\sigma}_N^2$	0.626*** (86.410)			0.431*** (78.345)
$\bar{\rho}_\Sigma$		0.153*** (83.855)		0.103*** (75.830)
$\bar{\sigma}_N^2 \times \bar{\rho}_\Sigma$			0.869*** (129.499)	
RMSE	0.016	0.016	0.012	0.011
Adjusted R^2	61.1%	59.7%	97.9%	82.4%
Constant	0.004*** (5.597)	0.016*** (18.069)	0.001*** (2.440)	0.021*** (23.594)
\bar{s}_N^3	0.744*** (28.995)			0.533*** (21.121)
$\bar{\rho}_\Gamma$		-0.088*** (33.479)		-0.070*** (26.578)
$\bar{s}_N^3 \times \bar{\rho}_\Gamma$			1.766*** (45.453)	
RMSE	0.004	0.007	0.004	0.004
Adjusted R^2	65.0%	29.1%	70.3%	66.0%
Constant	-0.007*** (5.791)	-0.022*** (17.136)	-0.005*** (5.956)	-0.031*** (22.488)
\bar{k}_N^4	0.481*** (22.787)			0.310*** (15.515)
$\bar{\rho}_\Theta$		0.165*** (36.212)		0.145*** (31.477)
$\bar{k}_N^4 \times \bar{\rho}_\Theta$			1.661*** (48.350)	
RMSE	0.004	0.008	0.003	0.004
Adjusted R^2	69.9%	21.6%	73.0%	65.4%

second moments with the R^2 being 63.9% and 61.2% for the third and fourth moments.

The average correlations alone do not act as good estimators in explaining the market index moments either, with R^2 to be 37.9%, 23.9%, and 21.2% respectively for the second, third and fourth moments. The linear combination of the average moments and the average correlations have done a fairly good job, explaining roughly more than 60% of the market index moments but still underperform the product of the average moments and the average correlations. Not surprisingly, moving from the second moments to third and fourth moments, the explanatory power for all of the potential independent variables drops gradually. It can be explained by the complex structures of the co-moments matrix in the higher dimensional and the higher dimensional correlations are approximations of the exact correlations. As the time to maturity increase, the explanatory power of the product of the average moments and the average correlations and that of the average moments alone also increase but that of the average moments decrease, which indicates that the time-varying average correlations play an important role in the long term.

Overall, the exercise demonstrates that the moments of the market portfolio can be decomposed into average moments and average correlations as shown in Equation 7.33. Both the value-weighted average moments and the option-implied average correlations play important role in explaining the variation of the market index moments. The value-weighted average moments dominate in the short run while in the longer time to maturity, the time-varying average correlations show significant explanatory power.

7.7 Concluding Remarks

Motivated by the growing literature on utilising the option-implied moments and co-moments to explain the cross-sectional stock returns, I introduce a set of ex ante measures to map the higher dimensional market average correlations based on the higher order moments and co-moments extracted from options written on the market index and individual components stocks. In particular, the quadratic, cubic, and quartic option-implied average correlations are

measures of the levels of diversification in the market portfolio from different dimensions. The validity of the diagonal decomposition of the co-moments tensors is demonstrated empirically by regression-based analyses, which shows that both the value-weighted average moments and the option-implied average correlations play significant roles in explaining the variation of the market index moments.

The future research will obvious be exploring the information content of the ex ante cross sectional correlation measures. In the next chapter, I demonstrate the applications of the higher dimensional option-implied average correlations in risk management and empirical asset pricing.

Chapter 8

The Information Content of Higher Dimensional Option-implied Average Correlations: Measuring Diversification Risk and Cross Sectional Asset Pricing

8.1 Introduction

This chapter intensively investigates the information content of the higher dimensional option-implied average correlations introduced in Chapter 7. The empirical analyses on the higher dimensional option-implied average correlations are based on two strands of papers. One strand lies in the literature on correlation risks. Various literature have documented evidence that the correlation risk is not only priced in equity market and option market but also shows forecasting ability for the future market aggregated risks, see for example [Driessen et al. \[2009\]](#), [Krishnan et al. \[2009\]](#), [Buraschi et al. \[2010\]](#), [Pollet and Wilson \[2010\]](#), [Markopoulou et al. \[2016\]](#).

The option-implied average correlations provide a time-varying forward looking benchmark of the market risks, see for example [Driessen et al. \[2009\]](#) and [Driessen et al. \[2013\]](#). Specifically, the conventional quadratic correlation shows the market-wide diversification level of the individual risky assets' returns in the market, a higher quadratic correlation implies the returns of the individual risky assets are correlated with each other. The conventional quadratic correlation implies the tendency among the assets in the market and the higher dimensional correlations provide the movement tendency of the assets in the situation when the market undergoes extreme positive or negative deviations.

Another main strand of literature is on the role of the risk-neutral moments in explaining cross-section expected stock returns. Contrary to the conventional [CAPM](#) intuition, recent studies by [Ang et al. \[2006\]](#), [Chang et al. \[2013\]](#), [Conrad et al. \[2013\]](#) demonstrate that the risk-neutral moments risks of either the market or the individual stocks are priced in cross sectional stock expected returns.

Standing questions in asset pricing factor models is (a) whether diversification risk is priced separately from the index benchmark and (b) what is the main property of the co-dependency of asset returns that is priced by investors? The capital asset pricing model ([CAPM](#)) and more sophisticated asset pricing models look at co-dependency solely in terms of an individual asset versus the factor. However, most common asset pricing models such as the [Fama and French \[1993\]](#), [Carhart \[1997\]](#) and [Pastor and Stambaugh \[2003\]](#) still do not capture all of the dependency structure between the cross section of asset returns.

A cottage of literature has been built up regarding the pricing puzzles that the traditional asset pricing model fails to explain in cross section stock returns. Along with the growing popularity of the option markets, a growing literature has been built up on investigating the relation between the risk-neutral factors extracted from option prices and the cross section stock returns. Unlike the factors extracted from the historical time-series, the risk-neutral factors implied by option prices are genuinely conditional and forward-looking. Vast studies document empirical evidence showing that both

the market volatilities, skewness, and kurtosis extracted from the individual equity options play important role in explaining and forecasting cross section stock returns, see [Chang et al. \[2013\]](#), [Conrad et al. \[2013\]](#), [Lopez Aliouchkin \[2015\]](#), and [Bali et al. \[2015\]](#) for the most recent examples.

In addition to the risk-neutral moments and co-moments, [Skintzi and Refenes \[2005\]](#) proposes an approach for extracting the option-implied correlations from the option prices of the individual stocks and the market index. [Driessen et al. \[2009\]](#) provide a stochastic correlation model to estimate the price of the correlation risk premium. The following work by [Krishnan et al. \[2009\]](#) and [Driessen et al. \[2013\]](#) document significant evidence that the option-implied average correlations have remarkable explanatory power for the variance premium. Specifically, my main focus is on investigating the relation between the option-implied average correlations and cross section stock returns. Simple ordinary least square regression analyses indicates that stocks with high exposure to the option-implied average correlations yield higher expected returns. I then form quintile portfolios by sorting individual stocks on their exposure to the option-implied average correlations respectively.

An aggregated market average correlation factor is formed by the average of the expected returns of the portfolios for each of the quintile portfolios. I examine the explanatory power of the market average correlation factor by performing a series of time-series regressions on the expected returns of the sector portfolios. I find the market average correlation factor largely increase the model fitting of the risk-adjusted models and maintain significance across different sectors. The risk premium of the market average correlations is further explored by performing the [Fama and MacBeth \[1973\]](#) cross-sectional regression across all individual stocks. The market average correlation factor reveals a significant positive risk premium after controlling other firm characteristic factors and existing risk factors.

The remainder of this chapter is organised as follows: Section [8.2](#) briefly describes the data and the construction of the independent variables. Various empirical analyses on the option-implied average correlations are performed in Section [8.3](#). I check the robustness of our empirical results in Section [8.4](#)

and Section 8.5 concludes this chapter.

8.2 Data and Variables

In this section I first describe the datasets used in the empirical analyses. I then list the control variables that are proposed in prior empirical studies related to the cross-sectional variation in stock returns and illustrate the estimation procedures.

8.2.1 Data

The cross-sectional dataset for the empirical analyses is formed by merging three separate data sources. The higher dimensional option-implied average correlations are estimated as described in Section 7.3 in Chapter 7. In parallel to the high-frequency option data panel, I obtain the cross section stock returns and firm characteristic data for the same sample from the [CRSP](#).

Specifically, the close price, trading volume, number of outstanding shares, and adjusted return for each stock in my sample are stored at daily frequency. To construct the book-to-market ratio, I get the annually accounting data for each stock from Compustat. The Fama-French 3-factor portfolios data source is Kenneth French's web site at Dartmouth.¹

The main focus in this chapter is to investigate the information contents of the option-implied average correlations in explaining the cross-sectional stock returns. To guard against some of the effects and anomalies in the prior empirical studies, I explicitly control for the most popular existing explanatory variables mentioned in the recent literature.

8.2.2 Firm-specific Control Variables

This part lists the firm-specific control variables calculated using firm-specific information, which act as the idiosyncratic factors in the later cross-sectional regressions.

¹Source: <http://mba.tuck.dartmouth.edu/pages/faculty/ken.french/>.

Market capitalisation – SIZE Following Bali et al. [2016], we control the market capitalisation for stock i with the firm characteristics factor **SIZE**, which is defined as the natural log of the market capitalisation such that:

$$\text{SIZE}_{i,t,\tau_j} = \frac{1}{\tau_j} \sum_{t=1}^{\tau_j} \log \left(\frac{|S_{i,t} \times \text{SHROUT}_{i,t}|}{10000} \right) \quad (8.1)$$

where $S_{i,t}$ is the stock price and $\text{SHROUT}_{i,t}$ represents the number of outstanding shares for equity i at day t . τ_j is the j th tenor consistent with the option data panel as defined before in days.

The data of the number of outstanding shares and the stock prices are from the **CRSP** daily stock file. Because the number of shares in **CRSP** is recorded in thousands of shares, the division by 1000 indicated that the market capitalisation is in millions of dollars. The absolute values is taken to account for the fact that **CRSP** reports a negative value price when the reported value is calculated as the average of a bid and ask price. When either the $\text{SHROUT}_{i,t}$ or $S_{i,t}$ are missing or set to zero, we take the SIZE_{i,t,τ_j} to be missing.

Book-to-Market Ratio – BM The book-to-market ratio (**BM**) for equity i is defined as the book value of the equity (**BE**) divided by the market capitalisation of the equity (**ME**),

$$\text{BM}_{i,t} = \frac{\text{BE}_{i,t}}{\text{ME}_{i,t}} \quad (8.2)$$

The book value of a company is released in the accounting data on a fiscal year pattern, thus to ensure the book-to-market information is available prior to the returns information, we follow Fama and French [1992] to calculate the book-to-market ratio in June of year y as the ratio of the book value of common equity in fiscal year $y - 1$ to the market value of the equity in December of year $y - 1$.

Calculation of the book value of common equity is done from balance sheet data provided by Compustat's North America Fundamentals Annual file. The

book value of the common equity is defined as:

$$BE_{i,t} = SEQ_{i,t} + TXDB_{i,t} + ITCB_{i,t} - BVPS_{i,t} \quad (8.3)$$

where $SEQ_{i,t}$ is the book value of the shareholders' equity, which is adjusted for tax effects by adding $TXDB_{i,t}$, the deferred taxes, and $ITCB_{i,t}$, the investment tax credit to it. The book value of preferred stock ($BVPS_{i,t}$) is then subtracted to obtain the book value of the common equity $BE_{i,t}$. Following the suggestions given in Bali et al. [2016], the book value of preferred stock ($BVPS_{i,t}$) is backed by the following:

$$BVPS_{i,t} = \begin{cases} \text{PRTKRV, if available} \\ \text{PSTKL, if available and PRTKRV not available} \\ \text{PSTK, if available and PRTKRV, PSTKL not available} \\ 0, \text{ otherwise.} \end{cases} \quad (8.4)$$

where $PRTKRV$, $PSTKL$, and $PSTK$ are the redemption value, the liquidating value, and the par value, respectively. If either the book value of the shareholders' equity SEQ or the deferred taxes $TXDB$ is missing, the book value of common equity is not calculated and the calculation of the book-to-market ratio then fails. If investment tax credit $ITCB$ is missing, it is taken to be zero. In some case, the calculation of the BE can be negative and I take these observations to be missing to avoid negative book-to-market ratio.

Realised Co-skewness and Co-kurtosis – CSK & CKT Following Ang et al. [2006], the 'downside risk' has been captured by the realised co-skewness and co-kurtosis measures such that:

$$CSK_{i,t,\tau_j} = \frac{\frac{1}{\tau_j} \sum_{t=1}^{\tau_j} (R_{i,t} - \mathbb{E}[R_{i,\tau_j}]) (R_{m,t} - \mathbb{E}[R_{m,\tau_j}])^2}{\sqrt{\frac{1}{\tau_j} \sum_{t=1}^{\tau_j} (R_{i,t} - \mathbb{E}[R_{i,\tau_j}])^2 \left(\frac{1}{\tau_j} \sum_{t=1}^{\tau_j} (R_{m,t} - \mathbb{E}[R_{m,\tau_j}])^2 \right)}} \quad (8.5)$$

and

$$\text{CKT}_{i,t,\tau_j} = \frac{\frac{1}{\tau_j} \sum_{t=1}^{\tau_j} (R_{i,t} - \mathbb{E}[R_{i,\tau_j}]) (R_{m,t} - \mathbb{E}[R_{m,\tau_j}])^3}{\sqrt{\frac{1}{\tau_j} \sum_{t=1}^{\tau_j} (R_{i,t} - \mathbb{E}[R_{i,\tau_j}])^2 \left(\frac{1}{\tau_j} \sum_{t=1}^{\tau_j} (R_{m,t} - \mathbb{E}[R_{m,\tau_j}])^2 \right)^{3/2}}} \quad (8.6)$$

where $R_{i,t}$ and $R_{m,t}$ are the i th equity and market portfolio return at day t and $\mathbb{E}[R_{i,\tau_j}]$ and $\mathbb{E}[R_{m,\tau_j}]$ are the average return of the i th equity and market portfolio over the period τ_j .

Realised Skewness and Kurtosis – RSK & RKT I construct the realised skewness and kurtosis measures for stock i at day t over period τ_j following [Amaya et al. \[2015\]](#) from the high frequency spot prices data as:

$$\text{RSK}_{i,t,\tau_j} = \frac{1}{\tau_j} \sum_{t=1}^{\tau_j} \frac{\sqrt{L} \sum_{l=1}^L R_{i,t,l}^3}{\left(\sum_{l=1}^L R_{i,t,l}^2 \right)^{3/2}}, \quad (8.7)$$

and

$$\text{RSK}_{i,t,\tau_j} = \frac{1}{\tau_j} \sum_{t=1}^{\tau_j} \frac{\sqrt{L} \sum_{l=1}^L R_{i,t,l}^4}{\left(\sum_{l=1}^L R_{i,t,l}^2 \right)^2}. \quad (8.8)$$

where $R_{i,t,l}$ is the l th intraday return for stock i at day t and L is the total number of the tick times over a day.

Following the convention in the literature in intraday realised volatility (see [Andersen et al. \[2003\]](#)) and [Amaya et al. \[2015\]](#), I calculate the realised skewness and kurtosis by resample the one-minute data into five-minute interval. For the trading day from 9:45 A.M. to 4:00 P.M. (ET), I have $L = 75$. The realised skewness and kurtosis over period τ_j are then calculated as the average of the daily realised skewness and kurtosis over the period.

Idiosyncratic Volatility – IDIO As defined in [Ang et al. \[2006\]](#), the idiosyncratic volatility as a risk factor for stock i is calculated by the standard deviation of the residuals ϵ_i from the Fama-French 3-factor regression such

that:

$$R_{i,t} - r_{f,t} = \alpha_i + \beta_i(R_{m,t} - r_{f,t}) + \xi_i \text{SMB}_t + \psi_i \text{HML}_t + \epsilon_{i,t} \quad (8.9)$$

$$\text{IDIO}_{i,t,\tau_j} = \frac{1}{\tau_j} \sum_{t=1}^{\tau_j} \sqrt{\text{var}(\epsilon_{i,t})} \quad (8.10)$$

where $R_{i,t}$, $R_{m,t}$, $r_{f,t}$ are the equity return, market return, and risk-free return and SMB_t and HML_t are the Fama-French size and book-to-market factors at given day t .

Illiquidity – ILLIQ The illiquidity measure is constructed following the method proposed by Amihud [2002] such that the illiquidity for stock i over a specific period τ_j is measured as the average daily ratio of the absolute stock return to the dollar trading volume over the period and to reduce the skewness we take the natural logarithm:

$$\text{ILLIQ}_{i,t,\tau_j} = \frac{1}{\tau_j} \sum_{t=1}^{\tau_j} \log \left(\frac{|R_{i,t}|}{\text{Volume}_{i,t} \times S_{i,t}} \right) \quad (8.11)$$

where $R_{i,t}$, $\text{Volume}_{i,t}$, and $S_{i,t}$ are the return, trading volume and price for stock i at a given day t and τ_j is the j th tenor consistent with the option data panel as defined before in days.

Reversal – REV Following Jegadeesh [1990] and Lehmann [1990], I control the short-term reversal variable at the end of each month by the return over the month such that:

$$\text{REV}_{i,M} = R_{i,M} \quad (8.12)$$

where $R_{i,M}$ is the stock return at month m .

Momentum – MOM Following Jegadeesh and Titman [1993], I further control the intermediate-term momentum variable at the end of each month by the compound gross returns over the past 12 months, ignoring the most

recent month such that:

$$\text{MOM}_{i,M} = \prod_{M \in [M-11:M-1]} (R_{i,M} + 1) - 1 \quad (8.13)$$

where $R_{i,M}$ represents the corresponding monthly return.

8.2.3 Portfolio-based Control Variables

This part provides the market common factors that formed based on portfolios, which are the systematic risk factors and the same across the market.

Market Factor – MKT The market factor is simply defined as the excess return of the market portfolio. There are two commonly used proxies for the market portfolio in empirical asset pricing research. The first one is the value-weighted portfolio of all U.S. based common stocks in the CRSP database. The second one is the CRSP value-weighted portfolio, which contains all securities in the CRSP database, but excluding American Depository Receipts (ADRs). The main difference between the two is that the later one contains shares of firms that are not based in the U.S., closed-end funds, and other securities that are not common stocks. As my sample is made up by the S&P 500 index components, I use the first proxy for the market portfolio and the daily and monthly excess return for the market portfolio is from the Fama-French database on WRDS.

Stock Size Factor – SMB Proposed by Fama and French [1993] for the portfolio analyses, the stock size factor SMB (small minus big) is meant to mimic the risk factor in returns related to firm size and constructed by the difference between the simple average of the returns on three small stock portfolios and the simple average of returns on the three big-stock portfolios at each month. The size factor SMB is the difference between the returns on small and big stock portfolios with about the same weighted-average book-to-market equity.

Book-to-market Factor – HML The **HML** (high minus low) factor is meant to mimic the risk factor in returns related to book-to-market equity, and is constructed by the difference between the simple average of the returns on the two high book-to-market equity portfolios and the average of the returns on the two low book-to-market equity portfolios. Similar to the **SMB**, the two portfolios are returns on high and low book-to-market equity portfolios with about the same weighted-average size.

Momentum Factor – UMD The **UMD** (up minus down) factor is proposed by **Carhart [1997]** to investigate the ability of momentum to explain the persistence in mutual fund performance documented in the previous empirical studies. In **Carhart [1997]**, the **UMD** factor is constructed as the equal-weighted average return of stocks in the top 30% of Mom portfolio minus that of stocks in the bottom 30% of Mom portfolio, where the Mom portfolio is formed by sorting the stocks by momentum.

Traded Liquidity Factor – LIQ **Pastor and Stambaugh [2003]** find strong empirical evidence that stock-level sensitivity to innovations in an aggregate liquidity factor plays an important role in determining expected stock returns. Following the same spirits of **Fama and French [1993]** and **Carhart [1997]**, **Pastor and Stambaugh [2003]** form a long minus short liquidity sensitivity portfolio, commonly referred as the traded liquidity factor, which is constructed based on a regression procedure.

8.3 Empirical Identification of the Price of Market Correlation Risk

In this section, I demonstrate the empirical identification of the price of market correlation risk. In particular, Section 8.3.1 investigates the relation between the higher dimensional option-implied average correlations and the market risks, which is proxied by the **CBOE** Volatility Index (VIX). The application of the higher dimensional option-implied average correlations in explaining

the cross section stock returns is examined in Section 8.3.2. I form a market average correlation factor based on the option-implied average correlations. I document significant evidence showing that the market average correlation factor is priced via both time-series regression on portfolios and cross-sectional regression across stocks.

8.3.1 Measure Market Diversification Risk

As shown in Corollary 7.1, the option-implied average correlation provide a measure of the diversification level across assets in the market portfolio. Considerable evidence has been documented over the past decades that correlations among assets are time varying. In particular, the correlations increase during volatile periods as diversification opportunities are least available when they are most needed, which is consistent with the dynamics of the estimated higher dimensional option-implied average correlations as displayed in Figure 7.8.

The CBOE Volatility Index (VIX) has often been referred to as the ‘fear index’ or the ‘fear gauge’, which provides a measure of the markets’ expectation of stock market volatility in the next 30 days. VIX has been widely used as an indicator of the market risks and various trading and portfolio management strategies have been developed around the application of VIX. The estimated option-implied average correlation is a benchmark of the level of the diversification level in the market, I explore the information content of the option-implied average correlation benchmark in explaining and forecasting the market risk index via the following regression:

$$\text{VIX}_{t+\Delta h} = \alpha + \beta_1 \bar{\rho}_{\Sigma_t} + \beta_2 \bar{\rho}_{\Gamma_t} + \beta_3 \bar{\rho}_{\Theta_t} + \epsilon_{t+h} \quad (8.14)$$

where h is the forecasting horizon. In this case, $\Delta h = 0$ gives the contemporaneous regression and $\Delta h = 5, 22, 66$ represent the one-week, one-month, and one-quarter ahead forecasting respectively.

Table 8.1 reports the contemporaneous and predictive regression results for the relationship between the option-implied average correlations and market risks. Recall that the option data is obtained from two separate data sources.

Table 8.1: Option-implied Average Correlations and the Market Risks

Table 8.1 reports the contemporaneous and predictive regression results for the relationship between the option-implied average correlations and the market risks. The market risks are proxied by the daily CBOE VIX data. The dependent variable is the CBOE VIX and the independent variables are our option-implied average correlations estimated from the second, third, and fourth central moments of the index and single-name equity options, namely, $\bar{\rho}_\Sigma$, $\bar{\rho}_\Gamma$, and $\bar{\rho}_\Theta$. As the CBOE VIX is estimated based on the S&P 500 index options with 30-day to maturity, we selectively use the one month to maturity option-implied average correlations as the independent variables. The estimated coefficients (with absolute value of the corresponding t-statistics in brackets underneath and *** indicates the significance at 1% level, ** at 5%, and * at 10%. < 0.01% indicates the value is less than 0.01%), the root mean squared error (RMSE), and the adjusted R^2 , and the number of observations are listed for each regression. Regression (1) is a contemporaneous regression between the CBOE VIX and the three option-implied average correlations. Regression (2), (3), and (4) are the predictive regressions between the CBOE VIX and the option-implied average correlations with forecasting horizons being 5 days (one week), 22 days (one month), and 66 days (one quarter), respectively. Panel A is for the whole sample, from January 1, 1996 to January 1, 2015. Panel B is for the pre-OPRA period, from January 1, 1996 to November 30, 2009. Panel C is for the post-OPRA period, from December 1, 2009 to January 1, 2015.

	(1) (VIX _t)	(2) (VIX _{t+5})	(3) (VIX _{t+22})	(4) (VIX _{t+66})
Panel A: Whole Sample (1996.01.01-2015.01.01)				
Constant	0.019*** (5.702)	0.026*** (7.495)	0.065*** (16.470)	0.129*** (28.639)
$\bar{\rho}_{\Sigma,t}$	0.648*** (66.661)	0.621*** (60.812)	0.519*** (44.589)	0.348*** (26.022)
$\bar{\rho}_{\Gamma,t}$	-0.256*** (25.356)	-0.238*** (22.422)	-0.242*** (19.867)	-0.196*** (13.808)
$\bar{\rho}_{\Theta,t}$	-0.052*** (4.615)	-0.053*** (4.543)	-0.032*** (2.361)	-0.065*** (4.203)
RMSE	0.057	0.060	0.068	0.078
Adjusted R^2	54.1%	49.5%	34.6%	14.6%
No. of Obs.	4751	4747	4730	4686
Panel B: Pre OPRA (1996.01.01-2009.11.30)				
Constant	0.024*** (6.459)	0.030*** (7.656)	0.062*** (13.920)	0.127*** (24.240)
$\bar{\rho}_{\Sigma,t}$	0.719*** (64.978)	0.696*** (59.806)	0.606*** (45.548)	0.441*** (28.558)
$\bar{\rho}_{\Gamma,t}$	-0.258*** (19.524)	-0.236*** (16.935)	-0.223*** (14.034)	-0.162*** (8.468)
$\bar{\rho}_{\Theta,t}$	-0.182*** (12.536)	-0.191*** (12.527)	-0.178*** (10.175)	-0.243*** (11.974)
RMSE	0.057	0.060	0.069	0.079
Adjusted R^2	58.9%	54.5%	40.8%	21.6%
No. of Obs.	3470	3466	3449	3405
Panel C: Post OPRA (2009.12.01-2015.01.01)				
Constant	-0.019*** (4.333)	-0.008* (1.638)	0.055*** (6.585)	0.088*** (8.442)
$\bar{\rho}_{\Sigma,t}$	0.530*** (47.850)	0.489*** (37.864)	0.337*** (15.678)	0.228*** (8.470)
$\bar{\rho}_{\Gamma,t}$	-0.227*** (14.583)	-0.205*** (11.332)	-0.209*** (7.003)	-0.041 (1.085)
$\bar{\rho}_{\Theta,t}$	0.455*** (16.553)	0.456*** (14.262)	0.447*** (8.401)	0.142** (2.165)
RMSE	0.025	0.029	0.047	0.058
Adjusted R^2	84.0%	78.6%	43.6%	17.1%
No. of Obs.	1281	1277	1260	1216

Thus, I run the regressions using data over three sample periods, mainly the whole sample period (January 1, 1996 to January 1, 2015), the pre-OPRA sample period (January 1, 1996 to November 30, 2009), and the post-OPRA sample period (December 1, 2009 to January 1, 2015). I use the CBOE VIX index to proxy the market risks. As the CBOE VIX is calculated using the out-of-the-money S&P 500 index options with 30-day to maturity, I selectively use the one month to maturity option-implied average correlations as the independent variables.

Regression (1) shows that the option-implied average correlations can explain up to 84.0% of the variation in the VIX contemporaneously for the post OPRA period while the explanatory power pre the OPRA period reduces down to 58.9% and for the whole sample to 54.1%. The predictive power of the option-implied average correlations of the market risks is investigated in the predictive regressions (2), (3), and (4). For the post OPRA period, the option-implied average correlations capture 78.6%, 43.6%, and 17.1% variation of the CBOE VIX for one-week (VIX_{t+5}), one-month (VIX_{t+22}), and one-quarter forecasting horizon (VIX_{t+66}), respectively. ²

The sign of the estimated coefficients for the quadratic option-implied average correlation is positive and significant across all sample periods for both contemporaneous and predictive regressions while that for the cubic and quartic option-implied average correlations is mixed across different sample period. Intuitively, the quadratic option-implied correlation is the diversification of the second moments (the variance) of the equities in the market and the CBOE VIX is a measure of the implied volatility. Thus, the VIX and quadratic correlation should move in the same direction such that during the crisis period, the market volatility increase and the level of diversification of the second moments of the equities decreases and the quadratic correlation increases.

²Comparing the adjusted R^2 for both the contemporaneous and predictive regressions across the whole sample, pre OPRA sample, and post OPRA, the pre OPRA period consistently shows lower explanatory power. Part of the reason is that the data on individual equity options before the OPRA period are very thin and source from different exchanges, which will cause ‘error in variable’ problem in the estimations of the option-implied average correlations.

The quartic option-implied correlation measures the diversification of the fourth moments of the equities in the market, which can be viewed as the ‘volatility of volatility’, hence, when the market volatility increases, the quartic correlation should also go up, indicating the low diversification level during volatile period. The cubic option-implied correlation captures the diversification of the third moments. Various studies show that people have opposite preference for the odd moments and even moments. Risk aversion makes investors averse to the even moments but prefer the odd moments, hence we expect the estimated coefficients of the cubic correlation are negative, indicating that when market risks increase the diversification of the equities third moments in fact also increase hence the cubic correlation drops.

As the main focus in this section is to investigate the information content of the higher dimensional option-implied average correlations in explaining the market risk rather forecasting the future market volatility, I do not explore more sophisticated volatility forecasting models, such as the heterogeneous autoregressive (HAR) model introduced by Corsi [2009]. Also, the predictive regression results reported in Table 8.1 are in sample results and the out-of-sample exercise for using the higher dimensional option-implied average correlations to forecast the future market volatility is beyond the subject of the current work.

8.3.2 Construct The Market Average Correlation Factor

In this section, I construct a market correlation factor (MAC) from the higher dimensional average option-implied correlations. Following Chang et al. [2013], I form the correlation portfolios based on the individual stock’s risk exposures to different market correlation risks. Specifically, I construct the market average correlation portfolios in the following procedure. I first run a time-series regression between the individual stock’s excess return and

the option-implied average correlations controlling the market excess return:

$$\begin{aligned}
 R_{i,h} - r_{f,h} &= c_i + \beta_i^{\text{MKT}} \text{MKT}_h + \beta_i^{\rho_{\Sigma}} \rho_{\Sigma,h} + \epsilon_h, \\
 R_{i,h} - r_{f,h} &= c_i + \beta_i^{\text{MKT}} \text{MKT}_h + \beta_i^{\rho_{\Gamma}} \rho_{\Gamma,h} + \epsilon_h, \\
 R_{i,h} - r_{f,h} &= c_i + \beta_i^{\text{MKT}} \text{MKT}_h + \beta_i^{\rho_{\Theta}} \rho_{\Theta,h} + \epsilon_h.
 \end{aligned}
 \tag{8.15}$$

The coefficients are estimated at each month using rolling overlapping regressions of the daily excess returns for each of the individual stocks over the past year on the daily market portfolio excess returns. At the end of each month, I sort the individual stocks into five value-weighted portfolios according to the estimated coefficients.

Table 8.2 reports the results of the univariate portfolio analyses of the relation between the risk exposures of the option-implied average correlation and the stock returns. The table shows the average sorted variable value, average value of the other variables, value-weighted excess returns (in percent), and the Fama-French-Carhart 4 factor (FFC4) alpha (in percent) for each of the five decile portfolios as well as for the long-short zero-cost portfolio that is long the 5th decile portfolio (high) and short the 1st decile portfolio (low).

A persistent pattern can be observed across all three sets of the risk exposure for the option-implied average correlations. Specifically, portfolios with higher risk exposure to the option-implied average correlations (i.e. Quintile 5) are expected to have higher excess returns than those with lower risk exposure (i.e. Quintile 1). Moreover, the Newey and West [1987] adjusted t-statistics in the parentheses show that the excess returns are also significant different from zero.

Apart from the quintile portfolios, I also form the long-short zero-cost portfolios that is long the 5th decile portfolio (highest exposure) and short the 1st decile portfolio (lowest exposure) to investigate whether there is a cross-sectional relation exists between the risk exposure of the option-implied average correlations and the stock excess returns. The Newey and West [1987] adjusted t-statistics confirm that the excess returns for the difference portfolios across all three sets of the risk exposures are significant

Table 8.2: Contemporaneous Univariate-sorted Portfolios on Option-implied Average Correlation Risk Exposure

Table 8.2 reports the results of the univariate portfolio analyses of the relation between the risk exposures of the option-implied average correlation and the stock returns. Monthly portfolios are formed by sorting all individual stocks in the sample into quintile portfolios using decile breakpoints calculated based on the given sort variables using all individual stocks in our sample. The monthly risk exposures of the option-implied average correlations, $\hat{\beta}^{\rho\Sigma}$, $\hat{\beta}^{\rho\Gamma}$, and $\hat{\beta}^{\rho\Theta}$, are estimated based on rolling window regressions (Equation 8.15) using daily excess returns for each of the individual stocks and the market portfolio returns over one year period. The table shows the average sort variable value, value-weighted excess returns (in percent per month), and the Fama-French-Carhart 4 factor (FFC4) alpha (in percent per month) for each of the 5 decile portfolios as well as for the long-short zero-cost portfolio that is long the 5th decile portfolio (highest exposure) and short the 1st decile portfolio (lowest exposure). Newey and West [1987] robust t-statistics, adjusted using six lags, testing the null hypothesis that the average portfolio excess return or the FFC4 alpha is equal to zero, are shown in parentheses. The whole sample period is from January 1, 1996 to January 1, 2015, with 228 monthly observations for 588 individual stocks included in the S&P 500 index over the whole sample period. Panel A is sorted by the estimated risk exposure of the quadratic option-implied average correlation, Panel B is sorted by that of the cubic option-implied average correlation, and Panel C is sorted by that of the quartic option-implied average correlation.

Panel A: Sorted by $\beta^{\rho\Sigma}$					
Quintile	$\hat{\beta}^{\rho\Sigma}$	$\hat{\beta}^{\rho\Gamma}$	$\hat{\beta}^{\rho\Theta}$	R_p	FFC4 α
1 (Low)	-2.287	-1.303	-1.564	0.331 (0.761)	-0.482 (2.266)
2	-0.817	-0.423	-0.492	0.738 (2.410)	0.135 (1.123)
3	-0.011	-0.001	0.024	0.832 (3.161)	0.320 (3.065)
4	0.758	0.430	0.550	0.924 (3.151)	0.412 (3.039)
5 (High)	2.000	1.142	1.495	1.151 (2.946)	0.624 (2.497)
5-1 (High-Low)	4.287	2.445	3.059	0.820 (2.001)	0.706 (2.670)
Panel B: Sorted by $\beta^{\rho\Gamma}$					
1 (Low)	-1.245	-2.304	-1.756	0.602 (2.394)	-0.124 (2.519)
2	-0.410	-0.810	-0.596	0.799 (2.609)	0.222 (1.715)
3	-0.008	0.006	0.034	0.721 (2.673)	0.186 (1.814)
4	0.408	0.787	0.640	0.915 (3.103)	0.395 (2.904)
5 (High)	1.020	2.071	1.695	0.839 (2.179)	0.280 (2.156)
5-1 (High-Low)	2.265	4.375	3.451	0.237 (2.562)	0.404 (2.928)
Panel C: Sorted by $\beta^{\rho\Theta}$					
1 (Low)	-1.500	-1.663	-2.291	0.563 (2.367)	-0.168 (2.795)
2	-0.471	-0.538	-0.781	0.720 (2.497)	0.151 (1.280)
3	0.026	0.051	0.055	0.885 (3.274)	0.356 (1.363)
4	0.482	0.566	0.867	0.928 (3.172)	0.418 (3.152)
5 (High)	1.272	1.496	2.258	0.949 (2.419)	0.382 (2.669)
5-1 (High-Low)	2.772	3.159	4.548	0.386 (2.022)	0.550 (2.405)

distinguishable from zero. The last columns of Panel A, B, and C report the Fama-French-Carhart 4 factor (FFC4) alpha of the quintile portfolios as well as the difference portfolios.

Insignificant FFC4 alpha indicates that the excess returns of the testing portfolio can be explained by the market, size, value and momentum factors given in Fama and French [1993] and Carhart [1997] and vice versa. There are occasionally slight insignificant FFC4 alphas across Panel A, B, and C for the quintile portfolios while those for the the difference portfolios show persistent strong significance, suggesting that the excess returns for the long-short zero-cost portfolios based on the risk exposure of the option-implied average correlations cannot be explained by the market, size, value, and momentum factors.

Given the evidence shown in Table 8.2, I construct a market average correlation factor based on the three sets of different portfolios. Specifically, for each set of correlation risk exposure I define the high and low portfolios as the value-weighted average excess returns for the 5th quintile portfolio and that of the 1st quintile portfolio, denoted by the pair $\{H_{\rho_{\Sigma}}, L_{\rho_{\Sigma}}\}$, $\{H_{\rho_{\Gamma}}, L_{\rho_{\Gamma}}\}$, and $\{H_{\rho_{\Theta}}, L_{\rho_{\Theta}}\}$ for the quadratic, cubic, and quartic option-implied average correlations respectively. The excess returns for the long-short zero-cost portfolios between the high and low correlation risk exposure portfolios are then expressed by:

$$\begin{aligned} \text{LS}_{\rho_{\Sigma},h} &= H_{\rho_{\Sigma},h} - L_{\rho_{\Sigma},h}, \\ \text{LS}_{\rho_{\Gamma},h} &= H_{\rho_{\Gamma},h} - L_{\rho_{\Gamma},h}, \\ \text{LS}_{\rho_{\Theta},h} &= H_{\rho_{\Theta},h} - L_{\rho_{\Theta},h}. \end{aligned} \tag{8.16}$$

Recall that in Table 7.1, the three option-implied average correlations are highly correlated with each other. Thus, instead of constructing three correlation portfolios respectively, I construct the market average correlation portfolio by the average of the three long-short zero-cost portfolios such that:

$$\text{MAC}_h = \frac{1}{3}\text{LS}_{\rho_{\Sigma},h} + \frac{1}{3}\text{LS}_{\rho_{\Gamma},h} + \frac{1}{3}\text{LS}_{\rho_{\Theta},h}. \tag{8.17}$$

The constructed market average correlation portfolio can be used as such a risk-adjusted factor similar to the [SMB](#), [HML](#), and [UMD](#) factors introduced in [Fama and French \[1992\]](#) and [Carhart \[1997\]](#).

8.3.3 Market Average Correlation Factor and Expected Stock Returns

In the following, I first examine the performance of the market average correlation factor with 11 sector portfolios by running a series of time-series regressions, including the conventional [CAPM](#), the [Fama and French \[1992\]](#) three-factor ([FF3](#)), the [Fama and French \[1992\]](#) and [Carhart \[1997\]](#) four-factor ([FFC4](#)), and [FFC4](#) with the [Pastor and Stambaugh \[2003\]](#) traded liquidity factor ([LIQ](#)).

The 588 individual companies are grouped into 11 sectors according to the Global Industry Classification Standard (GICS), namely Energy, Materials, Industrials, Consumer Discretionary, Consumer Staples, Health Care, Financial, Information Technology, Utilities, Telecommunication Services, and Real Estate. The monthly excess returns for each sector portfolio are formed by the value-weighted average excess returns of all the individual stocks in the sector at each month. For each sector p , I run a sets of time-series regressions with the market average correlation factor ([MAC](#)):

$$R_{p,h} - r_{f,h} = \alpha_p + \beta_p^{\text{MKT}} \text{MKT}_h + \beta_p^{\text{MAC}} \text{MAC}_h + \beta_p^{\mathbf{Z}} \mathbf{Z}_h + \epsilon_p, \quad (8.18)$$

where \mathbf{Z} stands for the control portfolio factors, including the [Fama and French \[1992\]](#) firm size and value factors ([SMB](#), [HML](#)), [Carhart \[1997\]](#) momentum factor ([UMD](#)), and the [Pastor and Stambaugh \[2003\]](#) traded liquidity factor ([LIQ](#)).

Table [8.3](#) reports the results for the time-series regressions between the expected excess returns for aa sector portfolios and the market average correlation factor controlling market portfolio factor controlling other market risk factors, including the market portfolio ([MKT](#)), firm size ([SMB](#)), firm value ([HML](#)), momentum ([UMD](#)), and liquidity ([LIQ](#)). In order to examine the role

Table 8.3: Market Average Correlation Factor and Sectors Portfolio Returns

Table 8.3 reports the estimated coefficients with the robust t-statistics (in parentheses, *** indicates the significance at 1% level, ** at 5%, and * at 10%. $< 0.01\%$ indicates the value is less than 0.01%), the adjusted R^2 and the root of mean standard errors (RMSE) for the time series regressions with market average correlation factor across sectors classified by the Global Industry Classification Standard (GICS). The null hypothesis is the alphas are joint zero. Panel A to K display the results for the CAPM (MKT), Fama-French 3 factor (MKT, SMB, HML), Fama-French-Carhart 4 factor (MKT, SMB, HML, UMD), and Fama-French-Carhart 4 factor and the Pastor and Stambaugh traded liquidity factor (MKT, SMB, HML, UMD, LIQ) for different sectors, respectively. The whole sample period is from January 1, 1996 to January 1, 2015, with 228 monthly observations for 588 individual stocks included in the S&P 500 index over the whole sample period.

Panel A: Energy								
	(1)	(2)	(3)	(4)	(5)	(6)	(7)	(8)
Alpha	0.568** (2.077)	0.589** (2.112)	0.486** (1.793)	0.485* (1.749)	0.437* (1.602)	0.440 (1.575)	0.291 (1.077)	0.298 (1.086)
MKT	0.666*** (11.258)	0.683*** (11.519)	0.692*** (11.540)	0.707*** (11.813)	0.720*** (11.329)	0.734*** (11.580)	0.703*** (11.299)	0.716*** (11.563)
MAC		0.111** (2.136)		0.132*** (2.487)		0.130*** (2.446)		0.120** (2.307)
SMB			0.016 (0.195)	0.048 (0.568)	0.003 (0.038)	0.035 (0.411)	$< 0.01\%$ (0.001)	0.031 (0.368)
HML			0.262*** (2.989)	0.269*** (3.026)	0.285*** (3.191)	0.290*** (3.215)	0.317*** (3.620)	0.324*** (3.663)
UMD					0.070 (1.307)	0.068* (1.287)	0.065 (1.241)	0.064 (1.234)
LIQ							0.225*** (3.456)	0.232*** (3.556)
R^2	35.93%	38.49%	38.54%	41.11%	39.01%	41.58%	42.12%	44.91%
RMSE	4.094	4.050	4.028	3.981	4.021	3.975	3.926	3.869
Panel B: Industrials								
	(1)	(2)	(3)	(4)	(5)	(6)	(7)	(8)
Alpha	0.490*** (2.836)	0.498*** (2.740)	0.367*** (2.690)	0.368*** (2.582)	0.436*** (3.259)	0.436*** (3.126)	0.453*** (3.345)	0.454*** (3.223)
MKT	0.945*** (25.298)	0.952*** (24.658)	1.017*** (33.671)	1.024*** (33.260)	0.978*** (31.394)	0.983*** (31.060)	0.980*** (31.339)	0.986*** (31.015)
MAC		0.040 (1.167)		0.048** (1.754)		0.051** (1.939)		0.053** (1.986)
SMB			-0.132*** (3.215)	-0.113*** (2.585)	-0.114*** (2.835)	-0.093** (2.193)	-0.113*** (2.823)	-0.093** (2.178)
HML			0.440*** (9.964)	0.459*** (10.049)	0.407*** (9.318)	0.428*** (9.489)	0.403*** (9.170)	0.423*** (9.335)
UMD					-0.099*** (3.801)	-0.101*** (3.821)	-0.099*** (3.773)	-0.100*** (3.796)
LIQ							-0.027 (0.816)	-0.030 (0.906)
R^2	73.90%	74.16%	84.08%	84.58%	85.05%	85.58%	85.09%	85.64%
RMSE	2.586	2.638	2.029	2.047	1.970	1.984	1.972	1.985

Table 8.3: Continued

Panel C: Materials								
	(1)	(2)	(3)	(4)	(5)	(6)	(7)	(8)
Alpha	0.533*** (2.239)	0.533*** (2.130)	0.356** (1.701)	0.307** (1.403)	0.433*** (2.078)	0.385* (1.775)	0.286 (1.415)	0.243 (1.161)
MKT	0.960*** (18.636)	0.968*** (18.215)	1.016*** (21.896)	1.023*** (21.690)	0.971*** (20.015)	0.977*** (19.830)	0.955*** (20.490)	0.958*** (20.346)
MAC		0.049 (1.053)		0.094** (2.235)		0.098*** (2.367)		0.087** (2.214)
SMB			0.041 (0.650)	0.095* (1.414)	0.061 (0.978)	0.117** (1.766)	0.058 (0.967)	0.113** (1.781)
HML			0.560*** (8.268)	0.593*** (8.461)	0.524*** (7.692)	0.556*** (7.933)	0.556*** (8.489)	0.590*** (8.777)
UMD					-0.111*** (2.719)	-0.117*** (2.841)	-0.116*** (2.971)	-0.121*** (3.096)
LIQ							0.226*** (4.636)	0.234*** (4.708)
R^2	60.58%	60.99%	70.21%	71.14%	71.16%	72.21%	73.71%	74.87%
RMSE	3.566	3.631	3.114	3.138	3.070	3.087	2.938	2.942

Panel D: Consumer Discretionary								
	(1)	(2)	(3)	(4)	(5)	(6)	(7)	(8)
Alpha	0.725*** (4.255)	0.748*** (4.176)	0.613*** (3.908)	0.607*** (3.692)	0.718*** (4.786)	0.712*** (4.562)	0.705*** (4.632)	0.696*** (4.408)
MKT	0.952*** (25.844)	0.947*** (24.869)	0.980*** (28.183)	0.978*** (27.604)	0.919*** (26.306)	0.916*** (25.861)	0.918*** (26.142)	0.914*** (25.684)
MAC		-0.018 (0.526)		0.012 (0.367)		0.017 (0.571)		0.016 (0.530)
SMB			0.062* (1.323)	0.072* (1.438)	0.090** (1.999)	0.102** (2.149)	0.090** (1.989)	0.102** (2.135)
HML			0.342*** (6.741)	0.362*** (6.879)	0.293*** (5.972)	0.313*** (6.208)	0.296*** (5.987)	0.317*** (6.239)
UMD					-0.151*** (5.154)	-0.157*** (5.303)	-0.152*** (5.160)	-0.157*** (5.313)
LIQ							0.020 (0.554)	0.026 (0.695)
R^2	74.72%	74.76%	79.03%	79.46%	81.26%	81.89%	81.29%	81.93%
RMSE	2.552	2.601	2.334	2.358	2.211	2.219	2.215	2.222

Panel E: Consumer Staples								
	(1)	(2)	(3)	(4)	(5)	(6)	(7)	(8)
Alpha	0.711*** (4.276)	0.643*** (3.799)	0.693*** (4.574)	0.638*** (4.113)	0.665*** (4.361)	0.613*** (3.924)	0.689*** (4.461)	0.635*** (4.021)
MKT	0.443*** (12.309)	0.453*** (12.593)	0.502*** (14.964)	0.506*** (15.109)	0.518*** (14.564)	0.521*** (14.685)	0.520*** (14.596)	0.524*** (14.711)
MAC		0.099*** (3.115)		0.077*** (2.591)		0.076*** (2.550)		0.077*** (2.599)
SMB			-0.247*** (5.435)	-0.216*** (4.538)	-0.254*** (5.562)	-0.223*** (4.664)	-0.254*** (5.549)	-0.222*** (4.648)
HML			0.139*** (2.847)	0.167*** (3.364)	0.152*** (3.054)	0.179*** (3.546)	0.147*** (2.930)	0.174*** (3.423)
UMD					0.039* (1.316)	0.038 (1.274)	0.040* (1.343)	0.038* (1.297)
LIQ							-0.037 (0.986)	-0.036 (0.960)
R^2	40.13%	43.08%	51.45%	53.67%	51.82%	54.02%	52.04%	54.22%
RMSE	2.490	2.456	2.252	2.226	2.249	2.223	2.249	2.223

Table 8.3: Continued

Panel F: Health Care								
	(1)	(2)	(3)	(4)	(5)	(6)	(7)	(8)
Alpha	0.774*** (4.463)	0.725*** (3.987)	0.783*** (4.646)	0.757*** (4.254)	0.747*** (4.405)	0.724*** (4.048)	0.822*** (4.857)	0.801*** (4.512)
MKT	0.569*** (15.158)	0.569*** (14.709)	0.607*** (16.249)	0.604*** (15.731)	0.628*** (15.885)	0.623*** (15.340)	0.636*** (16.295)	0.633*** (15.818)
MAC		0.040 (1.165)		0.015 (0.442)		0.013 (0.394)		0.019 (0.570)
SMB			-0.195*** (3.854)	-0.192*** (3.527)	-0.205*** (4.025)	-0.201*** (3.681)	-0.203*** (4.053)	-0.199*** (3.704)
HML			0.034 (0.625)	0.046 (0.801)	0.051 (0.921)	0.061 (1.052)	0.035 (0.629)	0.043 (0.748)
UMD					0.052* (1.565)	0.048* (1.430)	0.054** (1.667)	0.051* (1.529)
LIQ							-0.114*** (2.798)	-0.126*** (2.982)
R^2	50.41%	50.43%	54.20%	54.14%	54.69%	54.58%	56.24%	56.44%
RMSE	2.597	2.641	2.507	2.552	2.499	2.546	2.462	2.500

Panel G: Financials								
	(1)	(2)	(3)	(4)	(5)	(6)	(7)	(8)
Alpha	0.401 (1.313)	0.423 (1.308)	0.119 (0.547)	0.123 (0.533)	0.249 (1.183)	0.250 (1.126)	0.400** (1.968)	0.402** (1.887)
MKT	1.092*** (16.558)	1.096*** (15.963)	1.224*** (25.402)	1.230*** (24.779)	1.149*** (23.444)	1.154*** (22.891)	1.166*** (24.839)	1.174*** (24.451)
MAC		-0.013 (0.209)		0.020 (0.458)		0.027 (0.633)		0.038 (0.945)
SMB			-0.134*** (2.049)	-0.129** (1.833)	-0.100** (1.582)	-0.093** (1.363)	-0.096** (1.600)	-0.088* (1.362)
HML			0.954*** (13.561)	0.969*** (13.140)	0.893*** (12.984)	0.909*** (12.667)	0.859*** (13.007)	0.873*** (12.750)
UMD					-0.187*** (4.555)	-0.190*** (4.520)	-0.182*** (4.633)	-0.185*** (4.641)
LIQ							-0.233*** (4.735)	-0.250*** (4.927)
R^2	54.81%	54.91%	77.56%	77.86%	79.47%	79.82%	81.35%	81.92%
RMSE	4.569	4.691	3.234	3.303	3.101	3.160	2.962	2.999

Panel H: Information Technology								
	(1)	(2)	(3)	(4)	(5)	(6)	(7)	(8)
Alpha	0.884*** (3.594)	0.955*** (3.697)	1.057*** (4.979)	1.155*** (5.222)	1.161*** (5.564)	1.250*** (5.755)	1.131*** (5.352)	1.216*** (5.541)
MKT	1.272*** (23.913)	1.275*** (23.223)	1.197*** (25.454)	1.198*** (25.123)	1.138*** (23.415)	1.141*** (23.126)	1.134*** (23.263)	1.136*** (22.967)
MAC		-0.050 (1.033)		-0.077** (1.825)		-0.073** (1.753)		-0.075** (1.811)
SMB			0.053 (0.831)	0.032 (0.469)	0.080 (1.281)	0.059 (0.892)	0.079 (1.270)	0.058 (0.876)
HML			-0.576*** (8.390)	-0.606*** (8.562)	-0.625*** (9.167)	-0.651*** (9.274)	-0.618*** (9.014)	-0.643*** (9.110)
UMD					-0.149*** (3.656)	-0.143*** (3.476)	-0.150*** (3.678)	-0.144*** (3.502)
LIQ							0.046 (0.893)	0.056 (1.070)
R^2	71.67%	72.23%	79.36%	80.31%	80.52%	81.38%	80.59%	81.49%
RMSE	3.683	3.750	3.158	3.172	3.074	3.092	3.076	3.091

Table 8.3: Continued

Panel I: Telecommunication Services								
	(1)	(2)	(3)	(4)	(5)	(6)	(7)	(8)
Alpha	0.049 (0.165)	0.152 (0.498)	0.127 (0.433)	0.308 (1.029)	0.209 (0.712)	0.379 (1.262)	0.186 (0.627)	0.352 (1.157)
MKT	0.658*** (10.296)	0.653*** (10.088)	0.686*** (10.590)	0.677*** (10.473)	0.639*** (9.360)	0.635*** (9.305)	0.637*** (9.279)	0.632*** (9.209)
MAC		-0.129*** (2.257)		-0.186*** (3.241)		-0.183*** (3.194)		-0.185*** (3.219)
SMB			-0.266*** (3.026)	-0.328*** (3.574)	-0.244*** (2.781)	-0.308*** (3.347)	-0.245*** (2.782)	-0.308*** (3.351)
HML			-0.166** (1.758)	-0.224*** (2.328)	-0.205*** (2.139)	-0.257*** (2.643)	-0.200*** (2.072)	-0.250*** (2.559)
UMD					-0.118*** (2.063)	-0.106** (1.859)	-0.119*** (2.072)	-0.107** (1.871)
LIQ							0.035 (0.480)	0.045 (0.616)
R^2	31.93%	34.85%	34.81%	38.94%	36.03%	39.92%	36.10%	40.03%
RMSE	4.427	4.423	4.352	4.302	4.320	4.277	4.328	4.284

Panel J: Real Estate								
	(1)	(2)	(3)	(4)	(5)	(6)	(7)	(8)
Alpha	1.458*** (4.399)	1.513*** (4.321)	1.177*** (4.051)	1.117*** (3.646)	1.343*** (4.758)	1.278*** (4.306)	1.324*** (4.626)	1.257*** (4.183)
MKT	0.849*** (11.851)	0.842*** (11.320)	0.855*** (13.291)	0.860*** (13.021)	0.760*** (11.561)	0.764*** (11.332)	0.758*** (11.472)	0.761*** (11.233)
MAC		-0.052 (0.791)		0.060 (1.019)		0.068 (1.205)		0.067 (1.174)
SMB			0.454*** (5.204)	0.494*** (5.270)	0.497*** (5.882)	0.540*** (5.955)	0.497*** (5.866)	0.540*** (5.936)
HML			0.765*** (8.137)	0.803*** (8.187)	0.687*** (7.444)	0.727*** (7.584)	0.691*** (7.431)	0.732*** (7.578)
UMD					-0.239*** (4.333)	-0.241*** (4.288)	-0.240*** (4.335)	-0.242*** (4.291)
LIQ							0.028 (0.410)	0.034 (0.480)
R^2	38.33%	38.40%	53.67%	54.36%	57.27%	58.04%	57.30%	58.08%
RMSE	4.964	5.081	4.321	4.395	4.159	4.224	4.167	4.232

Panel K: Utilities								
	(1)	(2)	(3)	(4)	(5)	(6)	(7)	(8)
Alpha	0.675*** (2.765)	0.564*** (2.263)	0.566*** (2.474)	0.441** (1.897)	0.537** (2.324)	0.415** (1.771)	0.439** (1.905)	0.330* (1.409)
MKT	0.315*** (5.969)	0.320*** (6.051)	0.375*** (7.403)	0.380*** (7.573)	0.392*** (7.285)	0.395*** (7.420)	0.381*** (7.154)	0.384*** (7.281)
MAC		0.118*** (2.528)		0.130*** (2.907)		0.128*** (2.875)		0.122*** (2.763)
SMB			-0.096* (1.396)	-0.070 (0.986)	-0.103* (1.496)	-0.077 (1.081)	-0.106* (1.548)	-0.080 (1.133)
HML			0.383*** (5.177)	0.410*** (5.508)	0.397*** (5.257)	0.422*** (5.569)	0.418*** (5.587)	0.442*** (5.878)
UMD					0.042 (0.929)	0.038 (0.861)	0.039 (0.866)	0.036 (0.809)
LIQ							0.150*** (2.682)	0.141*** (2.531)
R^2	13.62%	15.78%	25.79%	29.15%	26.08%	29.40%	28.40%	31.50%
RMSE	3.653	3.618	3.401	3.334	3.402	3.336	3.356	3.294

of the aggregated market correlation portfolio, we compare the results for each of the conventional factor models with and without the market aggregated market correlation portfolio separately.

At a glance, the results are quite mixed across different sectors, which is similar to the inconsistent performance of the other portfolio factors in the literature. In fact, across the sector portfolios, 7 out of 11 sectors show consistent significance for the market aggregated factor controlling different sets of market risk factors. For example, for Energy sector, the inclusion of the market average correlation factor largely increase the model fitting of the **FFC4** and **LIQ** model with 2.79% increase of R^2 and the estimated α is insignificant from zero. The estimated coefficients of **MAC** also report a positive relation between the excess returns for the Energy sector portfolio and the aggregated correlation factor. However, the performance of the aggregated correlation factor in some sectors are very poor and fails to show any significance, such as the Financial sector in Panel G.

An interesting pair of sectors is the Consumer Discretionary (Panel D) and Consumer Staples (Panel E). Though both sectors are composed by companies focusing on individual consumer products, the Discretionary stock companies provide services and products that consumers find non-essential while Staple stocks involve products and services essential for day-to-day living. Thus, the Consumer Discretionary sector portfolio earns a much higher market beta than the Consumer Staples sector. Interestingly, the market average correlation factor maintain significant and largely increases the model-fitting of the **FFC4** factor model with a 2.22% increase in R^2 for the Consumer Staples sector portfolio while performs very poorly for the Consumer Discretionary sector portfolio.

It is not surprise that the performance of the market average correlation factor varies across different sectors. As currently, the higher dimensional option-implied average correlations are extracted from the S&P 500 index and all the components stocks, however, the weights of different sectors in the are unbalanced. Thus, the performance of the market average correlation factor is not universe across different sectors. In fact, the mixed results inspires us to further investigate the sector average correlations utilising the exchange-

traded Selected Sector SPDR ETFs index and the options written on the ETFs in the future work.³

After examining the performance of the market average correlation factor in risk-adjusted factor pricing models across the time-series regressions, I proceed now to further explore the relation between the risk premium of the market average correlation factor and cross section stock returns utilising the Fama and MacBeth [1973] methodology. Specifically, I first run the time-series regressions between the excess expected returns for each individual stocks and the market portfolio (MKT) and the market average correlation portfolio (MAC) to collect the estimated factor loadings with a rolling window of one year at monthly frequency:

$$R_{i,h} - r_{f,h} = \alpha_i + \beta_i^{\text{MKT}} \text{MKT}_{i,h} + \beta_i^{\text{MAC}} \text{MAC}_{i,h} + \epsilon_i \quad (8.19)$$

I then run the cross-sectional regression at each month with the estimated factor loadings for the market factor, i.e. $\hat{\beta}_i^{\text{MKT}}$ and $\hat{\beta}_i^{\text{MAC}}$, together with the set of firm-specific characteristic factors as control variables:

$$\mathbb{E}[R_{i,h}] - r_{f,h} = \lambda_0 + \lambda_h^{\text{MKT}} \hat{\beta}_i^{\text{MKT}} + \lambda_h^{\text{MAC}} \hat{\beta}_i^{\text{MAC}} + \boldsymbol{\lambda}_t^Z \mathbf{Z}_i + \epsilon_h \quad (8.20)$$

where \mathbf{Z}_i represents the firm-specific idiosyncratic factors, namely, the logarithm of firm size (SIZE), book-to-market ratio (BM), momentum (MOM), short-term reversal (REV), idiosyncratic volatility (IDIO), realised skewness (RSK), realised kurtosis (RKT), co-skewness (CSK), co-kurtosis (CKT), and liquidity (ILLIQ). The details of the calculations for these controlled variables are given in Section 8.2.2. The final estimated coefficients are calculated by the time-series average of the periodic cross-sectional regression coefficients and the standard errors and the associate t-statistics are adjusted following Newey and West [1987].

Table 8.4 summarise the results of Fama and MacBeth [1973] cross-sectional regression analyses of relation between expected stock returns and the risk premium of the market average correlation portfolio. The univariate

³Readers who are interested in this are welcome to contact the author for further information on the work on sectors average correlations.

Table 8.4: Fama-MacBeth Regression Analyses on Market Average Correlation Portfolio

Table 8.4 reports the results of Fama and MacBeth [1973] cross-sectional regression analyses of relation between expected stock returns and the market average correlation portfolio. Panel A presents the univariate regressions results between the expected stock returns and the each of the independent variables and control variables. Each row in Panel B displays results for a different cross-sectional regression specification. The dependent variable in all specifications is the monthly expected excess stock return. The independent variables are indicated in the first row. The independent variables are indicated in the first row. Following Bali et al. [2016], the firm-specific variables are winsorized at the 0.5% level. The dependent variable, i.e. stock excess expected returns, is in percent unit. The table presents average estimated coefficients along with the absolute value of the t-statistics (in parentheses, *** indicates the significance at 1% level, ** at 5%, and * at 10%. < 0.01% indicates the value is less than 0.01%), adjusted following Newey and West [1987] using six lags, testing the null hypothesis that the average coefficient is equal to zero. The whole sample period is from January 1, 1996 to January 1, 2015, with 228 monthly observations for 588 individual stocks included in the S&P 500 index over the whole sample period.

Panel A: Univariate Regressions						
	β^{MKT}	β^{MAC}	SIZE	BM	MOM	REV
	0.433 (6.288)	0.201 (2.425)	-0.105 (3.381)	0.001 (0.319)	0.070 (2.764)	0.614 (2.813)
Panel B: Multivariate Regressions						
	β^{MKT}	β^{MAC}	SIZE	BM	MOM	REV
(1)	0.212*** (3.486)		-0.013 (0.278)	< 0.01% (0.241)	0.055*** (6.131)	0.229*** (6.890)
(2)		0.102*** (2.676)	-0.040 (0.832)	< 0.01% (0.003)	0.055*** (6.115)	0.226*** (6.764)
(3)	0.472*** (6.824)	0.194*** (2.766)	-0.078*** (2.536)	< 0.01% (0.255)		
(4)	0.496*** (11.502)	0.214*** (4.902)	-0.061*** (3.169)	0.001* (1.312)	0.071*** (3.177)	
(5)	0.487*** (11.738)	0.223*** (5.310)	-0.076*** (4.095)	0.001* (1.480)	0.053*** (4.951)	0.238*** (6.882)
(6)	0.217*** (3.887)	0.148*** (3.466)	0.011 (0.522)	< 0.01% (0.040)	0.071*** (3.766)	
(7)	0.494*** (11.421)	0.211*** (4.806)	-0.062*** (3.228)	0.001* (1.320)	0.071*** (3.133)	
(8)	0.490*** (11.376)	0.203*** (4.625)	-0.050*** (2.509)	0.001* (1.439)	0.071*** (3.193)	
(9)	0.491*** (11.414)	0.214*** (4.929)	-0.065*** (3.395)	0.001* (1.375)	0.072*** (3.313)	
(10)	0.584*** (12.897)	0.157*** (3.574)	-0.004 (0.186)	0.001 (0.991)	0.071*** (3.949)	
(11)	0.493*** (11.347)	0.214*** (4.911)	-0.085** (1.750)	0.001* (1.390)	0.071*** (3.186)	
(12)	0.328*** (5.209)	0.126*** (3.056)	-0.018 (0.394)	0.001 (0.623)	0.054*** (6.373)	0.234*** (7.184)

Table 8.4: Continued

Panel A: Univariate Regressions						
	IDIO	RSK	RKT	CSK	CKT	ILLIQ
	0.385*	-1.579**	0.015***	-0.871	-0.275***	0.084***
	(1.283)	(2.257)	(3.183)	(1.073)	(2.363)	(2.770)
Panel B: Multivariate Regressions						
	IDIO	RSK	RKT	CSK	CKT	ILLIQ
(1)	-0.313***	-0.038	0.006***	1.737***	-0.296***	-0.047
	(5.349)	(0.090)	(2.059)	(3.730)	(3.278)	(1.053)
(2)	-0.423***	0.066	0.005**	1.664***	-0.052	-0.066*
	(4.101)	(0.156)	(1.751)	(3.557)	(0.659)	(1.460)
(3)						
(4)						
(5)						
(6)	-0.312***					
	(4.472)					
(7)		-0.348				
		(0.805)				
(8)			0.007**			
			(2.144)			
(9)				1.035**		
				(2.120)		
(10)					-0.447***	
					(5.299)	
(11)						-0.026
						(0.551)
(12)	-0.230***	0.039	0.005**	1.683***	-0.322***	-0.040
	(5.203)	(0.093)	(1.769)	(3.688)	(3.648)	(0.920)

regression results in Panel A show that the market average correlation factor earns a positive significant risk premium as expected. The significant positive risk premium of the market average correlation factor is consistent with the univariate portfolio sorting analyses in Table 8.2 that stocks with higher exposure to the market correlation risk outperform the stocks with lower exposure to the correlation risks.

The results of the multivariate regressions are summarised in Panel B. Specifically, Regression (1) and (2) regress the market portfolio (CAPM) and the market average correlation factor independently along with all of the controlled variables on the excess stock returns. Regression (3) tests the joint significance of the market average correlation factor with the three risk factors in Fama and French [1992] (FF3) while Regression (4) further examines the joint significance of the MAC together with the momentum factor (FFC4) as suggested in Carhart [1997]. It can be seen that the market average correlation factor consistently show positive significant coefficients across CAPM, FF3, and FFC4.

Regression (5) to (11) further investigate that whether the market average correlation can be explained by the firm-specific characteristic factors that are well-documented in the recent literature. Again, the market average correlation factor survives through the multivariate regressions with independent controlling variables. Finally, the joint significance of the market average correlation factor and all the firm-specific characteristic factors are confirmed in Regression 12.

To summarise, I investigate the information content of the higher dimensional option-implied average correlations via a series of empirical analyses. Specifically, I first demonstrate the explanatory power of the higher dimensional option-implied average correlations for the market risk, in this case proxy by the CBOE VIX. The option-implied average correlations could explain up to 84.0% of the variations in the VIX contemporaneously and capture 78.6%, 43.6%, and 17.1% variations of the CBOE VIX in the one-week, one-month, and one-quarter ahead forecasting horizons, respectively.

The implications of the higher dimensional option-implied average correlations in empirical asset pricing are then intensively examined. In

particular, I show that the option-implied quadratic, cubic, and quartic average correlations are priced market factors in cross-sectional stock returns via the [Fama and MacBeth \[1973\]](#) cross-sectional regressions. I then uniquely construct the market average correlation factor ([MAC](#)) by forming the zero-cost long-short portfolios by sorting stocks with respect to their risk exposures to the option-implied average correlations. Through a series of time-series regressions for different sector portfolios, I show that [MAC](#) largely increase the model-fittings of the traditional risk-adjusted factor models, such as the [CAPM](#), Fama-French three-factor, and Fama-French-Carhart four-factor models. Finally, I document significant evidence that the [MAC](#) is priced cross-sectional via the [Fama and MacBeth \[1973\]](#) cross-sectional regression after controlling other firm-specific characteristic factors.

8.4 Robustness Check

To further examine the robustness of my empirical findings, I carry out a series of robustness checks regarding on the various procedures in the empirical analyses.

8.4.1 Sub-Periods

The period between January 1, 1996 and January 1, 2015 in the U.S. market is characterised by various turbulences, such as the early 2000 recession, the 2001 Bursting of dot-com bubble, and the 2007 - 2008 Global financial crisis. As we mentioned in [Section 8.2.1](#), our high frequency option dataset is merged by the exchange-based option prices and the [OPRA](#) system, which is separated by the introduction of the National Market System in November 30, 2009. In order to verify that the results are not driven by the peculiar circumstances in this sample period, I repeat the empirical analyses in [Section 8.3](#) on two sub-periods: pre [OPRA](#) & Global financial crisis period: January 1, 1996 to November 30th, 2009, and the post [OPRA](#) & Global financial crisis period: December 1, 2009 to January 1, 2015.

Table [8.5](#) reports the results of [Fama and MacBeth \[1973\]](#) cross-sectional

Table 8.5: Fama-MacBeth Regression Analyses for the Pre and Post OPRA Sub-Periods

Table 8.5 reports the results of Fama and MacBeth [1973] cross-sectional regression analyses for the pre and post OPRA sub-periods as displayed in Table 8.4. In order to conserve space, we only present the results obtained using the most general multivariate regression for each analyses. I re-perform regression (12) in Table 8.4 investigating the cross-sectional risk premium of the market average correlation factor controlling all the other firm-specific characteristic factors. The independent variables are indicated in the first row. Independent variables are winsorised at the 0.5% level on a monthly basis. The dependent variable, i.e. stock excess expected returns, is in percent unit. The table presents average estimated coefficients along with the absolute value of the t-statistics (in parentheses, *** indicates the significance at 1% level, ** at 5%, and * at 10%. < 0.01% indicates value less than 0.01%), adjusted following Newey and West [1987] using six lags, testing the null hypothesis that the average coefficient is equal to zero. The whole sample period is from January 1, 1996 to January 1, 2015, with 228 monthly observations for 588 individual stocks included in the S&P 500 index over the whole sample period. The pre OPRA sample period is from January 1, 1996 to November 30th, 2009 with 167 observations and the post OPRA sample period is from December 1, 2009 to January 1, 2015 with 61 observations.

Market Average Correlation Portfolio and Cross Section Stock Returns						
	β^{MKT}	β^{MAC}	SIZE	BM	MOM	REV
Pre OPRA	0.500*** (6.699)	0.116 (1.178)	-0.005 (0.118)	0.001** (1.827)	0.051*** (3.574)	-0.258*** (3.311)
Post OPRA	0.305*** (2.652)	0.126*** (2.993)	-0.115*** (2.159)	-0.050* (1.600)	0.051*** (3.380)	-0.204*** (3.998)
	IDIO	RSK	RKT	CSK	CKT	ILLIQ
Pre OPRA	-0.266*** (6.036)	-0.105* (1.501)	0.001 (0.132)	1.855*** (3.040)	-0.168* (1.625)	0.009 (0.224)
Post OPRA	-0.151*** (2.582)	1.758*** (4.351)	0.017*** (5.581)	0.344 (0.981)	-0.061 (0.656)	-0.053 (0.953)

regression analyses for the pre and post OPRA sub-periods as displayed in Table 8.4. I re-perform regression (12) in Table 8.4 investigating the cross-sectional risk premium of the market average correlation factor controlling all the other firm-specific characteristic factors. Compared to the results in Table 8.4, the constructed market average correlation factor (MAC) returns a positive risk premium for both pre and post OPRA periods, but the pre OPRA risk premium is not statistically significant while that for the post OPRA period is strongly significant.

8.4.2 Length of the Portfolio Formation Period

In Section 8.3.2, I construct the monthly rebalanced market average correlation factor by sorting the stocks with their exposures to the option-implied average correlations estimating with over a one-year rolling window. As the higher dimensional option-implied average correlations are time-varying, I repeat the portfolio formation and the test procedures with individual correlation risk exposures estimating over samples longer or shorter than one month with rolling windows longer or shorter than one-year respectively. With the new sets of MAC factors, I re-run the Fama and MacBeth [1973] cross-sectional regressions in Table 8.4. I present the univariate-sorting portfolios results and the cross-sectional regression analyses for Equation 8.20 obtained using the risk exposures estimated every three-month over a one-year rolling window in detail.

Table 8.6 reports the results of the robustness check for using different length of the portfolio formation period. Specifically, Panel A reports the results of the univariate-sorted portfolios on the risk exposures of the option-implied average correlations estimating with three-month period over a one-year rolling window. The stocks are sorted by their risk exposures to the quadratic, cubic, and quartic option-implied average correlations in (I), (II), and (III) in Panel A, respectively. Monthly excess returns (in percent) and the Fama-French-Cahart four-factor alphas are reported with the the absolute value of the robust t-statistics (in parentheses).

To further explore the risk premium of the constructed market average

Table 8.6: Single-sorted Portfolios and Fama-MacBeth Regression Analyses with Different Length of Portfolio Formation Period

Table 8.6 displays the results of the robustness check of the length of the portfolio formation period. Panel A reports the results of the univariate-sorted portfolios on the risk exposures of the option-implied average correlations estimating with three-month period over a one-year rolling window. Panel B displays the the Fama and MacBeth [1973] cross-sectional regression analyses for the market average correlation factor formed by the re-estimated sorting portfolios in Panel A. The independent variables are indicated in the first row. Following Bali et al. [2016], firm-specific variables are winsorized at the 0.5% level on a monthly basis. The dependent variable, i.e. stock excess expected returns, is in percent unit. The table presents average estimated coefficients along with the absolute value of the t-statistics (in parentheses, *** indicates the significance at 1% level, ** at 5%, and * at 10%. < 0.01% indicates value less than 0.01%), adjusted following Newey and West [1987] using six lags, testing the null hypothesis that the average coefficient is equal to zero. The whole sample period is from January 1, 1996 to January 1, 2015, with 228 monthly observations for 588 individual stocks included in the S&P 500 index over the whole sample period.

Panel A: Univariate-sorted Portfolios on Option-implied Average Correlation Risk Exposure					
Sorted by $\beta^{P\Sigma}$					
Quintile	$\beta^{P\Sigma}$	$\beta^{P\Gamma}$	$\beta^{P\Theta}$	Return	FFC4
1 (Low)	-2.034	-1.130	-1.313	0.373 (0.926)	-0.463 (2.669)
2	-0.731	-0.398	-0.436	0.746 (2.480)	0.118 (1.000)
3	-0.003	-0.025	0.024	0.820 (3.024)	0.268 (2.468)
4	0.678	0.359	0.454	0.921 (3.120)	0.390 (2.957)
5 (High)	1.779	0.978	1.228	1.107 (3.024)	0.596 (2.942)
5-1 (High -Low)	3.813	2.107	2.540	0.734 (2.237)	1.060 (3.313)
Sorted by $\beta^{P\Gamma}$					
1 (Low)	-1.124	-2.051	-1.517	0.632 (1.529)	-0.173 (0.853)
2	-0.372	-0.725	-0.535	0.836 (2.790)	0.216 (1.811)
3	-0.007	-0.006	0.022	0.774 (2.925)	0.234 (2.188)
4	0.385	0.672	0.535	0.850 (2.893)	0.329 (2.496)
5 (High)	0.919	1.788	1.405	0.906 (2.428)	0.345 (1.646)
5-1 (High -Low)	2.042	3.839	2.922	0.274 (2.776)	0.518 (1.438)
Sorted by $\beta^{P\Theta}$					
1 (Low)	-1.325	-1.478	-1.945	0.586 (1.503)	-0.208 (1.220)
2	-0.427	-0.481	-0.674	0.772 (2.746)	0.170 (1.520)
3	0.040	0.046	0.038	0.873 (3.213)	0.347 (3.006)
4	0.442	0.490	0.730	0.851 (2.934)	0.331 (2.706)
5 (High)	1.120	1.270	1.905	0.905 (2.310)	0.318 (1.547)
5-1 (High -Low)	2.445	2.748	3.849	0.319 (2.026)	0.526 (1.658)

Table 8.6: Continued

Panel B: Market Average Correlation Portfolio and Cross Section Stock Returns						
Regressions	β^{MKT}	β^{MAC}	SIZE	BM	MOM	REV
(1)	0.417*** (9.612)	0.174*** (2.459)	-0.061*** (2.978)	0.001 (1.111)	0.071*** (2.532)	
(2)	0.409*** (9.787)	0.196*** (2.868)	-0.075*** (3.808)	0.001 (1.267)	0.053*** (4.185)	-0.245*** (3.709)
(3)	0.116*** (2.380)	0.087* (1.359)	0.012 (0.596)	-0.002 (0.168)	0.055*** (3.861)	-0.225*** (3.626)
(4)	0.119*** (2.439)	0.097* (1.505)	0.009 (0.461)	-0.001 (0.126)	0.054*** (3.825)	-0.226*** (3.667)
(5)	0.129*** (2.651)	0.119** (1.841)	0.022 (1.058)	< 0.01% (0.086)	0.054*** (3.861)	-0.227*** (3.748)
(6)	0.121*** (2.469)	0.109** (1.683)	0.019 (0.917)	< 0.01% (0.101)	0.055*** (3.013)	-0.228*** (3.784)
(7)	0.222*** (3.761)	0.147*** (2.248)	0.040** (1.830)	0.002 (0.179)	0.054*** (3.969)	-0.237*** (4.078)
(8)	0.219*** (3.716)	0.151*** (2.304)	-0.030 (0.637)	< 0.01% (0.509)	0.054*** (4.028)	-0.237*** (4.092)
Regressions	IDIO	RSK	RKT	CSK	CKT	ILLIQ
(1)						
(2)						
(3)	-0.373*** (4.784)					
(4)	-0.366*** (4.547)	-0.502 (1.230)				
(5)	-0.353*** (4.159)	-0.155 (0.363)	0.008*** (2.535)			
(6)	-0.360*** (4.330)	-0.086 (0.200)	0.008*** (2.430)	0.888** (1.929)		
(7)	-0.297*** (3.826)	-0.181 (0.424)	0.008*** (2.606)	1.129*** (2.433)	-0.276*** (3.006)	
(8)	-0.293*** (3.717)	-0.205 (0.481)	0.009*** (2.766)	1.228*** (2.632)	-0.279*** (3.049)	-0.075** (1.676)

correlation factor (MAC), we re-perform the Fama and MacBeth [1973] cross-sectional regression analyses as displayed in Table 8.4. Regression (1) shows that the constructed market average correlation factor returns a positive significant risk premium for the Fama-French-Carhart four-factor risk-adjusted model. Regressions (2) to (8) re-examine the consistence of the risk premium of the constructed market average correlation factor by controlling different firm-specific characteristic factors. As in Table 8.4, the constructed market average correlation factor maintain the positive significant risk premium in most of cases.

8.4.3 Options with Longer Time to Maturity

The risk-neutral moments and co-moments extracted from options with different time to maturities reflect investors' expectation of risk in the stock market over different horizons ahead. For instance, the one-month option-implied average correlations provides a proxy of investors' expectation over the future month and the three-month option-implied moments and average correlations reflect investors' expectation of risk and the market average correlation over the next quarter while the six-month to maturity estimations reflect the investors' expectation over a six-month ahead horizon.

I focus the empirical analyses on investigating the relation between the one-month option-implied average correlations and the monthly cross section stock returns, however, for other applications interested in the assets returns over longer periods in the future, such as quarterly or semi-annually cross section stock returns, the use of option-implied average correlations extracted from options with longer maturities would be more appropriate.

8.5 Concluding Remarks

In this Chapter, I intensively investigate the information content of the higher dimensional option-implied average correlations in explaining the market risk and cross section stock returns. As an aggregated measure of the market diversification level, the option-implied average correlations exhibit strong

explanatory power for the variations in the market risks, measured by the CBOE VIX. I also document significant evidence that the option-implied average correlations could explain the one-week, one-month, and one-quarter ahead CBOE VIX variations.

I then explore the role that the option-implied average correlations play in asset pricing, especially the relation between the option-implied average correlations and cross-sectional stock returns. Specifically, I sort the individual stocks on their exposures for the quadratic, cubic, and quartic option-implied average correlations individually and form zero-cost long-short portfolios on each of the average correlation exposures. I then construct an average correlation portfolio with the average of the excess returns of the three long-short portfolios. Rebalancing every month, I construct a portfolio-mimicking factor, namely the market average correlation factor (MAC).

Based on a series of time-series regressions on 11 sector portfolios, I show that the MAC plays an important role in the risk-adjusted factor pricing models and maintains statistically significant controlling the existing popular portfolio-mimicking factors. The risk premium of the market average correlation factor is further explored by a Fama and MacBeth [1973] cross-sectional regression across all of the individual stocks.

The robustness of the findings on the higher dimensional option-implied average correlations and the market average correlation factor is checked from various angles. Different holding periods have been used to construct the excess returns of the long-short correlation spread portfolios in Section 8.3.2. I address the effects of macroeconomic news announcements by excluding specific announcement days in the sample and re-run the cross-sectional regressions. I also perform the analyses with a sub-sample post the OPRA system as the out-of-sample check. As expected, no significant changes in the findings have been detected.

The future research will lie in three strands. As I mentioned in the sector portfolio analyses, I could build the sector-based average correlation index using options written on the ETFs exchange-traded sector indices and on the corresponding sector components individual equities. Another strand is to take advantage of the various term-structure of the option-implied correlations

to perform predictive analyses on the future stock returns. Lastly, as a proxy of the market diversification, the option-implied average correlation measures can also be included in various studies on the banking risk management, such as in explaining and forecasting the financial industry systemic risk.

Chapter 9

Conclusions

9.1 Summary and Remarks

The thesis demonstrates the information gains from high frequency option panels with applications in risk management and empirical asset pricing. First and foremost, inspired by the recent developed literature on the [RT](#), Chapter [5](#) and Chapter [6](#) investigate the empirical implementation of [RT](#) in practice with noisy market data. In Chapter [5](#), I specify a perturbation theory on the recovered discount factor, pricing kernel and the physical probability density. Utilising the results of the perturbation theory, in Chapter [6](#), I identify a set of linear and non-linear constraints that force the optimisation system to result in a transition matrix with desirable structure. A fast sequential optimisation algorithm is built and the efficiency of the algorithm is tested and checked through a series of simulations.

Following the theoretical development, I demonstrate the applications of the [RT](#) in two empirical examples. On the one hand, I provide new empirical evidence on the [RT](#) by applying the fast empirical recovery algorithm on both S&P 500 index options and options written on individual equities, AAPL.O. Consistent with the existing literature, the recovered physical probability distributions show thinner left tails than the risk-neutral probability distributions. In contrast to the example provided in [Ross \[2015\]](#), I recover U-shaped empirical pricing kernels across different numbers of states and tenors. Indeed, the empirical pricing kernel is known to be U-shaped

other than strictly decreasing in the literature. On the other hand, I build a market left tail index by aggregating the recovered physical probabilities for S&P 500 options with states being -50% and 25% over the sample period. The market left-tail index tracks the financial crisis and economic recessions well through the years.

Secondly, I extend the literature in spanning contracts by deriving the explicit formulas for extracting risk-neutral higher order central moments for asset returns from market option prices in Chapter 4. In Chapter 7, borrowing the algebra of symmetric multi-dimensional tensors, I uniquely introduce the option-implied average quadratic, cubic, and quartic correlations and derive the explicit formulas for calculating the option-implied average correlations for portfolios with high number of stocks. Utilising the high frequency data on S&P 500 index option and options written on all of index components, I estimate the time series of option-implied average correlations from January 1, 1996 through January 1, 2015.

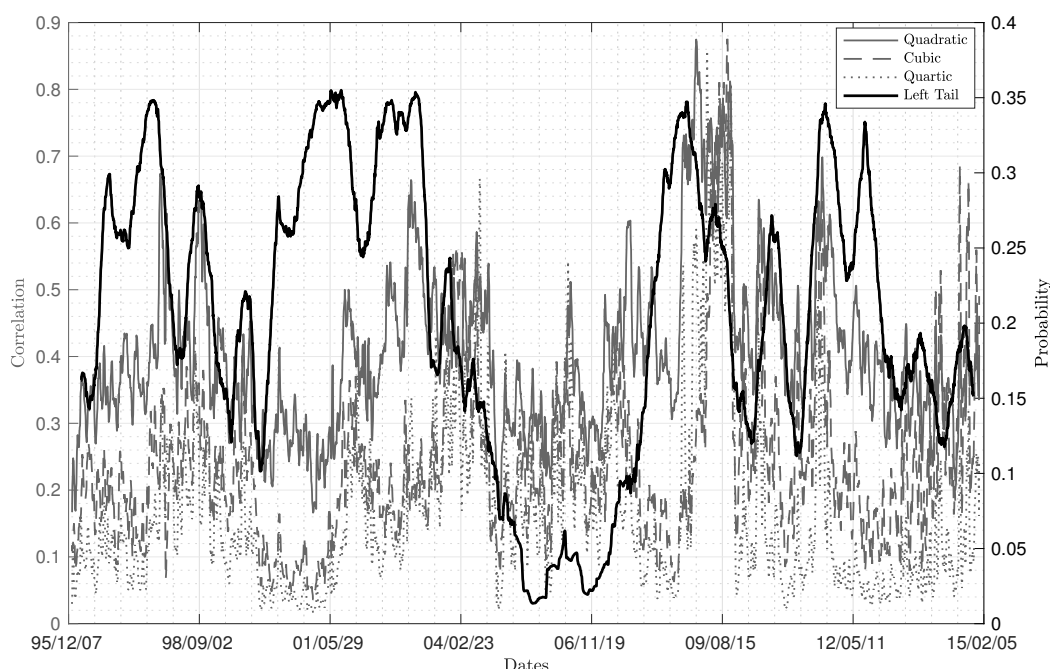
Finally, in Chapter 8, I explore the information content of higher dimensional option-implied average correlations from two perspectives. I first demonstrate that the option-implied average correlations have persistent explanatory powers for both contemporaneous and future market risks. I then show that the option-implied higher dimensional average correlations are priced in cross section stock returns. Moreover, a market average correlation factor is constructed by sorted stocks with respect to their individual exposure to the option-implied average correlations. I illustrate that the market average correlation factor largely enhance the fittings of the existing risk-adjusted asset pricing models via time-series regressions for 11 sector-based portfolios. A persistent positive risk premium is detected from two-stage [Fama and French \[1993\]](#) cross-sectional regressions.

9.2 Future Work

Various future research can build on the current content of the thesis. A obvious direction could be to investigate the dynamics between the two option-

implied risk measures. Figure 9.1 plots the market left tail index against the higher dimensional option-implied average correlations. The market left tail index represents the probability of the downside risk while the option-implied average correlations measure the diversification level in the market. It can be seen from the plot that the left tail index shows lower probabilities for downside risk when the correlations are low. Both the left tail index and the option-implied correlations track the markets very well. Thus, potential research can be conducted on investigating the dynamics of the interactions of these two option-implied risk measures.

Figure 9.1: The Two Option-implied Risk Measures



Note. Figure 9.1 plots the higher dimensional one-month to maturity option-implied average correlations against the left tail index over the sample period running from January 1, 1996 through January 31, 2015. The left y-axis represents the correlation level with the hard, dash, and dot grey lines representing the quadratic, cubic, and quartic option-implied average correlations respectively. The right y-axis demonstrates the probability for the downside risks measuring by the left tail index plotting as the black hard line.

Alternatively, both option-implied risk measures proposed in this thesis can be used as forward-looking measures for forecasting future market risks. For example, the option-implied average correlations for the financial sector can be used as a measure of the systemic risk. The existing measures

for systemic risk are mostly calculated either from accounting data for the financial sectors (such as the **CLASS** model, see for example **Hirtle et al. [2016]**) or based on specific time series models such as **GARCH** (for example the **SRISK** by **Brownlees and Engle [2017]**). As the option-implied average correlations are derived directly from option prices, which is forward-looking and conditional, the financial sector correlations can be used as indicators for future systemic risk.

Traditionally, market volatility is widely used as one of the measures for market uncertainty, however, a vast of literature also investigates the dynamics of the interaction between market-based indicators and the macroeconomic variables, such as the **GDP** (Gross Domestic Product), the **HPI** (House Price Index), and the **M2**, see for example **Jurado et al. [2015]**. As the market-wide left tail index provides the probabilities of the downside risks for the whole market, it can also be treated as a measure for uncertainty. Thus, a potential direction of future work could be to investigate the forecasting ability of the left tail index on various macroeconomic variables.

Lastly, though the dynamics of empirical pricing kernel is not the main focus of this thesis, the **RT** provides an alternative method for extracting the empirical pricing kernel to the existing literature on ‘pricing kernel puzzles’. Future research can be conducted on investigating the information content of the recovered empirical pricing kernel and calibrating the parameters in various utility functions to adjust the deviation between the theoretical pricing kernel and the empirical pricing kernel.

Chapter 10

Appendix

A.1 S&P 500 Index Constituents Sample List

Table A. 1: S&P 500 Index and Constituents

No.	Ticker	Name	Total Days	Total Obs.	Avg. Obs
1	A	Agilent Technologies Inc	4,319	63,515,389	14,706
2	AA	Alcoa Inc	2,281	27,509,567	12,060
3	AAPL	Apple Inc	4,702	526,224,432	111,915
4	ABBV	Abbvie Inc	504	12,793,579	25,384
5	ABC	Amerisourcebergen Corp	333	1,320,569	3,966
6	ABT	Abbott Laboratories	2,533	38,880,995	15,350
7	ACE	Ace Ltd	1,281	12,382,719	9,666
8	ACN	Accenture Plc	1,006	34,707,857	34,501
9	ACS	Affiliated Computer Services	47	66,074	1,406
10	ACT	Actavis Plc	489	20,571,318	42,068
11	ADBE	Adobe Systems Inc	3,033	48,093,625	15,857
12	ADI	Analog Devices	3,491	29,635,719	8,489
13	ADM	Archer-Daniels-Midland Co	3,284	46,595,877	14,189
14	ADP	Automatic Data Processing	2,053	25,629,641	12,484
15	ADS	Alliance Data Systems Corp	504	7,542,348	14,965
16	ADSK	Autodesk Inc	4,691	61,190,986	13,044
17	ADT	Adt Corp	565	12,302,067	21,774
18	AEE	Ameren Corp	4,273	4,672,625	1,094
19	AEP	American Electric Power Co	4,773	32,811,239	6,874
20	AES	Aes Corp	4,577	13,522,753	2,955
21	AET	Aetna Inc	4,773	67,022,419	14,042
22	AFL	Aflac Inc	4,773	54,023,445	11,319
23	AGN	Allergan Inc	4,773	38,137,327	7,990
24	AIG	American International Group	4,455	95,437,214	21,422

Continued on next page

Table A. 1 – continued from previous page

No.	Ticker	Name	Total Days	Total Obs.	Avg. Obs
25	AIV	Apartment Invst & Mgmt Co	3,021	2,981,357	987
26	AIZ	Assurant Inc	2,727	6,493,321	2,381
27	AKAM	Akamai Technologies Inc	2,936	91,647,998	31,215
28	AKS	Ak Steel Holding Corp	876	15,489,756	17,682
29	ALL	Allstate Corp	4,773	49,354,190	10,340
30	ALLE	Allegion Plc	273	801,468	2,936
31	ALTR	Altera Corp	4,773	62,564,414	13,108
32	ALXN	Alexion Pharmaceuticals Inc	1,281	27,276,919	21,293
33	AMAT	Applied Materials Inc	4,773	56,594,310	11,857
34	AMD	Advanced Micro Devices	4,451	33,754,429	7,584
35	AME	Ametek Inc	504	705,119	1,399
36	AMG	Affiliated Managers Grp Inc	252	3,119,043	12,377
37	AMGN	Amgen Inc	4,773	77,947,464	16,331
38	AMP	Ameriprise Financial Inc	2,329	18,547,112	7,964
39	AMT	American Tower Corp	3,021	39,139,921	12,956
40	AMZN	Amazon.Com Inc	3,021	243,909,237	80,738
41	AN	Autonation Inc	3,020	14,007,203	4,638
42	ANF	Abercrombie & Fitch -Cl A	1,452	54,621,118	37,618
43	ANR	Alpha Natural Resources Inc	337	17,268,967	51,243
44	ANTM	Anthem Inc	20	1,010,927	50,546
45	AON	Aon Plc	1,280	8,246,561	6,443
46	APA	Apache Corp	4,444	93,991,189	21,150
47	APC	Anadarko Petroleum Corp	4,773	105,861,413	22,179
48	APD	Air Products & Chemicals Inc	1,281	13,788,211	10,764
49	APH	Amphenol Corp	3,021	10,804,980	3,577
50	APOL	Apollo Education Group Inc	901	30,264,764	33,590
51	ARG	Airgas Inc	3,021	10,197,042	3,375
52	ATI	Allegheny Technologies Inc	3,884	49,812,338	12,825
53	AVB	Avalonbay Communities Inc	3,021	20,006,767	6,623
54	AVGO	Avago Technologies Ltd	252	5,378,954	21,345
55	AVP	Avon Products	4,773	28,742,713	6,022
56	AVY	Avery Dennison Corp	4,773	7,079,724	1,483
57	AXP	American Express Co	4,773	93,660,485	19,623
58	AYE	Allegheny Energy Inc	313	298,688	954
59	AZO	Autozone Inc	3,033	49,364,861	16,276
60	BA	Boeing Co	4,773	123,776,282	25,933
61	BAC	Bank Of America Corp	4,773	87,496,880	18,332
62	BAX	Baxter International Inc	4,772	65,192,108	13,661
63	BBBY	Bed Bath & Beyond Inc	4,773	78,264,177	16,397
64	BBT	Bb&T Corp	4,024	52,381,836	13,017
65	BBY	Best Buy Co Inc	4,773	104,629,651	21,921
66	BCR	Bard (C.R.) Inc	4,773	10,875,195	2,278
67	BDK	Black & Decker Corp	3,563	14,839,408	4,165
68	BDX	Becton Dickinson & Co	4,770	12,329,757	2,585
69	BEAM	Beam Inc	1,814	5,112,881	2,819
70	BEN	Franklin Resources Inc	4,772	39,242,542	8,224
71	BFB	Brown-Forman -Cl B	1,281	2,346,239	1,832
72	BHI	Baker Hughes Inc	4,773	105,965,217	22,201
73	BIG	Big Lots Inc	1,634	9,767,736	5,978
74	BIIB	Biogen Inc	870	6,350,344	7,299
75	BJS	Bj Services Co	2,000	22,214,134	11,107

Continued on next page

Table A. 1 – continued from previous page

No.	Ticker	Name	Total Days	Total Obs.	Avg. Obs
76	BK	Bank Of New York Mellon Corp	4,773	61,791,554	12,946
77	BLK	Blackrock Inc	1,281	26,057,585	20,342
78	BLL	Ball Corp	1,281	4,399,716	3,435
79	BMC	Bmc Software Inc	3,574	22,676,973	6,345
80	BMS	Bemis Co Inc	4,410	3,432,573	778
81	BMY	Bristol-Myers Squibb Co	4,773	73,381,221	15,374
82	BRCM	Broadcom Corp	3,899	107,353,530	27,534
83	BRKB	Berkshire Hathaway	1,281	30,811,334	24,053
84	BSX	Boston Scientific Corp	4,773	26,988,202	5,654
85	BTU	Peabody Energy Corp	1,972	85,449,132	43,331
86	BWA	Borgwarner Inc	1,281	11,494,143	8,973
87	BXP	Boston Properties Inc	2,685	12,653,676	4,713
88	C	Citigroup Inc	4,772	151,624,776	31,774
89	CA	Ca Inc	4,368	27,555,290	6,308
90	CAG	Conagra Foods Inc	4,773	20,923,433	4,384
91	CAH	Cardinal Health Inc	4,772	39,972,880	8,377
92	CAM	Cameron International Corp	3,021	49,428,388	16,362
93	CAT	Caterpillar Inc	4,773	133,047,147	27,875
94	CB	Chubb Corp	4,444	28,298,081	6,368
95	CBE	Cooper Industries Plc	256	157,003	613
96	CBG	Cbre Group Inc	2,482	15,266,177	6,151
97	CBS	Cbs Corp	2,875	48,384,573	16,829
98	CCE	Coca-Cola Enterprises Inc	4,773	21,855,051	4,579
99	CCI	Crown Castle Intl Corp	1,281	9,288,901	7,251
100	CCL	Carnival Corp/Plc (Usa)	4,773	51,985,897	10,892
101	CEG	Constellation Energy Grp Inc	3,238	6,064,898	1,873
102	CELG	Celgene Corp	3,021	97,040,846	32,122
103	CEPH	Cephalon Inc	735	5,082,286	6,915
104	CERN	Cerner Corp	1,281	20,549,222	16,042
105	CF	Cf Industries Holdings Inc	1,485	19,204,794	12,933
106	CFN	Carefusion Corp	1,281	6,633,130	5,178
107	CHK	Chesapeake Energy Corp	1,740	19,377,453	11,136
108	CHRW	C H Robinson Worldwide Inc	2,999	34,335,134	11,449
109	CI	Cigna Corp	4,730	55,246,338	11,680
110	CIEN	Ciena Corp	2,053	8,086,241	3,939
111	CINF	Cincinnati Financial Corp	4,064	2,478,444	610
112	CL	Colgate-Palmolive Co	4,773	48,534,982	10,169
113	CLF	Cliffs Natural Resources Inc	1,087	82,642,260	76,028
114	CLX	Clorox Co/De	4,773	24,581,825	5,150
115	CMA	Comerica Inc	3,033	30,024,254	9,899
116	CMCSA	Comcast Corp	1,281	44,755,545	34,938
117	CME	Cme Group Inc	2,450	58,027,725	23,685
118	CMG	Chipotle Mexican Grill Inc	1,281	175,535,207	137,030
119	CMI	Cummins Inc	2,784	86,492,948	31,068
120	CMS	Cms Energy Corp	4,444	3,024,675	681
121	CNP	Centerpoint Energy Inc	1,281	3,756,214	2,932
122	CNX	Consol Energy Inc	3,020	78,899,203	26,126
123	COF	Capital One Financial Corp	4,773	95,494,292	20,007
124	COG	Cabot Oil & Gas Corp	3,021	30,583,415	10,124
125	COH	Coach Inc	3,021	76,988,656	25,484
126	COL	Rockwell Collins Inc	3,217	5,536,677	1,721

Continued on next page

Table A. 1 – continued from previous page

No.	Ticker	Name	Total Days	Total Obs.	Avg. Obs
127	COP	Conocophillips	3,105	97,620,144	31,440
128	COST	Costco Wholesale Corp	4,498	83,962,638	18,667
129	COV	Covidien Plc	1,281	13,761,686	10,743
130	CPB	Campbell Soup Co	4,444	15,839,426	3,564
131	CPWR	Compuware Corp	3,270	2,698,525	825
132	CRM	Salesforce.Com Inc	2,631	116,285,467	44,198
133	CSC	Computer Sciences Corp	4,773	33,992,003	7,122
134	CSCO	Cisco Systems Inc	4,770	80,508,030	16,878
135	CSX	Csx Corp	4,773	48,142,578	10,086
136	CTAS	Cintas Corp	4,771	15,950,751	3,343
137	CTL	Centurylink Inc	4,772	22,362,338	4,686
138	CTSH	Cognizant Tech Solutions	3,021	64,534,056	21,362
139	CTXS	Citrix Systems Inc	4,663	57,983,833	12,435
140	CVC	Cablevision Sys Corp -Cl A	1,281	9,877,905	7,711
141	CVG	Convergys Corp	2,395	2,000,112	835
142	CVH	Coventry Health Care Inc	1,071	6,382,691	5,960
143	CVS	Cvs Health Corp	4,575	64,453,842	14,088
144	CVX	Chevron Corp	1,281	66,392,224	51,828
145	D	Dominion Resources Inc	2,284	14,455,037	6,329
146	DAL	Delta Air Lines Inc	1,281	49,932,209	38,979
147	DD	Du Pont (E I) De Nemours	3,518	76,341,656	21,700
148	DE	Deere & Co	4,773	99,557,443	20,858
149	DELL	Dell Inc	4,005	37,601,109	9,389
150	DF	Dean Foods Co	1,799	6,992,245	3,887
151	DFS	Discover Financial Svcs Inc	2,197	29,546,509	13,449
152	DG	Dollar General Corp	1,281	20,238,780	15,799
153	DGX	Quest Diagnostics Inc	3,521	24,672,719	7,007
154	DHI	D R Horton Inc	3,020	47,955,601	15,879
155	DHR	Danaher Corp	4,773	47,416,160	9,934
156	DIS	Disney (Walt) Co	4,773	80,846,477	16,938
157	DISCA	Discovery Communications Inc	1,281	4,101,592	3,202
158	DLPH	Delphi Automotive Plc	776	10,496,684	13,527
159	DLTR	Dollar Tree Inc	1,281	20,313,059	15,857
160	DNB	Dun & Bradstreet Corp	3,021	6,969,359	2,307
161	DNR	Denbury Resources Inc	1,281	12,099,282	9,445
162	DO	Diamond Offshre Drilling Inc	3,021	76,941,872	25,469
163	DOV	Dover Corp	1,281	7,514,922	5,866
164	DOW	Dow Chemical	3,518	76,921,591	21,865
165	DPS	Dr Pepper Snapple Group Inc	1,677	3,125,617	1,864
166	DRI	Darden Restaurants Inc	4,551	34,838,521	7,655
167	DTE	Dte Energy Co	4,773	4,531,957	949
168	DTV	Directv	1,532	35,241,574	23,004
169	DUK	Duke Energy Corp/Progress Energy Inc	4,773	25,207,134	5,281
170	DV	Devry Education Group Inc	715	3,929,967	5,496
171	DVA	Davita Healthcare Partners	3,021	10,950,825	3,625
172	DVN	Devon Energy Corp	2,574	75,414,852	29,299
173	DYN	Dynegy Inc	2,284	2,791,855	1,222
174	EA	Electronic Arts Inc	762	31,743,385	41,658
175	EBAY	Ebay Inc	3,979	104,850,257	26,351
176	ECL	Ecolab Inc	4,145	8,808,605	2,125
177	ED	Consolidated Edison Inc	4,773	19,701,896	4,128

Continued on next page

Table A. 1 – continued from previous page

No.	Ticker	Name	Total Days	Total Obs.	Avg. Obs
178	EFX	Equifax Inc	4,773	3,450,634	723
179	EIX	Edison International	4,749	19,736,124	4,156
180	EL	Lauder (Estee) Cos Inc -Cl A	3,021	28,991,298	9,597
181	EMC	Emc Corp/Ma	2,993	42,229,421	14,109
182	EMN	Eastman Chemical Co	4,773	42,185,190	8,838
183	EMR	Emerson Electric Co	4,772	56,856,389	11,915
184	EOG	Eog Resources Inc	4,773	102,799,494	21,538
185	EP	El Paso Corp	2,619	15,861,779	6,056
186	EQR	Equity Residential	4,476	12,912,775	2,885
187	EQT	Eqt Corp	3,021	11,818,568	3,912
188	ERTS	Electronic Arts	523	10,580,749	20,231
189	ES	Eversource Energy	486	358,451	738
190	ESRX	Express Scripts Holding Co	3,021	75,851,829	25,108
191	ESS	Essex Property Trust	252	1,216,569	4,828
192	ESV	Enesco Plc	2,014	50,281,801	24,966
193	ETFC	E Trade Financial Corp	2,018	19,008,319	9,419
194	ETN	Eaton Corp Plc	3,517	52,400,931	14,899
195	ETR	Entergy Corp	4,773	20,717,158	4,340
196	EW	Edwards Lifesciences Corp	1,281	10,310,610	8,049
197	EXC	Exelon Corp	2,076	24,707,645	11,902
198	EXPD	Expeditors Intl Wash Inc	3,018	34,777,719	11,523
199	EXPE	Expedia Inc	2,518	41,987,551	16,675
200	F	Ford Motor Co	4,772	64,923,557	13,605
201	FAST	Fastenal Co	3,018	29,587,313	9,804
202	FB	Facebook Inc	653	120,806,565	185,002
203	FCX	Freeport-Mcmoran Inc	4,773	134,616,749	28,204
204	FDO	Family Dollar Stores	3,372	26,506,467	7,861
205	FDX	Fedex Corp	4,773	93,562,826	19,603
206	FE	Firstenergy Corp	1,281	12,681,246	9,899
207	FFIV	F5 Networks Inc	1,281	66,055,633	51,566
208	FHN	First Horizon National Corp	2,309	4,078,861	1,767
209	FII	Federated Investors Inc	2,445	2,580,507	1,055
210	FIS	Fidelity National Info Svcs	2,186	6,807,954	3,114
211	FISV	Fiserv Inc	4,771	13,209,268	2,769
212	FITB	Fifth Third Bancorp	4,773	32,780,824	6,868
213	FLIR	Flir Systems Inc	3,021	10,763,367	3,563
214	FLR	Fluor Corp	4,773	65,272,105	13,675
215	FLS	Flowserve Corp	2,678	23,199,240	8,663
216	FMC	Fmc Corp	3,020	5,789,604	1,917
217	FOSL	Fossil Group Inc	1,281	23,793,517	18,574
218	FOXA	Twenty-First Century Fox Inc	380	8,018,565	21,101
219	FRX	Forest Laboratories -Cl A	3,419	22,172,792	6,485
220	FSLR	First Solar Inc	1,999	128,268,943	64,167
221	FTI	Fmc Technologies Inc	3,021	15,181,400	5,025
222	FTR	Frontier Communications Corp	2,322	3,242,314	1,396
223	GAS	Agl Resources Inc	1,281	466,540	364
224	GCI	Gannett Co	1,281	18,266,680	14,260
225	GD	General Dynamics Corp	3,880	61,124,716	15,754
226	GE	General Electric Co	4,773	73,907,739	15,485
227	GENZ	Genzyme Corp	2,341	30,145,292	12,877
228	GILD	Gilead Sciences Inc	3,021	113,680,954	37,630

Continued on next page

Table A. 1 – continued from previous page

No.	Ticker	Name	Total Days	Total Obs.	Avg. Obs
229	GIS	General Mills Inc	4,773	31,295,954	6,557
230	GLW	Corning Inc	4,681	49,559,720	10,587
231	GM	General Motors Co	4,392	92,866,623	21,144
232	GMCR	Keurig Green Mountain Inc	252	42,979,162	170,552
233	GME	Gamestop Corp	3,021	59,846,237	19,810
234	GNW	Genworth Financial Inc	2,660	27,426,988	10,311
235	GOOG	Google Inc	1,006	339,121,124	337,099
236	GPC	Genuine Parts Co	4,772	4,838,313	1,014
237	GPS	Gap Inc	4,772	58,176,618	12,191
238	GR	Goodrich Corp	4,163	11,860,263	2,849
239	GRMN	Garmin Ltd	1,281	25,576,769	19,966
240	GS	Goldman Sachs Group Inc	3,322	117,217,684	35,285
241	GT	Goodyear Tire & Rubber Co	4,264	17,070,533	4,003
242	GWW	Grainger (W W) Inc	4,773	20,121,242	4,216
243	HAL	Halliburton Co	4,772	122,598,095	25,691
244	HANS	Hansen'S Natural	531	7,330,435	13,805
245	HAR	Harman International Inds	3,021	23,268,390	7,702
246	HAS	Hasbro Inc	1,281	10,928,502	8,531
247	HBAN	Huntington Bancshares	4,771	6,719,810	1,408
248	HCBK	Hudson City Bancorp Inc	3,018	4,040,312	1,339
249	HCN	Health Care Reit Inc	2,310	9,844,636	4,262
250	HCP	Hcp Inc	2,999	6,190,824	2,064
251	HD	Home Depot Inc	4,773	97,064,504	20,336
252	HES	Hess Corp	1,281	59,275,558	46,273
253	HIG	Hartford Financial Services	3,033	44,786,748	14,766
254	HNZ	Heinz (H J) Corp Ii	885	5,877,207	6,641
255	HOG	Harley-Davidson Inc	2,111	50,577,239	23,959
256	HON	Honeywell International Inc	4,773	78,866,454	16,523
257	HOT	Starwood Hotels&Resorts Wrld	4,343	60,709,328	13,979
258	HP	Helmerich & Payne	1,281	28,821,634	22,499
259	HPQ	Hewlett-Packard Co	1,281	64,243,681	50,151
260	HRB	Block H & R Inc	3,033	18,099,940	5,968
261	HRL	Hormel Foods Corp	3,021	2,938,931	973
262	HRS	Harris Corp	3,021	9,432,223	3,122
263	HSP	Hospira Inc	2,823	5,804,957	2,056
264	HST	Host Hotels & Resorts Inc	2,194	7,625,993	3,476
265	HSY	Hershey Co	4,773	24,241,897	5,079
266	HUM	Humana Inc	3,033	48,969,000	16,145
267	IBM	Intl Business Machines Corp	4,751	135,207,617	28,459
268	ICE	Intercontinental Exchange	2,290	48,551,205	21,201
269	IFF	Intl Flavors & Fragrances	4,773	5,175,064	1,084
270	IGT	Intl Game Technology	3,218	22,377,337	6,954
271	INTC	Intel Corp	4,767	81,367,662	17,069
272	INTU	Intuit Inc	4,773	52,530,736	11,006
273	IP	Intl Paper Co	4,773	68,142,823	14,277
274	IPG	Interpublic Group Of Cos	4,443	9,763,945	2,198
275	IR	Ingersoll-Rand Plc	1,281	32,834,984	25,632
276	IRM	Iron Mountain Inc	3,021	7,801,713	2,582
277	ISRG	Intuitive Surgical Inc	2,988	147,352,910	49,315
278	ITT	Itt Corp	3,236	9,660,576	2,985
279	ITW	Illinois Tool Works	4,773	45,003,680	9,429

Continued on next page

Table A. 1 – continued from previous page

No.	Ticker	Name	Total Days	Total Obs.	Avg. Obs
280	IVZ	Invesco Ltd	1,914	12,200,184	6,374
281	JAVA	Sun Microsystems Inc	612	3,135,250	5,123
282	JBL	Jabil Circuit Inc	3,463	34,418,592	9,939
283	JCI	Johnson Controls Inc	4,773	42,747,334	8,956
284	JCP	Penney (J C) Co	4,500	78,669,605	17,482
285	JDSU	Jds Uniphase Corp	1,023	19,648,451	19,207
286	JEC	Jacobs Engineering Group Inc	3,021	34,611,724	11,457
287	JNJ	Johnson & Johnson	4,773	69,885,471	14,642
288	JNPR	Juniper Networks Inc	2,999	61,534,392	20,518
289	JNS	Janus Capital Group Inc	2,241	5,379,185	2,400
290	JOY	Joy Global Inc	520	25,629,991	49,288
291	JOYG	Joy Global Inc.	513	20,974,184	40,885
292	JPM	Jpmorgan Chase & Co	4,652	153,618,937	33,022
293	JWN	Nordstrom Inc	3,916	52,731,924	13,466
294	K	Kellogg Co	2,769	18,766,730	6,777
295	KBH	Kb Home	3,507	25,278,565	7,208
296	KEY	Keycorp	4,773	21,033,876	4,407
297	KFT	Kraft Foods	720	12,972,240	18,017
298	KG	King Pharmaceuticals Inc	2,320	4,287,607	1,848
299	KIM	Kimco Realty Corp	3,021	5,312,249	1,758
300	KLAC	Kla-Tencor Corp	4,773	80,748,794	16,918
301	KMB	Kimberly-Clark Corp	3,285	27,150,861	8,265
302	KMI	Kinder Morgan Inc	2,594	15,401,881	5,938
303	KMX	Carmax Inc	1,281	25,353,778	19,792
304	KO	Coca-Cola Co	4,773	76,851,496	16,101
305	KORS	Michael Kors Holdings Ltd	759	51,098,837	67,324
306	KR	Kroger Co	3,284	20,964,973	6,384
307	KRFT	Kraft Foods Group Inc	565	9,797,922	17,341
308	KSS	Kohl'S Corp	4,773	67,675,822	14,179
309	KSU	Kansas City Southern	1,281	14,165,655	11,058
310	L	Loews Corp	2,741	4,567,262	1,666
311	LB	L Brands Inc	273	8,427,001	30,868
312	LEG	Leggett & Platt Inc	4,773	6,287,627	1,317
313	LEN	Lennar Corp	3,021	75,564,802	25,013
314	LH	Laboratory Cp Of Amer Hldgs	3,021	15,297,553	5,064
315	LIFE	Life Technologies Corp	1,300	6,150,910	4,731
316	LLL	L-3 Communications Hldgs Inc	3,021	31,221,717	10,335
317	LLTC	Linear Technology Corp	4,773	65,764,302	13,778
318	LLY	Lilly (Eli) & Co	4,773	62,219,002	13,036
319	LM	Legg Mason Inc	3,021	45,911,520	15,197
320	LMT	Lockheed Martin Corp	1,281	33,270,268	25,972
321	LNC	Lincoln National Corp	4,773	42,407,749	8,885
322	LO	Lorillard Inc	1,653	26,959,802	16,310
323	LOW	Lowe'S Companies Inc	1,281	40,949,554	31,967
324	LRCX	Lam Research Corp	1,281	42,543,870	33,211
325	LSI	Lsi Corp	4,264	10,726,570	2,516
326	LTD	L Brands	1,008	28,822,624	28,594
327	LUK	Leucadia National Corp	2,741	10,860,265	3,962
328	LUV	Southwest Airlines	4,772	21,382,190	4,481
329	LVL	Level 3 Communications Inc	252	8,506,096	33,754
330	LXK	Lexmark Intl Inc -Cl A	3,305	37,106,935	11,228

Continued on next page

Table A. 1 – continued from previous page

No.	Ticker	Name	Total Days	Total Obs.	Avg. Obs
331	LYB	Lyondellbasell Industries Nv	1,059	27,990,409	26,431
332	M	Macy'S Inc	1,912	61,872,384	32,360
333	MA	Mastercard Inc	2,161	156,626,422	72,479
334	MAC	Macerich Co	1,281	3,032,333	2,367
335	MAR	Marriott Intl Inc	4,773	40,354,797	8,455
336	MAS	Masco Corp	4,773	20,417,826	4,278
337	MAT	Mattel Inc	1,326	22,300,578	16,818
338	MBI	Mbia Inc	3,278	17,497,835	5,338
339	MCD	Mcdonald'S Corp	4,773	83,550,716	17,505
340	MCHP	Microchip Technology Inc	3,021	32,288,384	10,688
341	MCK	Mckesson Corp	4,773	44,966,558	9,421
342	MCO	Moody'S Corp	3,581	44,791,845	12,508
343	MDLZ	Mondelez International Inc	564	16,313,958	28,925
344	MDP	Meredith Corp	2,908	1,769,920	609
345	MDT	Medtronic Plc	4,773	69,682,725	14,599
346	MEE	Massey Energy Co	743	21,903,381	29,480
347	MET	Metlife Inc	3,694	79,061,045	21,403
348	MFE	Mcafee Inc	550	3,400,964	6,184
349	MHFI	Mcgraw Hill Financial	413	4,153,387	10,057
350	MHK	Mohawk Industries Inc	1,281	11,954,254	9,332
351	MHP	Mcgraw Hill Financial	869	10,118,380	11,644
352	MHS	Medco Health Solutions Inc	2,171	20,799,739	9,581
353	MI	Marshall & Ilsley Corp	2,367	3,020,940	1,276
354	MIL	Millipore Corp	3,648	4,790,818	1,313
355	MJN	Mead Johnson Nutrition Co	1,281	10,765,610	8,404
356	MKC	Mccormick & Co Inc	3,021	2,419,481	801
357	MLM	Martin Marietta Materials	252	3,353,467	13,307
358	MMC	Marsh & Mclennan Cos	4,773	21,006,605	4,401
359	MMI	Motorola Mobility Hldgs Inc	349	2,023,052	5,797
360	MMM	3M Co	3,284	70,306,652	21,409
361	MNK	Mallinckrodt Plc	380	6,282,888	16,534
362	MNST	Monster Beverage Corp	750	31,476,583	41,969
363	MO	Altria Group Inc	3,285	43,173,251	13,143
364	MOLX	Molex Inc	3,452	4,049,674	1,173
365	MON	Monsanto Co	3,021	77,467,605	25,643
366	MOS	Mosaic Co	1,281	60,598,430	47,306
367	MRK	Merck & Co	3,285	65,779,370	20,024
368	MRO	Marathon Oil Corp	4,773	72,794,320	15,251
369	MS	Morgan Stanley	2,257	73,374,889	32,510
370	MSFT	Microsoft Corp	4,773	116,985,094	24,510
371	MSI	Motorola Solutions Inc	1,004	19,653,578	19,575
372	MTB	M & T Bank Corp	3,021	17,000,446	5,627
373	MU	Micron Technology Inc	4,773	81,384,044	17,051
374	MUR	Murphy Oil Corp	3,021	43,192,205	14,297
375	MWD	Morgan Stanley	2,167	15,633,316	7,214
376	MWV	Meadwestvaco Corp	3,211	5,052,181	1,573
377	MWW	Monster Worldwide Inc	784	5,678,401	7,243
378	MYL	Mylan Nv	2,789	28,044,366	10,055
379	NAVI	Navient Corp	170	303,513	1,785
380	NBL	Noble Energy Inc	3,021	50,838,897	16,828
381	NBR	Nabors Industries Ltd	2,306	50,562,416	21,926

Continued on next page

Table A. 1 – continued from previous page

No.	Ticker	Name	Total Days	Total Obs.	Avg. Obs
382	NDAQ	Nasdaq Omx Group Inc	2,440	32,532,923	13,333
383	NE	Noble Corp Plc	1,281	62,056,856	48,444
384	NEE	Nextera Energy Inc	1,140	19,358,930	16,982
385	NEM	Newmont Mining Corp	4,772	120,494,821	25,250
386	NFLX	Netflix Inc	1,281	282,853,266	220,807
387	NFX	Newfield Exploration Co	1,281	26,784,098	20,909
388	NI	Nisource Inc	4,507	6,859,627	1,522
389	NKE	Nike Inc	4,773	91,910,325	19,256
390	NLSN	Nielsen Holdings Nv	984	1,175,363	1,194
391	NOC	Northrop Grumman Corp	1,281	21,054,186	16,436
392	NOV	National Oilwell Varco Inc	2,470	94,246,543	38,156
393	NOVL	Novell Inc	3,847	3,570,509	928
394	NRG	Nrg Energy Inc	1,281	18,699,119	14,597
395	NSC	Norfolk Southern Corp	2,769	57,721,029	20,845
396	NSM	National Semiconductor Corp	3,951	27,185,966	6,881
397	NTAP	Netapp Inc	4,457	92,017,599	20,646
398	NTRS	Northern Trust Corp	4,768	21,848,086	4,582
399	NU	Northeast Utilities	1,281	694,583	542
400	NUE	Nucor Corp	1,281	58,334,655	45,538
401	NVDA	Nvidia Corp	3,883	63,024,442	16,231
402	NVLS	Novellus Systems Inc	1,772	33,998,310	19,186
403	NWL	Newell Rubbermaid Inc	4,443	16,979,243	3,822
404	NYT	New York Times Co -Cl A	3,326	3,969,173	1,193
405	NYX	Nyse Euronext	1,525	31,325,332	20,541
406	ODP	Office Depot Inc	2,885	6,335,973	2,196
407	OI	Owens-Illinois Inc	3,021	28,095,762	9,300
408	OKE	Oneok Inc	1,281	7,000,958	5,465
409	OMC	Omnicom Group	4,773	32,144,741	6,735
410	ORCL	Oracle Corp	4,772	107,302,279	22,486
411	ORLY	O'Reilly Automotive Inc	1,281	8,259,594	6,448
412	OXY	Occidental Petroleum Corp	4,773	104,220,012	21,835
413	PAYX	Paychex Inc	4,773	39,037,929	8,179
414	PBCT	People'S United Finl Inc	2,187	3,214,913	1,470
415	PBG	Pepsi Bottling Group Inc	2,210	1,588,023	719
416	PBI	Pitney Bowes Inc	4,773	16,179,765	3,390
417	PCAR	Paccar Inc	4,441	55,095,941	12,406
418	PCG	Pg&E Corp	4,773	8,648,668	1,812
419	PCL	Plum Creek Timber Co Inc	3,021	28,203,790	9,336
420	PCLN	Priceline Group Inc	1,920	199,660,629	103,990
421	PCP	Precision Castparts Corp	2,891	39,370,512	13,618
422	PCS	Metropcs Communications Inc	859	5,210,240	6,065
423	PDCO	Patterson Companies Inc	3,018	10,218,122	3,386
424	PEG	Public Service Entrp Grp Inc	4,773	9,652,298	2,022
425	PEP	Pepsico Inc	1,281	39,561,576	30,883
426	PETM	Petsmart Inc	1,281	11,381,740	8,885
427	PFE	Pfizer Inc	1,281	52,316,257	40,840
428	PFG	Principal Financial Grp Inc	1,281	13,444,813	10,496
429	PG	Procter & Gamble Co	4,773	78,182,094	16,380
430	PGR	Progressive Corp-Ohio	4,773	20,132,366	4,218
431	PH	Parker-Hannifin Corp	4,773	27,526,198	5,767
432	PHM	Pultegroup Inc	1,281	29,613,394	23,117

Continued on next page

Table A. 1 – continued from previous page

No.	Ticker	Name	Total Days	Total Obs.	Avg. Obs
433	PKI	Perkinelmer Inc	1,281	1,335,386	1,042
434	PLD	Prologis Inc	1,740	5,697,639	3,275
435	PLL	Pall Corp	4,755	5,394,790	1,135
436	PM	Philip Morris International	1,704	48,481,653	28,452
437	PNC	Pnc Financial Svcs Group Inc	4,773	65,574,535	13,739
438	PNR	Pentair Plc	1,281	2,808,964	2,193
439	PNW	Pinnacle West Capital Corp	4,773	1,572,724	330
440	POM	Pepco Holdings Inc	3,021	1,716,906	568
441	PPG	Ppg Industries Inc	2,769	32,006,491	11,559
442	PPL	Ppl Corp	2,734	9,350,108	3,420
443	PRGO	Perrigo Co Plc	1,281	9,888,848	7,720
444	PRU	Prudential Financial Inc	3,224	70,964,453	22,011
445	PSA	Public Storage	2,589	18,077,856	6,983
446	PSX	Phillips 66	672	27,776,885	41,335
447	PTV	Pactiv Corp	2,771	3,090,960	1,115
448	PVH	Pvh Corp	1,281	15,218,477	11,880
449	PWR	Quanta Services Inc	3,021	22,149,206	7,332
450	PX	Praxair Inc	4,773	23,111,176	4,842
451	PXD	Pioneer Natural Resources Co	3,021	67,386,872	22,306
452	Q	Qwest Communication Intl Inc	2,829	3,436,094	1,215
453	QCOM	Qualcomm Inc	4,544	104,107,218	22,911
454	QEP	Qep Resources Inc	1,134	5,278,315	4,655
455	QLGC	Qlogic Corp	2,538	24,122,067	9,504
456	R	Ryder System Inc	1,595	8,543,744	5,357
457	RAI	Reynolds American Inc	2,624	29,198,708	11,128
458	RCL	Royal Caribbean Cruises Ltd	252	8,071,292	32,029
459	RDC	Rowan Companies Plc	4,679	47,694,582	10,193
460	REGN	Regeneron Pharmaceuticals	1,278	72,878,860	57,026
461	RF	Regions Financial Corp	3,189	13,828,084	4,336
462	RHI	Robert Half Intl Inc	4,773	5,268,584	1,104
463	RHT	Red Hat Inc	1,281	38,774,075	30,269
464	RIG	Transocean Ltd	1,281	57,582,672	44,951
465	RL	Ralph Lauren Corp	3,021	48,423,358	16,029
466	ROK	Rockwell Automation	4,769	16,299,814	3,418
467	ROP	Roper Industries Inc/De	1,281	4,785,123	3,735
468	ROST	Ross Stores Inc	1,281	30,941,464	24,154
469	RRC	Range Resources Corp	2,645	55,547,931	21,001
470	RRD	Donnelley (R R) & Sons Co	2,132	5,491,110	2,576
471	RSG	Republic Services Inc	3,021	3,540,504	1,172
472	RTN	Raytheon Co	1,281	34,496,373	26,929
473	S	Sprint Corp	4,300	21,089,076	4,904
474	SAI	Sunamerica Inc	959	2,282,813	2,380
475	SBUX	Starbucks Corp	4,773	83,598,697	17,515
476	SCG	Scana Corp	2,768	1,472,447	532
477	SCHW	Schwab (Charles) Corp	2,274	22,523,440	9,905
478	SE	Spectra Energy Corp	2,015	17,256,152	8,564
479	SEE	Sealed Air Corp	4,770	15,679,353	3,287
480	SHLD	Sears Holdings Corp	697	20,479,150	29,382
481	SHW	Sherwin-Williams Co	4,773	34,600,963	7,249
482	SIAL	Sigma-Aldrich Corp	4,768	10,507,807	2,204
483	SII	Smith International Inc	984	12,931,422	13,142

Continued on next page

Table A. 1 – continued from previous page

No.	Ticker	Name	Total Days	Total Obs.	Avg. Obs
484	SJM	Smucker (Jm) Co	3,021	7,162,303	2,371
485	SLB	Schlumberger Ltd	4,773	129,767,507	27,188
486	SLE	Sara Lee Corp.	651	2,083,590	3,201
487	SNA	Snap-On Inc	4,772	5,835,145	1,223
488	SNDK	Sandisk Corp	1,281	91,454,230	71,393
489	SNI	Scripps Networks Interactive	1,601	3,753,348	2,344
490	SO	Southern Co	4,773	36,054,219	7,554
491	SPG	Simon Property Group Inc	4,292	50,731,931	11,820
492	SPLS	Staples Inc	4,773	27,434,774	5,748
493	SRCL	Stericycle Inc	3,019	8,480,275	2,809
494	SRE	Sempra Energy	4,149	9,458,914	2,280
495	STI	Suntrust Banks Inc	4,773	50,935,653	10,672
496	STJ	St Jude Medical Inc	4,545	26,527,600	5,837
497	STR	Questar Corp	901	6,433,197	7,140
498	STT	State Street Corp	4,773	58,659,316	12,290
499	STX	Seagate Technology Plc	1,281	72,804,039	56,834
500	STZ	Constellation Brands	3,021	18,454,843	6,109
501	SUN	Sunoco Inc	4,211	48,456,702	11,507
502	SVU	Supervalu Inc	4,101	6,860,443	1,673
503	SWK	Stanley Black & Decker Inc	4,773	30,299,593	6,348
504	SWN	Southwestern Energy Co	1,281	58,123,656	45,374
505	SWY	Safeway Inc	4,057	29,943,630	7,381
506	SYK	Stryker Corp	4,382	35,574,696	8,118
507	SYMC	Symantec Corp	3,021	34,063,407	11,276
508	SYU	Sysco Corp	2,704	20,064,162	7,420
509	T	At&T Inc	1,281	58,945,475	46,015
510	TAP	Molson Coors Brewing Co	3,484	21,162,037	6,074
511	TDC	Teradata Corp	1,281	9,764,923	7,623
512	TE	Teco Energy Inc	4,721	4,430,926	939
513	TEG	Integrus Energy Group Inc	1,981	1,790,989	904
514	TEL	Te Connectivity Ltd	1,281	3,426,678	2,675
515	TER	Teradyne Inc	3,548	22,119,232	6,234
516	TGT	Target Corp	3,749	86,448,250	23,059
517	THC	Tenet Healthcare Corp	4,767	27,131,420	5,692
518	TIE	Titanium Metals Corp	1,299	14,676,333	11,298
519	TIF	Tiffany & Co	4,773	67,949,176	14,236
520	TJX	Tjx Companies Inc	1,281	21,189,205	16,541
521	TLAB	Tellabs Inc	4,012	13,226,175	3,297
522	TMK	Torchmark Corp	4,773	5,161,156	1,081
523	TMO	Thermo Fisher Scientific Inc	4,444	14,964,779	3,367
524	TRIP	Tripadvisor Inc	758	42,647,493	56,263
525	TROW	Price (T. Rowe) Group	4,770	20,060,257	4,206
526	TRV	Travelers Cos Inc	1,978	20,662,553	10,446
527	TSCO	Tractor Supply Co	1,281	11,070,053	8,642
528	TSN	Tyson Foods Inc -Cl A	3,021	22,417,004	7,420
529	TSO	Tesoro Corp	3,021	76,558,098	25,342
530	TSS	Total System Services Inc	3,021	2,979,338	986
531	TWC	Time Warner Cable Inc	1,972	19,533,934	9,906
532	TWX	Time Warner Inc	4,085	53,282,409	13,043
533	TXN	Texas Instruments Inc	4,773	74,487,832	15,606
534	TXT	Textron Inc	4,759	40,228,669	8,453

Continued on next page

Table A. 1 – continued from previous page

No.	Ticker	Name	Total Days	Total Obs.	Avg. Obs
535	TYC	Tyco International Plc	1,281	23,253,461	18,153
536	UA	Under Armour Inc	1,281	58,853,171	45,943
537	UHS	Universal Health Svcs Inc	1,281	3,221,775	2,515
538	UNH	Unitedhealth Group Inc	4,254	68,412,694	16,082
539	UNM	Unum Group	4,773	16,415,227	3,439
540	UNP	Union Pacific Corp	4,773	82,911,142	17,371
541	UPS	United Parcel Service Inc	3,741	63,994,237	17,106
542	URBN	Urban Outfitters Inc	1,281	39,769,267	31,045
543	URI	United Rentals Inc	1,281	39,169,170	30,577
544	USB	U S Bancorp	4,376	71,345,602	16,304
545	UTX	United Technologies Corp	4,773	91,285,927	19,125
546	V	Visa Inc	1,281	71,903,040	56,130
547	VAR	Varian Medical Systems Inc	3,021	12,696,687	4,203
548	VFC	Vf Corp	4,444	20,748,710	4,669
549	VLO	Valero Energy Corp	3,021	111,599,427	36,941
550	VMC	Vulcan Materials Co	4,142	37,894,007	9,149
551	VNO	Vornado Realty Trust	3,021	21,100,217	6,985
552	VRSN	Verisign Inc	3,021	46,978,130	15,551
553	VRTX	Vertex Pharmaceuticals Inc	1,281	39,124,413	30,542
554	VTR	Ventas Inc	1,935	7,662,678	3,960
555	VZ	Verizon Communications Inc	3,647	96,670,205	26,507
556	WAT	Waters Corp	4,735	19,022,439	4,017
557	WDC	Western Digital Corp	3,021	65,744,917	21,763
558	WEC	Wisconsin Energy Corp	3,021	1,770,663	586
559	WFC	Wells Fargo & Co	4,065	94,027,770	23,131
560	WFM	Whole Foods Market Inc	920	60,728,536	66,009
561	WFMI	Whole Foods Market	362	12,241,414	33,816
562	WFR	Memc Electronic Materials Inc.	518	6,807,599	13,142
563	WHR	Whirlpool Corp	4,768	77,720,185	16,300
564	WIN	Windstream Holdings Inc	2,131	4,390,382	2,060
565	WLP	Wellpoint Health Netwrks Inc	1,262	50,880,852	40,318
566	WM	Waste Management Inc	3,826	32,415,622	8,472
567	WMB	Williams Cos Inc	4,771	68,072,877	14,268
568	WMT	Wal-Mart Stores Inc	4,773	86,443,694	18,111
569	WPX	Wpx Energy Inc	557	2,004,637	3,599
570	WU	Western Union Co	2,078	13,385,839	6,442
571	WY	Weyerhaeuser Co	3,204	28,012,317	8,743
572	WYN	Wyndham Worldwide Corp	2,121	20,946,288	9,876
573	WYNN	Wynn Resorts Ltd	2,998	130,340,043	43,476
574	X	United States Steel Corp	4,642	97,663,961	21,039
575	XEC	Cimarex Energy Co	252	5,859,807	23,253
576	XEL	Xcel Energy Inc	2,769	2,014,712	728
577	XL	Xl Group Plc	4,415	25,391,855	5,751
578	XLNX	Xilinx Inc	4,773	72,849,000	15,263
579	XOM	Exxon Mobil Corp	3,772	98,886,949	26,216
580	XRAY	Dentsply Internatl Inc	3,019	4,856,728	1,609
581	XRX	Xerox Corp	4,773	20,404,005	4,275
582	XTO	Xto Energy Inc	1,384	18,697,631	13,510
583	XYL	Xylem Inc	796	1,021,658	1,283
584	YHOO	Yahoo Inc	4,350	115,767,911	26,613
585	YUM	Yum Brands Inc	4,333	58,046,698	13,396

Continued on next page

Table A. 1 – continued from previous page

No.	Ticker	Name	Total Days	Total Obs.	Avg. Obs
586	ZION	Zions Bancorporation	4,414	34,934,046	7,914
587	ZMH	Zimmer Holdings Inc	1,281	10,486,882	8,186
588	ZTS	Zoetis Inc	477	7,489,223	15,701

A.2 Selected Sector Index Sample List

Table A. 2: Select Sector Index Components and Holdings

No.	Ticker	Company Name	Index Weight
XLB Materials			
1	ALB	Albemarle Corp	2.13%
2	APD	Air Products & Chemicals Inc	4.56%
3	AVY	Avery Dennison Corp	1.31%
4	BLL	Ball Corp	2.28%
5	CF	CF Industries Holdings	1.23%
6	DD	E. I. du Pont de Nemours and Company	12.10%
7	DOW	Dow Chemical	12.33%
8	ECL	Ecolab Inc	5.70%
9	EMN	Eastman Chemical Co	2.10%
10	FCX	Freeport-McMoRan Inc	3.18%
11	FMC	FMC Corp	1.75%
12	IFF	Intl Flavors & Fragrances	1.88%
13	IP	Intl Paper Co	3.69%
14	LYB	LyondellBasell Industries N.V.	4.49%
15	MLM	Martin Marietta Materials	2.43%
16	MON	Monsanto Co.	8.79%
17	MOS	Mosaic Co	1.83%
18	NEM	Newmont Mining Corp	3.24%
19	NUE	Nucor Corp	3.38%
20	PPG	PPG Industries Inc	4.69%
21	PX	Praxair Inc	5.86%
22	SEE	Sealed Air Corp	1.52%
23	SHW	Sherwin-Williams Co	4.43%
24	VMC	Vulcan Materials Co	2.79%
25	WRK	WestRock Co	2.31%
XLE Energy			
1	APA	Apache Corp	1.54%
2	APC	Anadarko Petroleum Corp	2.71%
3	BHI	Baker Hughes Inc	2.00%
4	CHK	Chesapeake Energy Corp	0.43%
5	COG	Cabot Oil & Gas A	0.95%
6	COP	ConocoPhillips	4.63%
7	CVX	Chevron Corp	15.51%
8	CXO	Concho Resources Inc	1.49%
9	DVN	Devon Energy Corp	1.71%
10	EOG	EOG Resources	4.30%
11	EQT	EQT Corporation	0.88%
12	FTI	TechnipFMC Ltd	1.23%
13	HAL	Halliburton Co	3.32%
14	HES	Hess Corp	1.02%
15	HP	Helmerich & Payne Inc	0.62%
16	KMI	Kinder Morgan Inc	3.17%
17	MPC	Marathon Petroleum Corp.	2.03%
18	MRO	Marathon Oil Corp	1.09%
19	MUR	Murphy Oil Corp	0.41%

Continued on next page

Table A. 2 – continued from previous page

No.	Ticker	Company Name	Index Weight
20	NBL	Noble Energy Inc	1.18%
21	NFX	Newfield Exploration Co	0.61%
22	NOV	National Oilwell Varco Inc	1.18%
23	OKE	ONEOK Inc	0.96%
24	OXY	Occidental Petroleum	3.71%
25	PSX	Phillips 66	2.64%
26	PXD	Pioneer Natural Resources	2.47%
27	RIG	Transocean Ltd	0.44%
28	RRC	Range Resources Corp	0.49%
29	SLB	Schlumberger Ltd	8.26%
30	TSO	Tesoro Corp	0.76%
31	VLO	Valero Energy Corp	2.27%
32	WMB	The Williams Companies Inc	1.91%
33	XEC	Cimarex Energy Co	0.91%
34	XOM	Exxon Mobil Corp	23.16%
XLF Financial			
1	AFL	AFLAC Inc	1.01%
2	AIG	American Intl Group Inc	1.99%
3	AIZ	Assurant Inc	0.18%
4	AJG	Gallagher Arthur J. & Co	0.35%
5	ALL	Allstate Corp	1.03%
6	AMG	Affiliated Managers Grp	0.31%
7	AMP	Ameriprise Financial Inc	0.69%
8	AON	Aon plc	1.09%
9	AXP	American Express Co	2.05%
10	BAC	Bank of America Corp	8.07%
11	BBT	BB&T Corp	1.24%
12	BEN	Franklin Resources Inc	0.50%
13	BK	The Bank of New York Mellon Corp	1.69%
14	BLK	BlackRock Inc	1.61%
15	BRKB	Berkshire Hathaway B	10.95%
16	C	Citigroup Inc	5.74%
17	CB	Chubb Limited	2.21%
18	CBOE	CBOE Holdings Inc	0.26%
19	CFG	Citizens Financial Group Inc	0.61%
20	CINF	Cincinnati Financial Corp	0.37%
21	CMA	Comerica Inc (MI)	0.41%
22	CME	CME Group Inc A	1.39%
23	COF	Capital One Financial	1.41%
24	DFS	Discover Financial Services	0.89%
25	ETFC	E*TRADE Financial Corp	0.33%
26	FITB	Fifth Third Bancorp (OH)	0.65%
27	GS	Goldman Sachs Group Inc	2.93%
28	HBAN	Huntington Bancshares (OH)	0.49%
29	HIG	Hartford Finl Services Group	0.62%
30	ICE	Intercontinental Exchange Inc	1.24%
31	IVZ	Invesco Ltd	0.42%
32	JPM	JP Morgan Chase & Co	10.70%
33	KEY	KeyCorp	0.64%
34	L	Loews Corp	0.45%

Continued on next page

Table A. 2 – continued from previous page

No.	Ticker	Company Name	Index Weight
35	LNC	Lincoln National Corp	0.51%
36	LUK	Leucadia National Corp (NY)	0.29%
37	MCO	Moody's Corp	0.65%
38	MET	Metlife Inc	1.96%
39	MMC	Marsh & McLennan Companies	1.31%
40	MS	Morgan Stanley	2.08%
41	MTB	M&T Bank Corp	0.82%
42	NAVI	Navient Corp	0.15%
43	NDAQ	Nasdaq Inc	0.28%
44	NTRS	Northern Trust Corp (IL)	0.64%
45	PBCT	People's United Financial Inc	0.21%
46	PFJ	Principal Financial Group	0.58%
47	PGR	Progressive Corp	0.79%
48	PNC	PNC Finl Services Group	2.00%
49	PRU	Prudential Financial Inc	1.58%
50	RF	Regions Financial Corp	0.60%
51	RJF	Raymond James Financial Inc	0.33%
52	SCHW	Schwab Charles Corp	1.67%
53	SPGI	S&P Global Inc	1.17%
54	STI	SunTrust Banks Inc (GA)	0.94%
55	STT	State Street Corp	0.98%
56	SYF	Synchrony Financial	0.89%
57	TMK	Torchmark Corp	0.29%
58	TROW	T Rowe Price Group Inc	0.58%
59	TRV	Travelers Cos Inc	1.18%
60	UNM	Unum Group	0.37%
61	USB	US Bancorp	2.82%
62	WFC	Wells Fargo & Co	8.60%
63	WLTW	Willis Towers Watson PLC	0.58%
64	XL	XL Group Ltd	0.36%
65	ZION	Zions Bancorp (UT)	0.29%
XLI Industrials			
1	AAL	American Airlines Group Inc.	0.98%
2	ALK	Alaska Air Group Inc	0.52%
3	ALLE	Allegion plc	0.33%
4	AME	AMETEK Inc	0.58%
5	ARNC	Arconic Inc	0.54%
6	AYI	Acuity Brands Inc	0.35%
7	BA	Boeing Co	4.97%
8	CAT	Caterpillar Inc	2.78%
9	CHRW	CH Robinson Worldwide Inc	0.51%
10	CMI	Cummins Inc	2.01%
11	COL	Rockwell Collins	0.78%
12	CSX	CSX Corporation	2.48%
13	CTAS	Cintas Corp	0.61%
14	DAL	Delta Air Lines	1.55%
15	DE	Deere & Co	1.69%
16	DOV	Dover Corp	0.71%
17	EFX	Equifax Inc	1.05%
18	EMR	Emerson Electric Co	1.92%

Continued on next page

Table A. 2 – continued from previous page

No.	Ticker	Company Name	Index Weight
19	ETN	Eaton Corp plc	1.94%
20	EXPD	Expeditors Intl of WA Inc	0.48%
21	FAST	Fastenal Co	0.71%
22	FBHS	Fortune Brands Home & Security Inc	0.44%
23	FDX	FedEx Corp	2.43%
24	FLR	Fluor Corp	0.50%
25	FLS	Flowserve Corp	0.29%
26	FTV	Fortive Corp	0.96%
27	GD	General Dynamics	2.72%
28	GE	General Electric Co	9.14%
29	GWW	Grainger W.W. Inc	0.78%
30	HON	Honeywell Intl Inc	4.68%
31	IR	Ingersoll-Rand Plc	1.00%
32	ITW	Illinois Tool Works Inc	2.05%
33	JBHT	Hunt J.B. Transport Services	0.38%
34	JCI	Johnson Controls International plc	1.82%
35	JEC	Jacobs Engineering Group Inc	0.31%
36	KSU	Kansas City Southern Inc	0.43%
37	LLL	L3 Technologies, Inc	0.60%
38	LMT	Lockheed Martin	3.33%
39	LUV	Southwest Airlines Co	1.70%
40	MAS	Masco Corp	0.56%
41	MMM	3M Co	5.49%
42	NLSN	Nielsen Holdings plc	0.66%
43	NOC	Northrop Grumman Corp	2.10%
44	NSC	Norfolk Southern Corp	1.85%
45	PCAR	PACCAR Inc	1.29%
46	PH	Parker-Hannifin Corp	1.27%
47	PNR	Pentair PLC	0.49%
48	PWR	Quanta Services Inc	0.25%
49	R	Ryder System Inc	0.34%
50	RHI	Robert Half Intl Inc	0.39%
51	ROK	Rockwell Automation Inc	1.22%
52	ROP	Roper Technologies, Inc	1.00%
53	RSG	Republic Services Inc	0.68%
54	RTN	Raytheon Co	2.27%
55	SNA	Snap On Inc	0.45%
56	SRCL	Stericycle Inc	0.33%
57	SWK	Stanley Black & Decker	0.94%
58	TDG	TransDigm Group	0.53%
59	TXT	Textron Inc	0.75%
60	UAL	United Continental Holding Inc	0.95%
61	UNP	Union Pacific Corp	4.46%
62	UPS	United Parcel Service Inc B	3.53%
63	URI	United Rentals Inc	0.48%
64	UTX	United Technologies Corp	4.13%
65	VRSK	Verisk Analytics Inc	0.58%
66	WM	Waste Management Inc	1.53%
67	XYL	Xylem Inc	0.43%

XLK Information Technology

Continued on next page

Table A. 2 – continued from previous page

No.	Ticker	Company Name	Index Weight
1	AAPL	Apple Inc.	15.19%
2	ACN	Accenture plc A	1.48%
3	ADBE	Adobe Systems Inc	1.31%
4	ADI	Analog Devices Inc	0.61%
5	ADP	Automatic Data Processing	0.93%
6	ADS	Alliance Data Systems Corp	0.30%
7	ADSK	Autodesk Inc	0.35%
8	AKAM	Akamai Technologies Inc	0.22%
9	AMAT	Applied Materials Inc	0.85%
10	AMD	Advanced Micro Devices	0.25%
11	APH	Amphenol Corp A	0.44%
12	ATVI	Activision Blizzard Inc	0.71%
13	AVGO	Broadcom Limited	1.77%
14	CA	CA Inc	0.21%
15	CRM	Salesforce.com	1.14%
16	CSCO	Cisco Systems Inc	3.34%
17	CSRA	CSRA Inc	0.10%
18	CTL	CenturyLink Inc	0.28%
19	CTSH	Cognizant Tech Solutions Corp	0.72%
20	CTXS	Citrix Systems Inc	0.27%
21	DXC	DXC Technology Company	0.41%
22	EA	Electronic Arts	0.56%
23	EBAY	eBay Inc.	0.70%
24	FB	Facebook Inc A	6.72%
25	FFIV	F5 Networks Inc	0.19%
26	FIS	Fidelity National Information	0.54%
27	FISV	Fiserv Inc	0.51%
28	FLIR	FLIR Systems Inc	0.11%
29	GLW	Corning Inc	0.51%
30	GOOG	Alphabet Inc C	4.94%
31	GOOGL	Alphabet Inc A	5.07%
32	GPN	Global Payments Inc	0.25%
33	HPE	Hewlett Packard Enterprise Co	0.61%
34	HPQ	HP Inc	0.62%
35	HRS	Harris Corp	0.29%
36	IBM	Intl Business Machines Corp	3.00%
37	INTC	Intel Corp	3.46%
38	INTU	Intuit Inc	0.58%
39	IT	Gartner Inc	0.20%
40	JNPR	Juniper Networks Inc	0.23%
41	KLAC	KLA-Tencor Corporation	0.32%
42	LRCX	Lam Research Corp	0.44%
43	LVLT	Level 3 Communications	0.36%
44	MA	Mastercard Inc A	2.14%
45	MCHP	Microchip Technology Inc	0.34%
46	MSFT	Microsoft Corp	10.18%
47	MSI	Motorola Solutions Inc	0.29%
48	MU	Micron Technology Inc	0.61%
49	NTAP	NetApp Inc	0.24%
50	NVDA	Nvidia Corp	1.21%
51	ORCL	Oracle Corp	2.69%

Continued on next page

Table A. 2 – continued from previous page

No.	Ticker	Company Name	Index Weight
52	PAYX	Paychex Inc	0.39%
53	PYPL	PayPal Holdings Inc.	0.98%
54	QCOM	QUALCOMM Inc	1.69%
55	QRVO	Qorvo, Inc	0.19%
56	RHT	Red Hat Inc	0.32%
57	SNPS	Synopsys Inc	0.22%
58	STX	Seagate Technology	0.30%
59	SWKS	Skyworks Solutions Inc	0.39%
60	SYMC	Symantec Corp	0.39%
61	T	AT&T Inc	5.12%
62	TDC	Teradata Corp	0.09%
63	TEL	TE Connectivity Ltd.	0.54%
64	TSS	Total System Services Inc	0.19%
65	TXN	Texas Instruments Inc	1.62%
66	V	Visa Inc A	3.34%
67	VRSN	VeriSign Inc	0.17%
68	VZ	Verizon Communications Inc	3.32%
69	WDC	Western Digital Corp	0.50%
70	WU	Western Union Co	0.20%
71	XLNX	Xilinx Inc	0.30%
72	XRX	Xerox Corp	0.13%
73	YHOO	Yahoo Inc	0.83%
XLP Consumer Staples			
1	ADM	Archer-Daniels-Midland Co	1.49%
2	BFB	Brown-Forman Corp B	0.50%
3	CAG	Conagra Brands, Inc	1.02%
4	CHD	Church & Dwight Co	0.67%
5	CL	Colgate-Palmolive Co	3.55%
6	CLX	Clorox Co	1.07%
7	COST	Costco Wholesale Corp	4.04%
8	COTY	Coty Inc.	0.43%
9	CPB	Campbell Soup Co	0.75%
10	CVS	CVS Health Corporation	4.30%
11	DPS	Dr Pepper Snapple Group	1.11%
12	EL	Estee Lauder Cos. A	1.14%
13	GIS	General Mills Inc	1.91%
14	HRL	Hormel Foods Corp	0.69%
15	HSY	Hershey Foods Corp	0.93%
16	K	Kellogg Co	1.11%
17	KHC	The Kraft Heinz Company	2.88%
18	KMB	Kimberly-Clark	2.61%
19	KO	Coca-Cola Co	8.70%
20	KR	Kroger Co	1.62%
21	MDLZ	Mondelez International Inc	3.35%
22	MJN	Mead Johnson Nutrition Co	0.95%
23	MKC	McCormick & Co	0.73%
24	MNST	Monster Beverage Corp New	1.13%
25	MO	Altria Group Inc	6.67%
26	PEP	PepsiCo Inc	4.84%
27	PG	Procter & Gamble	12.16%

Continued on next page

Table A. 2 – continued from previous page

No.	Ticker	Company Name	Index Weight
28	PM	Philip Morris International	9.29%
29	RAI	Reynolds American Inc	3.10%
30	SJM	Smucker J.M. Co	0.96%
31	STZ	Constellation Brands Inc A	2.22%
32	SYZ	Sysco Corp	1.49%
33	TAP	Molson Coors Brewing Co B	1.18%
34	TSN	Tyson Foods Inc A	1.23%
35	WBA	Walgreens Boots Alliance Inc	3.90%
36	WFM	Whole Foods Market Inc	0.56%
37	WMT	Wal-Mart Stores	5.71%
XLU Utilities			
1	AEE	Ameren Corp	2.07%
2	AEP	American Electric Power	5.15%
3	AES	AES Corp	1.14%
4	AWK	American Water Works Co Inc	2.15%
5	CMS	CMS Energy Corp	1.99%
6	CNP	Centerpoint Energy Inc	1.87%
7	D	Dominion Resources Inc	7.53%
8	DTE	DTE Energy Co	2.88%
9	DUK	Duke Energy Corp	8.22%
10	ED	Consolidated Edison Inc	3.71%
11	EIX	Edison Intl	4.06%
12	ES	Eversource Energy	2.89%
13	ETR	Entergy Corp	2.10%
14	EXC	Exelon Corp	5.14%
15	FE	FirstEnergy Corp	2.16%
16	LNT	Alliant Energy Corp	1.40%
17	NEE	NextEra Energy Inc	9.39%
18	NI	Nisource Inc	1.20%
19	NRG	NRG Energy	0.91%
20	PCG	PG&E Corporation	5.29%
21	PEG	Public Service Enterprise Grp	3.46%
22	PNW	Pinnacle West Capital (AZ)	1.47%
23	PPL	PPL Corp	3.94%
24	SCG	SCANA Corp	1.47%
25	SO	Southern Co	7.69%
26	SRE	Sempra Energy	4.24%
27	WEC	WEC Energy Group Inc	2.97%
28	XEL	Xcel Energy Inc	3.53%
XLV Health Care			
1	A	Agilent Technologies Inc	0.60%
2	ABBV	AbbVie Inc.	3.67%
3	ABC	AmerisourceBergen Corp	0.53%
4	ABT	Abbott Laboratories	2.27%
5	AET	Aetna Inc	1.63%
6	AGN	Allergan plc	2.98%
7	ALXN	Alexion Pharmaceuticals Inc	0.92%
8	AMGN	Amgen Inc	4.23%
9	ANTM	Anthem Inc	1.58%
10	BAX	Baxter Intl Inc	0.92%

Continued on next page

Table A. 2 – continued from previous page

No.	Ticker	Company Name	Index Weight
11	BCR	Bard C.R. Inc	0.68%
12	BDX	Becton Dickinson & Co	1.42%
13	BIIB	Biogen Inc	2.11%
14	BMY	Bristol-Myers Squibb	3.16%
15	BSX	Boston Scientific Corp	1.19%
16	CAH	Cardinal Health Inc	0.91%
17	CELG	Celgene Corp	3.42%
18	CERN	Cerner Corp	0.61%
19	CI	Cigna Corporation	1.41%
20	CNC	Centene Corp	0.43%
21	COO	Cooper Companies Inc	0.34%
22	DGX	Quest Diagnostics	0.49%
23	DHR	Danaher Corp	1.85%
24	DVA	DaVita Inc	0.37%
25	ESRX	Express Scripts Holding Co.	1.49%
26	EVHC	Envision Healthcare Corp	0.27%
27	EW	Edwards Lifesciences Corp	0.70%
28	GILD	Gilead Sciences Inc	3.08%
29	HCA	HCA Holdings Inc	0.90%
30	HOLX	Hologic Inc	0.42%
31	HSIC	Schein Henry Inc	0.47%
32	HUM	Humana Inc	1.19%
33	IDXX	IDEXX Laboratories Inc	0.52%
34	ILMN	Illumina Inc	0.87%
35	INCY	Incyte Corp	0.86%
36	ISRG	Intuitive Surgical Inc	0.99%
37	JNJ	Johnson & Johnson	11.99%
38	LH	Lab Corp of America Hldgs	0.52%
39	LLY	Lilly Eli & Co	2.94%
40	MCK	McKesson Corp	1.12%
41	MDT	Medtronic plc	3.91%
42	MNK	Mallinckrodt plc	0.16%
43	MRK	Merck & Co Inc	6.18%
44	MTD	Mettler-Toledo Intl	0.44%
45	MYL	Mylan NV	0.63%
46	PDCO	Patterson Cos Inc	0.13%
47	PFE	Pfizer Inc	7.21%
48	PKI	PerkinElmer Inc	0.22%
49	PRGO	Perrigo Company plc	0.34%
50	REGN	Regeneron Pharmaceuticals Inc	1.02%
51	SYK	Stryker Corp	1.46%
52	TMO	Thermo Fisher Scientific	2.11%
53	UHS	Universal Health Services B	0.39%
54	UNH	Unitedhealth Group Inc	5.68%
55	VAR	Varian Medical Systems Inc	0.30%
56	VRTX	Vertex Pharmaceuticals Inc	1.00%
57	WAT	Waters Corp	0.44%
58	XRAY	Dentsply Sirona Inc.	0.50%
59	ZBH	Zimmer Biomet Holdings Inc	0.87%
60	ZTS	Zoetis Inc	0.92%

Continued on next page

Table A. 2 – continued from previous page

No.	Ticker	Company Name	Index Weight
XLY Consumer Discretionary			
1	AAP	Advance Auto Parts Inc	0.42%
2	AMZN	Amazon.com Inc	14.53%
3	AN	AutoNation Inc	0.10%
4	AZO	AutoZone Inc	0.81%
5	BBBY	Bed Bath & Beyond Inc	0.23%
6	BBY	Best Buy Co Inc	0.52%
7	BWA	Borgwarner Inc	0.31%
8	CBS	CBS Corp B	1.04%
9	CCL	Carnival Corp	0.99%
10	CHTR	Charter Communications Inc A	2.88%
11	CMCSA	Comcast Corp A	7.13%
12	CMG	Chipotle Mexican Grill Inc.	0.53%
13	COH	Coach Inc	0.45%
14	DG	Dollar General Corp	0.70%
15	DHI	Horton D.R. Inc	0.46%
16	DIS	Walt Disney Co	6.63%
17	DISCA	Discovery Communications Inc A	0.18%
18	DISCK	Discovery Communications Inc C	0.25%
19	DISH	DISH Network Corp A	0.58%
20	DLPH	Delphi Automotive PLC	0.82%
21	DLTR	Dollar Tree Inc	0.73%
22	DRI	Darden Restaurants Inc	0.42%
23	EXPE	Expedia	0.61%
24	F	Ford Motor Co	1.77%
25	FL	Foot Locker Inc	0.38%
26	FOX	Twenty-First Century Fox Inc B	0.61%
27	FOXA	Twenty-First Century Fox Inc A	1.33%
28	GM	General Motors Company	1.87%
29	GPC	Genuine Parts Co	0.54%
30	GPS	Gap Inc	0.20%
31	GRMN	Garmin Ltd	0.23%
32	GT	Goodyear Tire & Rubber Co	0.35%
33	HAS	Hasbro Inc	0.44%
34	HBI	Hanesbrands Inc	0.31%
35	HD	Home Depot Inc	7.21%
36	HOG	Harley-Davidson Inc	0.43%
37	HRB	Block H & R Inc	0.19%
38	IPG	Interpublic Group Cos	0.39%
39	JWN	Nordstrom Inc	0.20%
40	KMX	Carmax Inc	0.43%
41	KORS	Michael Kors Holdings Ltd	0.24%
42	KSS	Kohl's Corp	0.27%
43	LB	L Brands Inc	0.42%
44	LEG	Leggett & Platt	0.27%
45	LEN	Lennar Corp A	0.42%
46	LKQ	LKQ Corp	0.35%
47	LOW	Lowe's Cos Inc	2.85%
48	M	Macy's Inc	0.35%
49	MAR	Marriott Intl A	1.17%
50	MAT	Mattel Inc	0.35%

Continued on next page

Table A. 2 – continued from previous page

No.	Ticker	Company Name	Index Weight
51	MCD	McDonald's Corp	4.31%
52	MHK	Mohawk Industries Inc	0.58%
53	NFLX	NetFlix Inc	2.49%
54	NKE	NIKE Inc B	2.94%
55	NWL	Newell Brands Inc	0.89%
56	NWS	News Corp B	0.06%
57	NWSA	News Corp A	0.19%
58	OMC	Omnicom Group	0.81%
59	ORLY	O'Reilly Automotive	0.94%
60	PCLN	The Priceline Group Inc	3.49%
61	PHM	Pulte Group Inc	0.27%
62	PVH	PVH Corp	0.33%
63	RCL	Royal Caribbean Cruises Ltd	0.66%
64	RL	Ralph Lauren Corp A	0.18%
65	ROST	Ross Stores Inc	0.99%
66	SBUX	Starbucks Corp	3.42%
67	SIG	Signet Jewelers Ltd	0.19%
68	SNI	Scripps Networks Interactive A	0.30%
69	SPLS	Staples Inc	0.26%
70	TGNA	TEGNA Inc	0.22%
71	TGT	Target Corp	1.18%
72	TIF	Tiffany & Co	0.40%
73	TJX	TJX Cos Inc	2.00%
74	TRIP	TripAdvisor Inc. A	0.19%
75	TSCO	Tractor Supply Co	0.36%
76	TWX	Time Warner Inc	3.07%
77	UA	Under Armour Inc-C	0.14%
78	UAA	Under Armour Inc A	0.15%
79	ULTA	Ulta Beauty, Inc	0.66%
80	VFC	VF Corp	0.72%
81	VIAB	Viacom Inc B	0.64%
82	WHR	Whirlpool Corp	0.50%
83	WYN	Wyndham Worldwide Corp	0.36%
84	WYNN	Wynn Resorts Ltd	0.37%
85	YUM	Yum! Brands Inc	0.87%

A.3 MATLAB Codes for Data Extraction

This appendix lists all of the MATLAB codes I used in data processing.

```
clear;clc;
repository='F:\Data\ZipTrades';
addpath(pwd);
```

```

addpath(repository);

datatype='quotes';
datatype='trades';
uname{1,1}='dubs.trth1@durham.ac.uk';
uname{2,1}='dubs.trth2@durham.ac.uk';
uname{3,1}='dubs.trth3@durham.ac.uk';

cd(repository);
dn=dir;
dn(1:2)=[];
nfiles=length(dn);
k=1;
%strip out the zip repository files from the others
for i=1:nfiles
    fname=dn(i).name;
    nmbytes=dn(i).bytes./1e9;
    fzip=strfind(fname, '.zip');%find Repositoryfiles
    if ~isempty(fzip)
        repfile{k,1}=fname;
        repfilesize(k,1)=nmbytes;
        k=k+1;
    end
end
%find multipart files and put them together
nrep=length(repfile);
for i=1:nrep
    rname=repfile{i,1};
    for ii=1:length(uname)
        rname=strrep(rname, [uname{ii,1}, '-'], '');
    end
    ii=strfind(rname, '-');
    if length(ii)>1
        FileNames{i,1}=rname(1:ii(1)-1);
        FileCodes{i,1}=rname(ii(1)+1:ii(2)-1);
    else
        FileNames{i,1}=rname(1:ii(1)-1); %#ok<SAGROW>
        FileCodes{i,1}=rname(ii(1)+1:end-4);
    end
end
for i=1:length(FileNames)
    df=FileNames{i,1};
    df(end-9:end)=[];
    RICNames{i,1}=df;
end
[uRIC]=unique(RICNames);
for i=1:length(uRIC)
    ric=uRIC{i,1};
    ii=find(strcmp(ric, RICNames));
    fn=repfile(ii);
    fc=FileCodes(ii);
    [ufc, IA, IC]=unique(fc);
    jj=1;
    for j=1:length(ufc)
        list=find(strcmp(fc, ufc{j,1}));
        for k=1:length(list)

```

```

        repfile=fn{list(k),1};
        FNAMES=unzip(repfile);FNAMES=FNAMES';
        for kk=1:length(FNAMES)
            FLIST{jj,1}=FNAMES{kk,1};
            jj=jj+1;
        end
    end
end
%File counter
jjj=1;
%Run the loop over the main code list.
for j=1:length(FLIST)
    datfile=gunzip(char(FLIST{j,1}));
    A=importdata(char(datfile));
    %this is a switch block between trades and quotes.
    switch lower(datatype)
        case 'trades'
            if ~iscell(A)
                RIC=unique(A.textdata(2:end,1));
                days=A.textdata(2:end,2);
                times=A.textdata(2:end,3);
                bt=find(strcmp(times,''));
                times(bt)=[];
                days(bt)=[];
                GMT=A.textdata(2:end,3);
                dv=datenum([char(days), repmat(' ',length(days),1), char(times)]);
                'dd-mmm-yyyy HH:MM:SS.FFF');
                dataM(jjj).dv=dv;
                dataM(jjj).RIC=RIC;
                dataM(jjj).Open=A.data(:,1);
                dataM(jjj).High=A.data(:,2);
                dataM(jjj).Low=A.data(:,3);
                dataM(jjj).Last=A.data(:,4);
                dataM(jjj).Volume=A.data(:,5);
                dataM(jjj).APrice=A.data(:,6);
                dataM(jjj).VWAP=A.data(:,7);
                dataM(jjj).NTrades=A.data(:,8);
                jjj=jjj+1;
                emptyfiles(j,1)=0;
                disp(['Completed: ',char(datfile)]);
            elseif iscell(A)
                disp([num2str(j), ' is empty.']);
                emptyfiles(j,1)=1;
            end
        case 'quotes'
            if ~iscell(A)
                RIC=unique(A.textdata(2:end,1));
                days=A.textdata(2:end,2);
                times=A.textdata(2:end,3);
                bt=find(strcmp(times,''));
                times(bt)=[];
                days(bt)=[];
                GMT=A.textdata(2:end,3);
                dv=datenum([char(days), repmat(' ',length(days),1), char(times)]);
                'dd-mmm-yyyy HH:MM:SS.FFF');
                dataM(jjj).dv=dv;
                dataM(jjj).RIC=RIC;

```

```

        dataM(jjj).OpenBids=A.data(:,1);
        dataM(jjj).HighBids=A.data(:,2);
        dataM(jjj).LowBids=A.data(:,3);
        dataM(jjj).CloseBids=A.data(:,4);
        dataM(jjj).NBids=A.data(:,5);
        dataM(jjj).OpenAsks=A.data(:,6);
        dataM(jjj).HighAsks=A.data(:,7);
        dataM(jjj).LowAsks=A.data(:,8);
        dataM(jjj).CloseAsks=A.data(:,9);
        dataM(jjj).NAsks=A.data(:,10);
        jjj=jjj+1;
        emptyfiles(j,1)=0;
        disp(['Completed: ',char(datfile)]);
    elseif iscell(A)
        disp([num2str(j), ' is empty.']);
        emptyfiles(j,1)=1;
    end
end
end
fname=[ric, '_data'];
save(fname, 'dataM', '-v7.3');
disp(['Completed Archiving of: ', num2str(i)])
end

```

```

function [K,T,Type,ticker] = parseTicker(RIC)
RIC = strrep(RIC, '.U', '');
Strike = RIC(end-4:end);RIC(end-4:end)=[];
year = RIC(end-1:end);RIC(end-1:end)=[];
day = RIC(end-1:end);RIC(end-1:end)=[];
month = RIC(end);RIC(end)=[];
ticker = RIC;
tf = strcmp(lower(month),month);
    if tf
        K = str2double(Strike)/10;
    else
        K = str2double(Strike)/100;
    end
CallMonths = 'abcdefghijkl';
mnth = strfind(CallMonths,lower(month));
    if isempty(mnth)
        PutMonths = 'mnopqrstuvwxyz';
        mnth = strfind(PutMonths,lower(month));
        Type = 0;
    else
        Type = 1;
    end
T = datenum(2000+str2double(year),mnth,str2double(day));

```

A.4 Proofs for Chapter 5

A.4.1 Proof for Lemma 5.1

Before moving on, let me first declare some background definitions that will be used in deriving the Lemma:

A M-matrix: $\mathbf{M}^{n,n} := \{\mathbf{M} = (q_{ij}) \in \mathbb{R}^{n,n} | q_{ij} \leq 0, i \neq j\}$;

B Identity Matrix: $\mathbf{I}_n := \{\mathbf{I} = (i_{ij}) \in \mathbb{R}^{n,n} | i_{ij} = 1, 1 \leq i, j \leq n\}$;

C Group Inverse: Let \mathbf{X} be a square \mathbf{M} matrix. The index of \mathbf{X} is the least non-negative integer k such that $\text{rank}(\mathbf{X}^{k+1}) = \text{rank}(\mathbf{X}^k)$. The Drazin inverse of \mathbf{X} is the unique matrix \mathbf{X}^D which satisfies:

$$\mathbf{X}^{k+1}\mathbf{X}^D = \mathbf{X}^k, \quad \mathbf{X}^D\mathbf{X}\mathbf{X}^D = \mathbf{X}^D, \quad \mathbf{X}\mathbf{X}^D = \mathbf{X}^D\mathbf{X}$$

The group inverse of matrix \mathbf{X} is the Drazin inverse of \mathbf{X} with index $k = 0, 1$, denoted by $\mathbf{X}^\#$. Equivalently, $\mathbf{X}^\#$ satisfies all the properties with \mathbf{X}^D .

Proof. C^2 -Continuity of Recovered Discount Factor. The derivatives of the Perron root have been studied in the statistics and linear algebra to a certain extent before. My derivation of Equation 5.12 and Equation 5.13 utilises the results *Theorem 2* and *Theorem 3* of [Deutsch and Neumann \[1985\]](#), however, in turn these borrow heavily from [Vahrenkamp \[1976\]](#), [Ben-Israel and Greville \[2003\]](#), [Berman and Plemmons \[1979\]](#) and [Seneta \[1973\]](#). The use of the group and Drazin inverse to provide the approximation of the second derivative is from [Robert \[1968\]](#) and this in turn relies on an application of *Bolzano-Weirestrass theorem*. The derivations for $\nabla P(\mathbf{x})$ and $\nabla^2 P(\mathbf{x})$ are less well-established.

Recall that $\mathcal{R} : \mathcal{N}^{n,n} \rightarrow \mathbb{R}_+$ and we define $\mathbf{x} = \text{vec}[\mathbf{Q}]$ and the inverse transformation $\text{mat}[\mathbf{x}] = \mathbf{Q}$ for a column-wise ‘vec’ and ‘mat’ operators respectively. Thus, the first and the diagonal of the second-order partial derivatives of the Perron root $\mathcal{R}(\mathbf{P})$ with respect to the the ij th entries of \mathbf{P} can be expressed in terms of the ∇ and ∇^2 in the constraint functions as follows

$$\nabla P(\mathbf{x}) = \text{vec} \left[\frac{\partial \mathcal{R}(\mathbf{P})}{\partial ij} \right], \quad \text{and} \quad \nabla^2 P(\mathbf{x}) = \text{diag} \left[\text{vec} \left[\frac{\partial^2 \mathcal{R}(\mathbf{P})}{\partial^2 ij} \right] \right]$$

If we define $\mathbf{M} = \mathcal{R}(\mathbf{Q})\mathbf{I} - \mathbf{Q}$ as a singular and irreducible M-matrix, where \mathbf{I} is a $M \times M$ identity matrix. Recall that $\delta = \mathcal{R}(\mathbf{Q})$, then the first and second-order derivatives of the recovered discount factor can be expressed by:

$$\left[\frac{\partial \delta}{\partial q_{ij}} \right] = \text{vec} \left[\frac{\partial \mathcal{R}(\mathbf{Q})}{\partial ij} \right] = \text{vec} [(\mathbf{I} - \mathbf{M}\mathbf{M}^\#)'], \quad (10.1)$$

$$\left[\frac{\partial^2 \delta}{\partial^2 q_{ij}} \right] = \text{vec} \left[\frac{\partial^2 \mathcal{R}(\mathbf{Q})}{\partial^2 ij} \right] = 2\text{vec} [(\mathbf{M}^\#)' \circ (\mathbf{I} - \mathbf{M}\mathbf{M}^\#)'] \quad (10.2)$$

where $'$ denotes a transpose of matrix, $\mathbf{M}^\#$ gives the group inverse of \mathbf{M} and \circ is the Hadamard product operator. I now derive Equation (10.1) and (10.2) respectively.

[Deutsch and Neumann \[1985\]](#) and [Vahrenkamp \[1976\]](#) provide partial results for a perturbation theorem for the first derivative $\mathcal{R}(\mathbf{Q})$ and our derivation modifies proof of [Deutsch and Neumann \[1985\]](#) approach with some additional steps to include the ‘mat’ operator and recovery theorem via the ‘vec’ operator to eliminate resorting errors inherent in these approaches, which utilises two of intermediate steps in [Vahrenkamp \[1976\]](#).

The derivation of $\text{vec} \left[\frac{\partial \mathcal{R}(\mathbf{Q})}{\partial_{ij}} \right]$ can be proved by use of *Theorem 3.1* of [Deutsch and Neumann \[1985\]](#). To derive the existence and form of the first derivative of the discount factor, we need to determine a matrix transform of $\mathcal{S}(\mathbf{Q})$, which is a simple eigenvalue of \mathbf{Q} .

Consider a neighbourhood of $\mathbf{Q} \in \mathbb{R}^{n,n}$ such that each $\mathbf{F} \in \mathcal{N}_Q$ has a simple eigenvalue $\mathcal{S}(\mathbf{F})$ and such that if $\mathbf{F} \in \mathcal{N}_Q \cap \mathbb{R}^{n,n}$, then $\mathcal{S}(\mathbf{F}) = \mathcal{R}(\mathbf{F})$. If $\mathcal{V}_R(\mathbf{F})$ be the corresponding right eigenvector of \mathbf{F} such that:

$$\max_{1 \leq i \leq n} |(\mathcal{V}_R(\mathbf{F}))_i| = 1.$$

Then $\mathcal{V}_R(\cdot)$ is analytic as a function of each of the n^2 entries of the elements of \mathcal{N}_Q . Thus the partial derivatives $\partial \mathcal{V}_R(\mathbf{F}) / \partial_{ij}$, $\partial^2 \mathcal{V}_R(\mathbf{F}) / \partial_{ij} \partial_{kl}, \dots$ of $\mathcal{V}_R(\cdot)$ at \mathbf{F} with respect to these entries exist and are well defined. Differentiate both sides of the equality:

$$\mathbf{F} \mathcal{V}_R(\mathbf{F}) = \mathcal{R}(\mathbf{F}) \mathcal{V}_R(\mathbf{F}) \tag{10.3}$$

with respect to the ij th entry of \mathbf{F} yields:

$$\frac{\partial \mathbf{F}}{\partial_{ij}} \mathcal{V}_R(\mathbf{F}) + \mathbf{F} \frac{\partial \mathcal{V}_R(\mathbf{F})}{\partial_{ij}} = \frac{\partial \mathcal{S}(\mathbf{F})}{\partial_{ij}} \mathcal{V}_R(\mathbf{F}) + \mathcal{S}(\mathbf{F}) \frac{\partial \mathcal{V}_R(\mathbf{F})}{\partial_{ij}}. \tag{10.4}$$

Now let $\mathcal{V}_L(\mathbf{F})$ be a left eigenvector of \mathbf{F} such that $(\mathcal{V}_L(\mathbf{F}))' \mathcal{V}_R(\mathbf{F}) = 1$. Let $\partial \mathbf{F} / \partial_{ij} = \mathbf{E}_{ij}$, where \mathbf{E}_{ij} is the n, n matrix whose i, j entry is 1 and other remaining entries are 0. Then $(\mathcal{V}_L(\mathbf{F}))' \mathbf{E}_{ij} \mathcal{V}_R(\mathbf{F}) = (\mathcal{V}_L(\mathbf{F}))'_i (\mathcal{V}_R(\mathbf{F}))_j$.

Premultiplying both sides of Equation (10.4) by $(\mathcal{V}_L(\mathbf{F}))'$ obtain:

$$\frac{\partial \mathcal{S}(\mathbf{F})}{\partial_{ij}} = (\mathcal{V}_L(\mathbf{F}))_i (\mathcal{V}_R(\mathbf{F}))_j \quad (10.5)$$

Recall that \mathbf{M} is a singular and irreducible M-matrix and $\mathbf{M}^\#$ is its group inverse. According to *Perron-Frobenius theory*, there exist positive vectors \mathbf{v}_R and \mathbf{v}_L as the right and left Perron vectors, such that $\mathbf{M}\mathbf{v}_R = 0$ and $\mathbf{v}_L'\mathbf{M} = 0$. $\mathbf{I} - \mathbf{M}\mathbf{M}^\#$ is the projection matrix of the $n \times n$ real matrix onto the null space of \mathbf{M} along the range of \mathbf{M} . Then

$$\mathbf{I} - \mathbf{M}\mathbf{M}^\# = \mathbf{v}_R\mathbf{v}_L' \quad (10.6)$$

Now set $\mathbf{Q} = \mathbf{F}$,

$$\mathcal{V}_R(\mathbf{Q})\mathcal{V}_L'(\mathbf{Q}) = \mathbf{I} - \mathbf{M}\mathbf{M}^\# \Rightarrow \mathcal{V}_L(\mathbf{Q})\mathcal{V}_R(\mathbf{Q}) = (\mathbf{I} - \mathbf{M}\mathbf{M}^\#)'$$

The limit of $(\partial \mathcal{S}(\mathbf{Q}))/\partial_{ij}$ is given by

$$\lim_{t \rightarrow 0} \frac{\mathcal{S}(\mathbf{Q} + t\mathbf{E}_{ij}) - \mathcal{S}(\mathbf{Q})}{t}$$

The *Bolzano-Weirestrass* approach to the derivative relies on $\mathbf{Q} + t\mathbf{E}_{ij} \in \mathcal{N}_Q$ for small t , the limit coincides with the partial derivative of the Perron root at \mathbf{Q} with respect to the ij th entry, which is

$$\lim \frac{\partial \mathcal{S}(\mathbf{Q})}{\partial_{ij}} \rightarrow \frac{\partial \mathcal{R}(\mathbf{Q})}{\partial_{ij}} \equiv \mathcal{V}_L(\mathbf{Q})\mathcal{V}_R(\mathbf{Q}) = (\mathbf{I} - \mathbf{M}\mathbf{M}^\#)'$$

and recall $\mathbf{x} = \text{vec}[\mathbf{Q}]$, by construction we get:

$$\left[\frac{\partial \delta}{\partial q_{ij}} \right] = \text{vec} \left[\frac{\partial \mathcal{R}(\mathbf{Q})}{\partial_{ij}} \right] = \text{vec}[(\mathbf{I} - \mathbf{M}\mathbf{M}^\#)']$$

hence $\mathcal{R}(\mathbf{Q})$ is at least \mathcal{C}^1 continuous w.r.t \mathbf{Q} .

In fact, $(\partial^2 \mathcal{R}(\mathbf{Q}))/\partial_{ij}^2$ is a special case of the more general second-order partial derivative problem $(\partial^2 \mathcal{R}(\mathbf{Q}))/(\partial_{ij}\partial_{lk})$, with $i = k, j = l$ on diagonal as second-order derivatives.

Let $1 \leq i, j \leq n$ and $1 \leq k, l \leq n$, the differentiation of Equation (10.3) on both sides with respect to the (k, l) th entry gives:

$$\begin{aligned} & \mathbf{E}_{ij} \frac{\partial \mathcal{V}_R(\mathbf{F})}{\partial_{kl}} + \mathbf{E}_{kl} \frac{\partial \mathcal{V}_R(\mathbf{F})}{\partial_{ij}} + \mathbf{F} \frac{\partial^2 \mathcal{V}_R(\mathbf{F})}{\partial_{ij}\partial_{kl}} \\ &= \frac{\partial^2 \mathcal{V}_R(\mathbf{F})}{\partial_{ij}\partial_{kl}} \mathcal{V}_R(\mathbf{F}) + (\mathcal{V}_L(\mathbf{F}))_i (\mathcal{V}_R(\mathbf{F}))_j \frac{\partial \mathcal{V}_R(\mathbf{F})}{\partial_{kl}} \\ &+ (\mathcal{V}_L(\mathbf{F}))_k (\mathcal{V}_R(\mathbf{F}))_l \frac{\partial \mathcal{V}_R(\mathbf{F})}{\partial_{ij}} + \mathcal{S}(\mathbf{F}) \frac{\partial^2 \mathcal{V}_R(\mathbf{F})}{\partial_{ij}\partial_{kl}} \end{aligned} \quad (10.7)$$

Premultiplying both sides of Equation (10.7) by $(\mathcal{V}_L(\mathbf{F}))'$ and considering $(\mathcal{V}_L(\mathbf{F}))'\mathbf{F} = \mathcal{S}(\mathbf{F})(\mathcal{V}_L(\mathbf{F}))'$ and $(\mathcal{V}_L(\mathbf{F}))'\mathcal{V}_R(\mathbf{F}) = 1$ yields:

$$\begin{aligned} & \frac{\partial^2 \mathcal{S}(\mathbf{F})}{\partial_{ij}\partial_{lk}} \\ &= (\mathcal{V}_L(\mathbf{F}))_i \left(\left(\frac{\partial \mathcal{V}_R(\mathbf{F})}{\partial_{kl}} \right)_j - (\mathcal{V}_R(\mathbf{F}))_i (\mathcal{V}_L(\mathbf{F}))' \frac{\partial \mathcal{V}_R(\mathbf{F})}{\partial_{kl}} \right) \\ &+ (\mathcal{V}_R(\mathbf{F}))_k \left(\left(\frac{\partial \mathcal{V}_R(\mathbf{F})}{\partial_{ij}} \right)_l - (\mathcal{V}_R(\mathbf{F}))_l (\mathcal{V}_L(\mathbf{F}))' \frac{\partial \mathcal{V}_R(\mathbf{F})}{\partial_{ij}} \right) \end{aligned} \quad (10.8)$$

Noted that the first-order derivative of the eigenvector at \mathbf{F} with respect to its elements is the main element inside the bracket in Equation (10.8). Let

$\tilde{\mathbf{F}} := \mathcal{S}(\mathbf{F})\mathbf{I} - \mathbf{F}$ and let $1 \leq u, v \leq n$. According to Equation (10.5),

$$\tilde{\mathbf{F}} \frac{\partial \mathcal{V}_R(\mathbf{F})}{\partial_{uv}} = \mathbf{E}_{uv} \mathcal{V}_R(\mathbf{F}) - (\mathcal{V}_L(\mathbf{F}))_u (\mathcal{V}_R(\mathbf{F}))_v \mathcal{V}_R(\mathbf{F}) \quad (10.9)$$

Premultiplying Equation (10.9) by the group inverse of $\tilde{\mathbf{F}}$ on both sides and as $\tilde{\mathbf{F}}^\# \mathcal{V}_R(\mathbf{F}) = 0$, we get

$$\tilde{\mathbf{F}} \tilde{\mathbf{F}}^\# \frac{\partial \mathcal{V}_R(\mathbf{F})}{\partial_{uv}} = \tilde{\mathbf{F}} \tilde{\mathbf{F}}^\# \mathbf{E}_{uv} \mathcal{V}_R(\mathbf{F})$$

and we know that $\tilde{\mathbf{F}} \tilde{\mathbf{F}}^\# = \mathbf{I} - (\mathbf{I} - \tilde{\mathbf{F}} \tilde{\mathbf{F}}^\#)$,

$$\frac{\partial \mathcal{V}_R(\mathbf{F})}{\partial_{uv}} - (\mathbf{I} - \tilde{\mathbf{F}} \tilde{\mathbf{F}}^\#) \frac{\partial \mathcal{V}_R(\mathbf{F})}{\partial_{uv}} = \tilde{\mathbf{F}}^\# \mathbf{E}_{uv} \mathcal{V}_R(\mathbf{F}) \quad (10.10)$$

According to Equation (10.5), $\mathcal{V}_R(\mathbf{F})(\mathcal{V}_L(\mathbf{F}))' = \mathbf{I} - \tilde{\mathbf{F}} \tilde{\mathbf{F}}^\#$. Then for the w th components of the vectors on both sides of Equation (10.10), we have the equality that

$$\left(\frac{\partial \mathcal{V}_R(\mathbf{F})}{\partial_{uv}} \right)_v - (\mathcal{V}_R(\mathbf{F}))_w (\mathcal{V}_L(\mathbf{F}))'_w \frac{\partial \mathcal{V}_R(\mathbf{F})}{\partial_{uv}} = (\tilde{\mathbf{F}}^\#)_{wv} (\mathcal{V}_R(\mathbf{F}))_v \quad (10.11)$$

Substituting Equation (10.11) into Equation (10.9), obtain

$$\frac{\partial^2 \mathcal{S}(\mathbf{F})}{\partial_{ij} \partial_{lk}} = (\mathbf{I} - \tilde{\mathbf{F}} \tilde{\mathbf{F}}^\#)_{li} (\tilde{\mathbf{F}}^\#)_{jk} + (\mathbf{I} - \tilde{\mathbf{F}} \tilde{\mathbf{F}}^\#)_{jk} (\tilde{\mathbf{F}}^\#)_{li} \quad (10.12)$$

Lastly, let $\mathbf{F} = \mathbf{Q}$, $\mathcal{S}(\mathbf{F}) = \mathcal{R}(\mathbf{Q})$ and $\tilde{\mathbf{F}} = \mathbf{M}$,

$$\frac{\partial^2 \mathcal{R}(\mathbf{Q})}{\partial_{ij} \partial_{kl}} = (\mathbf{I} - \mathbf{M} \mathbf{M}^\#)_{li} (\mathbf{M}^\#)_{jk} + (\mathbf{I} - \mathbf{M} \mathbf{M}^\#)_{jk} (\mathbf{M}^\#)_{li} \quad (10.13)$$

To get $(\partial^2 \mathcal{R}(\mathbf{Q}))/\partial_{ij}^2$, simply let $k = i$ and $l = j$ and use the element-wise Hadmard product

$$\frac{\partial^2 \mathcal{R}(\mathbf{Q})}{\partial_{ij}^2} = 2(\mathbf{I} - \mathbf{M}\mathbf{M}^\#)_{ji}(\mathbf{M}^\#)_{ji} = 2(\mathbf{M}^\#)' \circ (\mathbf{I} - \mathbf{M}\mathbf{M}^\#)'$$

Reconstructing the \mathbf{Q} into the ‘vec’ form,

$$\begin{bmatrix} \partial^2 \delta \\ \partial^2 q_{ij} \end{bmatrix} = \text{vec} \begin{bmatrix} \partial^2 \mathcal{R}(\mathbf{Q}) \\ \partial_{ij}^2 \end{bmatrix} = 2\text{vec} [(\mathbf{M}^\#)' \circ (\mathbf{I} - \mathbf{M}\mathbf{M}^\#)']$$

hence $\mathcal{R}(\mathbf{Q})$ is at least \mathcal{C}^2 continuous w.r.t \mathbf{Q} .

End of proof. □

Proof. C^1 -Continuity of the Pricing Kernel. To demonstrate the continuity of the pricing kernel we need to first derive the first-order derivative of the Perron vector. We follow the analysis in [Deutsch and Neumann \[1985\]](#). Different from the derivation of the Perron root, the derivations of the first-order of the derivative of the Perron vector vary across different normalizations. Following our notations, let $\delta = \mathcal{R}(\mathbf{Q})$ and $\mathbf{v} = \mathcal{V}(\mathbf{Q})$ be the Perron root and Perron vector of \mathbf{Q} and let \mathbf{z} be an v-vector whose entries are differentiable functions. Thus we have the normalisation of the Perron vector such that $\mathbf{z}'\mathcal{V}(\mathbf{Q}) = 1$. From the standard result that the Perron root and vector are a principal eigenvalue and eigenvector we find the standard identity:

$$\mathbf{Q}\mathcal{V}(\mathbf{Q}) = \mathcal{R}(\mathbf{Q})\mathcal{V}(\mathbf{Q})$$

expanding the terms as a derivative we define

$$\frac{\partial \mathbf{Q}}{\partial_{ij}} \mathcal{V}(\mathbf{Q}) + \mathbf{Q} \frac{\partial \mathcal{V}(\mathbf{Q})}{\partial_{ij}} = \frac{\partial \mathcal{R}(\mathbf{Q})}{\partial_{ij}} \mathcal{V}(\mathbf{Q}) + \mathcal{R}(\mathbf{Q}) \frac{\partial \mathcal{V}(\mathbf{Q})}{\partial_{ij}}$$

setting $\mathbf{M} = \mathcal{R}(\mathbf{Q})\mathbf{I} - \mathbf{Q}$, then

$$\mathbf{M} \frac{\partial \mathcal{V}(\mathbf{Q})}{\partial_{ij}} = \frac{\partial \mathbf{Q}}{\partial_{ij}} \mathcal{V}(\mathbf{Q}) - \frac{\partial \mathcal{R}(\mathbf{Q})}{\partial_{ij}} \mathcal{V}(\mathbf{Q}) \quad (10.14)$$

thus the first derivative of the Perron vector $\mathcal{V}(\mathbf{Q})$ is:

$$\begin{aligned} \frac{\partial \mathcal{V}(\mathbf{Q})}{\partial_{ij}} &= \mathbf{M}^\# \frac{\partial \mathbf{Q}}{\partial_{ij}} \mathcal{V}(\mathbf{Q}) - \frac{\partial \mathcal{R}(\mathbf{Q})}{\partial_{ij}} \mathbf{M}^\# \mathcal{V}(\mathbf{Q}) + \alpha \mathcal{V}(\mathbf{Q}) \\ &= \mathbf{M}^\# \frac{\partial \mathbf{Q}}{\partial_{ij}} \mathcal{V}(\mathbf{Q}) + \alpha \mathcal{V}(\mathbf{Q}) \end{aligned} \quad (10.15)$$

where α is the constant of normalisation. To determine α , premultiplying the above equation by \mathbf{z}' yields:

$$\mathbf{z}' \frac{\partial \mathcal{V}(\mathbf{Q})}{\partial_{ij}} = \mathbf{z}' \mathbf{M}^\# \frac{\partial \mathbf{Q}}{\partial_{ij}} \mathcal{V}(\mathbf{Q}) + \alpha \mathbf{z}' \mathcal{V}(\mathbf{Q}) = \mathbf{z}' \mathbf{M}^\# \frac{\partial \mathbf{Q}}{\partial_{ij}} \mathcal{V}(\mathbf{Q}) + \alpha \quad (10.16)$$

solving for α we get:

$$\alpha = -\mathbf{z}' \mathbf{M}^\# \frac{\partial \mathbf{Q}}{\partial_{ij}} \mathcal{V}(\mathbf{Q}) - \left(\frac{\partial \mathbf{z}}{\partial_i} \right)' \mathcal{V}(\mathbf{Q}) \quad (10.17)$$

By definition, $\mathbf{z}' \mathcal{V}(\mathbf{Q}) = 1$, so

$$\left(\frac{\partial \mathbf{z}}{\partial_{ij}} \right)' \mathcal{V}(\mathbf{Q}) + \mathbf{z}' \frac{\partial \mathcal{V}(\mathbf{Q})}{\partial_{ij}} = 0.$$

Substituting α back into the formula for the first derivative of the Perron vector we obtain:

$$\begin{aligned} \frac{\partial \mathcal{V}(\mathbf{Q})}{\partial_{ij}} &= \mathbf{M}^\# \frac{\partial \mathbf{Q}}{\partial_{ij}} \mathcal{V}(\mathbf{Q}) - \left(\left(\frac{\partial \mathbf{z}}{\partial_i} \right)' \mathcal{V}(\mathbf{Q}) \right) \mathcal{V}(\mathbf{Q}) \\ &\quad - \left(\mathbf{z}' \mathbf{M}^\# \frac{\partial \mathcal{V}(\mathbf{Q})}{\partial_{ij}} \right) \mathcal{V}(\mathbf{Q}) \end{aligned} \quad (10.18)$$

Noted, the first derivative of the Perron vector will be determined by different normalisation, which depends on the choice of \mathbf{z} . However, in most of cases, we can show that $\left(\frac{\partial \mathbf{z}}{\partial_i} \right)' \mathcal{V}(\mathbf{Q}) = 0$, so the formula of the first-order derivative of the Perron vector can be further reduced to:

$$\frac{\partial \mathcal{V}(\mathbf{Q})}{\partial_{ij}} = \mathbf{M}^\# \frac{\partial \mathbf{Q}}{\partial_{ij}} \mathcal{V}(\mathbf{Q}) - \left(\mathbf{z}' \mathbf{M}^\# \frac{\partial \mathcal{V}(\mathbf{Q})}{\partial_{ij}} \right) \mathcal{V}(\mathbf{Q}) \quad (10.19)$$

Note, that for each elements in the Perron vector $\mathcal{V}(\mathbf{Q})$ we can write down the first-order derivative in the form of Equation 10.19. For simplicity, let

$$\mathbf{\Upsilon} := \mathbf{M}^\# \frac{\partial \mathbf{Q}}{\partial_{ij}} \quad \text{and} \quad v := \mathbf{z}' \mathbf{M}^\# \frac{\partial \mathcal{V}(\mathbf{Q})}{\partial_{ij}}.$$

setting $\tilde{\mathbf{v}}_m$ be the m row of $\mathbf{\Upsilon}$, the i th element of the first-order derivative of the Perron vector is:

$$\frac{\partial \mathcal{V}_m(\mathbf{Q})}{\partial_{ij}} = \tilde{\mathbf{v}}_m' \mathcal{V}(\mathbf{Q}) - v \mathcal{V}_m(\mathbf{Q}) \quad (10.20)$$

Recall that the pricing kernel is formed by the normalisation of the inverse of the Perron vector of the state transition matrix about the central (current)

state $\tilde{c} = (M + 1)/2$, hence

$$\text{diag}[\mathbf{D}] := \{d_m = \frac{\dot{d}_m}{\dot{d}_{\tilde{c}}}, 1 \leq m \leq M\}, \quad \text{diag}[\mathbf{D}] = \mathbf{v}^{-1} = \mathcal{V}(\mathbf{Q})^{-1}$$

hence we evaluate

$$d_m = \frac{\mathcal{V}_{\tilde{c}}(\mathbf{Q})}{\mathcal{V}_m(\mathbf{Q})} \quad (10.21)$$

Thus the first-order derivative of the pricing kernel can be derived by the quotient rule such that:

$$\frac{\partial d_m}{\partial_{ij}} = \frac{\mathcal{V}_m(\mathbf{Q}) \frac{\partial \mathcal{V}_{\tilde{c}}(\mathbf{Q})}{\partial_{ij}} - \mathcal{V}_{\tilde{c}}(\mathbf{Q}) \frac{\partial \mathcal{V}_m(\mathbf{Q})}{\partial_{ij}}}{[\mathcal{V}_m(\mathbf{Q})]^2} \quad (10.22)$$

Substituting Equation 10.20 back into Equation 10.22 we have:

$$\frac{\partial d_m}{\partial_{ij}} = \frac{\mathcal{V}_m(\mathbf{Q})(\tilde{\mathbf{v}}_{\tilde{c}}' \mathcal{V}(\mathbf{Q}) - v \mathcal{V}_{\tilde{c}}(\mathbf{Q})) - \mathcal{V}_{\tilde{c}}(\mathbf{Q}) \tilde{\mathbf{v}}_m' \mathcal{V}(\mathbf{Q}) - v \mathcal{V}_m(\mathbf{Q})}{\mathcal{V}_m^2(\mathbf{Q})}$$

Simplification yields the explicit derivative for the pricing kernel:

$$\frac{\partial d_m}{\partial_{ij}} = \frac{\mathcal{V}(\mathbf{Q})(\tilde{\mathbf{v}}_{\tilde{c}}' \mathcal{V}_m(\mathbf{Q}) - \tilde{\mathbf{v}}_m' \mathcal{V}_{\tilde{c}}(\mathbf{Q}))}{\mathcal{V}_m^2(\mathbf{Q})}$$

End of proof. □

A.4.2 Proofs for Unimodality of the State Price Transition Matrix

Proof. Unimodality of the State Price Transition Matrix.

Constraint D.4 impose the unimodality constraint in the optimisation

system. We call a matrix unimodal if for each of its rows and columns the entries change from increasing to decreasing in either direction at most once. In our case, the unimodality constraint imposed on the transition matrix \mathbf{Q} ('mat'[\mathbf{x}]) is formed by row-wise and column-wise inequality conditions separately:

1. Row constraint \mathbf{A}_r : the rows of \mathbf{Q} are unimodal, with the modes lying on the main diagonal of \mathbf{Q} ;
2. Column constraint \mathbf{A}_c : the columns of \mathbf{Q} are unimodal, with the modes lying on the main diagonal of \mathbf{Q} .

I first illustrate the form of the inequality constraint for the rows. Let \mathbf{i} be the index of diagonal of $\mathbf{Q}^{M \times M}$, then we have the conditions such that:

For the diagonal elements:

$$q_{i+k,i} \geq q_{i+k+1,i}, \quad k = 1, \dots, M - i,$$

$$q_{i-k,i} \geq q_{i-k-1,i}, \quad k = 1, \dots, i - 1;$$

For the off-diagonal elements:

$$q_{i,j} \geq \{q_{i-1,j}, q_{i+1,j}, q_{i,j-1}, q_{i,j+1}\}, \quad i > j,$$

$$q_{i,j} \leq \{q_{i-1,j}, q_{i+1,j}, q_{i,j-1}, q_{i,j+1}\}, \quad i < j.$$

which ensures that the largest element in each row is lying on the diagonal, as such $q_{1,1} \geq \{q_{1,2}, q_{1,2}\}$ then $q_{2,2} \geq \{q_{2,3}, q_{2,1}, q_{3,2}, q_{1,2}\}$ to $q_{i,i} \geq$

$\{q_{i,i+1}, q_{i,i-1}, q_{i+1,i}, q_{i-1,i}\}$ to $q_{M,M} \geq \{q_{M-1,M}, q_{M,M-1}\}$, where $\{1 < i < M, 1 < j < M\}$. We could form the constraints for the columns with the same rationale. Formally, the linear constraint imposing on the row and column unimodality is in the form:

For row elements:

$$q_{i,j} > q_{i,j+k}, \quad j > i, \quad \text{and} \quad k \in \{1, M-i\},$$

$$q_{i,j+k} > q_{i,j} \quad j < i, \quad \text{and} \quad k \in \{1, i-1\};$$

For column elements:

$$q_{i,j} > q_{i+k,j}, \quad j > i, \quad \text{and} \quad k \in \{1, M-i\},$$

$$q_{i+k,j} > q_{i,j}, \quad j < i, \quad \text{and} \quad k \in \{1, i-1\}.$$

Recall that I utilise a ‘vec’ form that $\mathbf{x} = \text{vec}[\mathbf{Q}]$ and $\mathbf{Q} = \text{mat}[\mathbf{x}]$. I introduce $\mathbf{A}_r^{M(M-1) \times M}$ and $\mathbf{A}_c^{M(M-1) \times M}$ to impose the row and column uni-modality constraints separately and the final constraint matrix $\mathbf{A}^{2M(M-1) \times M}$ is formed via vertical concatenation of $\mathbf{A}_r^{M(M-1) \times M}$ and $\mathbf{A}_c^{M(M-1) \times M}$ as discussed in the main text.

Thus, the first sub-set of optimisation in my main System 6.10 is:

$$\begin{aligned} &\text{minimize} \quad H(\mathbf{x}) = \frac{1}{2} \|\mathbf{G}\mathbf{x} - \mathbf{s}_0\|^2 \\ &\text{subject to} \quad U(\mathbf{x}) = \mathbf{A}\mathbf{x} - \mathbf{0}_{2M(M-1) \times 1} \leq 0, \quad \text{where} \quad \mathbf{0}_{M \times 1} \leq \mathbf{x} \leq \mathbf{e} \end{aligned}$$

Define \mathbf{z}_1 as the vector of slack variables and the equivalent equality

constrained optimisation problem with the slack-variable formulation is:

$$\begin{aligned}
& \text{minimize} && H(\mathbf{x}) = \frac{1}{2} \|\mathbf{G}\mathbf{x} - \mathbf{s}_0\|^2 \\
& \text{subject to} && U(\mathbf{x}) + \mathbf{z}_1 = \mathbf{A}\mathbf{x} - \mathbf{0}_{2M(M-1) \times 1} + \mathbf{z}_1 = 0 \\
& \text{where} && \mathbf{0}_{M \times 1} \leq \mathbf{x} \leq \mathbf{e}, \quad \mathbf{z}_1 \geq 0
\end{aligned} \tag{10.23}$$

We can solve the numerical solution for system (10.23) by standard Lagrangian method. The Lagrange function for the system (10.23) is:

$$\mathcal{L}_1(\mathbf{x}, \boldsymbol{\lambda}_1) = H(\mathbf{x}) - \boldsymbol{\lambda}'_1(U(\mathbf{x}) + \mathbf{z}_1) \tag{10.24}$$

Let ∇ represents the first-order derivative operator that returns the first-order derivative of the Lagrange function with respect to \mathbf{x} and $\boldsymbol{\lambda}_1$ respectively and $\boldsymbol{\delta}_x$ be the feasible step (corrections) then the optimisation for Equation (10.24) can be re-written as:

$$\nabla \mathcal{L}_1(\mathbf{x}^*, \boldsymbol{\lambda}_1^*) = 0 \tag{10.25}$$

where $\mathbf{x}^* = \mathbf{x} + \boldsymbol{\delta}_x \mathbf{x}$ is the feasible point and $\boldsymbol{\lambda}_1^* = \boldsymbol{\lambda}_1 + \boldsymbol{\delta}_x \boldsymbol{\lambda}_1$ is a stationary point of the Lagrangian function. Let ∇ be the first-order partial derivative operator then Equation (10.25) yields:

$$\begin{aligned}
\nabla_x \mathcal{L}_1 &= \frac{\partial \mathcal{L}_1(\mathbf{x}, \boldsymbol{\lambda}_1)}{\partial \mathbf{x}} = \nabla H(\mathbf{x}) - \boldsymbol{\lambda}'_1 \nabla U(\mathbf{x}) = 0 \\
\nabla_{\lambda} \mathcal{L}_1 &= \frac{\partial \mathcal{L}_1(\mathbf{x}, \boldsymbol{\lambda}_1)}{\partial \boldsymbol{\lambda}_1} = U(\mathbf{x}) + \mathbf{z}_1
\end{aligned} \tag{10.26}$$

The derivations of $\nabla H(\mathbf{x})$ is quite straightforward. As $\nabla H(\mathbf{x})$ is the matrix form of the classic least squares derivative:

$$\nabla H(\mathbf{x}) = \frac{1}{2} \frac{d\|\mathbf{G}\mathbf{x} - \mathbf{s}_0\|^2}{d\mathbf{x}}$$

Taking out the constant, we get:

$$\nabla H(\mathbf{x}) = -\mathbf{G}'\mathbf{s}_0 + (\mathbf{G}'\mathbf{G})\mathbf{x} \quad (10.27)$$

The unimodality constraint function $U(\mathbf{x})$ is a linear function, thus $\nabla U(\mathbf{x})$ is simply:

$$\nabla U(\mathbf{x}) = \mathbf{A} \quad (10.28)$$

Substituting into Equation (10.26) yields:

$$\begin{aligned} \nabla_x \mathcal{L}_1 = 0 : \quad & (\mathbf{G}'\mathbf{G})\mathbf{x} - \mathbf{G}'\mathbf{s}_0 - \mathbf{A}\boldsymbol{\lambda}_1 = 0 \\ \nabla_{\boldsymbol{\lambda}} \mathcal{L}_1 = 0 : \quad & \mathbf{A}\mathbf{x} - \mathbf{0}_{2M(M-1) \times 1} + \mathbf{z}_1 = 0 \end{aligned} \quad (10.29)$$

Rearrange and we have the linear system

$$\begin{pmatrix} \mathbf{G}'\mathbf{G} & -\mathbf{A} \\ -\mathbf{A}' & 0 \end{pmatrix} \begin{pmatrix} \mathbf{x} \\ \boldsymbol{\lambda}_1 \end{pmatrix} = - \begin{pmatrix} \mathbf{G}'\mathbf{s}_0 \\ \mathbf{0}_{2M(M-1) \times 1} + \mathbf{z}_1 \end{pmatrix} \quad (10.30)$$

If the inverse of the Lagrangian matrix exists, such that:

$$\begin{pmatrix} \mathbf{G}'\mathbf{G} & -\mathbf{A} \\ -\mathbf{A}' & 0 \end{pmatrix}^{-1} = \begin{pmatrix} \mathbf{L} & -\mathbf{K} \\ -\mathbf{K}' & \mathbf{U} \end{pmatrix} \quad (10.31)$$

Then we can write down the numerical solution for system (10.30)

$$\begin{aligned}\mathbf{x}^* &= -\mathbf{L}\mathbf{G}'\mathbf{s}_0 + \mathbf{K}(\mathbf{0}_{2M(M-1)\times 1} + \mathbf{z}_1) \\ \boldsymbol{\lambda}_1^* &= \mathbf{K}'\mathbf{G}'\mathbf{s}_0 - \mathbf{U}(\mathbf{0}_{2M(M-1)\times 1} + \mathbf{z}_1)\end{aligned}\tag{10.32}$$

End of proof. □

A.4.3 Proofs for Sub-stochasticity of the State Price Transition Matrix

Proof. Sub-stochasticity of the State Price Transition Matrix.

Constraint E.2 states that the progression of the sum of the risk-neutral state price describes the equivalent risk free asset, such that $\sum_j \mathbf{Q}\mathbf{s}_n \equiv \sum_j \mathbf{s}_{n+1}$, where \mathbf{s}_n denotes the n th column summation of the state price transition matrix \mathbf{S} . Recall that \mathbf{B} is a matrix and \mathbf{b} is a target vector such that the equality constraint $\mathbf{B}\mathbf{x} = \mathbf{b}$, where \mathbf{b} denotes the column summation of the one-period forward shift matrix, such that $\mathbf{b} = \mathbf{1}'\mathbf{s}_{n+1}$ and \mathbf{B} is the column summation of the columns within the vector $\mathbf{x} = \text{vec}[\mathbf{Q}]$ such that $\mathbf{B} = [\mathbf{1}' \otimes \mathbf{s}'_n]$.

Thus, the second subset of the main optimisation System 6.10 is:

$$\begin{aligned}\text{minimize } & H(\mathbf{x}) = \frac{1}{2} \|\mathbf{G}\mathbf{x} - \mathbf{s}_0\|^2 \\ \text{subject to } & B(\mathbf{x}) = \mathbf{B}\mathbf{x} - \mathbf{b}\end{aligned}\tag{10.33}$$

We have the Lagrangian function:

$$\mathcal{L}_2(\mathbf{x}, \boldsymbol{\lambda}_2) = H(\mathbf{x}) - \boldsymbol{\lambda}'_2 B(\mathbf{x}) \quad (10.34)$$

and the stationary point condition yields:

$$\begin{aligned} \nabla_x \mathcal{L}_2 = 0 : \quad & (\mathbf{G}'\mathbf{G})\mathbf{x} - \mathbf{G}'\mathbf{s}_0 - \mathbf{B}\boldsymbol{\lambda}_2 = 0 \\ \nabla_{\boldsymbol{\lambda}} \mathcal{L}_2 = 0 : \quad & \mathbf{B}\mathbf{x} - \mathbf{b} = 0 \end{aligned} \quad (10.35)$$

Rearrange and we have the linear system

$$\begin{pmatrix} \mathbf{G}'\mathbf{G} & -\mathbf{B} \\ -\mathbf{B}' & 0 \end{pmatrix} \begin{pmatrix} \mathbf{x} \\ \boldsymbol{\lambda}_2 \end{pmatrix} = - \begin{pmatrix} \mathbf{G}'\mathbf{s}_0 \\ \mathbf{b} \end{pmatrix} \quad (10.36)$$

Let $\begin{pmatrix} \mathbf{L} & -\mathbf{V} \\ -\mathbf{V}' & \mathbf{U} \end{pmatrix}$ be the inverse of the Lagrangian matrix, then the numerical solution of system (10.36) can be derived:

$$\begin{aligned} \mathbf{x}^* &= -\mathbf{L}\mathbf{G}'\mathbf{s}_0 + \mathbf{V}\mathbf{b} \\ \boldsymbol{\lambda}_2^* &= \mathbf{V}'\mathbf{G}'\mathbf{s}_0 - \mathbf{U}\mathbf{b} \end{aligned} \quad (10.37)$$

End of proof. □

A.4.4 Full Steps of the SQP Process on the Discount Factor Constraint

Following the similar convention in the previous proofs, I provide the full steps of the SQP process in the optimisation system with the constraint on the discount factor D.5 as stated in Equation 6.16 here. The usage of this approach embedded in a quadratic programming set-up has, to our knowledge, never been attempted, hence the precise steps matter for verification purposes as these types of optimisation problems rely heavily on the continuity of the second derivative of the constraint.

The third sub-set of optimisation in the main System 6.10 is:

$$\begin{aligned} \text{minimize} \quad & H(\mathbf{x}) = \frac{1}{2} \|\mathbf{G}\mathbf{x} - \mathbf{s}_0\|^2 \\ \text{subject to} \quad & P(\mathbf{x}) = \mathcal{R}(\text{mat}(\mathbf{x})) - 1 \leq 0 \end{aligned}$$

Define \mathbf{z}_3 as the vector of slack variables and the equivalent equality constrained optimisation problem with the slack-variable formulation is:

$$\begin{aligned} \text{minimize} \quad & H(\mathbf{x}) = \frac{1}{2} \|\mathbf{G}\mathbf{x} - \mathbf{s}_0\|^2 \\ \text{subject to} \quad & P(\mathbf{x}) + \mathbf{z}_3 = \mathcal{R}(\text{mat}(\mathbf{x})) - 1 + \mathbf{z}_3 = 0, \quad \text{where } \mathbf{z}_3 \geq 0 \end{aligned} \quad (10.38)$$

The Lagrange function can be written as:

$$\mathcal{L}_3(\mathbf{x}, \boldsymbol{\lambda}_3) = H(\mathbf{x}) - \boldsymbol{\lambda}_3'(P(\mathbf{x}) + \mathbf{z}_3) \quad (10.39)$$

Let $\boldsymbol{\delta}_x$ be the vectors of feasible step to arriving the feasible point, then Equation (10.39) can be re-written as:

$$\nabla \mathcal{L}_3(\mathbf{x} + \boldsymbol{\delta}_x, \boldsymbol{\lambda}_3 + \boldsymbol{\delta}_x \boldsymbol{\lambda}_3) = 0 \quad (10.40)$$

the Taylor series expansion for Equation(10.40) about \mathbf{x} and $\boldsymbol{\lambda}_3$ gives:

$$\boldsymbol{\nabla} \mathcal{L}_3(\mathbf{x} + \boldsymbol{\delta}_x, \boldsymbol{\lambda}_3 + \boldsymbol{\delta}_x \boldsymbol{\lambda}_3) = \boldsymbol{\nabla} \mathcal{L}_3(\mathbf{x}, \boldsymbol{\lambda}_3) + [\boldsymbol{\nabla}^2 \mathcal{L}_3] \begin{pmatrix} \boldsymbol{\delta}_x \\ \boldsymbol{\delta}_x \boldsymbol{\lambda}_3 \end{pmatrix} + \dots \quad (10.41)$$

where

$$\boldsymbol{\nabla} = \begin{pmatrix} \nabla_x \\ \nabla_\lambda \end{pmatrix}, \quad \text{and} \quad \boldsymbol{\nabla}^2 = \begin{pmatrix} \nabla_x^2 \\ \nabla_\lambda^2 \end{pmatrix}$$

∇ and ∇^2 are the the first and second-order partial derivative operators, such that,

$$\begin{aligned} \nabla_x \mathcal{L}_3 &= \frac{\partial \mathcal{L}_3(\mathbf{x}, \boldsymbol{\lambda}_3)}{\partial \mathbf{x}} = \nabla H(\mathbf{x}) - \boldsymbol{\lambda}'_3 \nabla P(\mathbf{x}) \\ \nabla_x^2 \mathcal{L}_3 &= \frac{\partial^2 \mathcal{L}_3(\mathbf{x}, \boldsymbol{\lambda}_3)}{\partial^2 \mathbf{x}} = \nabla^2 H(\mathbf{x}) - \boldsymbol{\lambda}'_3 \nabla^2 P(\mathbf{x}) \\ \nabla_\lambda \mathcal{L}_3 &= \frac{\partial \mathcal{L}_3(\mathbf{x}, \boldsymbol{\lambda}_3)}{\partial \boldsymbol{\lambda}_3} = -(P(\mathbf{x}) + \mathbf{z}_3) \\ \nabla_\lambda^2 \mathcal{L}_3 &= \frac{\partial^2 \mathcal{L}_3(\mathbf{x}, \boldsymbol{\lambda}_3)}{\partial^2 \boldsymbol{\lambda}_3} = 0 \end{aligned} \quad (10.42)$$

The derivations of $\nabla H(\mathbf{x})$ and $\nabla^2 H(\mathbf{x})$ are quite straightforward. As $\nabla H(\mathbf{x})$ is the matrix form of the classic least squares derivative:

$$\nabla H(\mathbf{x}) = \frac{1}{2} \frac{d \|\mathbf{G}\mathbf{x} - \mathbf{s}_0\|^2}{d\mathbf{x}}$$

Taking out the constant, we get:

$$\nabla H(\mathbf{x}) = -\mathbf{G}'\mathbf{s}_0 + (\mathbf{G}'\mathbf{G})\mathbf{x} \quad \text{and} \quad \nabla^2 H(\mathbf{x}) = \mathbf{G}'\mathbf{G} \quad (10.43)$$

According to the results in Lemma 5.1, the non-linear constraint function on Perron root $P(\mathbf{x})$ are exist and at least \mathcal{C}^1 and \mathcal{C}^2 continuous w.r.t \mathbf{Q} . We

can now give the full expressions for Equation (10.42):

$$\begin{aligned}
\nabla_x \mathcal{L}_3 &= -\mathbf{G}'\mathbf{s}_0 + (\mathbf{G}'\mathbf{G})\mathbf{x} - \lambda_3 \text{vec}[(\mathbf{I} - \mathbf{M}\mathbf{M}^\#)'] \\
\nabla_x^2 \mathcal{L}_3 &= \mathbf{G}'\mathbf{G} - 2\lambda_3 \text{vec}[(\mathbf{M}^\#)' \circ (\mathbf{I} - \mathbf{M}\mathbf{M}^\#)'] \\
\nabla_\lambda \mathcal{L}_3 &= -P(\mathbf{x}) = 1 - \mathcal{R}(\text{mat}[\mathbf{x}]) \\
\nabla_\lambda^2 \mathcal{L}_3 &= 0
\end{aligned} \tag{10.44}$$

Neglecting the higher order terms in Equation (10.41) and we have the iteration

$$[\nabla^2 \mathcal{L}_3] \begin{pmatrix} \delta_{\mathbf{x}\mathbf{x}} \\ \delta_{\mathbf{x}\lambda_3} \end{pmatrix} = -[\nabla \mathcal{L}_3] \tag{10.45}$$

This can be solved by the Newton's method for the stationary point problem to give the corrections $\delta_{\mathbf{x}\mathbf{x}}$ and $\delta_{\mathbf{x}\lambda_3}$. Substituting the expression for $\nabla^2 \mathcal{L}_3$ and $\nabla \mathcal{L}_3$ gives the system:

$$\begin{pmatrix} \mathbf{W}^{(k)} & -\mathbf{J}^{(k)} \\ -\mathbf{J}^{(k)'} & 0 \end{pmatrix} \begin{pmatrix} \delta_{\mathbf{x}\mathbf{x}} \\ \delta_{\mathbf{x}\lambda_3} \end{pmatrix} = \begin{pmatrix} -\mathbf{g}^{(k)} + \mathbf{J}^{(k)}\lambda_3 \\ \mathbf{c}^{(k)} \end{pmatrix} \tag{10.46}$$

where \mathbf{J} and \mathbf{W} are the Jacobian matrix and Hessian matrix of constraint normals evaluated at \mathbf{x} respectively:

$$\begin{aligned}
\mathbf{J}^{(k)} &= \nabla_x \mathcal{L}_3 = -\mathbf{G}'\mathbf{s}_0 + (\mathbf{G}'\mathbf{G})\mathbf{x} - \lambda_3 \text{vec}[(\mathbf{I} - \mathbf{M}\mathbf{M}^\#)'] \\
\mathbf{W}^{(k)} &= \nabla_x^2 \mathcal{L}_3 = \mathbf{G}'\mathbf{G} - 2\lambda_3 \text{vec}[(\mathbf{M}^\#)' \circ (\mathbf{I} - \mathbf{M}\mathbf{M}^\#)']
\end{aligned} \tag{10.47}$$

For the k th iteration, we compute the update $\lambda_3^{(k+1)} = \lambda_3^{(k)} + \delta_{\mathbf{x}\lambda_3}$ and $\delta_{\mathbf{x}}^{(k)} = \delta_{\mathbf{x}\mathbf{x}}$. To determine $\lambda_3^{(k+1)}$ and $\delta_{\mathbf{x}}^{(k)}$, rearrange Equation (10.47) and we have the following equivalent system:

$$\begin{pmatrix} \mathbf{W}^{(k)} & -\mathbf{J}^{(k)} \\ -\mathbf{J}^{(k)'} & 0 \end{pmatrix} \begin{pmatrix} \delta_{\mathbf{x}} \\ \lambda_3 \end{pmatrix} = \begin{pmatrix} -\mathbf{g}^{(k)} \\ \mathbf{c}^{(k)} \end{pmatrix} \tag{10.48}$$

Given $\lambda_3^{(k+1)}$ and $\delta_{\mathbf{x}}^{(k)}$, then $\mathbf{x}^{(k+1)}$ is given by

$$\mathbf{x}^{(k+1)} = \mathbf{x}^{(k)} + \delta_{\mathbf{x}}^{(k)}. \quad (10.49)$$

Given a set of initial approximations $\mathbf{x}^{(0)}$ and $\lambda^{(0)}$, the iterative sequence $\{\mathbf{x}^{(k)}, \lambda^{(k)}\}$ can be generated by System (10.46) and (10.49).

To compute the root $\mathcal{R}(\text{mat}(\mathbf{x}))$, I use the algorithm in Chanchana [2007], which is very effective from a numerical perspective both in terms of error bounds and speed of convergence. To make the chapter self-contained I list here the key steps of the computation, slightly adjusted to account for numerical issues. At first I initialise the computation by setting $\mathbf{v}^0 = \mathbf{1}$ be the start value of the tentative Perron's vector and $\delta = \mathbf{Q} \cdot \mathbf{1}$ be the start value of the tentative Perron's root. Then I repeat the following procedure:

1. Compute $\mathbf{M} = \delta \cdot \mathbf{I}_M - \mathbf{Q}$, and make sure that by construction $\mathcal{R}(\text{mat}(\mathbf{Q})) \leq \delta$.
2. If \mathbf{M} is well conditioned (as we might have found the Perron root by chance), then I execute the following computation:
 - (a) We then solve $\mathbf{M}\mathbf{v}^1 = \mathbf{v}^0$ for \mathbf{v}^1 .
 - (b) Solve $\mathbf{M}\mathbf{v}^0 = \mathbf{v}^1$ for \mathbf{v}^0 where \mathbf{v}^1 is the value computed at the previous step.
 - (c) Compute the lower and upper bounds for the Perron root $\delta_{min} = \delta - \max_{i \in \{1 \dots M\}}(\mathbf{v}_i^1 / \mathbf{v}_i^0)$ and $\delta_{max} = \delta - \min_{i \in \{1 \dots M\}}(\mathbf{v}_i^1 / \mathbf{v}_i^0)$.
3. Set the new value of the Perron root as the obtained upper bound $\delta = \delta_{max}$ and repeat from step (1) until the error $(\delta_{max} - \delta_{min}) / \delta_{max}$ is below a desired threshold.

The Perron eigenvector \mathbf{v}_R is then be computed by dividing \mathbf{v}^1 for the sum of its elements so that it has norm equal to one, i.e. $\mathbf{v}_R = \mathbf{v}^1 / \sum_i \mathbf{v}_i^1$. A similar procedure can be used to compute the left eigenvector \mathbf{v}_L by using the transpose of \mathbf{Q} in the above algorithm, provided the left eigenvector is also

scaled so that the scalar product between the two eigenvector is equal to one (i.e. $\mathbf{v}'_R \cdot \mathbf{v}_L = 1$).

At this point we only need to compute the first-order derivative and, as I have mentioned, it is better to rely on [Vahrenkamp \[1976\]](#) and use Equation 5.15. Then we return to the main algorithm the following results:

$$\mathcal{R}(\text{mat}(\mathbf{x})) = \delta, \quad \text{and} \quad \frac{\partial \mathcal{R}(\text{mat}[\mathbf{x}])}{\partial \mathbf{x}'} = \text{vec}[\mathbf{v}_L \mathbf{v}'_R],$$

$$\text{where} \quad \begin{cases} \mathbf{x} = \text{vec}[\mathbf{Q}] \\ \mathbf{Q} \cdot \mathbf{v}_R = r \mathbf{v}_R \text{ and } \mathbf{v}'_L \cdot \mathbf{Q} = r \mathbf{v}_L \\ \mathbf{v}'_R \cdot \mathbf{1} = 1 \text{ and } \mathbf{v}'_R \cdot \mathbf{v}_L = 1 \end{cases} \quad (10.50)$$

Bibliography

- Aït-Sahalia, Y. and A. W. Lo (1998). Nonparametric estimation of state-price densities implicit in financial asset prices. *The Journal of Finance* 53(2), 499–547. [25](#), [59](#), [101](#), [103](#), [104](#)
- Amaya, D., P. Christoffersen, K. Jacobs, and A. Vasquez (2015). Does realized skewness predict the cross-section of equity returns? *Journal of Financial Economics* 118(1), 135 – 167. [196](#)
- Amihud, Y. (2002). Illiquidity and stock returns: cross-section and time-series effects. *Journal of financial markets* 5(1), 31–56. [197](#)
- Andersen, A. B. and T. Wagener (2002, December). Extracting risk neutral probability densities by fitting implied volatility smiles: Some methodological points and an application to the 3m euribor futures options prices. *ECB Working Paper No. 198*. Available at SSRN: <https://ssrn.com/abstract=359060>. [25](#)
- Andersen, T. G., T. Bollerslev, F. X. Diebold, and H. Ebens (2001). The distribution of realized stock return volatility. *Journal of financial economics* 61(1), 43–76. [77](#)
- Andersen, T. G., T. Bollerslev, F. X. Diebold, and P. Labys (2003). Modeling and forecasting realized volatility. *Econometrica* 71(2), 579–625. [46](#), [50](#), [78](#), [196](#)
- Andersen, T. G., N. Fusari, and V. Todorov (2015, May). Parametric inference and dynamic state recovery from option panels. *Econometrica* 83(3), 1081–1145. [25](#), [50](#)

- Ang, A., J. Chen, and Y. Xing (2006). Downside risk. *Review of Financial Studies* 19(4), 1191–1239. [195](#)
- Ang, A., R. J. Hodrick, Y. Xing, and X. Zhang (2006). The cross-section of volatility and expected returns. *The Journal of Finance* 61(1), 259–299. [191](#), [196](#)
- Anthony, J. H. (1988). The interrelation of stock and options market trading-volume data. *The Journal of Finance* 43(4), 949–964. [23](#)
- Arrow, K. J. (1964). The role of securities in the optimal allocation of risk-bearing. *The Review of Economic Studies*, 91–96. [24](#), [58](#), [86](#)
- Audrino, F., R. Huitema, and M. Ludwig (2014). An empirical analysis of the ross recovery theorem. *Available at SSRN 2433170*. [25](#), [61](#), [87](#), [102](#)
- Backwell, A. (2015). State prices and implementation of the recovery theorem. *Journal of Risk and Financial Management* 8(1), 2–16. [25](#), [61](#), [87](#)
- Bakshi, G., F. Chabi-Yo, and X. Gao (2017). A recovery that we can trust? deducing and testing the restrictions of the recovery theorem. *The Review of Financial Studies* 31(2), 532–555. [60](#), [87](#)
- Bakshi, G. and N. Kapadia (2003). Volatility risk premiums embedded in individual equity options: Some new insights. *The Journal of Derivatives* 11(1), 45–54. [176](#)
- Bakshi, G., N. Kapadia, and D. Madan (2003a). Stock return characteristics, skew laws, and the differential pricing of individual equity options. *Review of Financial Studies* 16(1), 101–143. [26](#), [74](#), [77](#), [78](#)
- Bakshi, G., N. Kapadia, and D. Madan (2003b). Stock return characteristics, skew laws, and the differential pricing of individual equity options. *Review of Financial Studies* 16(1), 101–143. [176](#)
- Bakshi, G. and D. Madan (2000). Spanning and derivative-security valuation. *Journal of Financial Economics* 55(2), 205–238. [26](#), [73](#), [74](#), [78](#), [80](#), [151](#)

- Bali, T. G., R. F. Engle, and S. Murray (2016). *Empirical asset pricing: the cross section of stock returns*. John Wiley & Sons. [194](#), [195](#), [214](#), [220](#)
- Bali, T. G., J. Hu, and S. Murray (2015). Option implied volatility, skewness, and kurtosis and the cross-section of expected stock returns. *Georgetown McDonough School of Business Research Paper*. [26](#), [147](#), [192](#)
- Barndorff-Nielsen, O. E. (2002). Econometric analysis of realized volatility and its use in estimating stochastic volatility models. *Journal of the Royal Statistical Society: Series B (Statistical Methodology)* *64*(2), 253–280. [77](#)
- Ben-Israel, A. and T. N. Greville (2003). *Generalized inverses: theory and applications*, Volume 15. Springer Science & Business Media. [255](#)
- Berman, A. and R. J. Plemmons (1979). Nonnegative matrices. *The Mathematical Sciences, Classics in Applied Mathematics* *9*. [255](#)
- Black, F. and M. Scholes (1973). The pricing of options and corporate liabilities. *The journal of political economy*, 637–654. [23](#)
- Bodurtha, J. N. and Q. Shen (1995). Historical and implied measures of value at risk: The dm and yen case. *Manuscript, Georgetown University*. [27](#), [148](#)
- Bollerslev, T., B. Hood, J. Huss, and L. H. Pedersen (2018). Risk everywhere: Modeling and managing volatility. *Review of Financial Studies, forthcoming*. *Review of Financial Studies, forthcoming*. *Review of Financial Studies, forthcoming*. [50](#)
- Bondarenko, O. (2003). Estimation of risk-neutral densities using positive convolution approximation. *Journal of Econometrics* *116*(1), 85–112. [85](#)
- Borovička, J., L. P. Hansen, and J. A. Scheinkman (2016, March). Misspecified recovery. *Journal of Finance*. [2](#), [24](#), [60](#), [61](#), [68](#), [70](#), [71](#), [72](#), [83](#), [84](#), [87](#), [88](#), [89](#), [90](#), [91](#), [99](#), [142](#), [143](#)
- Boudt, K., W. Lu, and B. Peeters (2015). Higher order comoments of multifactor models and asset allocation. *Finance Research Letters* *13*, 225–233. [154](#)

- Breeden, D. T. and R. H. Litzenberger (1978). Prices of state-contingent claims implicit in option prices. *Journal of Business*, 621–651. [24](#), [30](#), [58](#), [73](#), [85](#), [86](#), [87](#), [92](#), [101](#), [103](#), [105](#), [118](#), [121](#)
- Brown, D. J. and S. A. Ross (1991). Spanning, valuation and options. *Economic Theory* 1(1), 3–12. [26](#), [73](#), [80](#)
- Brown, D. P. and J. C. Jackwerth (2004). The pricing kernel puzzle: Reconciling index option data and economic theory. *Working paper, University of Konstanz*. [32](#), [139](#)
- Brownlees, C. and R. F. Engle (2017). Srisk: A conditional capital shortfall measure of systemic risk. *The Review of Financial Studies* 30(1), 48–79. [228](#)
- Buckle, M., J. Chen, and J. M. Williams (2014). Realised higher moments: theory and practice. *The European Journal of Finance*, 1–20. [78](#), [154](#)
- Buraschi, A., P. Porchia, and F. Trojani (2010). Correlation risk and optimal portfolio choice. *The Journal of Finance* 65(1), 393–420. [190](#)
- Campa, J. M., P. K. Chang, and R. L. Reider (1998). Implied exchange rate distributions: evidence from otc option markets. *Journal of International Money and Finance* 17(1), 117–160. [27](#), [148](#)
- Carhart, M. M. (1997). On persistence in mutual fund performance. *The Journal of finance* 52(1), 57–82. [191](#), [199](#), [206](#), [207](#), [216](#)
- Carr, P. and D. Madan (2001). Optimal positioning in derivative securities. *Quantitative Finance*. [26](#), [73](#), [74](#), [75](#), [76](#), [77](#), [78](#), [80](#), [81](#), [151](#)
- Carr, P. and J. Yu (2012). Risk, return, and ross recovery. *Journal of Derivatives* 20(1), 38. [2](#), [24](#), [59](#), [61](#), [65](#), [66](#), [67](#), [68](#), [72](#), [83](#), [86](#), [87](#), [145](#)
- Chanchana, P. (2007). *An algorithm for computing the Perron root of a nonnegative irreducible matrix*. Ph. D. thesis, NCSU. [274](#)

- Chang, B. Y., P. Christoffersen, and K. Jacobs (2013). Market skewness risk and the cross section of stock returns. *Journal of Financial Economics* 107(1), 46–68. [26](#), [147](#), [191](#), [192](#), [203](#)
- Conrad, J., R. F. Dittmar, and E. Ghysels (2013). Ex ante skewness and expected stock returns. *The Journal of Finance* 68(1), 85–124. [26](#), [147](#), [151](#), [191](#), [192](#)
- Corsi, F. (2009). A simple approximate long-memory model of realized volatility. *Journal of Financial Econometrics* 7(2), 174–196. [203](#)
- Cuesdeanu, H. (2017). *Three Essays on Option Pricing*. Ph. D. thesis, Universität Konstanz, Konstanz. [32](#), [139](#)
- De Jong, F., J. Driessen, and A. Pelsser (2004). On the information in the interest rate term structure and option prices. *Review of Derivatives Research* 7(2), 99–127. [27](#), [148](#)
- Debreu, G. (1987). *Theory of value: An axiomatic analysis of economic equilibrium*, Volume 17. Yale University Press. [24](#), [58](#), [86](#)
- Deutsch, E. and M. Neumann (1985). On the first and second order derivatives of the perron vector. *Linear algebra and its applications* 71, 57–76. [255](#), [256](#), [257](#), [261](#)
- Driessen, J., P. J. Maenhout, and G. Vilkov (2009). The price of correlation risk: Evidence from equity options. *The Journal of Finance* 64(3), 1377–1406. [27](#), [147](#), [148](#), [151](#), [190](#), [191](#), [192](#)
- Driessen, J., P. J. Maenhout, and G. Vilkov (2013). Option-implied correlations and the price of correlation risk. *Netspar Discussion Paper No. 07/2013-061*. Available at SSRN: <https://ssrn.com/abstract=2359380> or <http://dx.doi.org/10.2139/ssrn.2359380>. [27](#), [147](#), [148](#), [151](#), [191](#), [192](#)
- Dubynskiy, S. and R. S. Goldstein (2013, April). Recovering drifts and preference parameters from financial derivatives.

Available at SSRN: <https://ssrn.com/abstract=2244394> or <http://dx.doi.org/10.2139/ssrn.2244394>. 24, 60, 87

- Dupont, D. Y. (2001). Extracting risk-neutral probability distributions from option prices using trading volume as a filter. Technical report, Reihe Ökonomie/Economics Series, Institut für Höhere Studien (IHS). 129
- Easley, D., M. O'hara, and P. S. Srinivas (1998). Option volume and stock prices: Evidence on where informed traders trade. *The Journal of Finance* 53(2), 431–465. 23
- Fama, E. F. and K. R. French (1992). The cross-section of expected stock returns. *the Journal of Finance* 47(2), 427–465. 194, 207, 216
- Fama, E. F. and K. R. French (1993). Common risk factors in the returns on stocks and bonds. *Journal of financial economics* 33(1), 3–56. 191, 198, 199, 206, 226
- Fama, E. F. and J. D. MacBeth (1973). Risk, return, and equilibrium: Empirical tests. *Journal of political economy* 81(3), 607–636. 38, 39, 192, 213, 214, 217, 218, 219, 220, 222, 223
- Figlewski, S. (2008). Estimating the implied risk neutral density. Technical report, Volatility and Time Series Econometrics: Essays in honor of Robert F. Engle, Tim Bollerslev, Jeffrey R. Russell, Mark Watson, Oxford, UK: Oxford University Press. 101, 103, 104, 105
- Fletcher, R. (1971). A general quadratic programming algorithm. *IMA Journal of Applied Mathematics* 7(1), 76–91. 110
- Frobenius, G. (1908). Über matrizen aus positiven elementen i and ii. *Sitzungsber. Preuss. Akad. Wiss., Berlin*, 471–476. 97
- Ghalanos, A., E. Rossi, and G. Urga (2015). Independent factor autoregressive conditional density model. *Econometric Reviews* 34(5), 594–616. 154
- Hansen, L. P. and J. A. Scheinkman (2009). Long-term risk: An operator approach. *Econometrica* 77(1), 177–234. 68, 70, 83, 86, 87, 90, 143

- Hens, T. and C. Reichlin (2013). Three solutions to the pricing kernel puzzle. *Review of Finance* 17(3), 1065–1098. 32, 139
- Hirtle, B., A. Kovner, J. Vickery, and M. Bhanot (2016). Assessing financial stability: the capital and loss assessment under stress scenarios (class) model. *Journal of Banking & Finance* 69, S35–S55. 228
- Jackwerth, J. C. (2004). Option-implied risk-neutral distributions and risk aversion. *CFA Institute*. 85
- Jackwerth, J. C. and M. Rubinstein (1996). Recovering probability distributions from option prices. *The Journal of Finance* 51(5), 1611–1631. 85
- Jegadeesh, N. (1990). Evidence of predictable behavior of security returns. *The Journal of Finance* 45(3), 881–898. 197
- Jegadeesh, N. and S. Titman (1993). Returns to buying winners and selling losers: Implications for stock market efficiency. *The Journal of finance* 48(1), 65–91. 197
- Jensen, C. S., D. Lando, and L. H. Pedersen (2018). Generalized recovery. *Journal of Financial Economics, forthcoming*. 25, 60, 61, 87
- Jurado, K., S. C. Ludvigson, and S. Ng (2015). Measuring uncertainty. *The American Economic Review* 105(3), 1177–1216. 228
- Krishnan, C., R. Petkova, and P. Ritchken (2009). Correlation risk. *Journal of Empirical Finance* 16(3), 353–367. 147, 148, 190, 192
- Lehmann, B. N. (1990). Fads, martingales, and market efficiency. *The Quarterly Journal of Economics* 105(1), 1–28. 197
- Liu, F. (2014, December). Recovering conditional return distributions by regression: Estimation and applications. Available at SSRN: <https://ssrn.com/abstract=2530183> or <http://dx.doi.org/10.2139/ssrn.2530183>. 24, 60, 87

- Liu, J. and J. Pan (2003). Dynamic derivative strategies. *Journal of Financial Economics* 69(3), 401–430. [23](#)
- Long, J. B. (1990). The numeraire portfolio. *Journal of Financial Economics* 26(1), 29–69. [61](#), [65](#), [66](#), [87](#)
- Longin, F. and B. Solnik (1995). Is the correlation in international equity returns constant: 1960–1990? *Journal of international money and finance* 14(1), 3–26. [27](#), [148](#)
- Longstaff, F. A., P. Santa-Clara, and E. S. Schwartz (2001). The relative valuation of caps and swaptions: Theory and empirical evidence. *The Journal of Finance* 56(6), 2067–2109. [27](#), [148](#)
- Lopez Aliouchkin, R. (2015, November). Option-implied idiosyncratic and systematic risk in the cross-section of expected stock returns. *Swedish House of Finance Research Paper No 15-15*. Available at SSRN: <https://ssrn.com/abstract=2683914> or <http://dx.doi.org/10.2139/ssrn.2683914>. [192](#)
- Markopoulou, C., V. Skintzi, and A. Refenes (2016). On the predictability of model-free implied correlation. *International Journal of Forecasting* 32(2), 527–547. [190](#)
- Martellini, L. and V. Ziemann (2010). Improved estimates of higher-order comoments and implications for portfolio selection. *Review of Financial Studies* 23(4), 1467–1502. [154](#)
- Martin, I. and S. A. Ross (2013). The long bond. Technical report, Working Paper, Stanford University. [60](#)
- Merton, R. C. (1973). Theory of rational option pricing. *The Bell Journal of economics and management science*, 141–183. [23](#)
- Monteiro, A. M., R. H. Tütüncü, and L. N. Vicente (2008). Recovering risk-neutral probability density functions from options prices using cubic

- splines and ensuring nonnegativity. *European Journal of Operational Research* 187(2), 525–542. [85](#)
- Mueller, P., A. Stathopoulos, and A. Vedolin (2016). International correlation risk. *Journal of Financial Economics*. [27](#), [148](#)
- Neuberger, A. (2012). Realized skewness. *Review of Financial Studies* 25(11), 3423–3455. [78](#)
- Newey, W. K. and K. D. West (1987). Hypothesis testing with efficient method of moments estimation. *International Economic Review*, 777–787. [204](#), [205](#), [213](#), [214](#), [218](#), [220](#)
- Ngoc-Khanh, T. and S. Xia (2014). Specified recovery. Technical report, Washington University in St. Louis. [25](#), [60](#), [87](#), [102](#)
- Norris, J. (1998). *Markov Chains*. Cambridge University Press. [107](#)
- Park, H. (2015). The martin integral representation of markovian pricing kernels. *arXiv preprint arXiv:1504.00276*. [24](#), [60](#), [87](#)
- Pastor, L. and R. F. Stambaugh (2003). Liquidity risk and expected stock returns. *Journal of Political Economy* 111(3), 642–685. [191](#), [199](#), [207](#)
- Perron, O. (1907). Zur theorie der matrices. *Mathematische Annalen* 64(2), 248–263. [97](#)
- Pollet, J. M. and M. Wilson (2010). Average correlation and stock market returns. *Journal of Financial Economics* 96(3), 364–380. [183](#), [190](#)
- Protter, P. E. (2013). *Stochastic integration and differential equations*, Volume 21. Springer. [74](#)
- Qin, L. and V. Linetsky (2014). Ross recovery in continuous time. *Available at SSRN 2439002*. [60](#), [87](#)
- Qin, L. and V. Linetsky (2016). Positive eigenfunctions of markovian pricing operators: Hansen-scheinkman factorization, ross recovery, and long-term pricing. *Operations Research*. [24](#), [60](#), [87](#)

- Qin, L. and V. Linetsky (2017). Long term risk: A martingale approach. *Econometrica*. [24](#), [60](#)
- Robert, P. (1968). On the group-inverse of a linear transformation. *Journal of Mathematical Analysis and Applications* *22*(3), 658–669. [255](#)
- Ross, S. (2015). The recovery theorem. *The Journal of Finance* *70*(2), 615–648. [2](#), [23](#), [24](#), [25](#), [32](#), [33](#), [59](#), [60](#), [61](#), [62](#), [64](#), [66](#), [68](#), [70](#), [71](#), [72](#), [83](#), [84](#), [86](#), [87](#), [88](#), [90](#), [92](#), [93](#), [94](#), [96](#), [101](#), [116](#), [128](#), [129](#), [130](#), [139](#), [142](#), [225](#)
- Ross, S. A. (1976). Options and efficiency. *The Quarterly Journal of Economics* *90*(1), 75–89. [26](#), [73](#), [80](#)
- Schneider, P. and F. Trojani (2018). (almost) model-free recovery. *Journal of Finance*, *forthcoming*. [25](#), [61](#), [87](#)
- Seneta, E. (1973). *Non-Negative Matrices, An Introduction to Theory and Applications*. Wiley, New York. [255](#)
- Skintzi, V. D. and A.-P. N. Refenes (2005). Implied correlation index: A new measure of diversification. *Journal of Futures Markets* *25*(2), 171–197. [27](#), [147](#), [148](#), [192](#)
- Song, Z. and D. Xiu (2016). A tale of two option markets: Pricing kernels and volatility risk. *Journal of Econometrics* *190*(1), 176–196. [32](#), [102](#), [116](#), [139](#), [145](#)
- Spears, T. (2013). *On estimating the risk-neutral and real-world probability measures*. Ph. D. thesis, Oxford University. [25](#), [61](#), [87](#)
- Swan, E. (2000). *Building the Global Market: A 4000 Year History of Derivatives*. Springer Netherlands. [22](#)
- Vahrenkamp, R. (1976). Derivatives of the dominant root. *Applied Mathematics and Computation* *2*(1), 29–39. [97](#), [99](#), [255](#), [256](#), [275](#)

- Von Furstenberg, G. M., B. N. Jeon, N. G. Mankiw, and R. J. Shiller (1989). International stock price movements: links and messages. *Brookings Papers on Economic Activity* 1989(1), 125–179. [26](#), [148](#)
- Walden, J. (2017). Recovery with unbounded diffusion processes. *Review of Finance* 21(4), 1403–1444. [24](#), [59](#), [86](#)
- Walter, C. A. and J. A. Lopez (2000). Is implied correlation worth calculating? evidence from foreign exchange options. *The Journal of Derivatives* 7(3), 65–81. [27](#), [148](#)
- Yatchew, A. and W. Härdle (2006). Nonparametric state price density estimation using constrained least squares and the bootstrap. *Journal of Econometrics* 133(2), 579–599. [25](#), [59](#)
- Yuan, M. (2009). State price density estimation via nonparametric mixtures. *The Annals of Applied Statistics*, 963–984. [25](#), [59](#)
- Zhou, H. (2013). On the predictive power of the implied correlation index. Technical report, Boston College. [148](#)